NEW FUNCTIONALIZED POLYOXOMETALATES (POMs) FOR MOLECULAR MEMORY DEVICES COMPATIBLE WITH A CMOS PROCESSING

Nicoleta Joo

THÈSE

Pour obtenir le grade de

DOCTEUR DE L'UNIVERITÉ DE GRENOBLE
Spécialité « Chimie Inorganique et Bio-Inorganique »
Arrêté ministériel : 7 août 2006
Présentée et soutenue publiquement par

NICOLETA JOO

le 3 Septembre 2010

NOUVEAUX DÉRIVÉS DE POLYOXOMÉTALLATES (POMs) POUR DES MÉMOIRES MOLÉCULAIRES COMPATIBLES AVEC DES PROCÉDÉS DE FABRICATION CMOS

Thèse dirigée par DR Gérard BIDAN et codirigée par Dr. Guillaume NONGLATON

JURY

M. Pierre Mialane	Professeur, Université Versailles Saint Quentin en Yvelines	Président
M. Tim McCormack	Docteur, Dundalk Institute of Technology	Rapporteur
M. Jean-Christophe Lacroix	Professeur, Université Paris Diderot	Rapporteur
M. Guy Royal	Professeur, Université Joseph Fourier	Examinateurs
Mme. Anna Proust	Professeur, Université Pierre et Marie Curie	
M. Gérard Bidan	Directeur de Recherche, CEA-Grenoble, INAC	
M. Guillaume Nonglaton	Docteur, CEA-Grenoble, LETI	

Thèse préparée au sein du Laboratoire LETI dans l'Ecole Doctorale Chimie et Science du Vivant

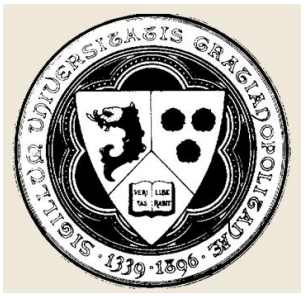

Ph.D. Thesis

NEW FUNCTIONALIZED POLYOXOMETALATES (POMs) FOR MOLECULAR MEMORY DEVICES COMPATIBLE WITH A CMOS PROCESSING

Ph.D. Student
NICOLETA JOO

Public Defence: September the 3rd, 2010

PhD advisor:
Dr. DR GÉRARD BIDAN

Supervisor:
Dr. GUILLAUME NONGLATON

Scientific advisors:
Prof. Dr. ANNA PROUST
Dr. RENÉ THOUVENOT
Prof. Dr. PIERRE GOUZERH

To Elena, Francisc,
Alexandra and Sorin.

ACKNOWLEDGMENTS

This thesis would not have been possible without their permanent involvement:

First of all, I sincerely thank to my PhD advisor DR Gérard Bidan, for giving me the opportunity to develop this work, for his generous support, guidance, encouragements and friendship during the course of this research.

I would like to express my sincere appreciation to my jury committee members for their kindness and patience to read my PhD thesis and for their considerations on it.

I would like to thank Prof. Anna Proust, Dr. René Thouvenot and Prof. Pierre Gouzerh from Pierre and Marie Curie University, Paris, France, for accepting me to work in their team during my 5 month stage in Paris. I would also like to thank them for their help, kindness, ideas and helpful discussions.

I would like to acknowledge the help, encouragements and friendship from Dr. Guillaume Nonglaton.

I want to thank Prof. Isabelle Schuster for her kindness, comments and useful advices during CHEMtronics meetings. Also thanks to Dr. Françoise Vinet and Dr. Christine Peponet for welcoming me in the LETI/LFCM laboratory.

Thanks go also to Tech. Séverine Renaudineau for permanently ensure the polyoxometalates precursors supply during these three years of thesis.

I am thankful to Dr. Julien Buckley for the electrical measurements and helpful discussions, to Dr. Nevine Rochat for the ATR measurements, to Dr. Christophe Lecitra for the ellipsometry measurements, and to Dr. Pierre Alain Bayle for the NMR measurements.

A number of other people have made my stay in a foreign country possible and enjoyable. My thanks in this regard go to Pommier family, my friends: Marius, Olga, Paul and Helga. Thanks also to my colleagues from LFCM, INAC and Marie and Pierre Curie University: Dr. Adeline Leyris, Dr. Yanxia Hou, Dr. Régis Barattin, Tech. Caroline Seraine, Dr. Fabien Lefloch, Dr. Cécile Halte, Dr. Gilles Marchand, Dr.

Guillaume Delapierre, Dr. Florence Duclairoir, Dr. Benoit Fleury, Dr. Richard Villanneau, Dr. Ruxandra Gheorghe, Dr. Carmen Paraschiv for all their support on professional and personal level.

I am also thankful to Prof. Mariana Rusu for introducing me to the wonderful field of polyoxometalates.

Special thanks to Sorin Puscas and Alexandra Joo for support, encouragements and help during my three years stay in France and to my parents for all their love and support.

The work and results reported in this publication were obtained with research funding from the European Community under the Sixth Framework Programme for the Marie Curie Host Fellowships for Early Stage Research Training (EST) “CHEMTRONICS” Contract Number MEST-CT-2005-020513.

Abstract – The microelectronics industry is presently close to the limit of this minimization trend dictated by both laws of physics and the cost of production. It is possible that electronically functional molecular components can not only address the ultimate limits of possible miniaturization but also provide promising new methodologies for novel architectures. The aim of the present thesis is to study the miniaturization of non-volatile memory devices, FLASH type, by replacing the floating gate with monolayers of redox molecules, polyoxometalates.

Towards this goal I was engaged in a program aimed at constructing devices that use the properties of polyoxometalates (POMs) to store information. In a general approach, a redox-active molecule attached to an electroactive surface serves as the active storage medium, and information is stored in the discrete redox states of the POM molecule.

This work is organized in four parts and begins with a short introduction into the molecular memory and polyoxometalates fields. It continues with the experimental results systematized in part 2, synthesis and characterization of functionalized polyoxometalates, part 3, polyoxometalates modified electrodes and part 4, electrical investigation of the polyoxometalates modified capacitors. Each part contains an abstract written in English and French.

The first part contains an introduction in the molecular electronics, the state of the art in the molecular memory is also presented and particularly the redox monolayers used as charge storage media in a memory device. Since the functionalized polyoxometalates constitute an important topic in this thesis, the hybrid polyoxometalates are reviewed and especially their electrochemical properties are stressed. Because of their reversible redox behavior, discrete structures in size from subnanometer to a few nanometers, and good solubility and stability in aqueous and organic solvents, POMs have been used widely as the inorganic components in functional molecular materials. An introduction into the polyoxometalates based materials is presented with an emphasis on in their electrical properties.

One of the most challenging objectives of the second part of the thesis is that of obtaining POMs derivatives with predetermined structures and properties. The derivatisation of POMs frameworks by replacing/derivatising the oxo ligands is an important aim since this it allows a much greater degree of control, potentially allowing the simultaneous exploitation of self assembly of the POMs fragments, and step wise synthesis to introduce pendant functionalities. However, the most common route to the

integration of POMs into functional architectures and devices rests on inorganic/organic hybrids. The second part describes the synthesis, the spectroscopic characterization and the electrochemical behavior in solution of some functionalized polyoxometalates. The surface attachment groups are synthetically designed for the molecule to attach on specific surfaces via covalent bonds.

The third part addresses the elaboration of a monolayer of POMs on silicon surface to form uniform and dense active storage medium. The attachment of polyoxometalate molecules onto the silicon surface by different linkers and using various grafting routes is described. The polyoxometalate modified silicon wafers were characterized by means of cyclic voltammetry (CV), X-ray photoelectron spectroscopy (XPS) and attenuated total reflection infrared spectroscopy (ATR-IR).

The fourth and last part contains information about the characterization of an electrode-molecule-silicon (EMS) capacitor which can provide critical information on the feasibility of using charge-trapping molecules in memory devices. Characterization by conventional capacitance and conductance techniques showed very high capacitance and conductance peaks associated with charging and discharging of electrons into and from discrete levels in the monolayer owing to the presence of the redox-active polyoxometalates.

Résumé – L'industrie de la microélectronique est aujourd'hui très proche de la limite de la tendance de miniaturisation dictée par les lois de la physique et les coûts de production. Il est possible que le composant moléculaire fonctionnalisé puisse non seulement répondre aux limites ultimes de miniaturisation mais aussi fournir de nouvelles méthodes prometteuses pour les nouvelles architectures. L'objectif de cette thèse est d'étudier la miniaturisation des dispositifs à mémoire non-volatile, de type FLASH, en remplaçant la grille flottante avec des monocouches de molécules redox, les polyoxométallates.

Dans ce but, j'ai été engagé dans un programme visant à construire des dispositifs qui utilisent les propriétés des polyoxométallates (POMs) pour stocker des informations. Dans une approche générale, une molécule redox-active fixée à une surface d'électrode de silicium sert de support de stockage actif, et l'information est stockée dans les états d'oxydo-réduction discrets de la molécule (POM).

Ce travail est organisé en quatre parties et commence par une brève introduction sur les mémoires moléculaires et les polyoxométallates. Il continue avec les résultats expérimentaux systématisés: en partie 2 : la synthèse et la caractérisation des polyoxométallates fonctionnalisés; en partie 3, les électrodes modifiées par des polyoxométallates et en partie 4, l'étude électrique des condensateurs modifiés par des polyoxométallates. Chaque partie contient un résumé rédigé en anglais et en français.

La première partie contient une introduction à l'électronique moléculaire. L'état de l'art sur les mémoires moléculaires est également présenté, notamment les monocouches redox utilisées comme supports de stockage de charges dans un dispositif de mémoire. Étant donné que les polyoxométallates fonctionnalisés constituent un sujet important dans cette thèse, les polyoxométallates hybrides sont examinés et en particulier leurs propriétés électrochimiques. En raison de leur comportement redox réversible, de leurs structures discrètes de taille du subnanométrique à quelques nanomètres, et d'une bonne solubilité et stabilité en milieux aqueux et solvants organiques, les POMs ont été largement utilisés comme composants inorganiques dans des matériaux moléculaires. Une introduction sur les matériaux basés sur les polyoxométallates est présentée et plus particulièrement sur leurs propriétés électriques.

L'un des objectifs les plus difficiles de la deuxième partie de la thèse est l'obtention de dérivés POMs avec des structures et des propriétés prédéterminées. La fonctionnalisation des structures de POMs en remplaçant les ligands oxo par des molécules organiques est un objectif important car cela permet un plus grand degré de contrôle, permettant potentiellement l'exploitation simultanée des auto-assemblages des fragments POMs, et la synthèse par étapes pour introduire des fonctionnalités sur la structure des POMs. Néanmoins, la route la plus commune pour l'intégration des POMs dans des architectures fonctionnelles ou des dispositifs repose sur des hybrides inorganiques/organiques. La deuxième partie décrit la synthèse, la caractérisation spectroscopique et le comportement électrochimique en solution de certains polyoxométallates fonctionnalisés. Les groupes d'attachement à la surface sont synthétiquement conçus pour que la molécule s'attache sur des surfaces spécifiques par des liaisons covalentes.

La troisième partie aborde l'élaboration d'une monocouche des POMs sur la surface de silicium pour former un milieu de stockage actif uniforme et dense. La fixation des molécules de polyoxométallates sur la surface de silicium par différents espaceurs utilisant différentes voies de greffage est décrite. Les surfaces de silicium modifiées par des polyoxométallates ont été caractérisées par voltamétrie cyclique (CV), spectrométrie de photoélectrons induits par rayons X (XPS) et spectrométrie infrarouge par réflexion totale atténuée (ATR-IR).

La quatrième et dernière partie contient des informations sur la caractérisation d'un condensateur de type électrode-molécule-silicium (EMS) qui peut fournir des informations critiques sur la possibilité d'utiliser le piégeage des charges par des molécules dans des dispositifs de mémoire. La caractérisation par des techniques de capacitance et de conductance conventionnelle ont montré des pics très élevés de capacitance et de conductance associée à la charge et la décharge d'électrons dans les niveaux discrets de la monocouche en raison de la présence de la couche de polyoxométallates redox-actifs.

TABLE OF CONTENT

Part 1

INTRODUCTION

1. First Part – Introduction

Abstract – An introduction in the molecular electronics and the state of the art in the molecular memory is presented within this chapter. Since the functionalized polyoxometalates constitute an important topic in this thesis, the hybrid polyoxometalates are reviewed and especially their electrochemical properties are stressed. Because of their impressive set of properties, POMs have been used widely as the inorganic components in functional molecular materials. An introduction into the polyoxometalates based materials is presented with an emphasis on in their electrical properties.

Résumé – Dans ce chapitre une introduction à l'électronique moléculaire et l'état de l'art sur les mémoires moléculaires est également présenté. Étant donné que les polyoxométallates fonctionnalisés constituent un sujet important dans cette thèse, les polyoxométallates hybrides sont examinés et en particulier leurs propriétés électrochimiques. En raison de leur ensemble impressionnant de propriétés, les POM ont été largement utilisés comme composants inorganiques dans des matériaux moléculaires. Une introduction sur les matériaux basés sur les polyoxométallates est présentée et plus particulièrement sur leurs propriétés électriques.

1.1. MOLECULAR ELECTRONICS – A GENERAL OVERVIEW

1.1.1. Introduction

When the microprocessor emerged 40 years ago, its impact on the semiconductor and computer industries was far from clear – and its ultimate impact not only on business of all kinds but also on everyday people was unthinkable. Indeed the microprocessors have transformed modern society. They affect the way we work and play, the way we travel and communicate, they offer remarkable processing power at remarkably low cost due to their progressive miniaturization.

The evolution of microprocessors has been known to follow Moore's Law when it comes to steadily increasing performance over the years. This law suggests that the complexity of an integrated circuit, with respect to minimum component cost, doubles every 24 months (Figure 1). This dictum has generally proven true since the early 1970s.

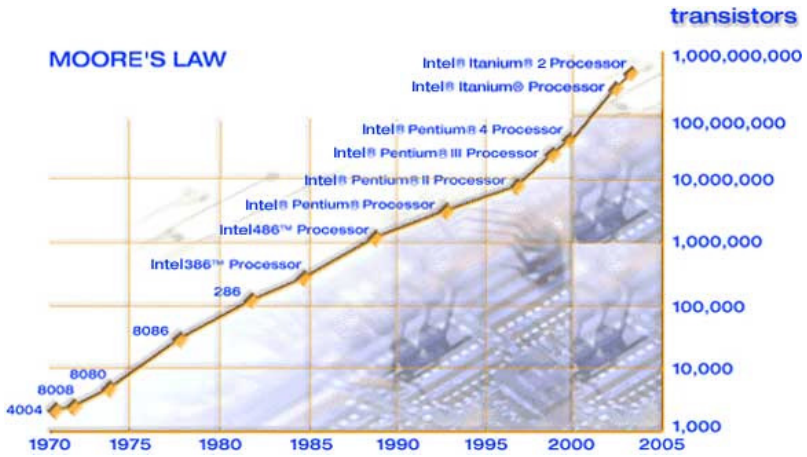

Figure 1. Moore's law which predicts that the number of transistors can be placed inexpensively on an integrated circuit will double approximately every two years. (image published by *Intel Corporation*)

Figure 2 depicts the reduction in size of amplification devices used in electronic circuits over the last century, and the further size reduction potential of molecules. Currently, integrated circuits can be produced with a resolution greater than 100 nm. Therefore, molecular electronics could be considered as the ultimate target to follow for the ongoing miniaturization trend in electronic circuitry.

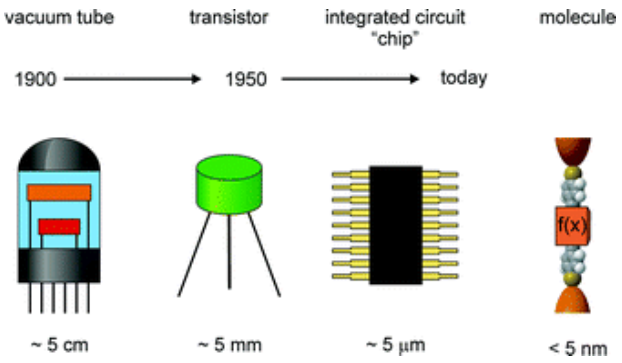

Figure 2. Miniaturization of amplification devices used in electronic circuits over the last century. From left to the right starting with the vacuum tube over the transistor to current integrated circuits.[1]

[1] N. Weibel, S. Grunder, M. Mayor, Functional molecules in electronic circuits, *Org. Biomol. Chem.* **2007**, *5*, 2343-2353.

The miniaturization trend known as Moore's law is only driven by the prospect of reducing the price per unit – more chips per silicon wafer reduces production costs. The latest *International Technology Roadmap for Semiconductors*[2] predicts that such scaling down approach will be pursued further in the nannoelectronics regime, and the 11 nm node technology will be reached by 2022. However, maintaining such aggressive top-down trend is getting increasingly difficult both technologycally and economically. Under these circumstances present nanoelectronics research is characterized by the migration of reasearch from pure down-scaling to the quest of new functionalities and other heterogenous technologies – referred to as 'More Moore' domains. The quest has become more urgent over the last decade, as traditional silicon circuitry continues to shrink towards a point where it can no longer function. Researchers hope to avoid this problem by using molecules and small chemical groups to create billions devices that could easily fit in the space of a current chip. Molecular electronics has developed to a mature research area in the past few years due to the increasing availability of investigative tools and the hope for appealing solutions at lower cost. With the contributions of physical and synthetic chemistry it has been possible over the last few years to correlate successfully molecular structure with physical properties, and design and synthesize tailor-made functional molecules which have been tried to use for electronic devices.

Modern molecular electronics began in 1974 when Aviram and Ratner[3] proposed a theoretical molecular rectifier based on an asymmetric molecular tunneling junction. A rectifier or diode is an important component in electronics that allows an electric current to flow in one direction, but blocks it in the opposite direction. They proposed the model molecule shown in **Figure 3**, (a). This molecule is composed of an electron-donor moiety, tetrathiafulvalene, and an electron acceptor moiety, tetracyanoquinodimethane, connected by methylene bridges. This structure is a molecular analogue of a *p-n* junction device (**Figure 3**, (b)). Indeed, the authors calculated the theoretical current-voltage (*I-V*) characteristics for this molecule and predicted the rectification behavior (**Figure 3**, (c)). Their contribution is very significant as a first step toward a molecular device.

[2] http://www.itrs.net/Links/2007ITRS/Home2007.htm
[3] A. Aviram, M. A. Ratner, Molecular Rectifiers, *Chem. Phys. Lett.* **1974**, *29*, 277-283.

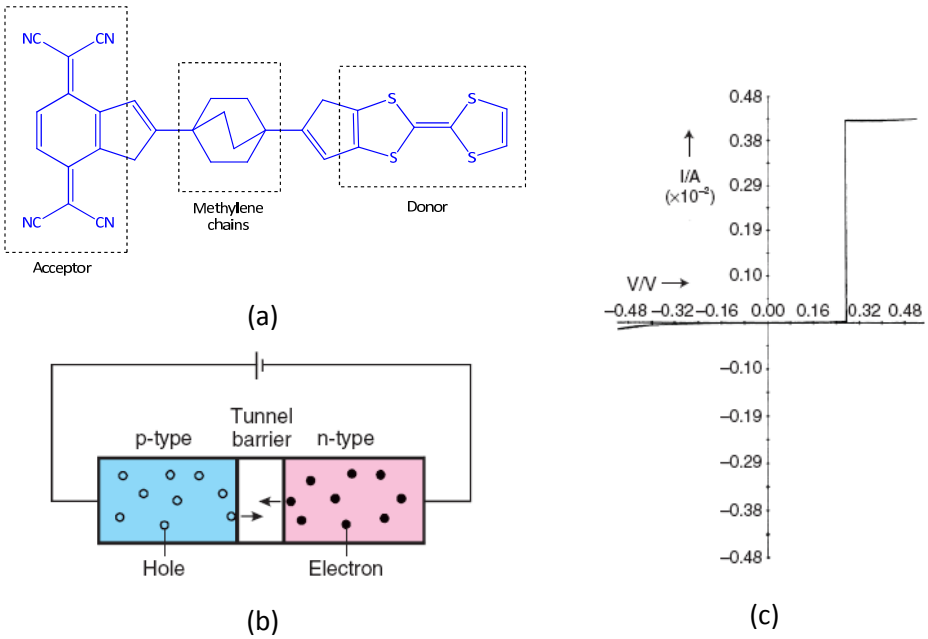

Figure 3. Explanation of molecular rectifier: (a) model molecule proposed by Aviram and Ratner, (b) *p-n* junction, and (c) calculated *I-V* characteristics.[3]

The past fifty years has witnessed continuous memory density increases and lower cost per bit, which has been powered by the startling downscaling of silicon memory devices. This trend, however, may soon end due to physical and technical limitations. This is because, as the projected size of the transistors goes down to 20 nm or below, the physics of the transistor leads to unacceptable power dissipation. In addition, technological and economic factors impose severe limits on the integration process. Continued growth of the semiconductor industry will likely rely on breakthroughs in both electronic materials and also device concepts. Extensive efforts have been devoted to address these two issues, and molecular memory is considered particularly promising. Such a memory has the potential to work on a few electrons at molecular scale and therefore promises low-power and ultradense systems. Important advancements have been made in this field since its conception. Multilevel molecular memory devices were proposed and demonstrated for data storage up to three bits per cell, in contrast to the standard one-bit-per-cell technology. This conceptual breakthrough in molecular memory yielded devices with on/off ratios exceeding 10^4 and retention times of 600 h.[4] The description of such devices is explained as follows.

[4] C. Li, W. Fan, B. Lei, D. Zhang, S. Han, T. Tang, X. Liu, Z. Liu, S. Asano, M. Meyyappan, J. Han, C. Zhou, Multilevel memory based on molecular devices, *Appl. Phys. Lett.* **2004**, *84*, 1949-1951.

1.1.2. Specificity of molecular electronics

It is well known that ***semiconductor devices are fabricated from the "top-down" approach*** that employs a variety of sophisticated lithographic and etch techniques to pattern a substrate. This approach has become increasingly challenging as feature size decreases. In particular, at nanometer scale, the electronic properties of semiconductor structures fabricated via conventional lithographic processes are increasingly difficult to control. In contrast, ***molecules are synthesized from the "bottom-up" approach*** that builds small structures from the atomic, molecular, or single device level. It in principle allows a very precise positioning of collections of atoms or molecules with specific functionalities. For example, one can selectively add an oxygen atom to a molecule with a precision far greater than an oxidation step in microfabrication using state of the art lithography and etching. Chemical synthesis makes it possible to make large quantities of nanometer-size molecules with the same uniformity but at significantly less cost, compared to other batch-fabrication processes such as microlithography. One can envision that in assembling molecular circuits, instead of building individual components on a chip one will synthesize molecules with structures possessing desired electronic configurations and attach/interconnect them into an electronic circuit using surface attachment techniques like self-assembly. ***Self-assembly is a phenomenon in which atoms, molecules, or groups of molecules arrange themselves spontaneously into regular patterns and even relatively complex systems without outside intervention***.

Essentially all electronic processes in nature, from photosynthesis to signal transduction, occur in molecular structures. For electronics applications, molecular structures have four major advantages:

− Size. The size scale of molecules is between 0.5 and 10 nm, a scale that permits functional nanostructures with accompanying advantages in cost, efficiency, and power dissipation.

− Assembly and recognition. One can exploit specific intermolecular interactions to form structures by nano-scale self-assembly. Molecular recognition can be used to modify electronic behavior, providing both switching and sensing capabilities on the single-molecule scale.

− Dynamical stereochemistry. Many molecules have multiple distinct stable geometric structures or isomers (an example is the rotaxane molecule, in which a rectangular slider has two stable binding sites along a linear track). Such geometric isomers can have distinct optical and electronic properties. Another example is the retinal molecule switches between two stable structures, a process that transduces light into a chemoelectrical pulse and allows vision.

− Synthetic tailorability. By choice of composition and geometry, one can extensively vary a molecule's transport, binding, optical, and structural properties. The tools of molecular synthesis are highly developed. [5]

Molecules have disadvantages, though, such as instability at high temperatures. But overall, the four advantages render molecules ideal for electronics applications, as Richard Feynman noted in his famous 1959 speech, *"There is Plenty of Room at the Bottom"*. ***In the present manuscript we explore the potential of polyoxometalates as suitable components for the fabrication of molecular devices, since they fulfill all the advantages of a molecule and exhibit high stability at elevated temperatures***.

1.1.3. Functional molecules for molecular electronics

To date, many molecules with wonderful electronic properties have been identified and more with desired properties are being synthesized in chemistry labs. In addition to electronic properties, many molecules posses rich optical, magnetic, thermoelectric, electromechanical and molecular recognition properties, which may lead to new devices that are not possible using conventional materials or approaches (Figure 4).

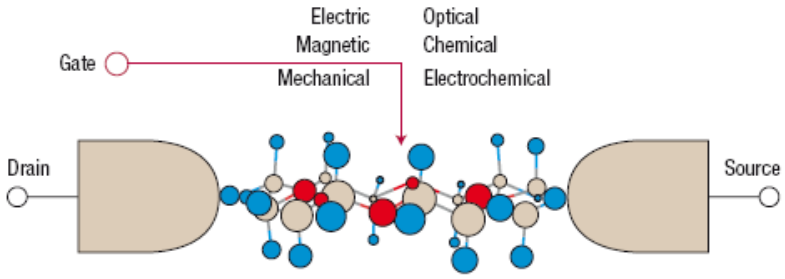

Figure 4. Illustration of a single molecule attached to two electrodes as a basic component in molecular electronics. Electron transport through the molecule may be controlled electrically, magnetically, optically, mechanically, chemically and electrochemically, leading to various potential device applications.[6]

Molecules designed and synthesized to be integrated into electronic circuits and to perform an electronic function are presented in this chapter. The ability of the chemist to correlate function with

[5] J. R. Heath, M. A. Ratner, Molecular Electronics, *Physics Today* **2003**, 43-49.
[6] N. J. Tao, Electron transport in molecular junctions, *Nat. Nanotechnol.* **2006**, *1*, 173-181.

structure, to design and to provide tailor-made functional molecules is central to molecular electronics. Several examples of such molecules will be illustrated as follows. They are classified in molecular rectifiers and switches comprising light-activated, redox active and hysteretic elements.

Molecule based rectifying systems

As already discussed in the introduction, rectification is of particular interest for the modular assembly of molecular devices. Since the principle of a molecular electronic device was proposed by Aviram and Ratner in 1974 (**Figure 3**), several molecular diodes have been realized.

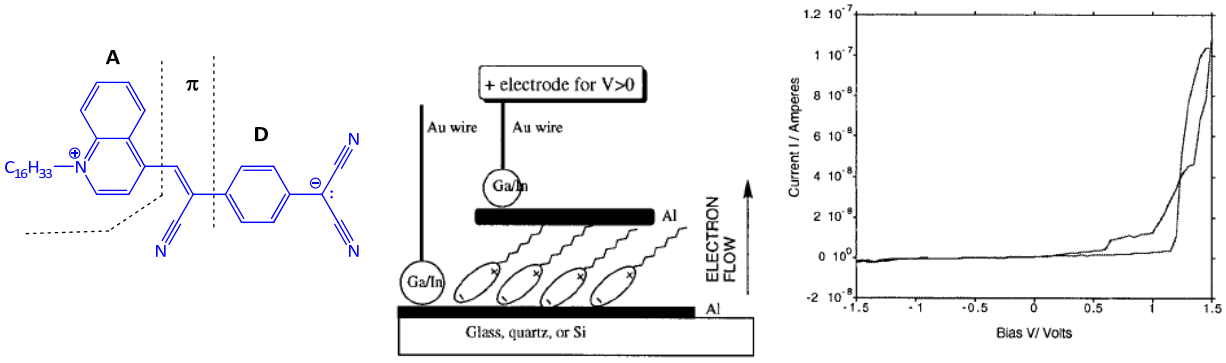

Figure 5. The zwitterionic molecule(a), sandwiched between Al electrodes (b), displaying rectification, plot of current *vs* applied voltage.[8]

To ensure correct functioning of the device, the donor and acceptor units need to be electronically separated from one another; if not, the two units interact and one single donor level is predicted. When the D-σ-A molecule is assembled between two metal electrodes M_1 and M_2, should form the rectifier $M_1|D\text{-}\sigma\text{-}A|M_2$, with easy electron transfer from M_2 to M_1 because of the "down-hill" tunnelling from excited state $D^+\text{-}\sigma\text{-}A^-$ to the ground state $D^0\text{-}\sigma\text{-}A^0$.[7] Metal-D-σ-A-metal molecular devices have been assembled with molecular films between two parallel planar electrodes, profiting from the self-assembly properties of amphiphilic molecules in Langmuir-Blodgett films at the water-air interface. Metzger investigated the zwitteronic molecule (**Figure 5**), carrying a positive charge on a

[7] R. M. Metzger, Electrical Rectification by a Molecule: The Advent of Unimolecular Electronic Device, *Acc. Chem. Res.* **1999**, *32*, 950-957.

quinolinium part a negative charge on a dicyanomethylene moiety in a Langmuir-Blodgett film between two aluminium electrodes. This is the first proven two-terminal molecular device.[8]

Light-activated molecular switches

Light turns out to be an attractive physical stimulus as it can be easily addressed in various media with short response times. Photochromic systems displaying light-induced reversible transformation (*e.g.* an isomerisation) accompanied by spectral changes in absorption are particularly appealing (**Figure 6**). The most prominent photoswitches are dithienylethene derivatives, which have been investigated in detail by Irie.[9] The most striking feature of the compounds is their resistance to fatigue. The coloration/decoloration cycle could be repeated more than 10^4 times without loss of their spectral features due to side reactions or decomposition. Their absorption properties, together with their stability features, make them ideal subunits for material displaying light-activated alteration of physical properties. In solution, the open-ring isomer can be irradiated with UV light to form the close-ring isomer. The open-state can be reached again by exposing the close-ring isomer to visible light (**Figure 6**).

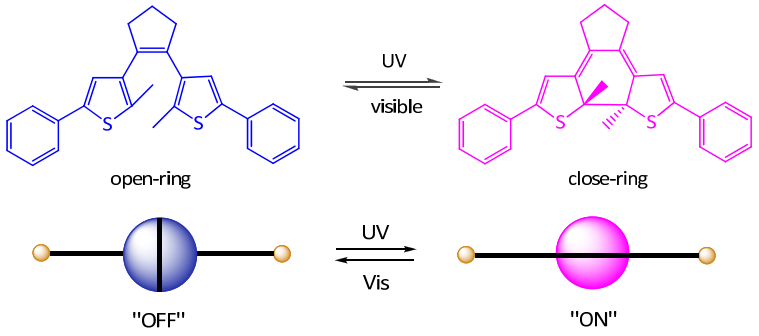

Figure 6. Principle of reversible photoswitching between the open ring (open) and the closed ring (close) isomers of a dithienylethene in solution.

The two isomers offer different absorption spectrum that of the closed form extends towards longer wavelengths up to the visible region, suggesting the delocalization of π-electrons over the entire structure in the close-ring isomer. In open-ring isomer, delocalization of π-electrons is restricted to each half of the molecule and electronic communication through the unsaturated bond of the middle ring is interrupted. Functionalized with suitable anchor groups and immobilized

[8] R. M. Metzger, B. Chen, U. Höpfner, M. V. Lakshmikantham, D. Vuillaume, T. Kawai, X. Wu, H. Tachibana, T. V. Hughes, H. Sakurai, J. W. Baldwin, C. Hosch, M. P. Cava, L. Brehmer, G. J. Ashwell, Unimolecular Electrical Rectification in Hexadecylquinolinium Tricyanoquinodimethanide, *J. Am. Chem. Soc.* **1997**, *119*, 10455-10466.
[9] M. Irie, Diarylethenes for Memories and Switches, *Chem. Rev.* **2000**, *100*, 1685-1716.

between two electrodes in a junction, the close-ring would then correspond to the "ON" state while the less conducting form open-ring would be referred as to the "OFF" state. Both, thermal stability and fatigue resistance are indispensable for applications to optoelectronic devices, such as memories and switches.

Electrochemically-activated molecular switches

In analogy with to the optically addressed dithienylethene derivatives, the conjugation through a redox chromophore may be addressed electrochemically. A model anthraquinone system bearing thioacetyl end groups for gold electrode binding is described by Hummelen and coworkers.[10] The anthraquinone-based molecular wire can be reversibly switched from cross conjugated (low conductance "OFF") to linear conjugated (high conductance "ON") (**Figure 7,** (a)). The molecular wire consists of the central electrochemical active moiety as a conjugation divider and is functionalized with terminal acetyl-protected sulfur anchor groups.

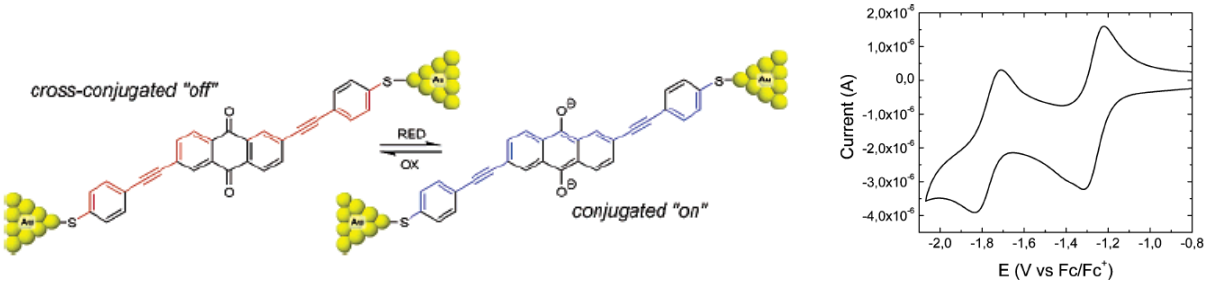

(a) (b)

Figure 7. Antraquinone based molecular wire proposed as potential electrochemically addressable molecular switch. The extent of expected π-delocalization in the oxidized (left) and reduced (right) form is represented in red and blue, respectively (a). Cyclic voltammogram of the anthraquinone derivative (b).[10]

Cyclic voltammetry investigations displayed a two-step reversible redox process with a semiquinone intermediate upon reduction to the hydroquinone dianion (**Figure 7**, (b)). Considerable differences are reported for the absorption spectra of the fully conjugated reduced state and the oxidized state already pointing at the differences of delocalization of the chromophore's π-system. Molecular orbital calculations have further supported the proposed switch, but transport

[10] E. H. van Dijk, D. J. T. Myles, M. H. van der Veen, J. C. Hummelen, Synthesis and Properties of an Antraquinone-Based Redox Switch for Molecular Electronics, *Org. Lett.* **2006**, *8*, 2333-2336.

investigation through an immobilized molecule in an electrochemically junction have, to the best of my knowledge, not been reported yet.

Voltage-activated hysteretic molecular switches

To achieve hysteretic switching in molecular devices, Stoddart and coworkers[11,12] combined electrochemical triggered systems with supramolecular rearrangement reactions. These most advanced and sophisticated hysteretic molecular switches are based on interlocked supermolecules like catenanes or rotaxanes. The goal here is to design a molecule that, at specific voltage, switches from a stable structure (isomer) to another, metastable isomer with a different conductivity and remains in the latter state until either another voltage pulse is applied or thermal fluctuation causes a return to the original isomer. The two states of the molecule correspond to the "ON" and "OFF" states of the switch, and the finite stability of the metastable state leads to a hysteretic current/voltage response that forms the basis of the switch.

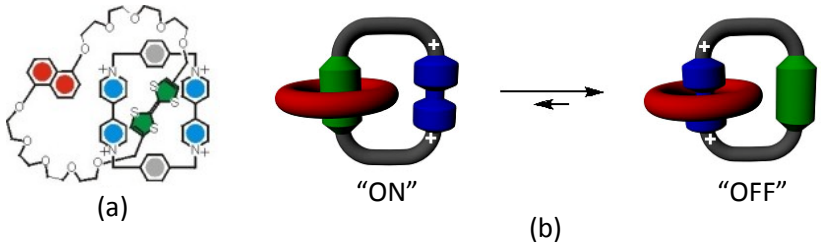

Figure 8. Structural formula of a representative bistable catenane molecule (a) and the operating principle (b).

The bistable rotaxanes (**Figure 9** (a)) behave as switches by incorporating two different recognition sites for the ring and the ring can be induced by applying modest voltages to move from one site to the other site and then reside there for many minutes. Consequently these molecules turn into on (high conductivity) state from off (low conductivity state). Operating principle is almost similar for catenanes (**Figure 8**). In catenane the circumrotation of macrocyclic components through each other cavities can be reversible controlled by oxidation/reduction of a metal ion introduced in the macrocyclic structure. The relative movements of the interlocked components of such catenanes and

[11] Y. Luo, C. P. Collier, J. O. Jeppesen, K. A. Nielsen, E. Delonno, G. Ho, J. Perkins, H.-R. Tseng, T. Yamamoto, J. F. Stoddart, J. R. Heath, Two-Dimensional Molecular Electronics Circuits, *Chem. Phys. Chem.* **2002**, *3*, 519-525.
[12] J. E. Green, J. W. Choi, A. Boukai, Y. Bunimovich, E. Johnston-Halperin, E. Delonno, Y. Luo, B. A. Sheriff, K. Xu, Y. S. Shin, H.-R. Tseng, J. F. Stoddart, J. R. Heath, A 160-kilobit molecular electronic memory patterned at 10^{11} bits per square centimeter, *Nature* **2007**, *445*, 414-417.

rotaxanes can be controlled from outside by means of chemical, electrochemically, and/or photochemical stimuli, if one introduce some chemically, electrochemically active groups which will represent the on and off state.

The switching mechanism is discussed briefly with the rotaxane molecule (**Figure 9**) as an example. It is based on oxidation of tetrathiafulvalene (TTF) unit (green) to the TTF^{+1} or TTF^{+2}, followed by Coulombic repulsion-driven motion of the tetracationic cyclophane ($CBQT^{4+}$) ring (blue) so that it encircles the dioxynaphthalene (DNP) unit (red). The TTF^{+} is reduced back to the TTF^{0} oxidation state to form the metastable state co-conformer, which is high-conductance. After reducing the TTF unit back to its initial state, the $CBQT^{4+}$ ring remains at the DNP unit for a while providing the required hysteretic features.

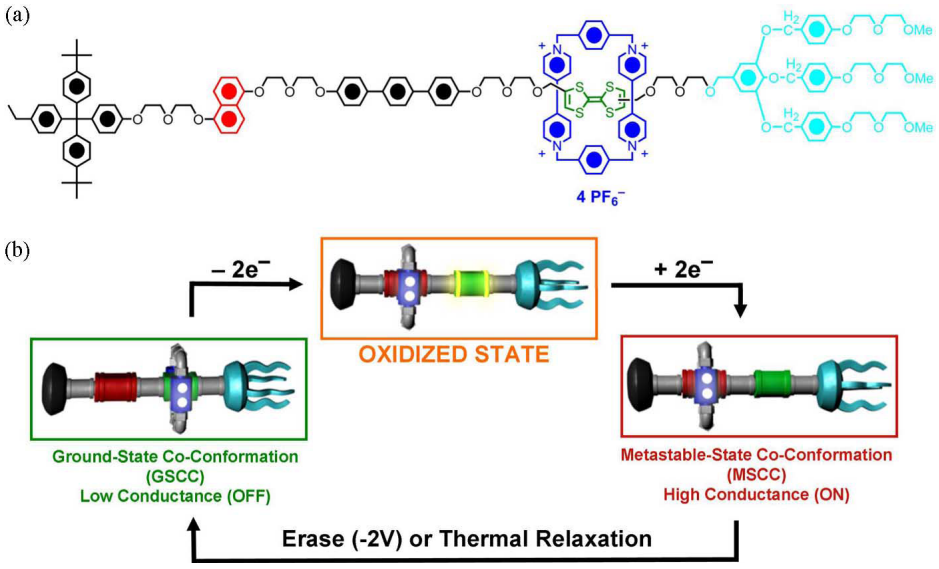

Figure 9. Rotaxane molecule. (a) Structural formula of a representative bistable rotaxane used in molecular electronic devices. (b) Switching mechanism of a rotaxane molecule. In the OFF (ground) state, the tetracationic $CBPQT^{4+}$ ring encircles the electron-rich TTF unit. Oxidation of the TTF unit produces its dication (TTF^{2+}), which results in Coulombic repulsion of the $CBPQT^{4+}$ ring to the neutral DNP site. Two electron reduction of the TTF^{2+} back to its neutral form results in a metastable ON state in which the $CBPQT^{4+}$ has not yet returned to the more favourable TTF station.[13, 14]

In this approach, the switching element is a metal/molecule/metal sandwich junction wherein molecules are placed at the cross section of two nanoscale metal wires. This sandwich molecular device has two stable, highly-retentive and reversible states: high-resistance state and low-resistance

state.[13, 14] An example of this memory was recently shown by the Hewlett Packard Research group. This example consisted of an 8 × 8 crossbar circuit,[15] where a monolayer of the [2]rotaxane molecules was sandwiched between bottom Ti (3 nm)/Pt (5 nm) and top Ti (11nm)/ Pt(5 nm) nanowires. The basic element in the circuit is the Pt/rotaxane/Ti junction formed at each cross point that acts as a reversible and nonvolatile switch, and 64 such switches are connected to form 8 × 8 crossbar circuit within a 1 μm^2 area (**Figure 10**).

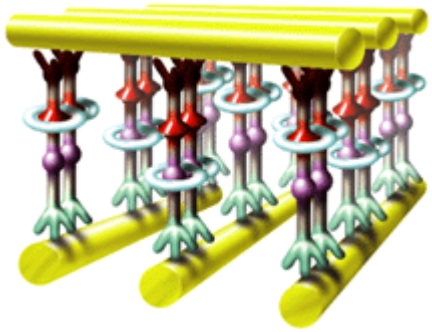

Figure 10. Crossbar architecture for a memory using molecular switches. An information bit is stored in the resistance of the rotaxane molecule at each intersection of a top and bottom bitline.[17]

This approach has the advantage of architectural simplicity and potential of high density via fabrication of highly dense nanowires. However, it has two major disadvantages including high rate of defective switching elements and the difficulty in controlling metal/molecule interface. However, as shown in their recent publications,[16, 17] the earlier results on electron transport phenomena in metal/molecule/metal junction may not be truly molecular but instead be dominated by electrode reactions with molecules.

---

[13] Y. Chen, D. A. A. Ohlberg, X. Li, D. R. Stewart, R. S. Williams, J. O. Jeppesen, K. A. Nielsen, J. F. Stoddart, D. L. Olynick, E. Anderson, Nanoscale molecular-switch devices fabricated by imprint lithography, *Appl. Phys. Lett.* **2003**, *82*, 1610-1612.

[14] C. P. Collier, E. W. Wong, M. Belohradsky, F. M. Raymo, J. F. Stoddart, P. J. Kuekes, R. S. Williams, J. R. Heath, Ellectronically Configurable Molecular-Based Logic Gates, *Science* **1999**, *285*, 391-394.

[15] Y. Chen, G.-Y. Jung, D. A. A. Ohlberg, X. Li, D. R. Stewart, J. O. Jeppesen, K. A. Nielsen, J. F. Stoddart, R. S. Williams, Nanoscale molecular-switch crossbar circuits, *Nanotechnology* **2003**, *14*, 462-468.

[16] D. R. Stewart, D. A. A. Ohlberg, P. A. Beck, Y. Chen, R. S. Williams, J. O. Jeppesen, K. A. Nielsen, J. F. Stoddart, Molecule-Independent Electrical Switching in Pt/Organic Monolayer/Ti devices, *Nano Lett.* **2004**, *4*, 133-136.

[17] J. R. Heath, J. F. Stoddart, R. S. Williams, More on Molecular Electronics, *Science* **2004**, *303*, 1136-1137.

1.2. MOLECULAR MEMORIES

The workhorse of today's electronic computer is the metal-oxide-semiconductor transistor, or MOSFET; the basic structure of a silicon MOSFET is shown in **Figure 11**. The transistor, which is based on the transport of electrons in a solid, comprises three electrodes (anode, cathod and gate), two of which serve as an electron reservoir: the source, which acts as the emitter filament of an electron tube, the drain, which acts as the collector plate, with the gate as "controller".

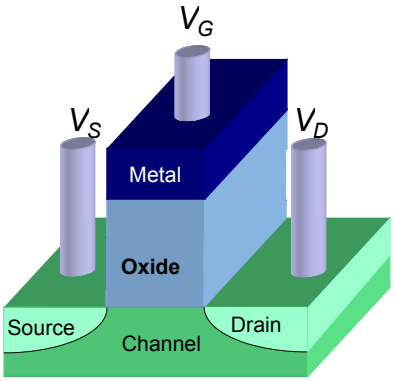

Figure 11. Schematic diagram of a MOSFET.

In this context, 'More Moore' is not sufficient anymore; 'More than Moore' is required to meet such challenges, to enable implementation of new functionalities while making the resulting subsystems smaller, lighter, more cost effective and more power efficient. The 'More than Moore' domain deals with ***hybrid co- integration of conventional Si CMOS*** and many other technologies, such as mechanics, fluidics, optics, etc. Such hybrid components will integrate nano-objects or molecules in "classical" CMOS devices.

1.2.1. Non-volatile flash memory

Flash memory is a type of non-volatile memory with many applications like: USB keys, MP3 players, cell phones etc. It was discovered in 1984 by Fujio Masuoka at Toshiba. ***Since flash memory is non-volatile, no power is needed to maintain the information stored in the chip***. This type of memory device can be electrically erased and reprogrammed. A typical example of flash memory device is the MOSFET.

The market for non-volatile memory devices is growing rapidly. Today, the vast majority of non-volatile memory devices are based on the floating gate device which is facing serious scaling limitations. An alternative path is to replace the floating gate by a charge trapping material. The integration of a layer of polyoxometalates into such hybrid components is the main objective of the present thesis.

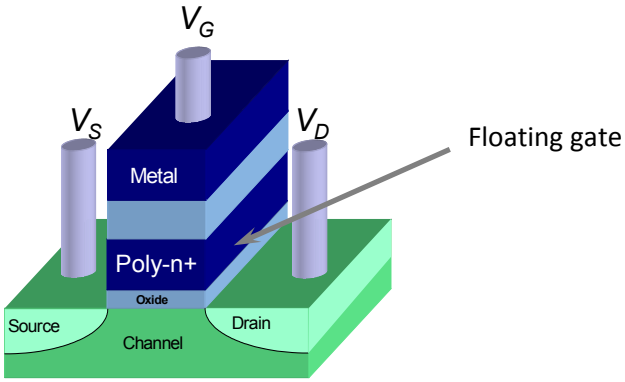

Figure 12. Cross section of Flash Memory cell.

A flash memory device contains a MOSFET transistor plus a floating gate situated between the gate and the channel (**Figure 12**). The floating gate is surrounded by insulators and traps the electrons inside it (~50 years). Flash memory costs far less and therefore has become the dominant technology wherever a significant amount of non-volatile, solid state storage is needed. In addition, flash memory offers fast read access times and better kinetic shock resistance than hard disks. These characteristics explain the popularity of flash memory in portable devices. Another feature of flash memory is that when packaged in a "memory card," it is enormously durable, being able to withstand intense pressure, extremes of temperature, and even immersion in water.

The extensive use of this kind of devices requires miniaturization. A very important issue in the scaling process is linked to the stored charges leakage through the oxide tunnel as the thickness of the latest decreases. Among the various approaches towards building new smaller and high-performance devices, the hybrid silicon/molecular approach, the use of redox active molecules instead of the silicon floating gate seems to be a promising solution.

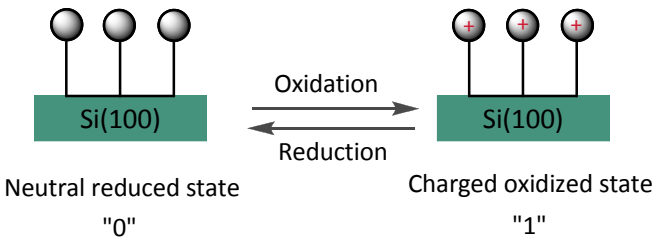

Figure 13. The operating principle of a memory device based on redox molecules.

So, the redox-active molecules are incorporated into silicon structures to generate a new class of electronic devices. These redox-active molecules, which can be design to self-assemble on surfaces as monolayers, exhibit charge storage states at distinct voltages. Application of an oxidizing voltage causes the redox-active monolayer to lose electrons, resulting in a positively charged monolayer. When a reducing voltage is applied, electrons are transferred to the molecules to the neutral state (**Figure 13**). The two states "0" and "1" are defined by the presence or absence of electrons into the floating gate.

1.2.1.1. Hybrid CMOS/Molecular Memory

Hybrid complementary metal oxide semiconductor (CMOS)/molecular memory devices are based on a dynamic random-access memory (DRAM) architecture, are fast, have high density, and exhibit low power consumption. These devices use a well-characterized charge storage mechanism to store information based on the intrinsic properties of molecules attached to a CMOS platform. The molecules are designed in a rational way to have known electrical properties and can be incorporated into CMOS devices with only minor modification of existing fabrication methods. Each memory element contains a monolayer of molecules (typically 100,000-1,000,000) to store charge; this process yields a structure that has many times the charge density of a typical DRAM capacitor, obviating the necessity for a trench or stacked capacitor geometry. The magnitude of voltage required to remove each electron is quantized (typically a few hundred millivolts per state), making it much easier to put molecules in a known state and to detect that state with low-power operation. Existing devices have charge retention times that are >1000 times that of semiconductors, and nonvolatile strategies based on simple modifications of existing systems are possible. All of these

devices are ultimately scalable to molecular dimensions and will enable the production of memory products as small as state-of-the-art lithography will allow.[18]

Storage of multiple bits on a single memory cell multiplies the density in the same space and has received increasingly more attention from the semiconductor industry. These devices rely on hot electron injection from the channel into the floating gate through a tunneling oxide layer, and different memory states are represented by different amount of charge stored. Further decreasing the cell size or increasing the number of levels for higher density, however, is extremely difficult, as the complicated device structure and the topdown fabrication approach inevitably leads to significant device variation and a blurring of the multiple levels. Molecular electronics may offer a solution to this scaling limit by taking advantage of the bottom-up self-assembling process. Discrete multilevels naturally exist in an ensemble of redox-active molecules, or even one molecule containing multiple redox centers.

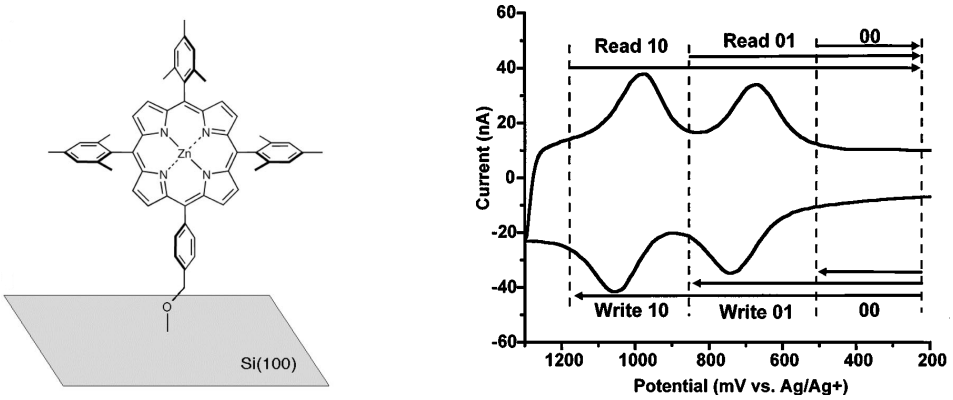

(a) (b)

Figure 14. Structure of the Si-tethered porphyrin molecule (a). The operating principle of a porphyrin based molecular memory device, information is stored by removing electrons from the porphyrins units (b).[19, 20]

Several universities and a number of companies (Hewlett Packard, ZettaCore) have announced work on molecular memories. ZettaCore molecular memory (**Figure 14**)[19, 20] is based on the properties of specially-designed molecules. These molecules are used to store information by adding or removing

[18] W. G. Kuhr, A. R. Gallo, R. W. Manning, C. W. Rhodine, Molecular Memories Based on a CMOS Platform, *MRS Bulletin* **2004**, 838-842.
[19] Q. Li, S. Surthi, G. Mathur, S. Gowda, Q. Zhao, T. A. Sorenson, R. C. Tenent, K. Muthukumaran, J. S. Lindsey, V. Misra, Multi-bit storage properties of porphyrin monolayers on SiO_2, *Appl. Phys. Lett*. **2004**, *85*, 1829-1831.
[20] Q. Li, G. Mathur, S. Gowda, S. Surthi, Q. Zhao, L. Yu, J. S. Lindsey, D. F. Bocian, V. Misra, Multibit Memory Using Self-Assembly of Mixed Ferrocene/Porphyrin Monolayers on Silicon, *Adv. Mater.* **2004**, *16*, 133-137.

electrons and then detecting the charge state of the molecule. The molecules, called multi-porphyrin nanostructures, can be oxidized and reduced (electrons removed or replaced) in a way that is stable, reproducible, and reversible. [21, 22, 23] In this way, molecules can be used as reliable memory locations for electronic devices. In many ways, each molecule acts like an individual capacitor device, similar to a conventional capacitor, but storing only a few electrons of charge that are accessible only at specific, quantized voltage levels. The key difference between ZettaCore memory and conventional memory is that as the size of a memory element becomes smaller using conventional electronic manufacturing, the properties of those semiconductor or polymer materials change in undesirable ways. In the ZettaCore approach the properties of these molecular capacitors remain the same. This allows scaling to very small size elements.

In 2004, two teams from University of Southern California and NASA,[24] have reported a multilevel molecular memory device for nonvolatile data storage application, which can store up to three bits (eight levels) per cell, in contrast to the standard one-bit-per-cell (two levels) technology. A self-assembled monolayer of Fe^{2+}-terpyridine molecules was formed on a 10 nm In_2O_3 nanowire. Charges were precisely placed at up to eight discrete levels in redox active molecules self-assembled on single-crystal semiconducting nanowire field-effect transistors. Gate voltage pulses and current sensing were used for writing and reading operations, respectively. Charge storage stability was tested up to retention of 600 h and on/off ratios exceeding 10^4. The data storage can be carried out by altering the population of the reduced/oxidized molecules, while the readout can be implemented by measuring the conduction of the nanowire. A two-level memory has been demonstrated before with excellent performance.[25, 26]

---

[21] K. M. Roth, N. Dontha, R. B. Dabke, D. T. Gryko, C. Clausen, J. S. Lindsey, D. F. Bocian, W. G. Kuhr, Molecular approach toward information storage based on the redox properties of porphyrins in self-assembled monolayers, *J. Vac. Sci. Technol. B* **2000**, *18*, 2359-2364.

[22] Z. Liu, A. A. Yasseri, J. S. Lindsey, D. F. Bocian, Molecular Memories That Survive Silicon Device Processing and Real-World Operation, *Science* **2003**, *302*, 1543-1545.

[23] Q. Li, G. Mathur, M. Homsi, S. Surthi, V. Misra, V. Malinovskii, K.-H. Schweikart, L. Yu, J. S. Lindsey, Z. Liu, R. B Dabke, A. Yasseri, D. F. Bocian, W. G. Kuhr, Capacitance and conductance characterization of ferrocene-containing self-assembled monolayers on silicon surfaces for memory applications, *Appl. Phys. Lett.* **2002**, *81*, 1494-1496.

[24] C. Li, W. Fan, B. Lei, D. Zhang, S. Han, T. Tang, X. Liu, Z. Liu, S. Asano, M. Meyyappan, J. Han, C. Zhou, Multilevel memory based on molecular devices, *Appl. Phys. Lett.* **2004**, *84*, 1949-1951.

[25] X. Duan, Y. Huang, C. M. Lieber, Nonvolatile Memory and Programmable Logic from Molecule-Gated Nanowires, *Nano Lett.* **2002**, *2*, 487-490.[2]

[26] C. Li, B. Lei, W. Fan, D. Zhang, M. Meyyappan, C. Zhou, Molecular Memory Based on Nanowire-Molecular Wire Heterostructures, *J. Nanosci. Nanotechnol*. **2007**, *7*, 138-150.

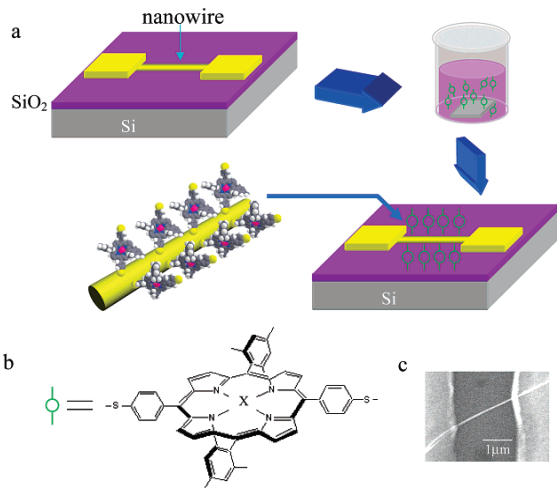

Figure 15. (a) Fabrication process of the memory device. An as-fabricated In_2O_3 nanowire was first immersed in a solution of the porphyrin molecules, and self-assembly was employed to coat the In_2O_3 nanowire with porphyrin molecules. (b) Molecule structure of the porphyrins used in this process. (c) SEM image of an In_2O_3 nanowire device.[27]

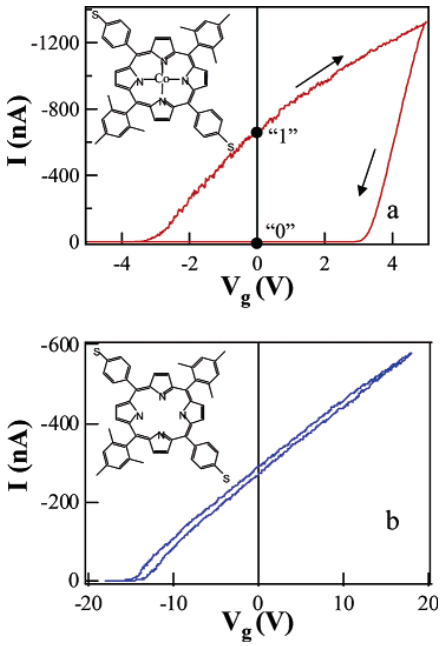

Figure 16. *I*-V_g characteristics of In_2O_3 nanowire device decorated with Co-porphyrins (a) and non-metallated porphyrins (b), respectively. Insets: structures of the corresponding porphyrins.[27]

Figure 15 and **Figure 16** describes in detail memory studies that have been carried out based on In_2O_3 nanowires coated with self-assembled monolayers of porphyrins. Devices with redox-active Co-metallated porphyrins coatings exhibited proeminent memory effects. These devices exhibited reliable operation with significant on/off ratios and were electronically programmable and erasable. While devices with Co-porphyrin coatings showed efficient memory operation, pronounced hysteresis in the *I*-V_g sweeps, the analogous non-metallated porphyrin coated nanowire devices exhibited no memory effects (**Figure 16**). A largely metal-centered oxidation (*e.g.* $Co^{2+/3+}$) appears to be important for achieving a memory effect in these devices.

[27] C. Li, J. Ly, B. Lei, W. Fan, D. Zhang, J. Han, M. Meyyappan, M. Thompson, C. Zhou, Data Storage Studies on Nanowire Transistors with Self-Assembled Porphyrin Molecules, *J. Phys. Chem. B* **2004**, *108*, 9646-9649.

1.2.1.2. Approaches Towards Multibit Memory in One Cell

The availability of charged states at distinct voltages is highly advantageous for memory applications. One strategy to increase memory density entails a multibit approach wherein the charge-storage element contains molecules with multiple redox states. There are several ways to obtain multiple redox states:

Synthesis of molecule with multiple redox states. Such complex molecules include ferrocene-porphyrin conjugate bearing a single tether,[28, 29] strongly/weakly bonded porphyrins,[30, 31] triple deckers of porphyrin,[32] and dyad of triple deckers.[33] This approach is limited only by the requirements for chemical synthesis of the covalently linked multi-redox molecule.

Mixed monolayers. An alternative and perhaps simpler strategy for achieving multibit functionality is afforded by mixing in one monolayer different redox-active molecules whose potentials are well-separated. It has been demonstrated this method using mixed SAMs of Fc-BzOH and Por-BzOH on the Si surface to achieve a four-state (two-bit) memory element. The four states include the neutral state and three distinct cationic states obtained upon oxidation of Fc-BzOH (monopositive) and Por-BzOH (monopositive, dipositive) molecules.

---

[28] R. S. Loewe, A. Ambroise, K. Muthukumaran, K. Padmaja, A. B. Lysenko, G. Mathur, Q. Li, D. F. Bocian, V. Misra, J. S. Lindsey, Porphyrins Bearing Mono or Trpodal Benzylphosphonic Acid Tethers for Attachment to Oxide Surfaces, *J. Org. Chem.* **2004**, *69*, 1453-1460.

[29] D. T. Gryko, C. Clausen, K. M. Roth, N. Dontha, D. F. Bocian, W. G. Kuhr, J. S. Lindsey, Synthesis of "Porphyrin-Linker-Thiol" Molecules with Diverse Linkers for Studies of Molecular-Based Information Storage, *J. Org. Chem.* **2000**, *65*, 7345-7355.

[30] C. Clausen, D. T. Gryko, A. A. Yasseri, J. R. Diers, D. F. Bocian, W. G. Kuhr, J. S. Lindsey, Investigation of Tightly Coupled Porphyrin Arrays Comprised of Identical Monomers for Multibit Information Storage, *J. Org. Chem.* **2000**, *65*, 7371-7378.

[31] C. Clausen, D. T. Gryko, R. B. Dabke, N. Dontha, D. F. Bocian, W. G. Kuhr, J. S. Lindsey, Synthesis of Thiol-Derivatized Porphyrin Dimers and Trimers for Studies of Architectural Effects on Multibit Information Storage, *J. Org. Chem.* **2000**, *65*, 7363-7370.

[32] A. Balakumar, A. B. Lysenko, C. Carcel, V. L. Malinovskii, D. T. Gryko, K.-H. Schweikart, R. S. Loewe, A. A. Yasseri, Z. Liu, D. F. Bocian, J. S. Lindsey, Diverse Redox-Active Molecules Bearing O-, S-, or Se-Terminated Tethers for Attachment to Silicon in Studies of Molecular Information Storage, *J. Org. Chem.* **2004**, *69*, 1435-1443.

[33] K.-H. Schweikart, V. L. Malinovskii, J. R. Diers, A. A. Yasseri, D. F. Bocian, W. G. Kuhr, J. S. Lindsey, Design, synthesis, and characterization of prototypical multistate counters in three distinct architectures, *J. Mater. Chem.* **2002**, *12*, 808-828.

Substrate engineering. In this approach, we attached Fc-BzOH on a Si substrate with arrays of *n*-type and *p*-type area. Since the redox potentials of molecules on n and p substrate are different and well-separated, it is achievable to obtain multiple redox states.[34, 35]

In our general approach, a monolayer of polyoxometalates covalently attached to a silicon substrate should have important significance towards multibit memory applications, since they exhibit multible reversible stable redox states.

1.3. POLYOXOMETALATES

1.3.1. Definition

Polyoxometalates, POMs, (isopoly- and heteropolyanions) ***are a class of inorganic, anionic, nanometre size metal-oxide cluster compounds with great variety in charge and framework structure***. They may be represented by the general formulae:

$[M_mO_y]^{p-}$ Isopolyanions

$[X_xM_mO_y]^{q-}$ Heteropolyanions

where M is usually Mo^{6+} or W^{6+}, less frequently V^{5+}, Nb^{5+} or Ta^{5+} or a mixture of these elements. M is called the addenda atom and X is a main group or transition-metal heteroatom. The chemistry of molybdenum (VI), tungsten (VI), and vanadium (V) in aqueous solution is dominated by the formation of polyoxoanions, as exemplified by **Equations 1** and **2**.[36]

$$8H^+ + 7[WO_4]^{2-} \rightarrow [W_7O_{24}]^{6-} + 4H_2O \qquad \textbf{Equation 1}$$

$$23H^+ + [HPO_4]^{2-} + 12[MoO_4]^{2-} \rightarrow [PMo_{12}O_{40}]^{3-} + 12H_2O \qquad \textbf{Equation 2}$$

---

[34] S. Gowda, G. Mathur, Q. Li, S. Surthi, Q. Zhao, J. S. Lindsey, K. Mobley, D. F. Bocian, V. Misra, Hybrid Silicon/Molecular Memories: Co-Engineering for Novel Functionality, *IEEE Int. Electron Devices Meeting* **2003**, 22.1.1.

[35] S. Gowda, G. Mathur, V. Misra, Valence band tunneling model for charge transfer of redox-active molecules attached to n- and p-silicon substrates, *Appl. Phys. Lett.* **2007**, *90*, 142113.

[36] M. T. Pope, A. Müller, Polyoxometalate Chemistry: An Old Field with New Dimensions in Several Disciplines, *Angew. Chem. Int. Ed. Engl.* **1991**, *30*, 34-48.

Historically, Berzelius is credited for reporting the first POM in 1826,[37] namely the ammonium salt of $[PMo_{12}O_{40}]^{3-}$. This heteropoly salt was later utilized by Svanberg and Struve[38] for the gravimetric and volumetric determination of phosphorus. However it would be almost another 100 years before its structure was determined by Keggin.[39] It is important to remember that there are hundreds of structures pertaining to POMs both isopoly and heteropoly; three of the most common structures are shown in **Figure 17**.

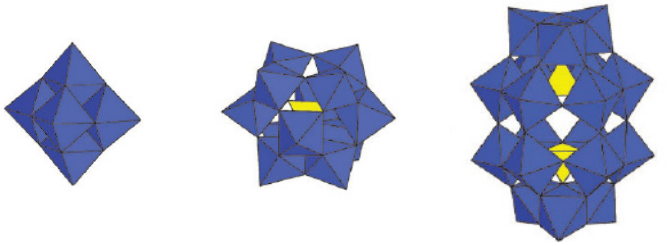

Figure 17. Polyhedral representation of the most common polyoxometalates structures.

The Keggin structure is perhaps the most commonly adopted structure and has a diameter of ~ 1.2 nm. It is composed of 12 vertex- and edge-sharing MO_6 octahedra surrounding a central XO_4 tetrahedron; X can be a wide range of elements typically from group 4 or 5 (e.g. P^{5+}, As^{5+}, Si^{4+}, Ge^{4+}). Most of POMs with a general ratio of 1:12 are labeled as 'Keggin' and those with a ratio of 2:18 are labeled 'Dawson' types.

Keggin POMs overall exhibit virtual tetrahedral (T_d) symmetry, with a central XO_4 tetrahedral unit surrounded by 12 MO_6 octahedral units which are arranged into four groups of three edge sharing M_3O_{13} units. Each of the four M_3O_{13} groups is linked to the central XO_4 unit and to each other by the corresponding corners. It was later found by Baker and Figgis that when groups of one, two, three or four of the M_3O_{13} units are rotated by $\pi/3$, different isomers of the Keggin POM can be related.

In addition to the isomeric forms of the complete (or 'plenary') Keggin structure, there are also 'lacunary' derivatives in which one, two or three oxo-metal vertices have been removed by treating the complete Keggin ion with a suitable base such as bicarbonate. An example illustrating the

[37] J. J. Berzelius, *Pogg. Ann.* **1826**, *61*, 380.
[38] K. Svanberg, H. Struve, *J. Prakt. Chem.* **1848**, *44*, 257-291.
[39] J. Keggin, *Nature* **1933**, *131*, 908.

formation of the lacunary $[XM_{11}O_{39}]^{n-}$ and $[XM_9O_{34}]^{n-}$ systems is shown in **Figure 18**. It has also been shown that certain lacunary species can be synthesized via stoichiometric and pH control.

POMs are structurally and compositionally diverse and they also typically exhibit rich electrochemistry. This can be attributed to their fully oxidized framework. It is common for POMs to display multiple and reversible one- or two-electron reductions often leading to mixed valence species referred to as 'heteropoly blues' due to their characteristic intense blue coloring. Perhaps this was why initial efforts of POM research focused greatly on their behavior as 'heteropoly acids' and more recently as catalysts. In their fully oxidized state POMs tend to be thermally, oxidatively and hydrolytically stable. However, cluster decomposition can occur even at mildly basic conditions. Physically, POMs can range anywhere between 6-25 Å in diameter with ionic weights upwards of 10,000 amu. Industrially, POMs have been utilized mainly as acid-, oxygenation- and photo-catalysts. In the early 1970's, Japan developed and commercialized the heteropoly salt, $H_4[SiW_{12}O_{40}]$ for the homogeneous catalytic hydration of propene to 2-propanol.

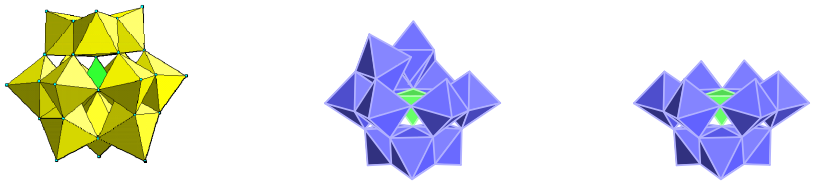

Keggin Structure $[XM_{12}O_{40}]^{n-}$ | Monolacunary Keggin $[XM_{11}O_{39}]^{n-}$ | Trilacunary Keggin $[XM_9O_{34}]^{n-}$

Figure 18. Examples of lacunary polyoxometalates derived from Keggin structure.

The removal of an MO_6 unit from the Keggin exposes a 'cavity' within the lacunary species. This cavity presents five oxygen donors in a roughly square pyramidal arrangement and therefore is ideally suited for incorporating an added $[ML]^{n+}$ unit in a pseudo-octahedral geometry. Exploitations of such vacant sites have afforded an enormous range of complexes (M = e.g., Co(II), Co(III), Zn(II), Ni(II), etc.; L = H_2O, halide, NH_3, pyridine, etc.). However, it should be noted that not all lacunary Keggins are hydrolytically or thermodynamically stable and can often revert back to their parent Keggin. Similar lacunary species are also known with the Dawson series of POMs.

1.3.2. FUNCTIONALIZED POLYOXOMETALATES

There continues to be extensive interest in hybrids containing both POMs and organometallic components. The motivation lies not only in chemists' steady desire to bring different structural units together but also in the prospect of generating new functional and multifunctional materials, although the overwhelming interest in organometallic/POM hybrids has so far been focused to their catalytic activity. A significant number of organometallic/POM hybrids have already been reported, [40] most of which anchor the organometallic component by either the surface oxygen atoms of POM clusters or active metal centers incorporated within the POM cluster. A commonly adopted synthetic approach relies on a self-assembly process in which attachment of the organometallic component and assembly of the POM cluster occur simultaneously. However, all the Keggin type functionalized POMs reported to date have been obtained from lacunary POMs. Although various other preparation methods have been reported, one which allows rational design and predetermination of structure and properties remains elusive.

In a restrictive sense, derivatized polyoxometalates might be defined as species where some oxo ligands have been replaced by other (inorganic or organic) ligands. One of the most challenging objectives is that of obtaining derivatives with predetermined structures and properties. Although systematic studies in non-aqueous solutions have allowed the synthesis of a number of covalent derivatives, hydrolytically stable derivatives are clearly needed in order to enhance the potential utility of polyoxometalates in catalysis, chemotherapy, and material science. Increasing attention is currently being paid to polyoxometalates for the synthesis of molecular materials with unusual associations of properties, *e.g.*, electrical and magnetic properties. With respect to the field of molecular materials, derivatization of polyoxometalates might provide efficient pathways to favor electronic coupling within charge-transfer materials based on organic donors and might allowed the incorporation of polyoxometalates in conducting polymers. [41]

The derivatization of POM frameworks by replacing/derivatizing the oxo ligands is an important aim since it will allow a much greater degree of control, potentially allowing the simultaneous exploitation of self assembly of the POM fragments, and step wise synthesis to introduce pendant functionalities.

---

[40] P. Gouzerh, A. Proust, Main-Group Element, Organic, and Organometallic Derivatives of Polyoxometalates, *Chem. Rev.* **1998**, *98*, 77-111.

[41] A. Proust, R. Thouvenot, P. Gouzerh, Functionalization of polyoxometalates: towards advances applications in catalysis and materials science, *Chem. Commun.* **2008**, 1837-1852.

1.3.2.1. Trilacunary Keggin Functionalized Polyoxometalates

The reactivity of organosilanes with multivacant heteropolytungstates was first investigated by the group of Proust *et al*. Under phase-transfer conditions, the trivacant anion α-A-$[XW_9O_{34}]^{n-}$ reacts with trichlorosilanes, $RSiCl_3$, to give the "capped-structures" derivatives α-A-$[XW_9O_{34}(RSiO)_3(RSi)]^{n-}$ (X = Si, P; R = H, Me, C_2H_3, Et, *n*Bu; *n* = 3, 4) [42, 43] with a variety of silanes. Whereas n-$BuSiCl_3$ reacts with α-A-$[PW_9O_{34}]^{9-}$ to give the "capped-structure" anion α-A-$[PW_9O_{34}(n\text{BuSiO})_3(n\text{BuSi})]^{3-}$, the corresponding reaction with *t*$BuSiCl_3$ yields the "open-structure" anion α-A-$[PW_9O_{34}(t\text{BuSiOH})_3]^{3-}$,[44, 45] presumably because of steric crowding (**Figure 19**). Its analog with As(III) as heteroatom, α-B-$[AsW_9O_{33}(t\text{BuSiOH})_3]^{3-}$, was obtained also by the same group.

Under similar conditions, reactions of the α-A-$[XW_9O_{34}]^{n-}$ with dichlorosilanes R_2SiCl_2 yields ions of the type α-A-$[XW_9O_{34}(R_2Si)_3]^{n-}$ where X = Si, P, R = Me, Ph and *n* = 3, 4.[46]

The reactivity of polyvacant polytungstates with organostannanes was systematically investigated by Pope and co-workers. Because of the preference of tin for six-coordination, the structures of organotin derivatives are different from those of organosilyl hybrids, for example in $[\{\beta\text{-A-}(PW_9O_{34})\}_2(PhSnOH)_3]^{12-}$ (**Figure 20**) and $[\{\alpha\text{-A-}(SiW_9O_{34})\}_2(BuSnOH)_3]^{14-}$ three organostannyl groups are embedded in between two 9-tungsto anions. [47, 48]

---

[42] N. Ammari, G. Hervé, R. Thouvenot, A new class of organosilyl derivatives of polyoxoanions: attachment of alkyl- and arylsilyl groups on trivacant tungstosilicate, *New. J. Chem.* **1991**, *15*, 607-608.

[43] J. Niu, M. Li, J. Wang, Organosilyl derivatives of trivacant tungstophosphate of general formula α-A-$[PW_9O_{34}(RSiO)_3(RSi)]^{3-}$. Synthesis and structure determination by X-ray crystallography, *J. Organomet. Chem.* **2003**, *675*, 84-90.

[44] D. Agustin, C. Coelho, A. Mazeaud, P. Herson, A. Proust, R. Thouvenot, Organic-Inorganic Hybrids based on Polyoxometalates. Part 8. Synthesis and Spectroscopic Characterization of the Heterosilylated Anions $[PW_9O_{34}(^t\text{BuSiO})_3(SiR)]^{3-}$ (R = $-CH_3$, $-CH{=}CH_2$, $-CH_2{-}CH{=}CH_2$, $-(CH_2)_4{-}CH{=}CH_2$) – X-ray Crystal Structure of $[^n\text{Bu}_4\text{N}]_3[PW_9O_{34}(^t\text{BuSiO})_3(SiCH_2{-}CH{=}CH_2)]$, *Z. Anorg. Allg. Chem.* **2004**, *630*, 2049-2053.

[45] A. Mazeaud, N. Ammari, F. Robert, R. Thouvenot, Coordination Chemistry of Polyoxometalates: Rational Synthesis of the Mixed Organosilyl Derivatives of Trivacant Polyoxotungstates α-A-$[PW_9O_{34}(t\text{BuSiO})_3(SiR)]^{3-}$ and α-A-$[AsW_9O_{33}(t\text{BuSiO})_3(HSi)]^{3-}$, *Angew. Chem. Int. Ed. Engl.* **1996**, *35*, 1961-1964.

[46] A. Mazeud, PhD Thesis, Université Pierre et Marie Curie, **1997**.

[47] F. Xin, M. T. Pope, Polyoxometalate Derivatives with Multiple Organic Groups. 1. Synthesis and Structures of tris(organotin) β-Keggin and α-Dawson Tungstophosphates, *Organometallics* **1994**, *13*, 4881-4886.

[48] F. Xin, M. T. Pope, G. J. Long, U. Russo, Polyoxometalate Derivatives with Multiple Organic Groups. 2. Synthesis and Structures of Tris(organotin) α, β-Keggin Tungstosilicates, *Inorg Chem.* **1996**, *35*, 1207-1213.

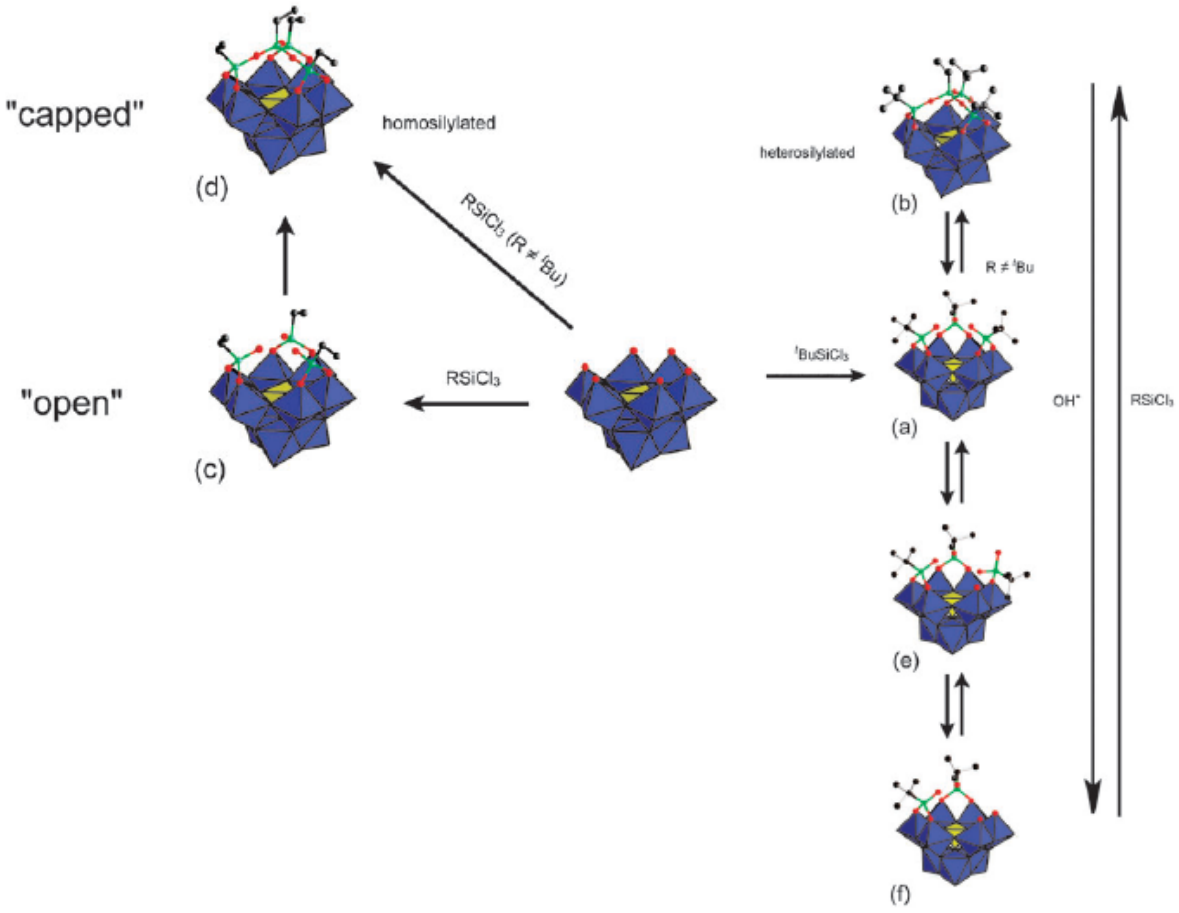

Figure 19. Organosilyl derivatives obtained from α-A-$[PW_9O_{34}]^{7-}$: (a) α-A-$[PW_9O_{34}(t\text{BuSiOH})_3]^{3-}$, (b) α-A-$[PW_9O_{34}(t\text{BuSiO})_3(\text{SiEt})]^{3-}$, (c) α-A-$[PW_9O_{34}(\text{EtSiOH})_3]^{3-}$, (d) α-A-$[PW_9O_{34}(\text{EtSiO})_3(\text{SiEt})]^{3-}$, (e) α-A-$[PW_9O_{34}(t\text{BuSiOH})_2\{t\text{BuSi(OH)}_2\}]^{4-}$, (f) α-A-$[PW_9O_{34}(t\text{BuSiOH})]^{5-}$. Color code: MoO_6 octahedra, blue; PO_4 tetrahedron, yellow; organic Si, green; C, black. [49]

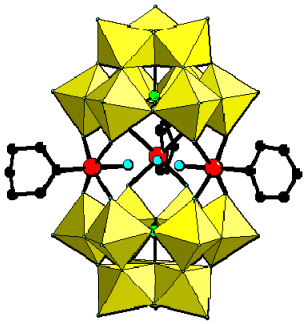

Figure 20. Polyhedral representation of the $[\{\beta\text{-A-}(PW_9O_{34})\}_2(PhSnOH)_3]^{12-}$ anion. Color code: WO_6 octahedra, yellow; PO_4, green; Sn, red; organic part, black; OH groups, blue.[47]

[49] A. Proust, R. Thouvenot, P. Gouzerh, Functionalization of polyoxometalates: towards advanced applications in catalysis and materials science, *Chem. Commun.* **2008**, 1837-1852.

Reaction of the trichlorogermanium precursors with the lacunary polyoxotungstate anions proceeds smoothly in aqueous or aqueous/organic solvents to give the desired derivatives in good yield. Recently, Zhang has reported the synthesis of trisubstituted heteropolytungstates containing $[RGe]^{3+}$ group, starting from trichlorogermanium precursors and lacunary polyoxometalates $[PW_9O_{34}]^{9-}$ and $[SbW_9O_{33}]^{9-}$ which lead to the formation of derivatives of the type $[Me_4N]_4H_5[(RGe)_3(XW_9O_{34-n})_2]$ (R = $HOOCCH_2CH_2$, $HOOCCH_2(m\text{-}NO_2C_6H_4)CH$, X = P, n = 0; X = Sb, n = 1).[50]

1.3.2.2. Monolacunary Keggin Functionalized Polyoxometalates

Organosilyl derivatives of polyoxometalates have been first reported by Knoth who obtained the anions $\alpha\text{-}[SiW_{11}O_{40}\{O(SiR)_2\}]^{4-}$ (Figure 21) by reacting $RSiCl_3$ (R = C_2H_5, $CH{=}CH_2$, $C_{10}H_{21}$, Ph, $NC(CH_2)_3$, C_3H_5) [51] with $[\alpha\text{-}SiW_{11}O_{39}]^{8-}$ in unbuffered solutions. These reactions have been extended by Judenstein.[52, 53] Similar compounds have been obtained from $\alpha\text{-}[PW_{11}O_{39}]^{7-}$. The organic part of the $[PW_{11}O_{39}(Si\text{-}CH{=}CH_2)_2O]^{3-}$ anion may be extended by hydrosilylation with Et_3SiH and $PhSiMe_2H$ (Figure 22). These are the first examples of hydrosilylation on a hybrid tungstophosphate core.[54]

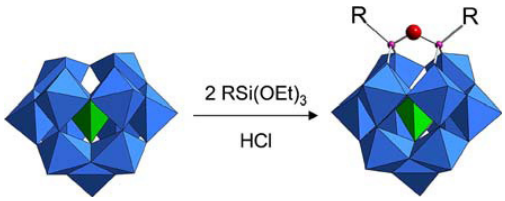

Figure 21. Schematic procedure of silanes grafting on a $[XW_{11}O_{39}]^{7-}$.

[50] J. Li, F. Zhai, X. Wang, E. Li, S. Zhang, Q. Zhang, X. Du, Synthesis and biological activity of triorganogermanium substituted heteropolytungstates, *Polyhedron*, **2008**, *27*, 1150-1154.
[51] W. H. Knoth, Derivatives of Heteropolyanions. 1. Organic derivatives of $W_{12}SiO_{40}^{4-}$, $W_{12}PO_{40}^{3-}$, and $Mo_{12}SiO_{40}^{4-}$, *J. Am. Chem. Soc.* **1979**, *101*, 759-760.
[52] P. Judenstein, C. Deprun, L. Nadjo, Synthesis and Multispectroscopic Charaterization of Organically Modified Polyoxometalates, *J. Chem. Soc. Dalton Trans.* **1991**, 1991-1997.
[53] P. Judenstein, Synthesis and Properties of Polyoxometalates Based Inorganic-Organic Polymers, *Chem. Mater.* **1992**, *4*, 4-7.
[54] D. Agustin, J. Dallery, C. Coelho, A. Proust, R. Thouvenot, Synthesis, characterization and study of the chromogenic properties of the hybrid polyoxometalates $[PW_{11}O_{39}(SiR)_2O]^{3-}$ (R = Et, $(CH_2)_nCH{=}CH_2$ (n = 0, 1, 4), $CH_2CH_2SiEt_3$, $CH_2CH_2SiMe_2Ph$), *J. Organomet. Chem.* **2007**, *692*, 746-754.

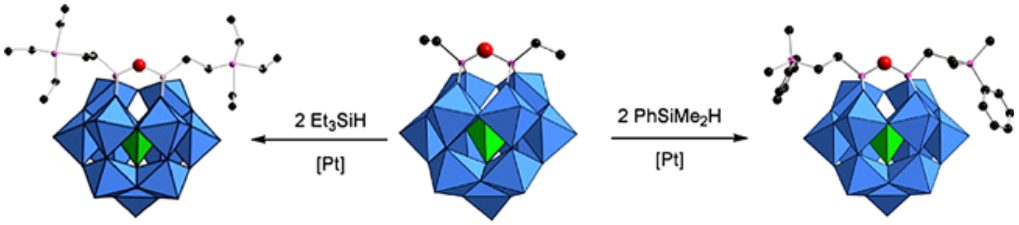

Figure 22. Schematic representation of hydrosilylation of $[PW_{11}O_{39}(Si\text{-}CH{=}CH_2)_2O]^{3-}$.[54]

The incorporation of organostannyl groups into polyoxometalate structures can be easily achieved by reaction of $RSnCl_3$ with appropriate lacunary anions. These reactions result in polyoxoanions in which $(O)_5WO^{4+}$ octahedra are replaced by $(O)_5SnR^{3+}$ to afford derivatives of type $[\alpha\text{-}XW_{11}O_{39}(SnR)]^{n-}$ (X = P, As, Si; R = Me, *n*Bu, Ph, $CH_2C_6H_5$, $(CH_2)_3Br$, $(CH_2)_4Cl$, $(CH_2)_{11}CH_3$, $(CH_2)_6Br$, $C_{27}H_{45}$, CN; *n* = 5, 6).[55, 56, 57] The stability of Sn-carbon bonds towards hydrolysis makes the resulting polyoxometalate derivatives particularly suitable for further derivatization and applications in aqueous solution. However, this strategy suffers from incompatibility of the trichlorotin moiety with most organic functions. A notable contribution has been recently reported by Neumann[58] who developed a simple method for the preparation of tin-substituted hybrid POM compounds with readily available amines. Such compounds are formed upon the interaction of the amine with Sn-Cl center of the polyoxometalate.

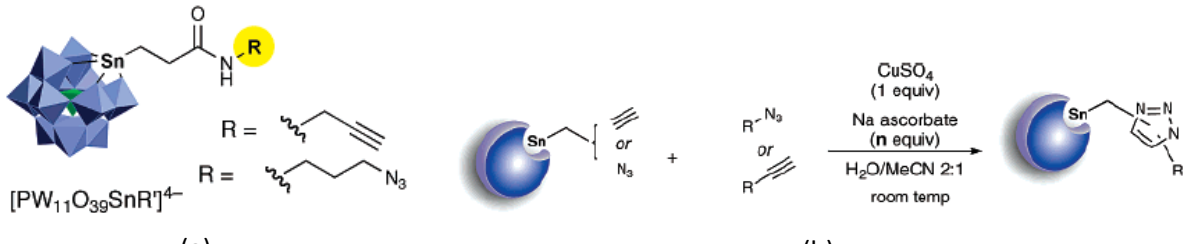

Figure 23. (a) Polyoxotungstic platform chosen for ligation. (b) General procedure of grafting organic molecules to polyoxotungstates through copper-catalyzed dipolar cycloaddtion.[59]

---

[55] W. H. Knoth, Derivatives of Heteropoyanions. 2. Metal-Metal-Bonded Derivatives, *J. Am. Chem. Soc.* **1979**, *101*, 2211-2213.
[56] F. Zonnevijlle, M. T. Pope, Attachement of Organic Groups to Heteropoly Oxometalate Anions, *J. Am. Chem. Soc.* **1979**, *101*, 2731-2732.
[57] G. S. Chorghade, M. T. Pope, Heteropolyanions as Nucleophiles. 1. Synthesis, Characterization, and Reaction of Keggin- Dawson- Type Tungstostannates (II), *J. Am. Chem. Soc.* **1987**, *109*, 5134-5138.
[58] I. Bar-Nahum, J. Ettedgui, L. Konstantinovski, V. Kogan, R. Neumann, A New Method for the Synthesis of Organopolyoxometalate Hybrid Compounds, *Inorg. Chem.* **2007**, *46*, 5798-5804.

The copper-catalyzed azide/alkyne cycloaddition (click chemistry) is reported for the first time in polyoxometalate chemistry, to graft different organic moieties to polyoxotungstates to generate hybrids (**Figure 23**).[59] This opens the way to varied functionalized POMs and applications.

Earlier work has demonstrated that the isolated $[RGe]^{3+}$ group can be incorporated into mono-lacunary Keggin structure polyanions. Acrylate derivatives provide a simple route to functionalization of organogermanium trihalides. [60]

1.4. ELECTROCHEMICAL PROPERTIES OF POMs

1.4.1. General Overview

The heteropolyanions undergo several rapid one- and two-electron reversible reductions to produce the so-called "heteropoly blue", and further irreversible multielectron reductions with possible decomposition. The electrons are accepted by the addenda ions of the heteropolyanions $[XM_{12}O_{40}]^{n-}$. If the addenda ions are all identical, the electrons are delocalized on the addenda ion oxide framework at room temperature by rapid electron hopping (intramolecular electron transfer). The reduction increases the negative charge density at the heteropolyanions and thus their basicity. It is well known that the one-electron waves in acidified media, where protonation accompanies the reduction, are converted into two-electron waves. [61] Both Keggin- and Dawson-type heteropolyanions undergo several one-electron reductions in neutral aqueous or organic solution where no protonation can occur.

Keggin-type heteropolyanions can accept a limited number of electrons without decomposition, and in some cases the reduced compounds have been isolated. In general, the reduction potentials of the Keggin-type heteropolytungstates are controlled by the following factors: 1) the reducibility increases in the sequence α-, β-, and γ-isomers according to the number of rotated M_3O_{13} groups; 2)

[59] K. Micoine, B. Hasenknopf, S. Thorimbert, E. Lacôte, M. Malacria, A General Strategy for Ligation of Organic and Biological Molecules to Dawson and Keggin Polyoxotungstates, *Org. Lett.* **2007**, *9*, 3981-3984.
[60] G. Sazani, M. T. Pope, Organotin and organogermanium linkers for simple, direct functionalization of polyoxotungstates, *Dalton Trans.* **2004**, 1989-1994.
[61] M. T. Pope, Heteropoly and Isopoly Oxometalates, Springer-Verlag, Berlin **1983**.

the reduction potential of the one-electron waves decreases linearly with a decrease in the valence of the central metal, *i.e.*, an increase in the negative charge of the heteropolyanions.[61, 62]

1.4.2. Electrochemical behavior of functionalized polyoxometalates

The electrochemical behavior of several silyl species derived from the $[PW_{11}O_{39}]^{7-}$ were investigated in acetonitrile solution at the glassy carbon electrode by the group of Proust.[54] For the $(Bu_4N)_3[PW_{11}O_{39}(SiR)_2O]$ derivative, where R is $-CH_2-CH_3$ and $-CH=CH_2$ four monoelectronic W(VI→V) reduction processes are observed (**Figure 24**), shifted to less negative values with respect to $[PW_{11}O_{39}]^{7-}$ anion. This is consistent with the lowering of the charge of complete structures which become more easily reduced. On the other hand when the organosilyl fragment R is $-CH_2-CH_2SiEt_3$ and $-CH_2-CH_2SiMe_2Ph$, the corresponding derivatives exhibit three monoelectronic reduction waves. Also, the first reduction potential is slightly dependent on the nature of the organic fragment grafted to the $\{PW_{11}\}$ unit.

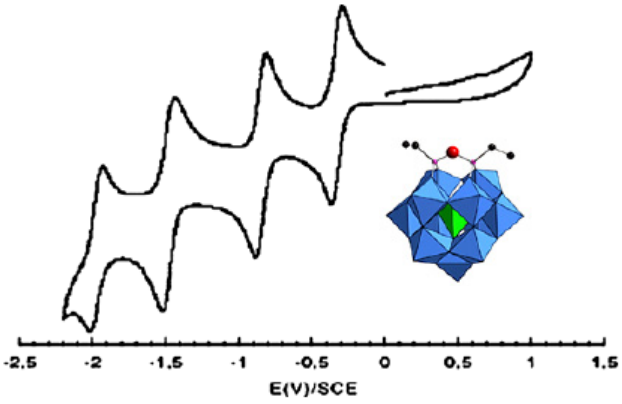

Figure 24. Cyclic voltammogram of $(Bu_4N)_3[PW_{11}O_{39}(SiR)_2O]$ (R = $-CH_2-CH_3$) derivative at the glassy carbon electrode.[56]

Pope *et al.*[60] investigated the electrochemical behavior organo-stannyl and germyl derivatives of the type $[XW_{11}O_{39}M(CH_2)_2COOH]^{n-}$ where X = Si, Ga; M = Sn, Ge. Their characteristic cyclic voltammogram showed two-electron quasi-reversible tungsten reduction at pH = 2.9.

The redox properties of POMs will be examined in details in the second part of this manuscript.

[62] M. Sadakane, E. Steckhan, Electrochemical Properties of Polyoxometalates as Electrocatalysts, *Chem. Rev.* **1998**, *98*, 219-237.

1.5. POLYOXOMETALATES BASED MATERIALS

1.5.1. Introduction

With sizes just one order of magnitude smaller than the smallest of living biological structures such as the Rhinovirus (approx. 20 nm) they are not colloids but soluble polynuclear species. Yet, they not only share structural and topological features with related transition metal oxides but also resemble them concerning their redox, electron transfer or ion transport behavior. In all these respects, polyoxometalates can be generically considered as the perfect models for quantum-sized transition metal oxide nanoparticles. For example, the electrochemical or photochemical injection of electrons in heteropolyanions (HPA) with the concomitant induction of thermally activated delocalization between metal centers and IVCT (Intervalence Charge Transfer Bands) leading to change in color, closely parallel the corresponding electrochromic properties of the corresponding oxides upon doping. [63] On the other hand, POMs are ultimately dispersed species where most, if not all the metal centers that conform the cluster are not part of a bulk extended structure but are effectively located at surface sites, with all the implications this has concerning interfacial chemistry/electrochemistry and surface properties.

Because of their reversible redox behavior, discrete structures in size from subnanometer to a few nanometers, and good solubility and stability in aqueous and organic solvents, POMs have been used widely as the inorganic components in functional molecular materials. Surface-confined thin films and two-dimensional arrays of POMs have been constructed to produce POM-containing molecular materials and devices. Ordered monolayers of POMs on gold or silver were obtained by spontaneous adsorption from solution. By solvent casting, POMs on carbon were prepared with active catalytic properties and ordered mesoporous SiO_2 functionalized with cationic groups was used as substrates for ionic immobilization of POMs. However, the majority of work aimed to make films of POMs utilizes the Langmuir-Blodgett (LB) technique. By taking advantage of the ionic interaction of positively charged organic molecules or polymers and negative charged POM polyanions, both monolayers and multilayers of POMs have been prepared by the LB technique on various substrates

[63] N. Casañ-Pastor, P. Gómez-Romero, Polyoxometalates: from inorganic chemistry to materials science, *Frontiers in Bioscience*, **2004**, *9*, 1759-1770.

including glass, quartz, ITO, glassy carbon, silicon, and silica. These LB films of POMs have been found to have interesting photo and electrical properties.

The majority of these monolayers and multilayers of POMs were deposited on substrates by physical adsorption or electrostatic forces. There are few examples of POMs that were attached through covalent bonds to the substrates to form well-defined monolayers. One example is the bonding of thiol-derived POM clusters to gold nanoparticles. There is one report of covalently bonding POMs to a Si surface by Errington's group, a stepwise method by which $TiWO_{18}$ clusters are attached to Si through covalent Ti-O-C bonds by alcoholysis of the Ti-OR bond in $[(RO)TiW_5O_{18}]^{3-}$ with a preassembled alkanol monolayer on Si.[67]

To the best of my knowledge the only reference which deals with the covalent grafting of polyoxometalates onto a silicon surface towards the construction of hybrid molecular/semiconductor devices, has been reported in 2009 by the group of Tour.[64] Using a one-step method, organically functionalized hexamolybdate cluster were grafted onto Si(111) and Si(100) surfaces through a conjugated linkage by diazonium chemistry (**Figure 25**, (a)). In their approach, the organic conjugated bridges between the cluster and Si substrates in combination with Si-C bond of the molecule with the Si surface, without the interfering oxide, could provide better electronic interaction between the electrically active POM clusters and the semiconductor substrate.

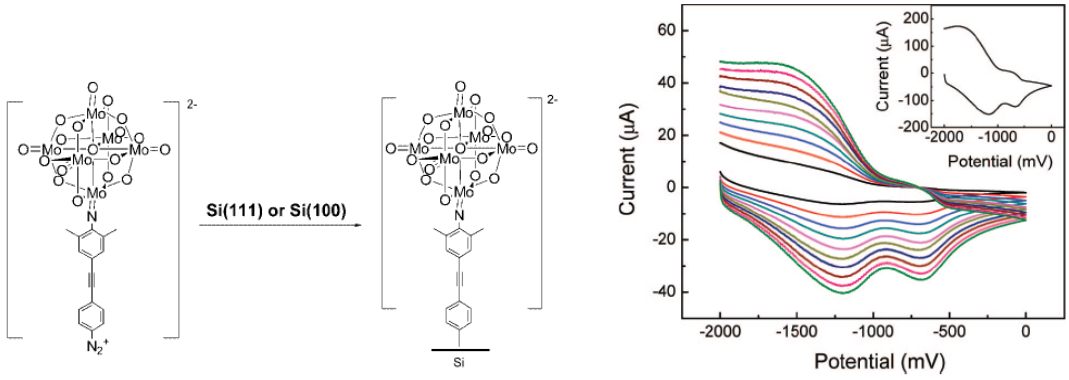

(a) (b)

Figure 25. (a) Surface grafting of diazonium derived hexamolybdate. (b) Cyclic voltammograms of hexamolybdate film on *p*-type Si(111), the scan rates are from 1 V/s (black line) to 10 V/s (green line) with increaments of 1 V/s. Inset is a representative cyclic voltammogram with a scan rate of 10 V/s.[28]

[64] M. Lu, W. M. Nolte, T. He, D. A. Corley, J. M. Tour, Direct Covalent Grafting of Polyoxometalates onto Si Surface, *Chem. Mater.* **2009**, *21*, 442-446.

Cyclic voltammetry was used to study the electrical properties of the covalently surface attached hexamolybdate clusters. The electrochemical results indicate that the hexamolybdate clusters covalently bonded onto Si surface are electrochemically accessible, and there are strong electronic interactions between the clusters and the Si substrate (**Figure 25**, (b)). This electronic interaction, in addition to the accessible and reversible redox behavior of hexamolybdates, could have applications in the bottom-up design of functional molecular materials or future generation of hybrid molecular devices.

The polyoxometalates are able to be attached onto the electrode by using an interaction between the polyoxometalates and the electrode. There are three methods commonly used to immobilize polyoxometalates onto the electrode surface. The first method is the adsorption of polyoxometalates on the electrode surface by dip coating. The second method is to entrap polyoxometalates into polymers on the electrode surface. The third method is the electrodeposition of polyoxometalates onto the electrode surface within the polyoxometalate solution under constant potential at -1.2 V.[65] Dilute solutions of POMs were used to activate vitreous carbon or graphite electrodes resulting in potential gains up to 1 V *vs* the unmodified version for the reaction of H_2 evolution from H_2O. A few examples of POMs-modified materials and their applications are given in **Table 1**.

Table 1. POMs-modified materials and their application.

Type of POM	***Substrate***	***Method***	***Application***
$[SiW_{10}O_{36}(HSC_3H_6)_2O]^{4-}$	Gold nanoparticles	Covalent bonding	Hybrid organic-inorganic materials[66]
$[(MeO)TiW_5O_{18}]^{3-}$	Silicon and porous silicon	Covalent bonding	Active materials[67]
$[Mo_6O_{18}(NC_{16}H_{12})N_2^{+}]^{2-}$	Silicon Si(111) or Si(100)	Covalent bonding	Hybrid molecular/semiconductor electronic devices[68,69]

[65] B. Keïta, L. Nadjo, Activation of electrode surfaces. Application to the electrocatalysis of the hydron evolution reaction, *J. Electroanal. Chem.* **1985**, *191*, 441-448.
[66] C. R. Mayer, S. Neveu, V. Cabuil, A Nanoscale Hybrid System Based on Gold Nanoparticles and Heteropolyanions, *Angew. Chem. Int. Ed.* **2002**, *41*, 501-503.
[67] R. J. Errington, S. S. Petkar, B. R. Horrocks, A. Houlton, L. H. Lie, S. N. Patole, Covalent Immobilization of TiW5 Polyoxometalates on Derivatized Silicon Surface, Angew. Chem. Int. Ed. **2005**, *44*, 1254-1257.
[68] M. Lu, W. M. Nolte, T. He, D. A. Corley, J. M. Tour, Direct Covalent Grafting of Polyoxometalates onto Si Surfaces, *Chem. Mater.* **2009**, *21*, 442-446.

$(NC_{26}H_{55}S(CO)CH_3)_6H_2[Co(H_2O)CoW_{11}O_{39})]$ $(NC_{26}H_{55}S(CO)CH_3)_{13}H_3[Co_4(H_2O)_2(P_2W_{15}O_{56})_2]$ $(NC_{26}H_{55}S(CO)CH_3)_{13}[Fe(H_2O)_2(P_2W_{15}O_{56})_2]Br$	Au(111)	Covalent bonding SAMs	Functional materials with electrocatalytic activity[70]
DODA [i]/POMs	ITO	LB	Films with electrochromic or magnetic properties[71]
OMA/ODA/ [ii] POMs	SiO_2, ITO, quartz	LB	Luminescent functional materials[72]
$[NaP_5W_{30}O_{110}]^{14-}$/PEI [iii] $[W_{10}O_{32}]^{4-}$/PEI	Silicon	LB	Materials in optical data storage[73]
$[\gamma\text{-}1,2\text{-}H_2SiV_2W_{10}O_{40}]^{4-}$	SiO_2 mesoporous	Ionic immobilization	Catalytic oxidation of olefins and sulfides[74]
$[\equiv Si(CH_2)_3N^+(CH_3)_3]_4PMo_{11}V^VO_{40}{}^{4-}$	SiO_2	Ionic immobilization	Catalytic oxidation of alcohols [75]
$\alpha\text{-}SiW_{12}O_{40}{}^{4-}$	Ag(111), Cu	Spontaneous adsorption	Functionalized surfaces [76]
$(NH_4)_3PMo_{12}O_{40}$ or $(NH_4)_4SiMo_{12}O_{40}$	Carbon fiber microelectrode	Dip coating	Electrocatalytic activity for the reduction of chlorate ion (ClO_3^-)[77]

[69] T. He, J. He, M. Lu, B. Chen, H. Pang, W. F. Reus, W. M. Nolte, D. P. Nackashi, P. D. Franzon, J. M. Tour, Controlled Modulation of Conductance in Silicon Devices by Molecular Monolayers, *J. Am. Chem. Soc.* **2006**, *128*, 14537-14541.

[70] H. Sun, W. Bu, Y. Li, H. Li, L. Wu, C. Sun, B. Dong, R. Dou, L. Chi, A. Schaefer, Self-Assembled Monolayers of CH3COS – Terminated Surfactant-Encapsulated Polyoxometalate Complexes, *Langmuir* **2008**, *24*, 4693-4699.

[71] M. Clemente-León, E. Coronado, C. J. Gómez-García, C. Mingotaud, S. Ravaine, G. Romualdo-Torres, P. Delhaès, Polyoxometalate Monolayers in Langmuir-Blodgett Films, *Chem. Eur. J.* **2005**, *11*, 3979-3987.

[72] L. Liu, W.-H. Ai, M.-J. Li, S.-Z. Liu, Langmuir – Blodgett Films of Heteropolyoxometalate/Organomercury Acetylide Hybrid Composites: Characterization and Photoelectric Properties, *Chem. Mater.* **2007**, *19*, 1704-1711.

[73] M. Jiang, E. Wang, G. Wei, L. Xu, Z. Li, Photochromic inorganic-organic multilayer films based on polyoxometalates and poly(ethylenimine), *J. Colloid Interface Sci.* 2004, *275*, 596-600.

[74] J. Kasai, Y. Nakagawa, S. Uchida, K. Yamaguchi, N. Mizuno, $[\gamma\text{-}1,2\text{-}H_2SiV_2W_{10}O_{40}]$ Immobilized on Surface-Modified SiO_2 as a Heterogeneous Catalyst for Liquid-Phase Oxidation with H_2O_2, *Chem. Eur. J.* **2006**, *12*, 4176-4184.

[75] C. N. Kato, A. Tanabe, S. Negishi, K. Goto, K. Nomiya, An Efficient $PMo_{11}V^VO_{40}{}^{4-}$/Silica Material Having Cationic Ammonium Moiety: Synthesis, Characterization, and Catalytic Performance for Oxidation of Alcohols xith Dioxygen, *Chem. Lett*. **2005**, *34*, 238-239.

[76] M. Ge, B. Zhong, W. G. Klemperer, A. A. Gewirth, Self-Assembly of Silicotungstate Anions on Silver Surfaces, *J. Am. Chem. Soc.* **1996**, *118*, 5812-5813.

[77] B. Wang, S. Dong, Electrochemical studyof isopoly- and heteropoly-oxometalates film modified microelectrodes – VI. Preparation and redox properties of 12-molybdophosphoric acid and 12-molybdosilicic acid modified carbon fiber microelectrodes, *Electrochim. Acta* **1996**, *41*, 895-902.

$K_7[SiW_{11}O_{39}(H_3P_2O_7)]$/ diazoresin	quartz, silicon, mica, ITO	LbL	Composite films with photosensitive properties[78]
$[P_2W_{18}O_{62}]^{6-}$/$[Fe(bpy)_3]^{2+}$	Glassy carbon	LbL	Electrocatalytic activity for the reduction of NO_2^-, H_2O_2, BrO_3^- [79]
$[P_8W_{48}O_{184}]^{40-}$/BPPA-Os *iv)*	Glassy carbon	LbL	Electrocatalytic activity for the reduction of HNO_2, H_2O_2[80]
polyamidoamine dendrimers/$PMo_{12}O_{40}^{3-}$ or $P_2W_{18}O_{62}^{6-}$	Quartz, Au	LbL	Electrocatalytic activity for the reduction of nitrite and iodate anions (NO_2^- and IO_3^-) [81]
Au/Cysteamine/*n*$SiW_{12}O_{40}$/ (*n*-1)QPVP-Os *v)*	Au	LbL	Potential applications in electrochromism, photoelectrochemistry, sensors, catalysis, light imaging and other thin-film molecular devices [82]

i) DODA = dimethyldioctadecylammonium cation
ii) OMA/ODA = organomercury acetylide complex/octadecylamine
iii) PEI = poly(ethylenimine)
iv) BPPA-Os = osmium-bis-N,N'-(2,2'-bipyridyl)-N-(pyridine-4-yl-methyl-(8-pyrrole-1-yl-octyl)-amine)chloride
v) QPVP-Os = poly(4-vinylpyridine) partially quaternized with bromoethane and complexed with osmium bis(2,2'-bipyridine) chloride

1.5.2. ELECTRONICS PROPERTIES OF POMs – based MATERIALS

The main part of applications, literature and patents regarding these systems is in the field of catalysis. However, there is a potential for exploitation of their electronic and optical properties. The successful

[78] Y. Feng, J. Peng, Z. Han, H. Ma, Fabrication of photosensitive multilayer films based on polyoxometalate and diazoresin, *J. Colloid Interace Sci.* **2005**, *286*, 589-595.
[79] N. Fay, E. Dempsey, T. McCormac, Assembly, electrochemical characterization and electrocatalytic ability of multilayer films based on $[Fe(bpy)_3]^{2+}$, and the Dawson heteropolyanion, $[P_2W_{18}O_{62}]^{6-}$, *J. Electroanal. Chem.* **2005**, *574*, 359-366.
[80] L.-H. Bi, K. Foster, T. McCormac, E. Dempsey, Preparation of multilayer films containing a crown heteropolyanion and an osmium functionalised pyrrole monomer, *J. Electroanal. Chem.* **2007**, *605*, 24-30.
[81] L. Cheng, J. A. Cox, Preparation of multilayered nanocomposites of polyoxometalates and poly(amidoamine) dendrimers, *Electrochem. Commun.*, **2001**, *3*, 285-289.
[82] Z. Cheng, L. Cheng, Q. Gao, S. Dong, X. Yang, Characterization of organic-inorganic multilayer films by cyclic voltammetry, UV-Vis spectrometry, X-ray photoelectron spectroscopy, small-angle X-ray diffraction and electrochemical impedance spectroscopy, *J. Mater. Chem.* **2002**, *12*, 1724-1729.

implementation of molecules in electronic devices depends to a great extend on our controlling of the material's structural parameters and our understanding of the complex electron-transport phenomena accompanying molecular conductance.[83]

The first attempts of electrical measurements on POM-based systems have been carried out by the groups of Glezos and Tour. Polyoxometalates were examined as components of polymeric materials with potential use in nanolithography, molecular devices and also properties such as charging and electron tunnelling through molecules in quantum switching applications were exploited. The one important requirement in this case is that the guest POM molecule should not interact chemically with the polymer guest material. POMs are embedded into resist systems with the intention to formulate an active molecular material that can be patterned by electron beam lithography. Such a system would allow patterning of the active material itself without any additional lithographic step. A few types of materials were considered for this procedure: poly(vinyl alcohol) (PVA), poly(methyl methacrylate) (PMMA) and a (meth)acrylate copolymer of hydroethyl methacrylate, cyclohexyl methacrylate, isobornyl methacrylate and acrylic acid (PHECIMA). Electrical characterization was carried out for POMs embedded in PHECIMA and PMMA. The PVA material was not tested for electrical properties because the concentration of the guest molecules varies during resist processing thus making it inappropriate for molecular device applications. The transport properties of these materials were investigated varying the interelectrode spacing and the POM concentration. Tunneling effects expressed as conductivity peak at room temperature were revealed for the PMMA composites. Another interesting result obtained was resonant tunneling at room temperature conditions for film thickness in the range of 10nm.[84, 85, 86] Quantum tunneling effects depend strongly on three factors, primarily on a) the POM concentration and therefore the intermolecular distance, b) the electrode distance and less on c) the electrode material.[87] This study concluded that the selective charging of POMs can be exploited in future memory devices.

---

[83] J. He, B. Chen, A. K. Flatt, J. S. Stephenson, C. D. Doyle, J. M. Tour, Metal-free silicon-molecule-nanotube testbed and memory device, *Nat. Mat.* **2006**, *5*, 63-68.

[84] N. Glezos, D. Velessiotis, G. Chaidogiannos, P. Argitis, D. Tsamakis, X. Zianni, Transport properties of polyoxometalate containing polymeric materials, *Synth. Met.* **2003**, *138*, 267-269.

[85] G. Chaidogiannos D. Velessiotis, P. Argitis P. Koutsolelos, C. D. Diakoumakos, D. Tsamakis, N. Glezos, Tunneling and negative resistance effects for composite materials containing polyoxometalate molecules, *Microelectron. Eng.* **2004**, *73-74*, 746-751.

[86] N. Glezos, P. Argitis, D. Velessiotis, C. D. Diakoumakos, Tunneling transport in polyoxometalate based composite materials, *Appl. Phys. Lett.* **2003**, *83*, 488-490.

[87] D. Velessiotis, N. Glezos, V. Ioannou-Sougleridis, Tungstate polyoxometalates as active components of molecular devices, *J. Appl. Phys.* **2005**, *98*, 084503.

A volatile metal-insulator-semiconductor (MIS) capacitor-like memory device based on a molecular proton storage element was reported in 2008. [88] In this type of memory device a hybrid organic/inorganic proton-conducting-polymeric layer is incorporated by spin coating of PMMA solutions containing 12-tungstophophoric acid ($H_3PW_{12}O_{40}$). The storage element can be placed in two readily discernible physical states that modulate the transistor's channel conductivity enabling data to be read electrically by sensing the current level of the transistor. These storage elements comprise at least a first layer made of a proton-conducting polymeric material (referred as proton-conducting-layer, PCL) in which protons are the mobile carriers, in this case PMMA/$H_3PW_{12}O_{40}$. Additionally, they may comprise a second proton-trapping layer (PTL) made of material which contains basic sites for ensuring the non-volatile function to a memory device. Application of an electric field across the PCL produces anions and protons. The protons can be moved at either side of the PCL depending on the direction of the applied electric field. This temporary transfer of protons confers bistability and long-refresh volatile memory properties to the devices. Application of an electric field across the storage element allows trapping of protons in the PTL and thereby, offers a non-volatile function to the memory device. Finally, the proton storage element can be easily incorporated in a modified CMOS platform technology and may be further exploited in a memory transistor.

A systematic study of the charge transport mechanisms on a multilayer film composed of POMs has been conducted by the same group of Glezos.[89, 90, 91] The multilayer film consists of a Keggin POM ($H_3PW_{12}O_{40}$) and a twelve carbon-chain diamine (DD), and they are fabricated on 3-aminopropyltriethoxysilane (APTES)-modified silicon substrates via the LBL self-assembly method (**Figure 26**). The aim of the electrical characterization is to determine the leakage currents through the molecular layer as well as the charging properties of ordered POM molecules. It was shown that POM molecule act as electron traps and that tunnelling is the dominant transport mechanism. The hybrid films prepared were also examined as dielectric components in silicon-based capacitance

[88] E. Kapetanakis, A. M. Douvas, D. Velessiotis, E. Makarona, P. Argitis, N. Glezos, P. Normand, Molecular Storage Elements for Proton Memory Devices, *Adv. Mater.* **2008**, *20*, 4568-4574.
[89] A. M. Douvas, E. Makarona, N. Glezos, P. Argitis, J. A. Mielczarski, E. Mielczarski, Polyoxometalate-Based Layered Structures for Charge Transport Control in Molecular Devices, *ACS NANO* **2008**, *2*, 733-742.
[90] E. Makarona, E. Kapetanakis, D. M. Velessiotis, A. Douvas, P. Argitis, P. Normand, T. Gotszalk, M. Woszczyna, N. Glezos, Vertical devices of self-assembled hybrid organic/inorganic monolayers based on tungsten polyoxometalates, *Microelectron. Eng.* **2008**, *85*, 1399-1402.
[91] N. Glezos, A. M. Douvas, P. Argitis, F. Saurenbach, J. Chrost, C. Livitsanos, Electrical characterization of molecular monolayers containing tungsten polyoxometalates, *Microelectron. Eng.* **2006**, *83*, 1757-1760.

structures. The dependence of charging upon the structure layer was demonstrated, and the distance between the active molecules was estimated.

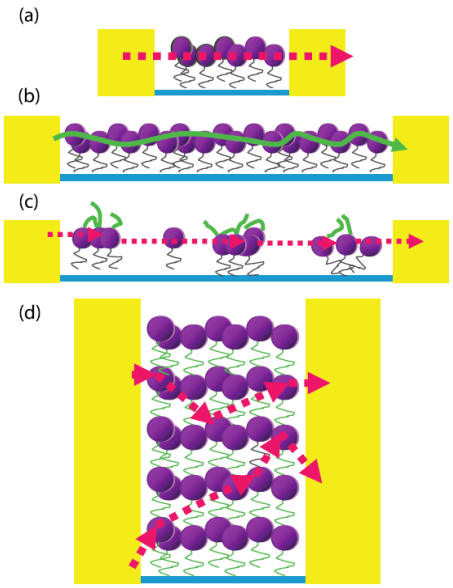

Figure 26. Schematic diagram of the transport mechanism model through the various film types at the high-voltage regime. For POM-ending films electron transport occurs through POM molecules: (a) When the gap between the electrodes is relatively short (50 nm) and the applied bias sufficient, the electrons can tunnel to the other electrode. (b) When the gap becomes relatively wide (150 nm), the electrons can never acquire enough energy to tunnel through to the other electrode and the percolation dominates. (c) In case of DD-ending films the electrons tunnel through the aggregates formed (due to the presence of the DD final layer) independent of gap width. (d) When more layers are added to the structure, alternative paths are offered to the electrons and Fowler-Nordheim tunneling.[89]

Consequently, a reproducible LbL method was established in order to fabricate POM-based molecular films with electrical properties fine-tuned *via* their structure and tailored for a novel molecular electronics material.

With respect to the electrical properties, many important achievements were obtained in the 1970s with the discovery of the first molecule-based metal in 1972,[92] namely the π-electron donor-acceptor complex [TTF][TCNQ] (TTF = tetrathiafulvalene, TCNQ = tetracyano-*p*-quinodimethane),[93] and the report of the first molecule-based superconductors in 1979 based on the Bechgaard salts $[TMTSF]_2X$ (X = PF_6^-, AsF_6^-; TMTSF = tetramethyltetraselena fulvalene).[94] In this context, POM anions combined with TTF-type organic donor molecules has proven to be a successful approach for preparing new types of POM-based materials. By altering the shapes, sizes, and charges on the

[92] Actually several years before the discovery of [TTF][TCNQ] the organic compound [*N*-methylphenazenium][TCNQ] was reported to show a metal-like conductivity (L. R. Melby, Substituted quinodimethans: VIII. Salts derived from the 7,7,8,8 – tetracyanoquinodimethan anion-radical and benzologues of quaternary pyrazinium cations, *Can. J. Chem.* **1965**, *43*, 1448-1453).

[93] J. Ferraris, D. O. Cowan, V. Walatka, Jr., J. H. Perlstein, Electron Transfer in a New Highly Conducting Donor-Acceptor Complex, *J. Am. Chem. Soc.* **1973**, *95*, 948-949.

[94] A. Andrieux, C. Duroure, D. Jérome, K. Bechgaard, The metallic state of the organic conductor TMTSF-DMTCNQ at low temperature under pressure, *J. Phys. Lett.* **1979**, *40*, 381-384.

polyanion, novel series of organic/inorganic radical cation salts which can undergo electron delocalization and even a metallic-like behaviour have been obtained.[95]

Today, POM chemistry is a key emerging area that promises to allow the development of sophisticated designer molecule-based materials and devices that exploit developments in instrumentation, nanoscale science, and material fabrication methods. There are highlighted POM systems that show or have potential to present a hierarchy of properties that may be successively "designed-in" to make highly sophisticated materials.[96]

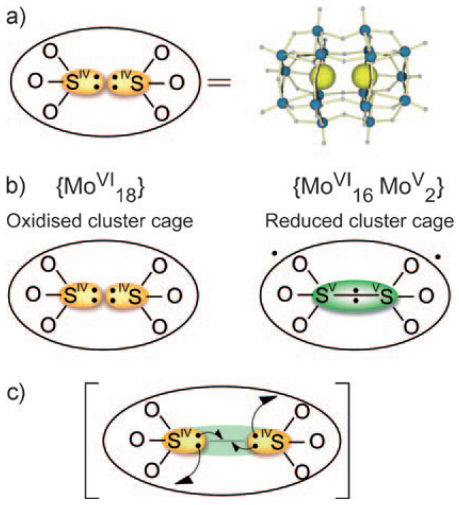

Figure 27. Schematic of the reversible S-S bond formation and electronic reorganization within the cluster cage.[97]

A strategy to create new functional POMs involves the encapsulation of redox-active template as heteroatoms. The POM cluster $[Mo_{18}O_{54}(SO_3)_2]^{4-}$, which contain two embedded redox-active sulfite templates (**Figure 27**), can be activated by a metallic surface and can reversibly interconvert between two electronic states. Upon thermal activation, two electrons are ejected from the active sulfite anions and delocalized over the metal oxide cluster cage, switching it from a fully oxidized state to a two-electron reduced state. The hypothesis is that there is a concomitant formation of an S-S bond between the two sulphur centers inside the cluster shell. This system is rather intriguing as it may be

[95] E. Coronado, C. J. Gómez-García, Polyoxometalate-Based Molecular Materials, *Chem. Rev.* **1998**, *98*, 273-296.
[96] D.-L. Long, R. Tsunashima, L. Cronin, Polyoxometalates: Building Blocks for Functional Nanoscale Systems, *Angew. Chem. Int. Ed.* **2010**, *49*, 1736-1758.
[97] C. Fleming, D.-L. Long, N. McMillan, J. Johnston, N. Bovet, V. Dhanak, N. Gadegaard, P. Kögerler, L. Cronin, M. Kadodwala, Reversible electron-transfer reactions within a nanoscale metal oxide cage mediated by metallic substrates, *Nat. Nanotechnol.* **2008**, *3*, 229-233.

possible to build a type of field-effect transistor based upon single clusters of this type. By placing the cluster in a circuit and applying a potential to the base of the cluster, the internal redox centers could be activated, thus causing electron transfer and reduction of the cluster shell and thereby switching the electronic state of the cluster from the oxidized to the mixed-valence reduced state.

1.6. CONCLUSIONS

Semiconductor technology continues to extend into regimes previously thought inaccessible. Despite this progress, it is uncertain whether devices that rely on the bulk properties of materials will retain the required characteristics to function when feature sizes ultimately reach nanoscale dimensions. As a consequence, there has been an intense interest in developing molecular-based electronic materials. A large number of redox active molecules have been implemented into hybrid molecular/semiconductor architectures *via* covalent linkage to afford molecular-based information storage.

Since the polyoxometalates are well known redox molecules, they represent prefect candidates for molecular memory devices. A common route to the integration of POMs into functional architectures and devices is by means of inorganic/organic hybrids. However, the most POM-based hybrid materials reported to date involves noncovalent interaction. In this context, the main objective of this thesis is the design and synthesis of functionalized POMs and their implementation in molecular/semiconductor architectures *via* covalent bonds for molecular memory applications.

Part 2

SYNTHESIS AND CHARACTERIZATION OF FUNCTIONALIZED POLYOXOMETALATES

2. Second Part – Synthesis and Characterization of Functionalized Polyoxometalates

Abstract – This chapter describes the synthesis, the spectroscopic characterization and the electrochemical behavior in solution of some functionalized polyoxometalates. The ***surface attachment groups are synthetically design for the molecule to attach on specific surfaces via covalent bonds***.

Résumé – Ce chapitre décrit la synthèse, la caractérisation spectroscopique et le comportement électrochimique en solution de certains polyoxométallates fonctionnalisés. Les ***groupes d'attachement à la surface sont synthétiquement conçus pour la molécule s'attache sur des surfaces spécifiques par des liaisons covalentes***.

2.1. INTRODUCTION

The area of POM-based inorganic/organic hybrids has greatly expanded over the last three decades. Due to their size and especially to their multifunctionalities POMs set to play an important role in the development of new materials. The current challenge is to incorporate POMs into functional devices. Functionalisation of polyoxometalates is quite atractive for its relevance to quite diverse disciplines. Generally speaking, POM are attractive components for the design of advanced materials and devices. One of the most challenging objectives is that of obtaining derivatives with predetermined structures and properties. The derivatisation of POM frameworks by replacing/derivatising the oxo ligands is an important aim since this will allow a much greater degree of control, potentially allowing the simultaneous exploitation of self assembly of the POM fragments, and step wise synthesis to introduce pendant functionalities. The most common route to the integration of POMs into functional architectures and devices rests on inorganic/organic hybrids.

2.2. OBJECTIVES

The main purpose of this work is ***to obtain different polyoxometalates derivatives with various terminal functions able to graft further onto a silicon wafer***. Polyoxometalates can act as multidentate inorganic ligands; they can bind most of the transition metals leading to a family of compounds exhibiting a huge diversity of structures. Their morphologies (shape and size) and their electronic, electrochemical and acido-basic properties can be finely tuned, making them useful as attractive components for the design of advanced materials and devices.

Considering all these features, ***POMs represent the perfectly suitable choice for molecular-based devices due to their redox properties***, they can be easily and reversibly reduced several times, ***and they are thermally stable*** (up to 350°C). Redox-active molecules have potential as charge storage materials because of their ability to undergo facile electron-transfer reactions at low potentials. POMs are able to graft organic fragments on the nucleophilic oxygen atoms of the core and to introduce organometallic fragments into vacant POM complex leading to the formation of various types of derivatives with different terminal functions able to graft further onto a silicon surface.

Table 1. Polyhedral representation of the four types of "platform", the $[PW_{11}O_{39}]^{7-}$ (**1**), $[PW_9O_{34}]^{9-}$ (**2**), $[PW_9O_{34}(t\text{BuSiOH})_3]^{3-}$ (**3**) and $[PW_9O_{34}(CH_3CH_2SiOH)_3]^{3-}$ (**12'**) anions.

$[PW_{11}O_{39}]^{7-}$ (**1**)	$[PW_9O_{34}]^{9-}$ (**2**)	$[PW_9O_{34}(t\text{BuSiOH})_3]^{3-}$ (**3**)	$[PW_9O_{34}(CH_3CH_2SiOH)_3]^{3-}$ (**12'**)
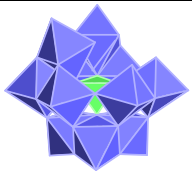	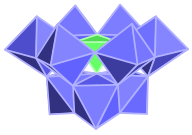	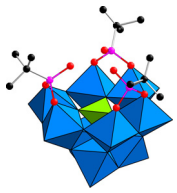	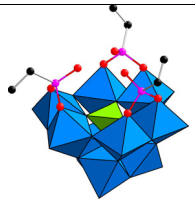
		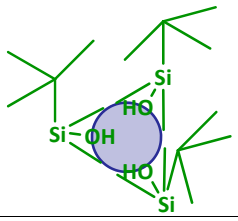	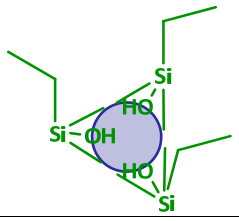

Towards the synthesis of the functionalized polyoxometalates, several aspects were taken into account:

i) the phosphorus (V) is among the elements best known to afford heteropolytungstates, the one which gives the highest number of species, as a result the POMs described in this chapter are phosphorus (V) based;

ii) the phosphorus (V) POMs purity can be easily checked, as a first method of characterization, by ^{31}P NMR;

iii) although heteropolymolybdates are reduced more easily than heteropolytunstates, the latter are more stable;

iv) four types of "platforms" (*see* **Table 1**) were envisaged at the beginning of this project which served as precursors for the functionalized POMs (**Scheme 1**) (we define a "platform" as an POM which is able to graft further the organic pendant which contains the functionality of our interest, *e.g.* double bond, triple bond, carboxylic or diazo function).

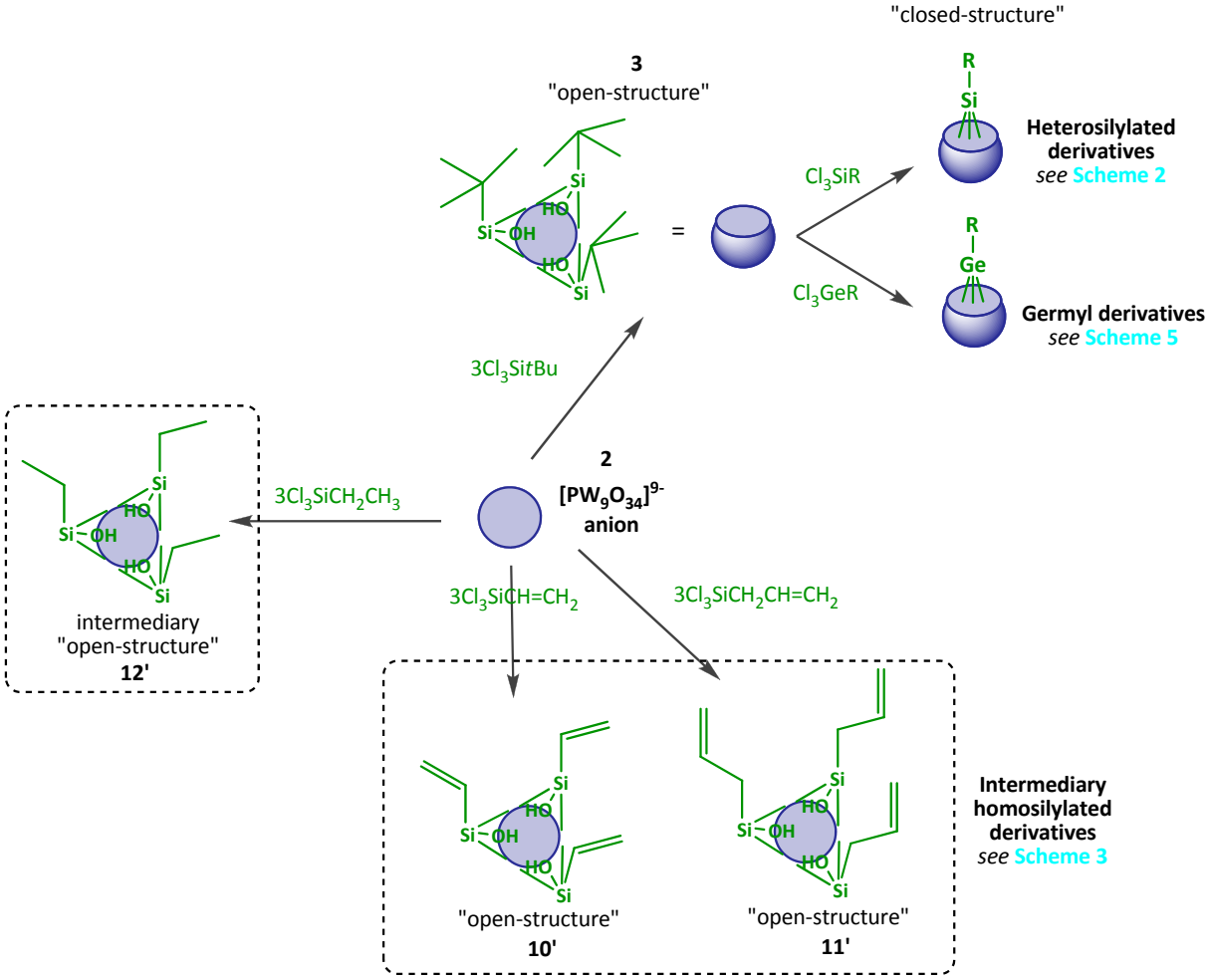

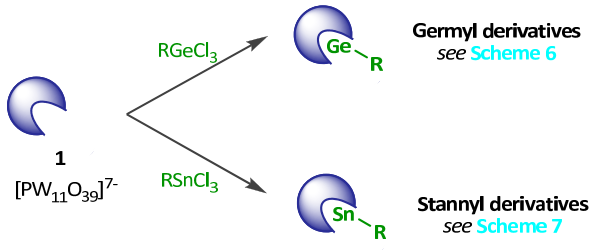

Scheme 1. General synthetic approach for the functionalized POMs used in this work.

For a better understanding of all the synthetic routes approached in this chapter, you can find at the end of this thesis all the POMs derivatives used in the following pages, together with their cartoon representation (*see Appendix*). A general synthetic approach of the POMs derivatives is presented in **Scheme 1**.

2.3. RESULTS AND DISCUSSIONS

2.3.1. Synthetic Routes for *Organosilyl Derivatives*

Starting from the trivacant highly-charged tungstophosphate $[PW_9O_{34}]^{9-}$, it has been possible to graft directly RSi moieties and, depending on R, "open-structure" $[PW_9O_{34}(RSiOH)_3]^{3-}$ (R = *t*Bu) or capped "closed-structure" $[PW_9O_{34}(RSiO)_3SiR]^{3-}$ (R ≠ *t*Bu) derivatives were obtained. Actually, the formation of the "closed-structures" takes place in two steps: the chemical grafting of three {RSi} groups onto the trivacant structure leading to the formation of the "open-structures", followed by the closing of the structure with a fourth {RSi} group.

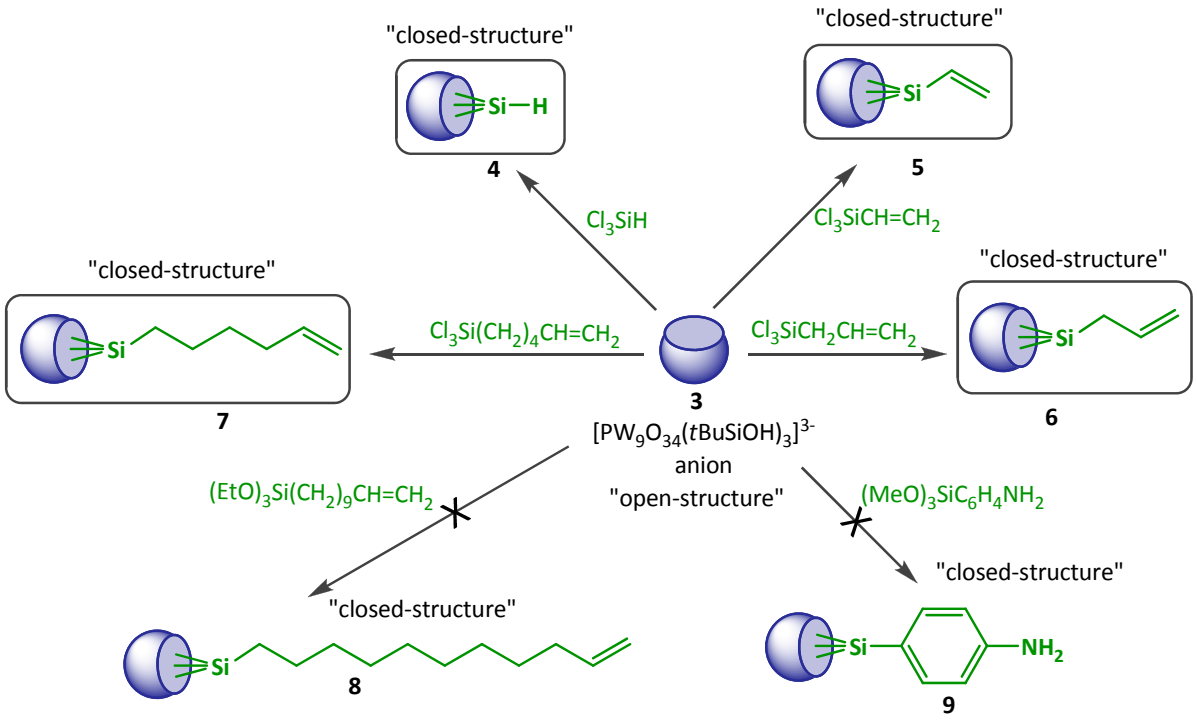

Scheme 2. Synthetic routes for heterosilylated compounds derived from $[PW_9O_{34}(t\text{BuSiOH})_3]^{3-}$ anion.

The reaction of the $[PW_9O_{34}]^{9-}$ with $t\text{BuSiCl}_3$ yields only the "open-structure" presumably because of the steric crowding. The "open-structure" anion is able to react with various $RSiCl_3$, to afford heterosilylated hybrid compounds (with a "closed-structure") with the general formula $[PW_9O_{34}(t\text{BuSiO})_3SiR]^{3-}$ (**3**) where R = -H (**4**), $-CH=CH_2$ (**5**), $-CH_2-CH=CH_2$ (**6**), $-(CH_2)_4-CH=CH_2$ (**7**) (Scheme 2).

The trivacant polyoxotungstate $[PW_9O_{34}]^{9-}$ (**2**) reacts readily with organochlorosilanes to yield directly "closed-structures" of the type $[PW_9O_{34}(RSiO)_3(RSi)]^{3-}$, where R = $-CH=CH_2$ (**10**), $-CH_2-CH=CH_2$ (**11**), $-CH_2-CH_3$ (**12**) (Scheme 3). Unfortunately, our efforts to stop the reaction after the first step towards the formation of "open-structures" of the type $[PW_9O_{34}(RSiOH)_3]^{3-}$ (R = $-CH=CH_2$, $-CH_2-CH=CH_2$, $-CH_2-CH_3$) proved to be unsuccessful. Our objective was to use the three vinyl or allyl organic pendants attached to the $[PW_9O_{34}]^{9-}$ framework as "tripods" for a better attachment of the POM derivatives to the silicon surface *via* hydrosilylation. Anyways, the two derivatives can be useful to our project and they were further investigated. As for derivative **12**, whose "open-structure" was envisaged as a new type of platform able to graft organic pendants, its investigation was abandoned since it presents no interest for our project.

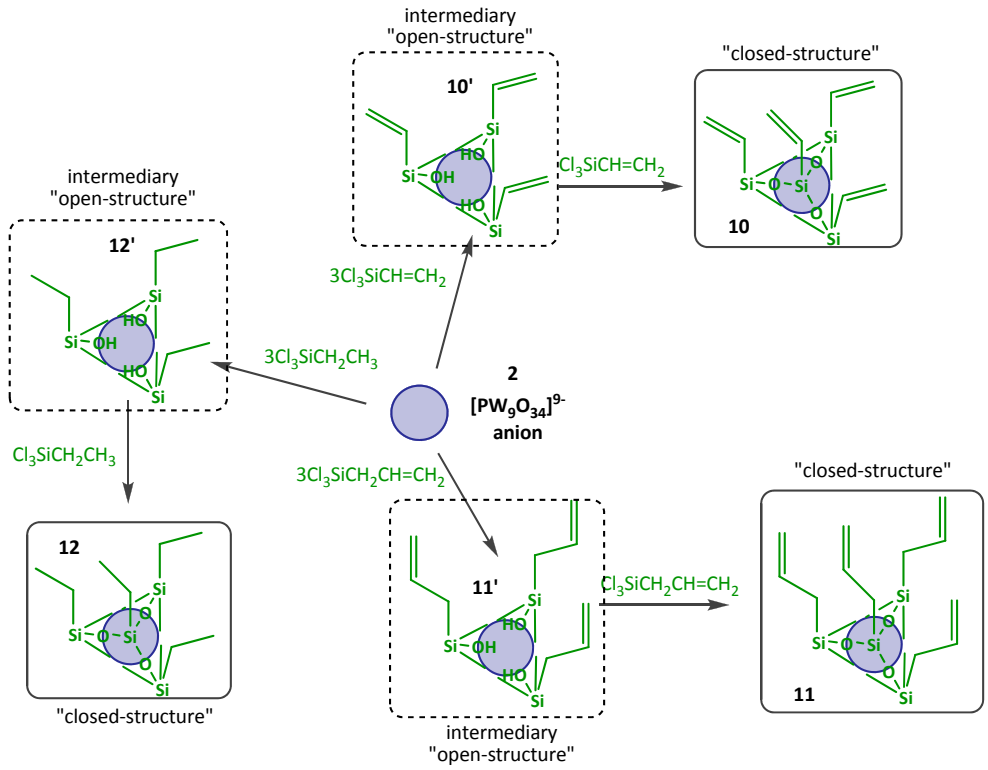

Scheme 3. Synthetic routes for homosilylated compounds derived from $[PW_9O_{34}]^{9-}$ anion.

2.3.1.1. Spectroscopic Characterization

Vibrational spectroscopy techniques are capable of giving useful information about the structure and the dynamics of a system.

Wavenumbers, characteristic of W-O_i, W-O_c-W, W-O_e-W, W=O_t, P-O_i (**Scheme 4**) bonds vibrations are expressed in cm^{-1}. The oxygen linked to the heteroatom was abbreviated with O_i, O_c (O_e, respectively) represent the oxygen atoms in corner (edge, respectively) shared octahedron, while O_t represents the terminal oxygen atom. Intensity of the bands characterizing the above mentioned asymmetric frequencies were classified in very strong (vs), strong (s), medium (m), weak (w) and very weak (vw). The shape of the same bands was classified in sharp (sp) and broad (b), while (sh) abbreviation was used when a shoulder was present.

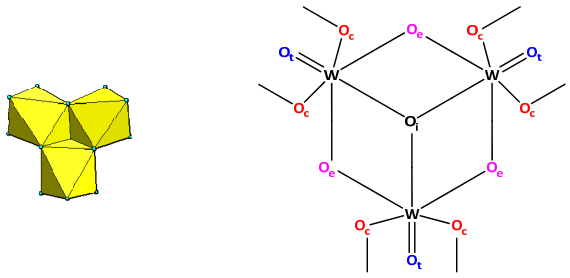

a ***b***

Scheme 4. The trimetallic W_3O_6 unit: a) the octahedral and b) the Sidgwick representation.

The characteristic group frequencies of the trimetallic unit W_3O_6 can be recognized in all the compounds. The $\nu_{as}(W\text{-}O_t)$ stretchings appear as a strong IR band between 1000-950 cm^{-1} and the $\nu_{as}(W\text{-}O_e\text{-}W)$ stretchings appear between 800-750 cm^{-1}. The vibrations between the trimetallic units have to be considered also: the $\nu_{as}(W\text{-}O_c\text{-}W)$ stretchings appear as an IR band in the 920-850 cm^{-1} region. The spectral changes in the low frequency region (below 400 cm^{-1}) give useful information about the type of isomer. All the spectra of the α isomers exhibit the same pattern of two bands: the former strong and sharp at about 370-380 cm^{-1} and the latter medium or weak at about 340 cm^{-1}. This spectral region is deeply modified for β isomers: the two bands above are replaced by a set of several well-defined and sharp bands (**Figure 1**). These changes with respect to α isomer spectra can be related to the different types of inter-unit W_3O_6 junctions, the modifications of the $W\text{-}O_c\text{-}W$ angles giving rise to several well-separated bands. The PO_4 tetrahedron vibrates almost independently from the rest of the polyanion. [1, 2] The occurrence of a vacancy in the Keggin structure leads to a weakening of the $P\text{-}O_i$ bond, as shown by the change of mean $\nu_{as}(P\text{-}O_i)$ frequencies, and induces a increase of the δ value in the ^{31}P NMR spectrum also. This also leads to a splitting of the $\nu(P\text{-}O_i)$ bands.

[1] R. Thouvenot, M. Fournier, R. Franck, C. Rocchiccioli-Deltcheff, Vibrational Investigations of Polyoxometalates. 3. Isomerism in Molybdenum (VI) and Tungsten (VI) Compounds Related to the Keggin Structure, *Inorg. Chem.* **1984**, *23*, 598-605.

[2] C. Rocchiccioli-Deltcheff, M. Fournier, R. Franck, R. Thouvenot, Vibrational Investigations of Polyoxometalates. 2. Evidence for Anion-Anion Interactions in Molybdenum (VI) and Tungsten (VI) compounds Related to the Keggin Structure, *Inorg. Chem.* **1983**, *22*, 207-216.

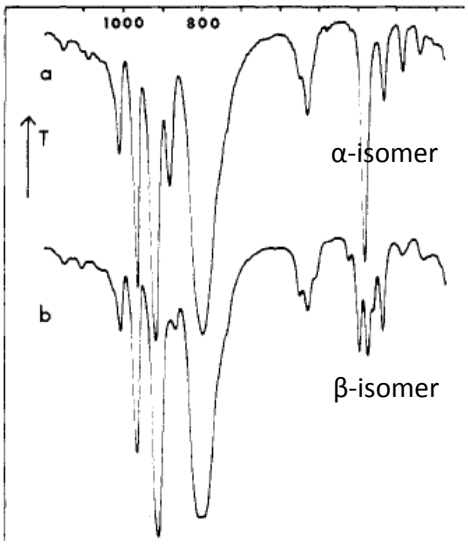

Figure 1. IR spectra of tungstic α and β isomers (as RbI): (a) α-$(Bu_4N)_4[SiW_{12}O_{40}]$, (b) β-$(Bu_4N)_4[SiW_{12}O_{40}]$.[1]

The precursors monolacunary Keggin α-$K_{7-x}Na_x[PW_{11}O_{39}]\cdot 14H_2O$ (**1**) and trilacunary Keggin A,α-$K_9[PW_9O_{34}]\cdot 16H_2O$ (**2**) were prepared according to the method of Contant[3]. Infrared spectroscopy analysis showed two bands at 1086 and 1043 cm^{-1} for **1** and, 1054 and 1003 cm^{-1} for **2** (**Figure 2** and **Figure 3**) assigned to the P-O_i stretching modes of the central PO_4 tetrahedron which are in agreement with literature data. Some frequencies of relevance for the two compounds **1** and **2**, together with their assignments are presented in **Table 2**. The formation of **1** and **2**, respectively, supports the reaction pathways shown bellow, the acidification of an aqueous solution of the oxoanion WO_4^{2-} affords the formation of compound **1** (**Equation 1**), and a controlled alkalinisation of a solution of compound **1** affords compound **2** (**Equation 2**), respectively.

$$11[WO_4]^{2-} + H_3PO_4 + 15H^+ \rightarrow [PW_{11}O_{39}]^{7-} + 9H_2O \qquad \textbf{Equation 1}$$

$$[PW_{11}O_{39}]^{7-} + 6OH^- \rightarrow [PW_9O_{34}]^{9-} + 2[WO_4]^{2-} + 3H_2O \qquad \textbf{Equation 2}$$

Table 2. Infrared data (cm^{-1}) for α-$K_{7-x}Na_xPW_{11}O_{39}\cdot 14H_2O$ (**1**) and A, α-$K_9PW_9O_{34}\cdot 16H_2O$ (**2**).

Compound	ν_{as}*(P-O_i)*	ν_{as}*(W-O_t)*	ν_{as}*(W-O-W)*
1	1086, 1043	952	903, 858, 810, 730
2	1054, 1003	929, 909	821, 733

[3] R. Contant, Relations entre les tungstophosphates apparentés à l'anion $PW_{12}O_{40}^{3-}$. Synthèse et propriétés d'un nouveau polyoxotungstophosphate lacunaire $K_{10}P_2W_{20}O_{70}\cdot 24H_2O$, *Can. J. Chem.*, **1987**, *65*, 568-573.

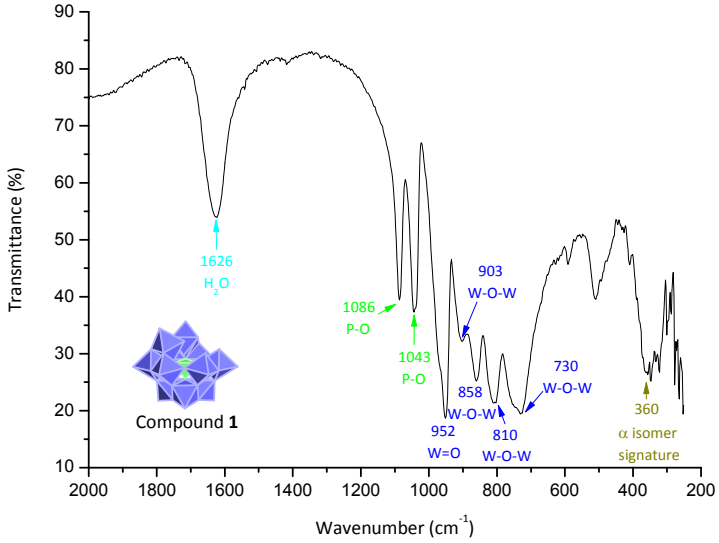

Figure 2. The IR spectrum of the precursor α-$K_{7-x}Na_xPW_{11}O_{39}\cdot 14H_2O$ (**1**).

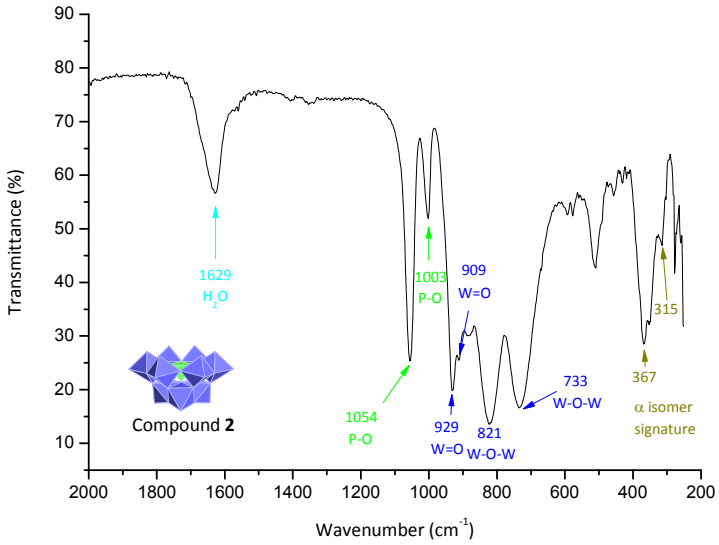

Figure 3. The IR spectrum of the precursor A, α-$K_9PW_9O_{34}\cdot 16H_2O$ (**2**).

The ^{31}P NMR was very often used to characterize the phospho-polyoxometalates and it was shown that the chemical shift of the ^{31}P in the Keggin polyoxoanions is very sensitive at slightly structural changes (*e.g.*, substitution) of the polyoxoanion framework. In particular, the formation of a lacuna in a complete Keggin polyanion induces a strong deshielding of the phosphorus central atom.

The ^{31}P NMR spectrum of $\{PW_{11}\}$ in D_2O solution presents one resonance at δ = - 10.31 ppm, also in agreement with the literature data (Figure 4).[4]

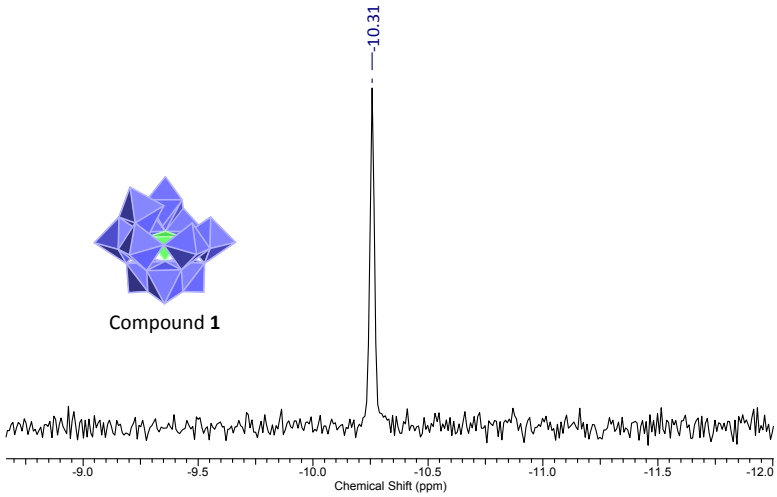

Figure 4. The ^{31}P NMR spectrum (121.49 MHz, D_2O) of compound **1**.

The following derivatives are obtained by reaction of trichlorosilanes with the trivacant species $[PW_9O_{34}]^{9-}$ (**2**) reported by Thouvenot *et al.*[5] All these hybrid anions are built up by grafting three organosilyl groups on the polyoxometalate surface which becomes saturated by formation of six Si-O-W bridges. The reaction of α-A-$[PW_9O_{34}]^{9-}$ anion with *t*BuSiCl$_3$ yields the "open-structure" (Equation 3) most likely because of the steric crowding.

$$3t\text{BuSiCl}_3 + 9H_2O \rightarrow 3t\text{BuSi(OH)}_3 + 9HCl$$

$$\text{A-}[PW_9O_{34}]^{9-} + 3t\text{BuSiCl}_3 + 3H_2O \rightarrow [PW_9O_{34}(t\text{BuSiOH})_3]^{3-} + 6Cl^- + 3HCl \qquad \textbf{Equation 3}$$

The structure of the anion $[PW_9O_{34}(t\text{BuSiOH})_3]^{3-}$ (**3**) is built up by the trivacant α-A-Keggin $\{PW_9O_{34}\}$ backbone on which three *t*BuSiOH fragments are grafted. Every one of these fragments is connected via two μ-oxo Si-O-W bonds from the same trimetallic group of the trilacunary Keggin.

[4] R. Massart, R. Contant, J.-M. Fruchart, J.-P. Ciabrini, M. Fournier, ^{31}P NMR Studies on Molybdic and Tungstic Heteropolyanions. Correlation between Structure and Chemical Shift, *Inorg. Chem.* **1977**, *16*, 2916-2921.

[5] A. Mazeud, N. Ammari, F. Robert, R. Thouvenot, Coordination Chemistry of Polyoxometalates: Rational Synthesis of the Mixed Organosilyl Derivatives of Trivacant Polyoxotungstates α-A-$[PW_9O_{34}(t\text{BuSiO})_3(\text{RSi})]^{3-}$ and α-B-$[AsW_9O_{33}(t\text{BuSiO})_3(\text{HSi})]^{3-}$, *Angew. Chem. Int. Ed. Engl.* **1996**, *35*, 1961-1964.

Every silicon atom has one group *t*Bu oriented to the outside and one group OH oriented to the inside of the polyoxometalate framework (**Figure 5**).

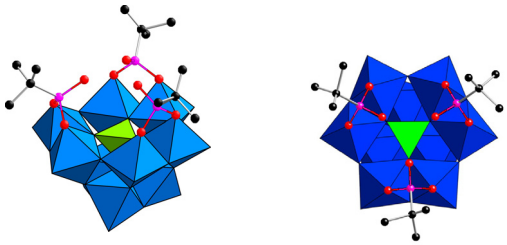

Figure 5. Polyhedral representation of compound **3**. Color code: WO_6 octahedron, blue; PO_4 tetrahedron, green; organic Si, pink; C, black; O, red.

Infrared spectroscopy analysis of the compound **3** showed the shift of the stretching vibration bands towards higher energies (with respect to the initial compound **2**) according to the polyoxometalate framework saturation (**Figure 6**). The ^{31}P NMR spectrum depends on saturation state of the polyoxotungstate. In the case of compound **3**, the signal for the phosphorus is observed at δ = -15.7 ppm (**Figure 7**).

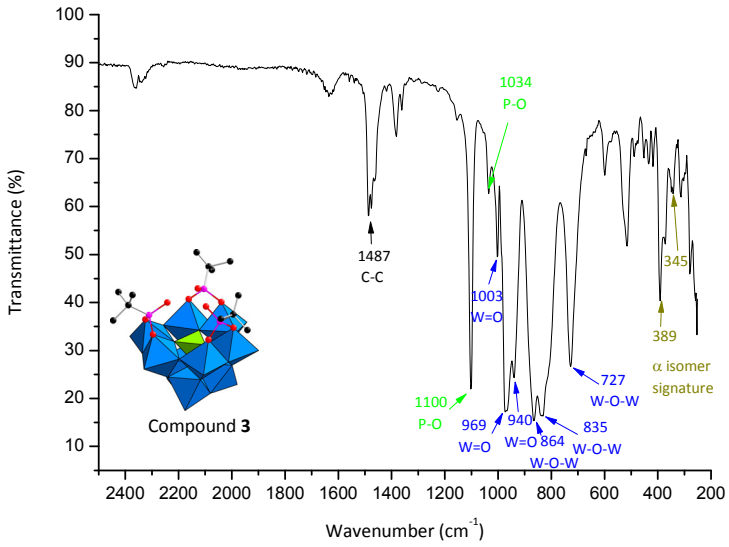

Figure 6. The IR spectrum of $(NBu_4)_3[PW_9O_{34}(tBuSiOH)_3]$ compound **3**.

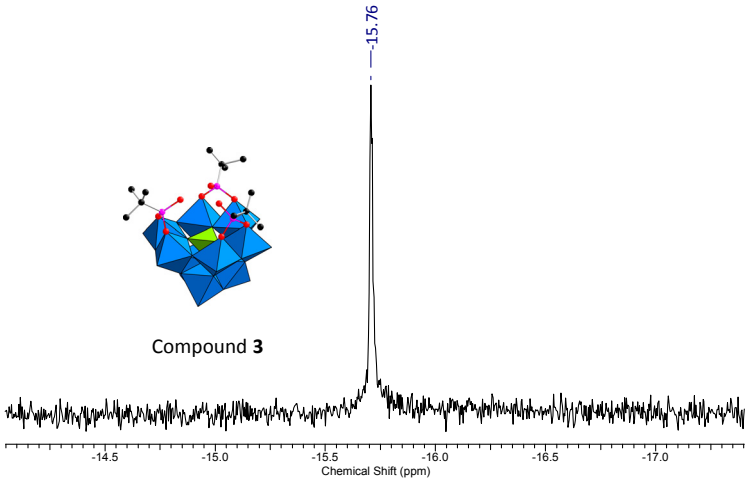

Figure 7. The ^{31}P NMR spectrum (121.49 MHz, $(CD_3)_2CO$) of $(NBu_4)_3[PW_9O_{34}(t\text{BuSiOH})_3]$ compound **3**.

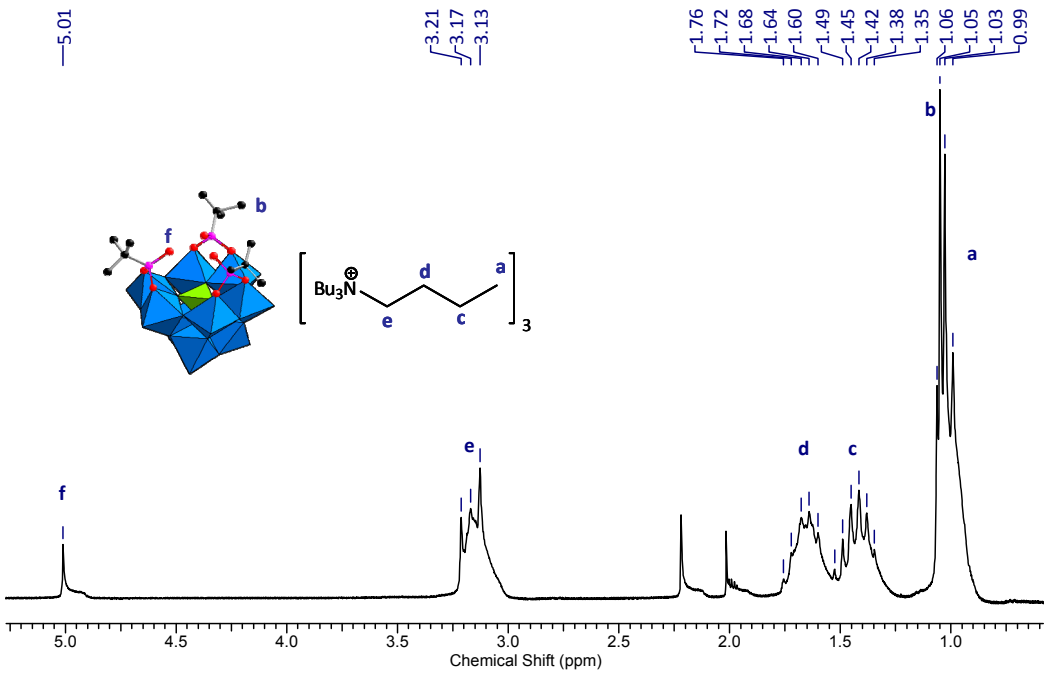

Figure 8. The ^{1}H NMR (200.13 MHz, CD_3CN) spectrum of compound **3**.

For a complete structural analysis in solution of compound **3**, ^{1}H NMR has been performed in CD_3CN. In addition to the $[nBu_4N]^+$ resonances, the ^{1}H NMR spectrum of **3** (Figure 8) shows also two singlets at 5.01 and 1.05 ppm, assigned to the Si-OH and *t*BuSi moieties respectively. The relative integration of these signals agrees with the formula, that are three *t*BuSiOH groups grafted on a $[PW_9O_{34}]^{9-}$ anion (**2**) and there are three $[nBu_4N]^+$ cations. The presence of a singlet for the 27 protons

of the three *t*Bu groups indicates the equivalence of the 9 methyl groups; this implies a trifold symmetry of the whole anion. These informations are in agreement with literature data.[5]

The "open-structure" anion $[PW_9O_{34}(t\text{BuSiOH})_3]^{3-}$ (**3**) is able to react in acetonitrile or DMF with various $RSiCl_3$ derivatives, to afford heterosilylated hybrid compounds with the general formula $[PW_9O_{34}(t\text{BuSiO})_3(SiR)]^{3-}$ (R = -H (**4**), $-CH=CH_2$ (**5**), $-CH_2-CH=CH_2$ (**6**), $-(CH_2)_4-CH=CH_2$ (**7**)) reported also in the literature.[6] The characterization of those compounds and their formation, respectively, support the reaction pathway shown in **Equation 4**, for the reactivity of trichlorosilanes with trivacant polyoxotungstates.

$$\alpha\text{-A-}[PW_9O_{34}(t\text{BuSiOH})_3]^{3-} + RSiCl_3 \rightarrow \alpha\text{-A-}[PW_9O_{34}(t\text{BuSiO})_3(SiR)]^{3-} + HCl \qquad \textbf{Equation 4}$$

(R = -H (**4**), $-CH=CH_2$ (**5**), $-CH_2-CH=CH_2$ (**6**), $-(CH_2)_4-CH=CH_2$ (**7**))

The structure of the hybrid anion is built up by the trivacant α-A-Keggin $\{PW_9O_{34}\}$ backbone on which three *t*BuSiO moieties are grafted, the structure being closed by a "capping" Si-R group (**Figure 9**).

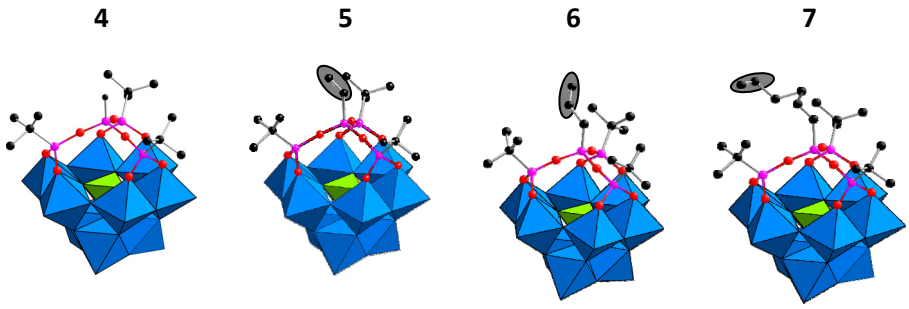

Figure 9. Polyhedral representation of compounds **4**, **5**, **6**, and **7**. Color code: WO_6 octahedron, blue; PO_4 tetrahedron, green; organic Si, pink; C, black; O, red. The double bond is underlined by the circled area.

The characteristic vibration bands in the spectrum for the capped heterosilylated derivatives $(NBu_4)_3[PW_9O_{34}(t\text{BuSiO})_3(SiH)]$ ($(NBu_4)_3$-**4**), $(NBu_4)_3[PW_9O_{34}(t\text{BuSiO})_3(SiCH=CH_2)]$ ($(NBu_4)_3$-**5**),

[6] D. Agustin, C. Coelho, A. Mazeaud, P. Herson, A. Proust, R. Thouvenot, Organic-Inorganic Hybrids based on Polyoxometalates. Part 8. Synthesis and Spectroscopic Characterization of the Heterosilylated Anions $[PW_9O_{34}(^t\text{BuSiO})_3(SiR)]^{3-}$ (R = $-CH_3$, $-CH=CH_2$, $-CH_2-CH=CH_2$, $-(CH_2)_4-CH=CH_2$) – X-ray Crystal Structure of $[^n\text{Bu}_4\text{N}]_3[PW_9O_{34}(^t\text{BuSiO})_3(SiCH_2\text{-}CH=CH_2)]$, *Z. Anorg. Allg. Chem.* **2004**, *630*, 2049-2053.

$(NBu_4)_3[PW_9O_{34}(t\text{BuSiO})_3(SiCH_2CH=CH_2)]$ ($(NBu_4)_3$-**6**) and $(NBu_4)_3[PW_9O_{34}(t\text{BuSiO})_3(Si(CH_2)_4CH=CH_2)]$ ($(NBu_4)_3$-**7**) are listed in **Table 3** in comparison with the uncapped derivative (**3**).

Table 3. Infrared data (cm^{-1}) for the silylated compounds derived from $[PW_9O_{34}(t\text{BuSiOH})_3]^{3-}$ anion (**3**).

Compound	ν(C=C)	ν(Si-R)	ν(Si-O-Si)	ν(P-O)	ν(W=O)	ν(W-O-W)	α isomer signature
3	-		-	1100vs 1034w	1003m 969vs 940vs	864vs 835vs 727s	389s 345w
4	-	2200s	1127vs	1095w 1040m	1000w 976vs 957vs	893w 874vs 834s 802vs	-
5	1603w	1278w	1120vs	1086w 1037m	1000m 975s 955s	864vs 810vs 730s	392s 341w
6	1634w	1256vw	1118vs	1092sh 1037m	1000w 975s 958s	864s 813vs 764w 727s	392s 341w
7	1641w	1228vw	1117vs	1082w 1040m	1000w 975s 955vs	867s 813vs 727s	392s 340w

Infrared spectroscopy is a very sensitive method to observe even small modifications in polyoxometalate structure. In the IR spectrum, the two bands at around 1090 and 1035 cm^{-1}, for **4** – **7** are assigned to the P-O stretching modes of the central PO_4 tetrahedron; they lie close to those of the open parent (1100 and 1034 cm^{-1}) in $[PW_9O_{34}(t\text{BuSiOH})_3]^{3-}$ anion (**3**). This suggests that the C_{3v} local symmetry around the phosphorus is retained upon grafting the SiR group (R = -H (**4**), $-CH=CH_2$ (**5**), $-CH_2-CH=CH_2$ (**6**), $-(CH_2)_4-CH=CH_2$ (**7**)). In the 1000-700 cm^{-1} region, corresponding to the W=O and W-O-W stretching modes, most of the bands are shifted to higher wavenumbers in comparison with $[PW_9O_{34}(t\text{BuSiOH})_3]^{3-}$. These high frequency shifts are also characteristic of the saturation of the structure, as a consequence of the grafting of silyl groups. A strong sharp band at about 1120 cm^{-1} which was assigned, with respect to the "open structure" derivative (**3**), to a vibration mode Si-O-Si indicates the grafting of the RSi capping group onto the open anion. In the low-frequency IR spectrum ($\nu < 400$ cm^{-1}) the bands observed at approximately 390 and 340 cm^{-1}, characteristic to the α isomer, suggests that no isomerisation occurs during the synthesis of the "closed structure" derivatives.

For structural analysis in solution, NMR measurements have been performed in acetonitrile or acetone solution. For all the capped species, compounds **5 – 7**, the ^{31}P NMR spectrum in acetone D6 solution presents one resonance at δ = -16.4 ± 0.1, shifted to low frequency with respect to that of the precursor (**3**) (δ = -15.6) (Table 4), in agreement with the saturation of the framework. All these features indicate that grafting of the RSi capping group onto the open anion does not affect markedly the structure of the organic-inorganic backbone, which keeps its trifold symmetry.

Table 4. ^{31}P NMR (300 MHz, acetone D6) data for the compounds **3**; **5 – 7**.

Compound	**3**	**4**	**5**	**6**	**7**
Chemical shift, δ ppm	-15.76	-16.64	-16.44	-16.45	-16.51

The NMR chemical shifts in the ^{1}H NMR spectra of compounds **4** and **5** are not very different from those of the parent anion **3**. Actually, for **4** and **5** respectively, the signals of the hydroxyl groups from the *t*BuSiOH moieties are missing indicative for the closure of the structure with the SiR group. The proton from Si-H group exhibit one signal at around 4.36 ppm (Figure 10) for compound **4** and at around 6 ppm, the ^{1}H NMR spectrum of compound **5** (Figure 11) exhibit the typical pattern characteristic of the ABX system of the $CH=CH_2$ vinylic group. In all the spectra, the integration of selected signals with respect to those of the tetrabutylammonium cations, $[nBu_4N]^+$, agrees with one SiR fragment for three tetrabutylammonium cations.

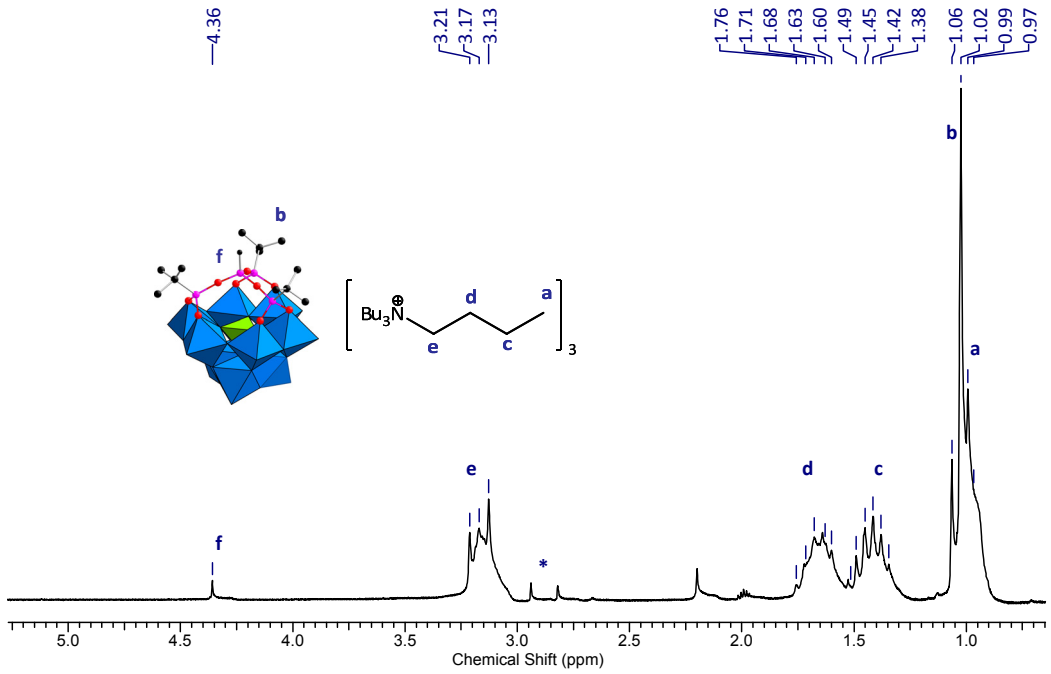

Figure 10. The ^{1}H NMR (200.13 MHz, CD_3CN) spectrum of compound **4** (* = DMF).

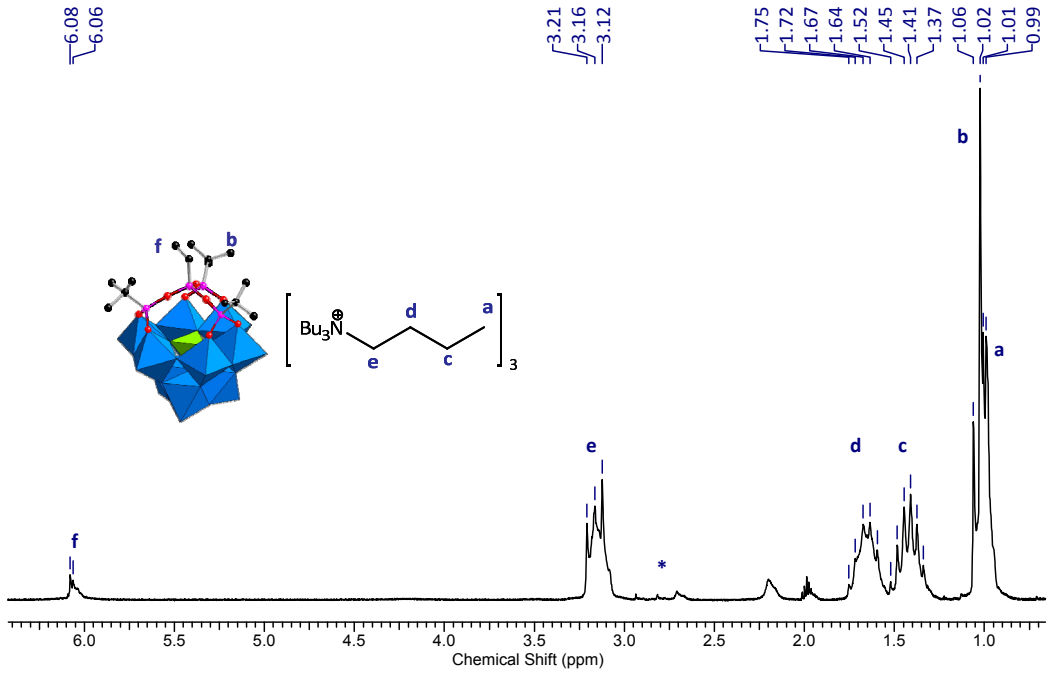

Figure 11. The ^{1}H NMR (200.13 MHz, CD_3CN) spectrum of compound **5** (* = DMF).

Since the list of trichlorosilanes commercially available is to a certain extent limited for double bond ended trichlorosilanes, our attention was focused on trimethoxy-/triethoxysilanes with some

rather interesting functionality like: amino, *p*-aminophenyl, 10-undecenyl, very appealing to this project. The reaction between the open structure anion $[PW_9O_{34}(t\text{BuSiOH})_3]^{3-}$ (**3**) and 10-undecenyltriethoxysilane, *p*-aminophenyltrimethoxysilane to give the isostructural compounds **8** and **9** respectively, didn't take place as expected. The experimental procedure used was the same as for the compounds **4 – 7**, in a few days crystals appeared in the solution, which proved to be the starting compound according to the ^{31}P NMR measurements. It seems that the triethoxy- and trimethoxysilanes are not so reactive in comparison with trichlorosilanes derivatives, so we tried to increase the reactivity of these compounds by adding a base (Bu_4NOH) in the reaction mixture in order to deprotonate the hydroxylic groups from the *t*BuSiOH moieties. The ^{31}P NMR spectra display two signals, the former situated at -15.34 ppm characteristic for the "open-structure" starting compound (**3**) and the latter at around -12 ppm attributed for an unidentified product of degradation of the polyoxometalate framework, as a result of alkalinisation of the reaction mixture. As it can be seen from the ^{31}P NMR spectra (Figure 12) as the quantity of TBAOH added to the reaction mixture is increased, the POM degradation becomes more pronounced.

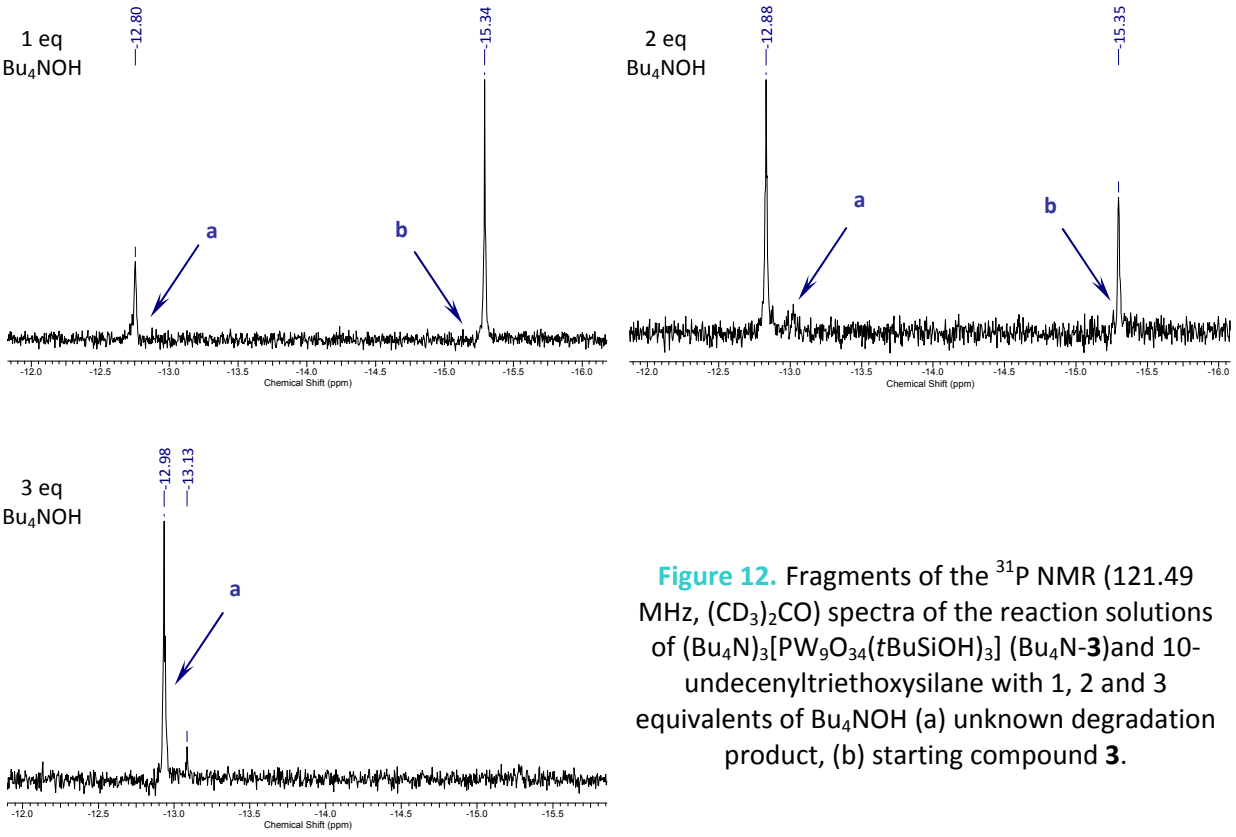

Figure 12. Fragments of the ^{31}P NMR (121.49 MHz, $(CD_3)_2CO$) spectra of the reaction solutions of $(Bu_4N)_3[PW_9O_{34}(t\text{BuSiOH})_3]$ (Bu_4N-**3**)and 10-undecenyltriethoxysilane with 1, 2 and 3 equivalents of Bu_4NOH (a) unknown degradation product, (b) starting compound **3**.

To reach a vast diversity of organic/inorganic hybrid polyoxometalates was an issue very challenging for this work. One approach towards this goal is the synthesis of a "tripod", namely to decorate the {PW_9} framework with three vinyl or allyl organic pendants which are able to connect onto a surface via three vinyl, allyl connectors, respectively. A cartoon representation of such molecule is shown in **Figure 13**. Another approach, as mentioned in the introduction, is to conceal another type of platform, similar to compound **3**, where the *t*BuSiOH moieties are replaced by CH_3CH_2SiOH (*see* **Figure 14** left, **Scheme 3**).

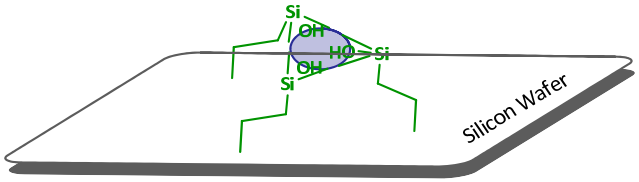

Figure 13. Cartoon representation of a "tripod".

To obtain silylated uncapped hybrid compounds, using the trilacunary Keggin derivative A, α-$K_9PW_9O_{34}{\cdot}16H_2O$ and $RSiCl_3$ (R ≠ *t*Bu, R = -CH=CH_2, -CH_2-CH=CH_2, -CH_2-CH_3) by reacting them in 1:3 molar ratio (**Equation 5**).

$$A\text{-}[PW_9O_{34}]^{9-} + 3RSiCl_3 + 3H_2O \rightarrow [PW_9O_{34}(RSiOH)_3]^{3-} + 6Cl^- + 3HCl \qquad \textbf{Equation 5}$$

R = -CH=CH_2, -CH_2-CH=CH_2, -CH_2CH_3

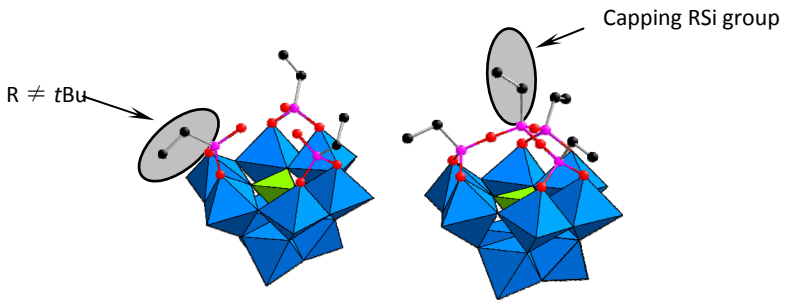

Intermediary $[PW_9O_{34}(RSiOH)_3]^{3-}$ $[PW_9O_{34}(RSiO)_3(RSi)]^{3-}$

Figure 14. Polyhedral representation of compounds with the general formula $[PW_9O_{34}(RSiOH)_3]^{3-}$ (R = -CH=CH_2 (**10'**), -CH_2-CH=CH_2 (**11'**), -CH_2-CH_3 (**12'**)) [7] and $[PW_9O_{34}(RSiO)_3(RSi)]^{3-}$ (R = -CH=CH_2 (**10**), -CH_2-

[7] N.B. – Compound **10'**, **11'** and **12'** are intermediary products which were unattainable in pure state.

$CH=CH_2$ (**11**), $-CH_2-CH_3$ (**12**)). Color code: WO_6 octahedron, blue; PO_4 tetrahedron, green; organic Si, pink; C, black; O, red.

To achieve the α-A-$[PW_9O_{34}(RSiOH)_3]^{3-}$ homosilylated derivatives we reconsidered the synthesis conditions and we tried to control the reactivity of trichlororganosilanes $RSiCl_3$. The α-A-{PW_9} and the $RSiCl_3$ were reacted in a 1:3 molar ratio in an anhydrous acetonitrile solution. Actually, the formation of the capped species $[PW_9O_{34}(RSiO)_3(RSi)]^{3-}$ takes place in two steps: i) the chemical grafting of three {RSi} groups onto the trivacant structure leading to the formation of the "open-structure" (**Equation 6**), followed by: ii) the closing of the structure with a fourth {RSi} group (**Equation 7**). We tried to stop the reaction after the first step by a controlled alcalinisation of the reaction mixture adding an NBu_4OH methanolic solution (tetra-*n* butylammonium hydroxide).

$$\alpha\text{-A-}[PW_9O_{34}]^{9-} + 3RSiCl_3 + 3H_2O \rightarrow \alpha\text{-A-}[PW_9O_{34}(RSiOH)_3]^{3-} + 3HCl + 6Cl^- \qquad \textbf{Equation 6}$$

$$\alpha\text{-A-}[PW_9O_{34}(RSiOH)_3]^{3-} + RSiCl_3 \rightarrow \alpha\text{-A-}[PW_9O_{34}(RSiO)_3(RSi)]^{3-} + 3HCl \qquad \textbf{Equation 7}$$

($R \neq t$Bu, R = $-CH=CH_2$, $-CH_2-CH=CH_2$, $-CH_2-CH_3$)

However, according to ^{31}P NMR spectrum (**Figure 15**) we didn't succeed to obtain a pure compound but a mixture of capped and uncapped species. In some cases we observed many signals in ^{31}P NMR spectrum which means that alkalinisation of the reaction medium is responsible for partial degradation of the polyoxometalate.

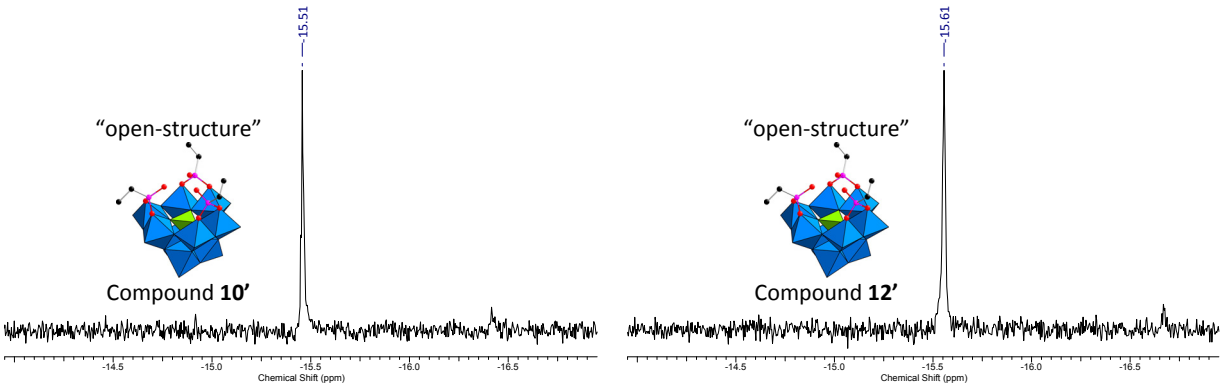

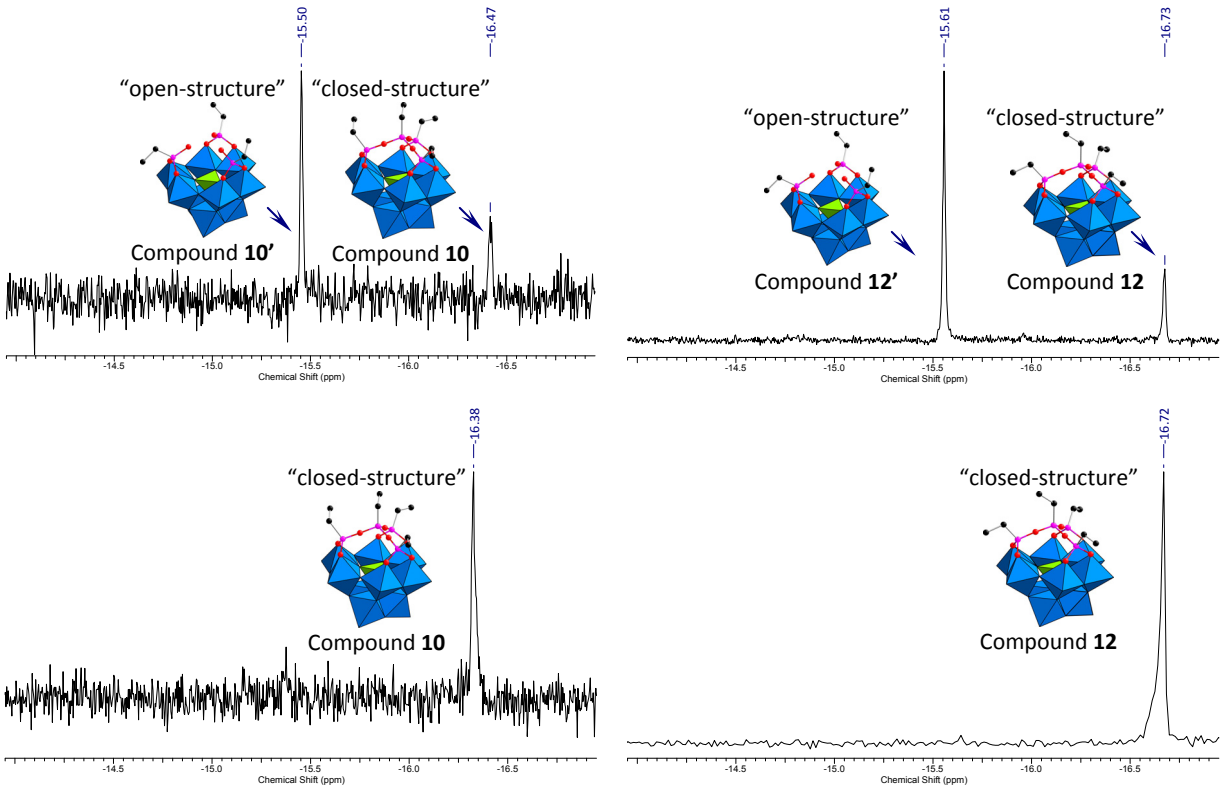

Figure 15. The ^{31}P NMR (121.49 MHz, $(CD_3)_2CO$) monitoring of the evolution towards capped species of the compounds **10** and **12**.

We reduced the reaction time to one hour and then to half an hour without adding TBAOH. After half an hour from the moment when the reaction was started, the ^{31}P NMR spectrum showed that the uncapped species were major species and the reaction mixture was set aside for crystallization. After a few days, when the crystals appeared, the ^{31}P NMR spectrum of the same solution showed evolution towards the capped ones. It appears then very difficult to obtain the pure uncapped species with non bulky R group (R ≠ *t*Bu).

The capped species with vinyl and allyl groups, namely compound **10** and **11** respectively, can be useful to our project and it can be obtained pure in large scale by recrystallisation. On the other hand, the investigation of compound **12** was abandoned since it presents no interest to our purpose. Compounds **10** and **12** were already reported in the literature by the group of Wang; [8, 9] they were

[8] J. Niu, M. Li, J. Wang, Organosilyl derivatives of trivacant tungstophosphate of general formula α-A-$[PW_9O_{34}(RSiO)_3(RSi)]^{3-}$. Synthesis and structure determination by X-ray crystallography, *J. Organomet. Chem.* **2003**, *675*, 84-90.

obtained from the trivacant polyoxotungstate β-A-$[PW_9O_{34}]^{9-}$ anion. It seems that the incorporation of the RSiO groups (R = -CH=CH_2, -CH_2-CH_3) into lacunary Keggin polytungstate structure induced a β→α isomerisation of the $PW_9O_{34}^{9-}$ structure.

For all capped species the ^{31}P NMR spectrum in CD_3CN solution presents one resonance at δ = -16.7, shifted to low frequency with respect to that of the uncapped species δ = - 15.6, in agreement with the saturation of the framework (Table 5).

Table 5. ^{31}P NMR (300 MHz, acetone D6) data for the compounds **10** – **12**.

Compound	**10**	**11**	**12**
Chemical shift, δ ppm	-16.38	-16.12	-16.72

Infrared spectroscopy spectra of compounds **10** and **11**, respectively reveals important information about the modification of the polyanion structure. In the range 1200-200 cm^{-1}, both compounds exhibit a spectrum similar to, but slightly different from that of the $[PW_9O_{34}]^{9-}$ precursor. The two bands assigned to P-O vibrations of the central PO_4 tetrahedron are observed around 1097 and 1037 cm^{-1} for compounds **10** and **11**. In the 1000-700 cm^{-1}, region of the W-O stretchings, the bands are shifted to high wavenumbers, characteristic of the saturation of the structure, as a consequence of the grafting of the four SiR groups (R = -CH=CH_2 (**10**), -CH_2-CH_3 (**11**)). The strong sharp band at 1125 and 1123 cm^{-1}, respectively, is assigned to the μ-oxo bridge Si-O-Si (Table 6).

Table 6. Infrared data (cm^{-1}) for the silylated compounds derived from $[PW_9O_{34}]^{7-}$ anion (**2**).

Compound	**ν(C=C)**	**ν(Si-R)**	**ν(Si-O-Si)**	**ν(P-O)**	**ν(W=O)**	**ν(W-O-W)**	**α isomer signature**
2	-	-	-	1054s 1003m	929vs 909s	821vs 733vs	367s 315w
10	1600w	1276w	1125vs	1097m 1037m	1006m 975vs 960vs	867vs 818vs 730vs	389s 334w
11	1634w	1256w	1123vs	1098m 1036m	1001m 975vs 960vs	868vs 817vs 725s	389s 343w

[9] J. Niu, J. Zhao, J. Wang, M. Li, An organosilyl derivative of trivacant tungstophosphate. Synthesis, characterization and crystal structure determination of α-A-[NBu^n_4][$PW_9O_{34}(C_2H_5SiO)_3(C_2H_5Si)$], *J. Molec. Struct.* **2003**, *655*, 243-250.

2.3.1.2. Electrochemical Behavior in Solution at the Glassy Carbon Electrode

Generally speaking, polyoxometalates can be rapidly reduced reversibly forming so called "heteropoly blue", polyoxometallic species reduced with one and two electrons in the first stages. Subsequently, the reduction process becomes irreversible, simultaneously with the decomposition of the polyoxometalate framework. If the addenda atoms are all identical, the electrons are delocalized on the addenda ion oxide framework at room temperature by rapid electron hopping (intramolecular electron transfer). In the reduction process, the electrons are accepted by the addenda atoms. ***Each electron which is added to an addenda atom, gets into an non-bonding orbital without an important alteration of the M-O bond length, therefore with minor structural changes***. The reduction increases the negative charge density at the heteropolyanions and thus their basicity. As a consequence, the reduction can be accompanied by protonation. The following study was performed in acetonitrile solution where no protonation can occur.

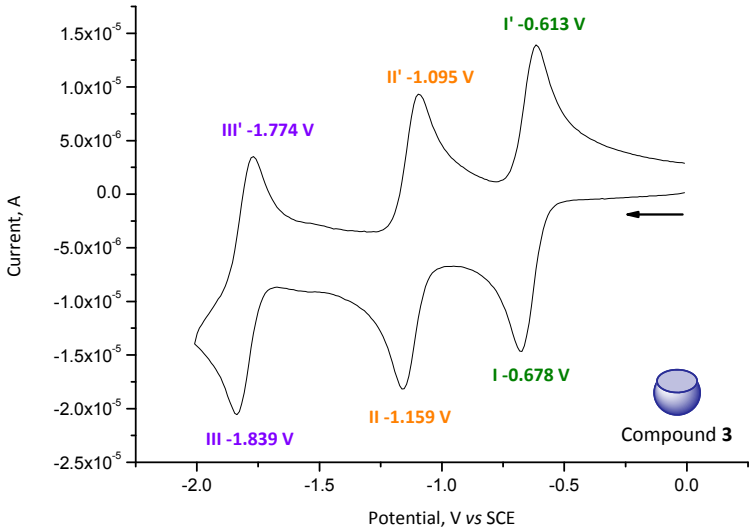

Figure 16. Cyclic voltammogram of compound **3** at glassy carbon electrode. [**3**] = 1×10^{-3} M in acetonitrile with 10^{-1} M Bu_4NBF_4 as supporting electrolyte. Scanning rate: 100 mV/s.

The electrochemical study of the POMs derivatives in solution, undertaken in this section, was done in order to follow the redox behavior of the POMs derivatives in solution and to examine the characteristic signature for each derivative. The electrochemical behavior of organosilyl derivatives was investigated by cyclic voltammetry in acetonitrile at a glassy carbon electrode, by using NBu_4BF_4 as the supporting electrolyte. A comparative study was performed in order to examine the influence

of the silyl groups on the reduction potential values. Figures 16-21 display the typical voltammograms for compounds **3** – **7**, **10** are represented below and the results are summarized in Table 7.

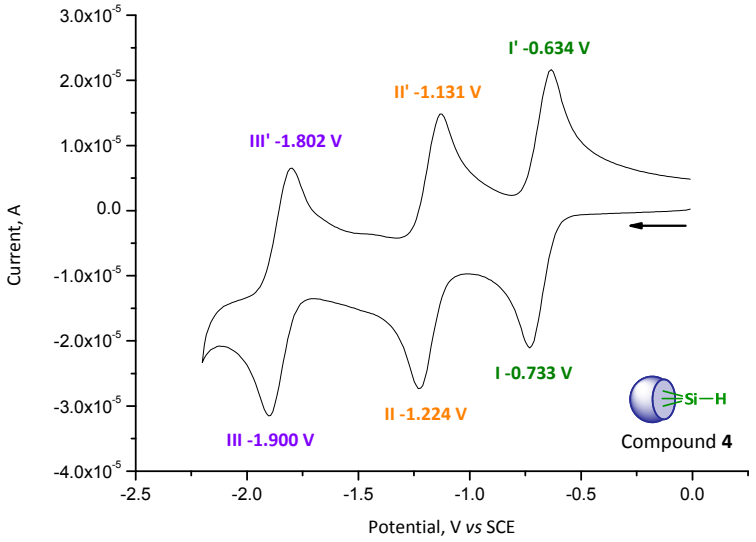

Figure 17. Cyclic voltammogram of compound **4** at glassy carbon electrode. [**4**] = 1 × 10^{-3} M in acetonitrile with 10^{-1} M Bu_4NBF_4 as supporting electrolyte. Scanning rate: 100 mV/s.

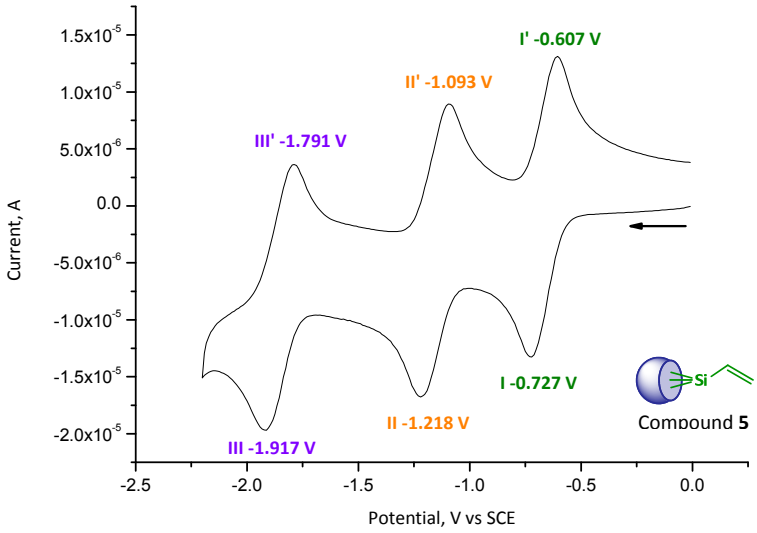

Figure 18. Cyclic voltammogram of compound **5** at glassy carbon electrode. [**5**] = 1 × 10^{-3} M in acetonitrile with 10^{-1} M Bu_4NBF_4 as supporting electrolyte. Scanning rate: 100 mV/s.

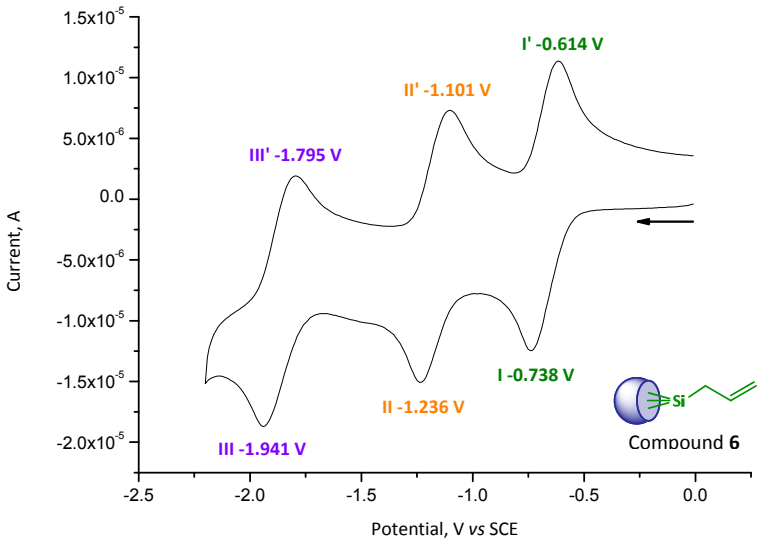

Figure 19. Cyclic voltammogram of compound **6** at glassy carbon electrode. [**6**] = 1 × 10^{-3} M in acetonitrile with 10^{-1} M Bu_4NBF_4 as supporting electrolyte. Scanning rate: 100 mV/s.

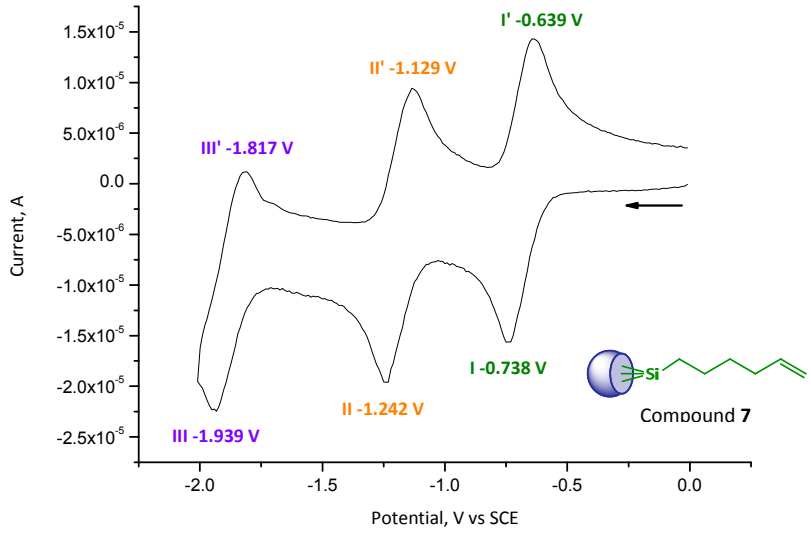

Figure 20. Cyclic voltammogram of compound **7** at glassy carbon electrode. [**7**] = 1 × 10^{-3} M in acetonitrile with 10^{-1} M Bu_4NBF_4 as supporting electrolyte. Scanning rate: 100 mV/s.

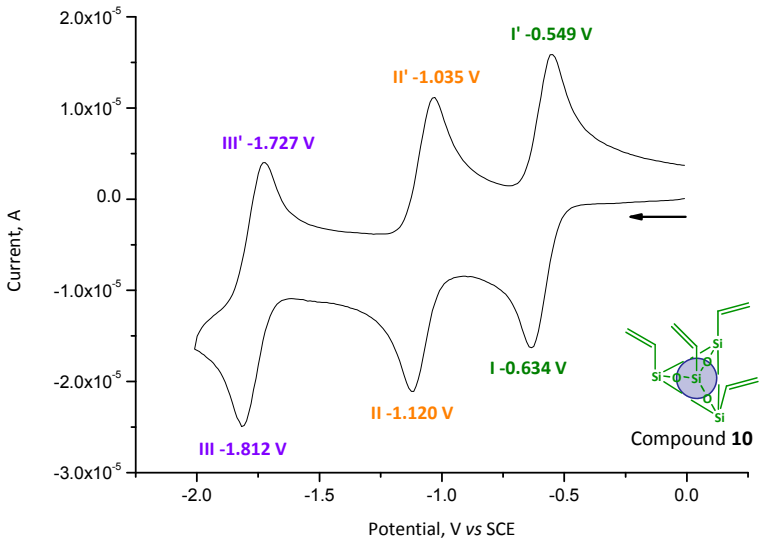

Figure 21. Cyclic voltammogram of compound **10** at glassy carbon electrode. [**10**] = 1×10^{-3} M in acetonitrile with 10^{-1} M Bu_4NBF_4 as supporting electrolyte. Scanning rate: 100 mV/s.

Table 7. Representative cyclic voltammetric data for compounds **3 – 7** and **10** *vs* SCE electrode.

Compounds[a]	$E(I)^b(\Delta E(I))^c$	$E(II)^b(\Delta E(II))^c$	$E(III)^b(\Delta E(III))^c$
3	-0.645 V (65 mV)	-1.127 V **(64 mV)**	**-1.806 V (65 mV)**
4	-0.683 V(99 mV)	-1.177 V(93 mV)	-1.851 V(98 mV)
5	-0.667 V (120 mV)	-1.155 V (125 mV)	-1.854 V (126 mV)
6	-0.676 V (124 mV)	-1.168 V (135 mV)	-1.868 V (146 mV)
7	-0.688 V (99 mV)	-1.185 V (113 mV)	-1.878 V (122 mV)
10	-0.591 V (85 mV)	-1.077 V (85 mV)	-1.769 V (85 mV)

[a] [POM] = 1×10^{-3} M in acetonitrile with 10^{-1} M Bu_4NBF_4 as supporting electrolyte.
[b] $E(i) = 1/2\ (E(i)_{ox} + E(i)_{red})$
[c] $\Delta E(i) = E(i)_{ox} - E(i)_{red}$

Between 0 and -2.5 V, three monoelectronic reduction waves at equal height are observed for all the compounds in the negative potential and they are assigned to tungsten-centered single electron processes. With the exception of compound **4**, the reduction potentials are slightly dependent on the nature of the organic fragment grafted on the $[PW_9O_{34}]^{9-}$ unit and they are slightly shifted towards more negative values as the length of the SiR capping group increases.

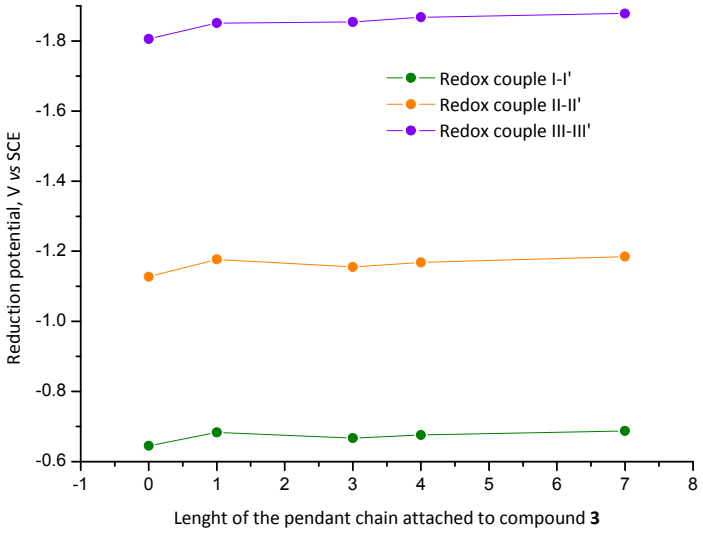

Figure 22. Reduction potential values as a function of the length of the pendant chain attached to the platform **3**.

Figure 22 displays the dependence of the reduction potential values *vs.* the length of the pendant chain attached to the compound **3**. From this representation one can conclude that with the increase of the length of the chain, the polyoxotungstate framework becomes slightly more difficult to reduce. This assumption is valid for all three redox couples. At one end is situated compound **10**, with four $SiCH=CH_2$ groups attached to the $\{PW_9\}$ unit, the easiest to reduce, has its reduction potentials situated at -0.591, -1.077, and -1.769 V, respectively. At the other end compound **7**, with three *t*BuSiO and one $Si(CH_2)_4CH=CH_2$ is the most difficult to reduce, and its reduction potentials situated at -0.688, -1.185, and 1.878 V, respectively. The only derivative that doesn't follow this tendency is compound **4**, which includes three *t*BuSiO groups and one capping group SiH. Its reduction potentials are positioned between the reduction potentials of compounds **6** and **7**, with pendant chains $SiCH_2$-$CH=CH_2$ and $Si(CH_2)_4CH=CH_2$ respectively.

For the $[PW_9O_{34}(t\text{BuSiO})_3SiR]^{3-}$ the variation of the reduction potential values shift follows the trend of the R moiety hexenyl > allyl > vinyl and shifts the reduction potential towards more negative values.

2.3.2. Synthetic Routes for *Organogermyl Derivatives*

We have achieved the synthesis of silyl derivatives of POMs, however to reach new functions we are limited by the commercially available silane derivatives. Since the triethoxy- and trimethoxysilanes do not react readily with compound **3** (*see* **Scheme 2**), we turned to another chemistry also well developed by the Paris 6 "Chimie Inorganique et Matériaux Moléculaires" laboratory. The incorporation of organic groups into polyoxometalate structures is easily achieved, for example by reaction of $RGeCl_3$ with appropriate monolacunary anions. These reactions results in polyoxoanions in which $(O)_5WO^{4+}$ octahedron is replaced by a $(O)_5GeR^{3+}$ unit. The stability of the M-carbon bonds towards hydrolysis makes the resulting polyoxometalate derivatives particularly suitable for further derivatization.

The $[PW_9O_{34}(t\text{BuSiOH})_3]^{3-}$ (**3**) is able to react cleanly with organogermyl fragments of the type $RGeCl_3$, to give $[PW_9O_{34}(t\text{BuSiO})_3Ge(CH_2)_2CO_2H]^{3-}$ (**14**) anion. A subsequent coupling with propargylamine afforded $[PW_9O_{34}(t\text{BuSiO})_3Ge(CH_2)_2CONHCH_2\text{-}C{\equiv}CH]^{3-}$ (**15**) anion which is able to react further with a iodotriazene (**16**) to give compound (**17**) $[PW_9O_{34}(t\text{BuSiO})_3Ge(CH_2)_2CONHCH_2\text{-}C{\equiv}C\text{-}C_6H_4\text{-}N_3Et_2]^{3-}$ (**Scheme 5**). Whereas trichlorosilanes react with monovacant POMs α-$[XW_{11}O_{39}]^{n-}$ to yield disubstituted hybrid anions of the type α-$[XW_{11}O_{39}\{O(SiR)_2\}]^{(n-4)-}$,[10] the corresponding reaction with trichloro-germanes give monosubstituted derivatives of the type α-$[XW_{11}O_{39}(GeR)]^{(n-3)-}$. Thus, organogermyl derivatives $[PW_{11}O_{39}Ge(CH_2)_2CO_2H]^{4-}$ (**21**) by reaction of $(NBu_4)_4[H_3PW_{11}O_{39}]$ with $Cl_3Ge(CH_2)_2CO_2H$ in homogeneous conditions, and then $[PW_{11}O_{39}Ge(CH_2)_2CONHCH_2C{\equiv}CH]^{4-}$ (**22**) by subsequent coupling with propargylamine, were prepared (**Scheme 6**). The tetramethylammonium salt of $[PW_{11}O_{39}Ge(CH_2)_2CO_2H]^{4-}$ has already been reported; it was obtained from $K_7[PW_{11}O_{39}]\cdot 13H_2O$.[11]

To afford the diazonium ended function on a polyoxometalate structure, the ethynyl ended compound **15** was reacted with 4-iodophenyl triazene/ 4-iodoaniline, to give compounds **17** and **20**, respectively, in a Pd-catalyzed Sonogashira reaction. The first Pd-catalyzed coupling reaction was demonstrated for the first time, on a iodo-functionalized hexamolybdate with ethynylarenes, by the group of Peng.[12] However, to the best of my knowledge this is the first Sonogashira coupling

---

[10] A. Proust, R. Thouvenot, P. Gouzerh, Functionalization of polyoxometalates: towards advanced applications in catalysis and material science, *Chem. Commun*. **2008**, 1837-1852.

[11] J. Li, R. Tan, R. Li, X. Wang, E. Li, F. Zhai, S. Zhang, Syntheses, properties and biological activity of organogermanium substituted heteropolytungstates, *Inorg. Chem. Commun.* **2007**, *10*, 216-219.

[12] B. Xu, Y. Wei, C. L. Barnes, Z. Peng, Hybrid Molecular Materials Based on Covalently Linked Inorganic Polyoxometalates and Organic Conjugated Systems, *Angew. Chem. Int. Ed.* **2001**, *40*, 2290-2292.

demonstrated on a Keggin polyoxometalate. The first attempts to obtain compound **20** (*see* Scheme 5) proved that the reaction was not 100% complete towards coupling with 4-iodoaniline, but I am confident that this compound can be obtained in pure state. Our attention was focused on the preparation of compound **17**, since it offers a protected diazonium group.

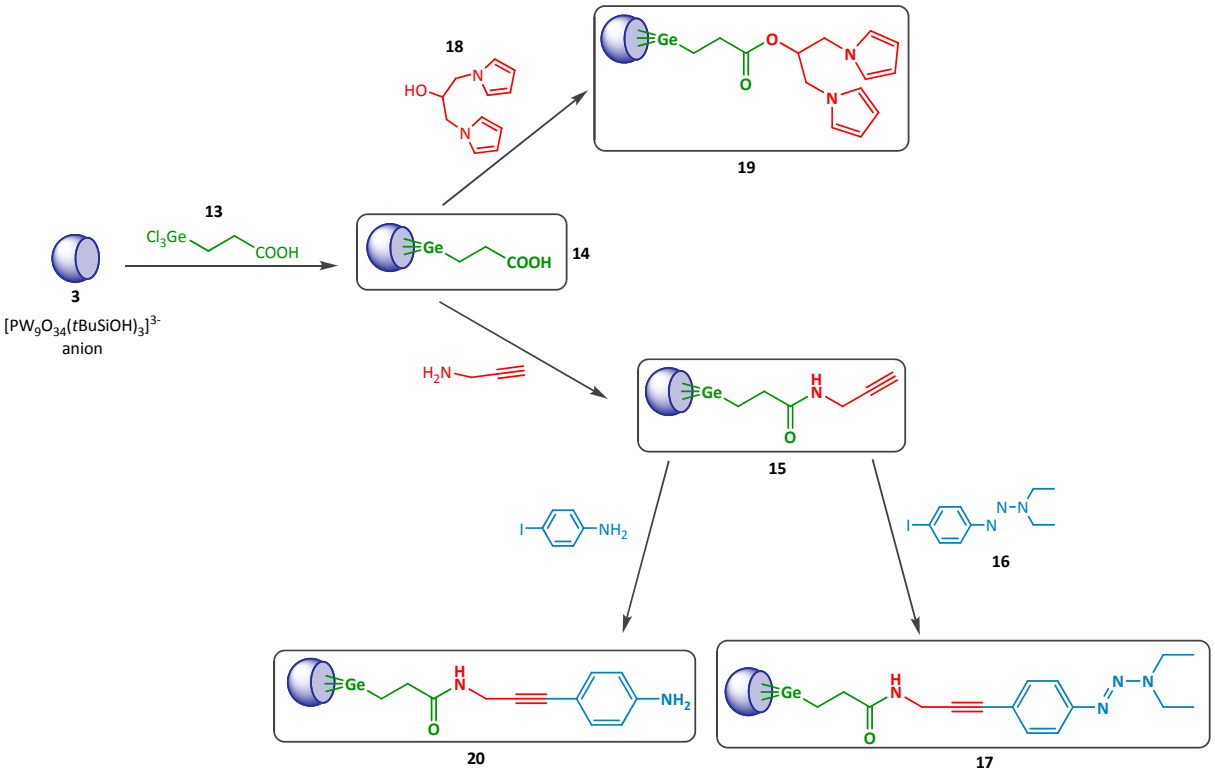

Scheme 5. Synthetic routes for organogermyl compounds derived from $[PW_9O_{34}(t\text{BuSiOH})_3]^{3-}$ anion.

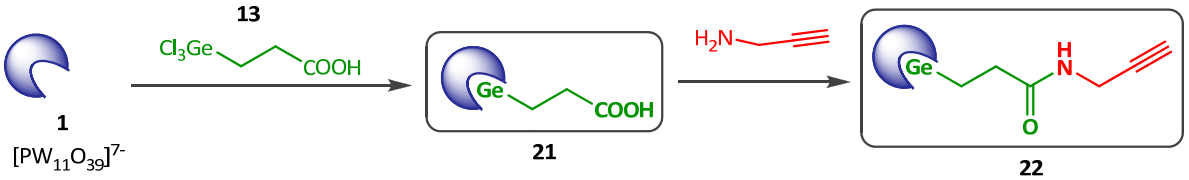

Scheme 6. Synthetic routes for organogermyl compounds derived from $[PW_{11}O_{39}]^{7-}$ anion.

2.3.2.1. Spectroscopic Characterization

The spectroscopic characterization of compounds **14**, **15**, **21** and **22** is depicted in details in *Appendix*.

The IR spectra of compounds **14**, **15**, **17** and **19** are represented in Figure 23, Figure 24, Figure 25 and Figure 26, respectively. Their main bands and their assignments together with those of reference compound (**3**) are presented in Table 8.

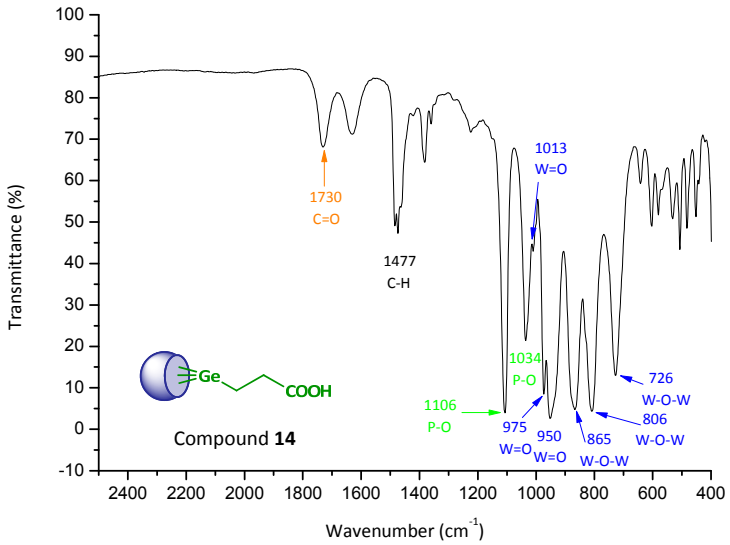

Figure 23. The IR spectrum of the $[PW_9O_{34}(t\text{BuSiO})_3Ge(CH_2)_2CO_2H]^{3-}$ anion (**14**).

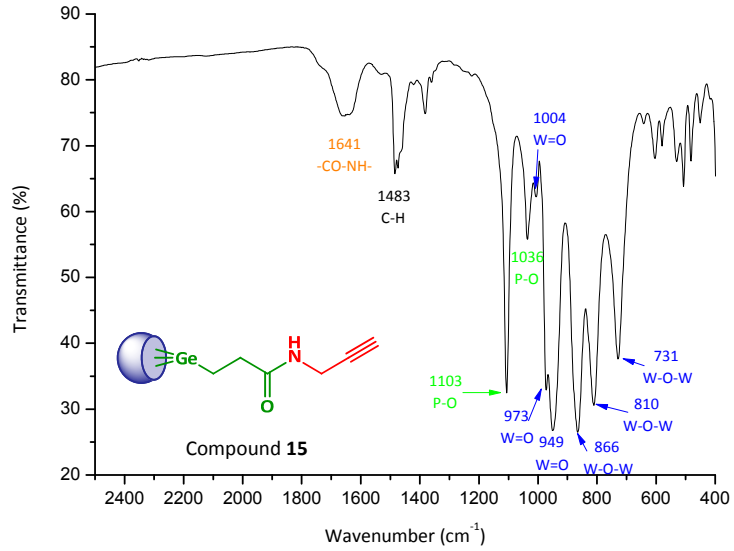

Figure 24. The IR spectrum of the $[PW_9O_{34}(t\text{BuSiO})_3Ge(CH_2)_2CONHCH_2\text{-}C{\equiv}CH]^{3-}$ anion (**15**).

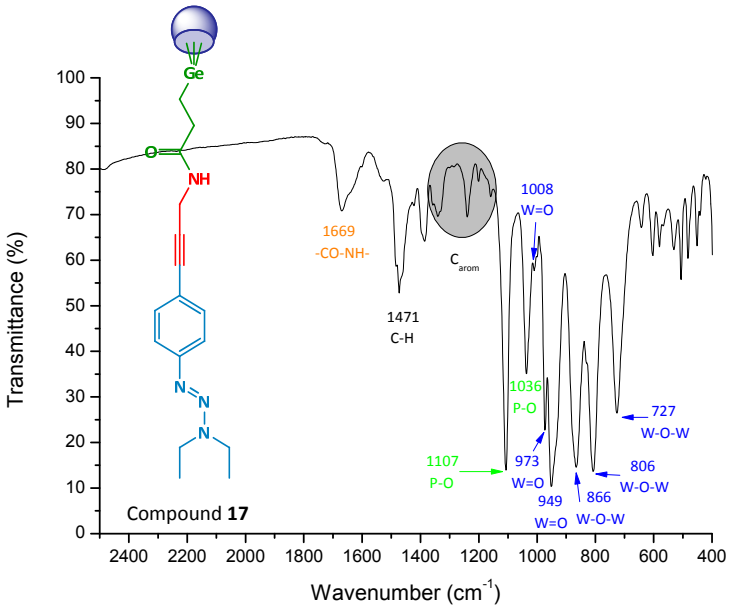

Figure 25. The IR spectrum of the $[PW_9O_{34}(t\text{BuSiO})_3Ge(CH_2)_2CONHCH_2\text{-}C{\equiv}C\text{-}C_6H_4\text{-}N_3Et_2]^{3-}$ anion (**17**).

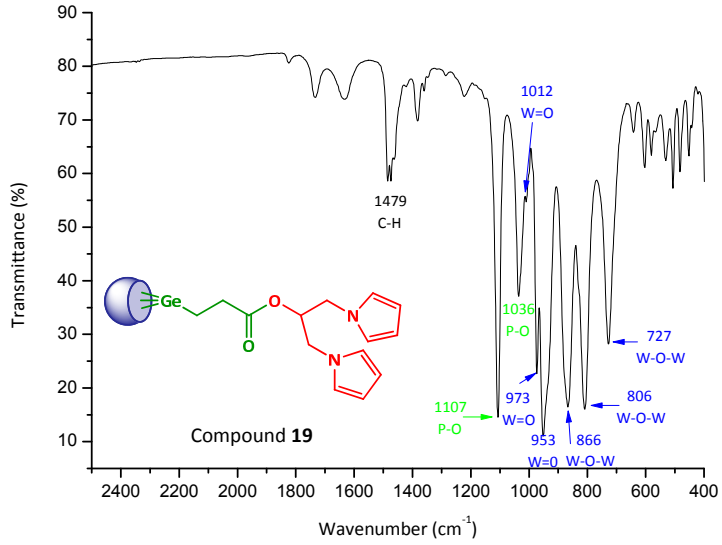

Figure 26. The IR spectrum of the $[PW_9O_{34}(t\text{BuSiO})_3Ge(CH_2)_2COOCH(CH_2Py)_2]^{3-}$ anion (**19**).

In the range 1200-400 cm^{-1}, all compounds exhibit a spectrum similar to that of the precursor which is $[PW_9O_{34}(t\text{BuSiOH})_3]^{3-}$ anion (**3**). In the stretching vibration part, a shift to higher wavenumbers indicates stabilization of the polyoxometalate framework, which becomes saturated by grafting the organogermyl groups. Relative to the $[PW_9O_{34}(t\text{BuSiO})_3(CH_2)_2CO_2H]^{3-}$, compounds **15**, **17** and **19** display no changes in the W-O stretching region, since the $\{PW_9\}$ backbone is not modified

during derivatization, the chemical transformation occurred far enough to the inorganic skeleton. Moreover, a band at 1730 cm^{-1} assigned to the ν(C=O) stretching vibrations from the carboxylic group of **14**, disappears in the IR spectrum of **15**, simultaneously with the apparition of two new bands of ν(C(O)NH) at 1641 cm^{-1} and ν(≡C-H) at 3312 cm^{-1} (**Figure 27**).

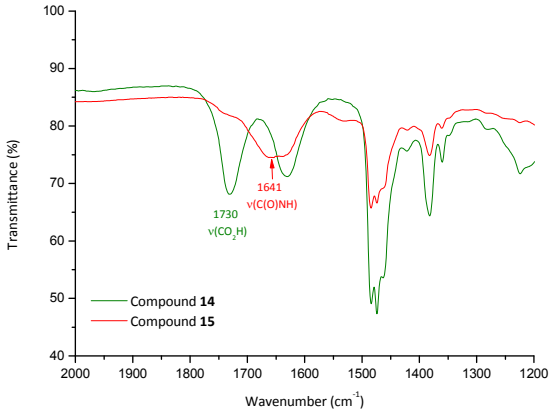

Figure 27. Fragment of the overlaid infrared spectra of compounds **14** and **15**.

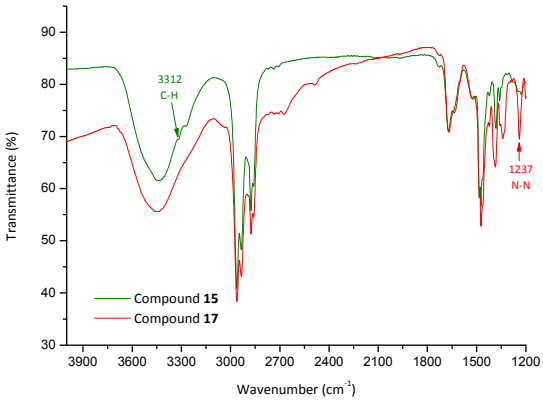

Figure 28. Fragment of the overlaid infrared spectra of compounds **15** and **17**.

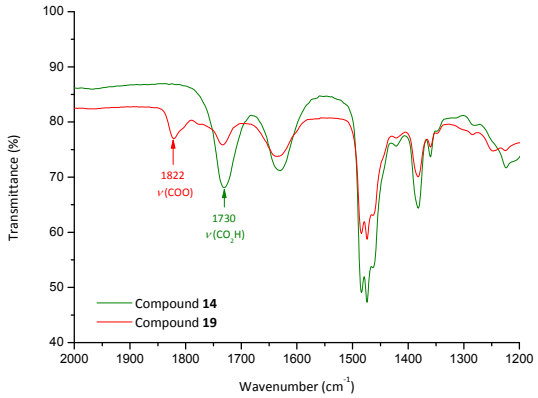

Figure 29. Fragment of the overlaid infrared spectra of compounds **14** and **19**.

For **17** the absence of ν(≡C-H) band at 3312 cm^{-1}, simultaneously with the occurrence of ν(N-N) at 1238 cm^{-1} (**Figure 28**) is indicative of the coupling between the -C≡CH ended group of **15** and iodotriazene **16**. The ν(N=N) stretching vibration band position, from the triazene moiety, expected at 1416 cm^{-1} could not be identified and it is probably hidden under ν(C-H) stretching vibrations of the *t*Bu group. A weak band in the IR spectrum of compound **19**, at 1822 cm^{-1} can be assigned to the ν(CO-O) stretching modes. However, since the band characteristic of carboxylic group of **14** has not completely disappeared, one can assume that the reaction was not complete and compound **19** is

impurified with the starting compound **14** (Figure 29). Nevertheless further spectroscopic investigations were performed to ensure these assumptions.

Table 8. Infrared data (cm^{-1}) for the germyl compounds derived from $[PW_9O_{34}(t\text{BuSiOH})_3]^{3-}$ anion (**3**).

Compound	ν(≡C-H)	ν(COO)	ν(C=O)	ν(CO-NH)	ν(N-N)[13]	ν(P-O)	ν(W=O)	ν(W-O-W)
3	-	-	-	-	-	1100vs 1034w	1003m 969vs 940vs	864vs 835vs 727s
14	-	-	1730w	-	-	1106vs 1034s	1013w 975vs 950vs	865vs 806vs 727s
15	3312w	-	-	1653w	-	1103vs 1036m	1004w 973vs 949vs	866vs 810vs 731s
17	-	-	-	1669w	1238w	1107vs 1036s	1008w 973s 949vs	866vs 806vs 727s
19	-	1822w	1730w	-	-	1107vs 1036s	1012w 973s 953vs	866vs 806vs 727s

The formation of $[PW_9O_{34}(t\text{BuSiO})_3Ge(CH_2)_2CO_2H]^{3-}$ (**14**) by reaction of $[PW_9O_{34}(t\text{BuSiOH})_3]^{3-}$ (**3**) with $Cl_3Ge(CH_2)_2CO_2H$ is conveniently monitored by ^{31}P NMR spectroscopy: the signal of **14** (δ = -16.34 ppm) is shifted to low frequency by ca. 0.5 ppm with respect to that of the "open-structure" platform $[PW_9O_{34}(t\text{BuSiOH})_3]^{3-}$ (δ = -15.9 ppm), which is consistent with a closed, *i.e.* capped structure.

The ^1H NMR spectrum of **14** (Figure 30) exhibits the four multiplets from the tetrabutylammonium cations and three signals of the hybrid anion, *i.e.* one singlet at 0.99 ppm (*t*Bu) and two AA'XX' complex multiplets centered at 2.57 and 1.55 ppm, which are assigned to the methylene groups adjacent to CO_2H and Ge respectively. Relative integration of the various multiplets agrees with the chemical formula, *i.e.* three NBu_4^+ cations for one hybrid anion.

[13] F. Zimmermann, TH. Lippert, CH. Beyer, J. Stebani, O. Nuyken, A. Wokaun, N=N Vibrational Frequencies and Fragmentation Patterns of Substituted 1-Aryl-3,3-Dialkyl-Triazene: Comparison with Other High-Nitrogen Compounds, *Appl. Spectroscopy* **1993**, *47*, 986-993.

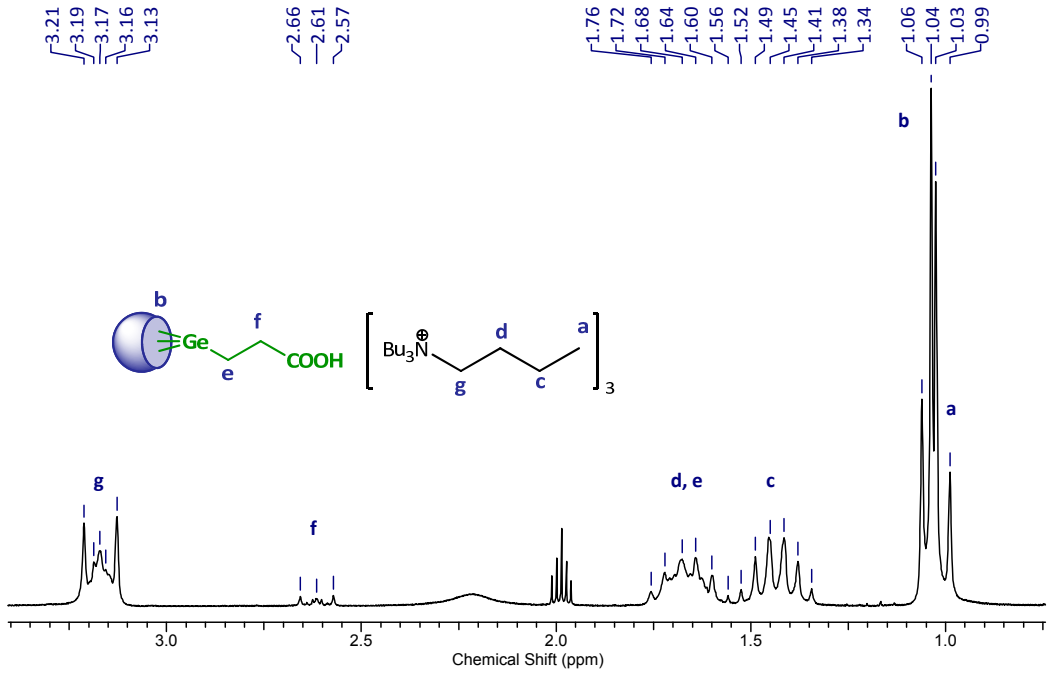

Figure 30. The ^{1}H NMR (200 MHz, CD_3CN) spectrum of compound $(NBu_4)_3$-**14**.

While conversion of **14** into **15** does not shift the ^{31}P NMR signal (δ = -16.35 ppm), since the reaction takes place away from the {PW_9} skeleton, the completion of the amide-coupling reaction can be demonstrated by ^{1}H NMR spectroscopy (**Figure 31**). The amide and ethynyl protons give rise to triplets at 6.69 and 2.42 ppm, respectively, due to coupling with the propargylic protons (complex multiplet, 3.91 ppm). The signals from the *t*Bu groups (singlet, 1.02 ppm) and the methylene groups adjacent to CO and Ge (complex multiplets centered at 2.45 and 1.55 ppm, respectively) are nearly unaffected by the coupling. As for **14**, relative integration of the different multiplets is consistent with the chemical formula, *i.e.* three NBu_4^+ cations for one hybrid anion.

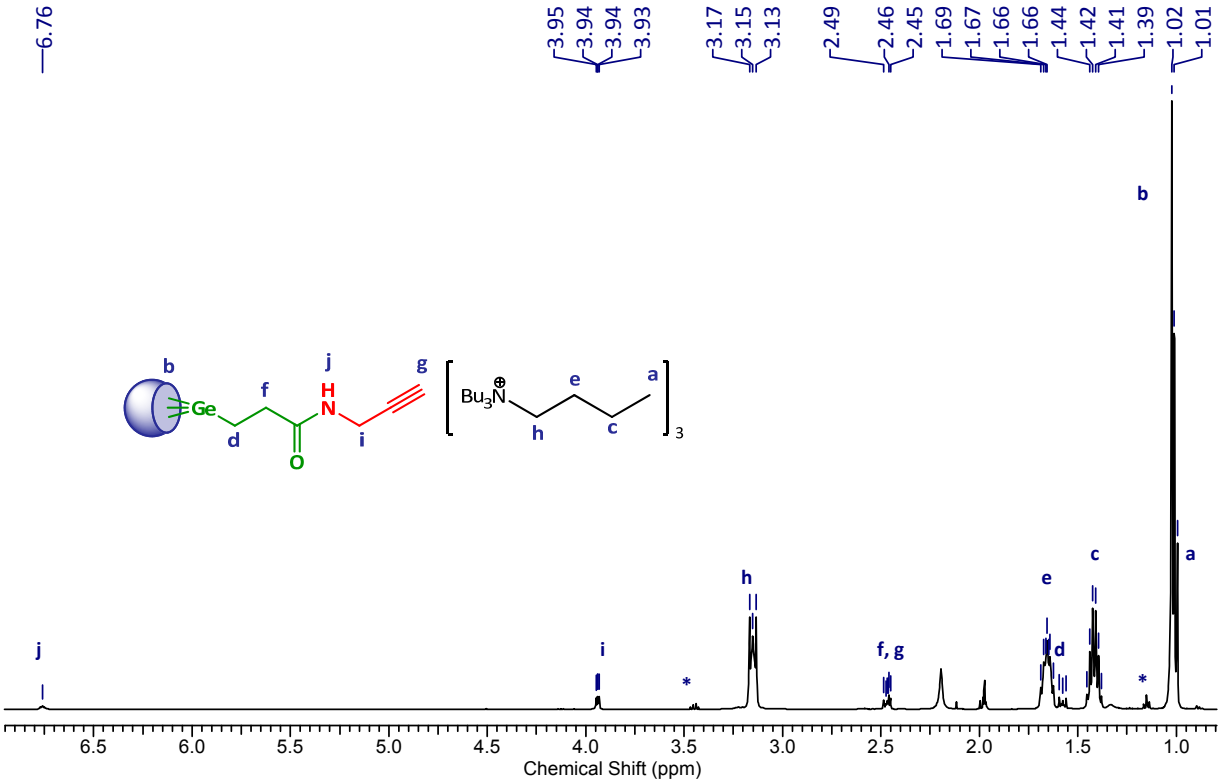

Figure 31. The ^{1}H NMR (500 MHz, CD_3CN) spectrum of compound $(NBu_4)_3$-**15** (* = diethyl ether).

The Sonogashira coupling between compound **15** and 4-iodophenyl triazene to afford compound **17** (*see* Scheme 5), was verified by ^{1}H NMR. In the spectrum of compound **17** (Figure 32) the signal of methylene group, close to NH, becomes a doublet instead of a doublet of doublets at 4.13 ppm. The pseudo doublet at 7.4 ppm arises from the four protons of the aromatic ring (strongly-coupled system) and the quadruplet at 3.8 ppm from the methylene group of the triazene moiety. A strong indication that the coupling took place should be the disappearance of the triplet at approximately 2.4 ppm assigned to the ethynyl proton. However, the absence of the ethynyl protons is not very easy to appreciate, since the signal is so closed the methylene multiplet (adjacent to the CO). Nevertheless, the integration of all these signals agrees with the expected formula, three NBu_4^+ cations for one polyoxometalate anion.

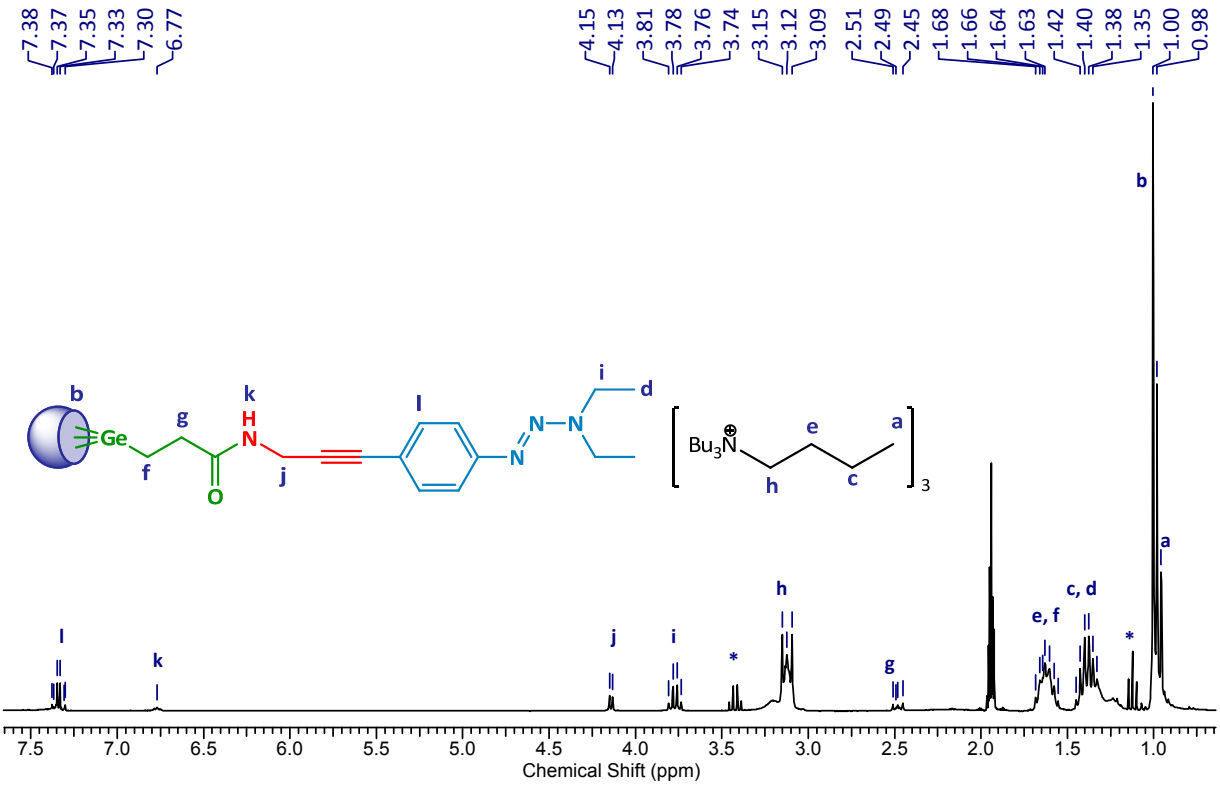

Figure 32. The ^{1}H NMR (300 MHz, CD_3CN) spectrum of compound $(NBu_4)_3$-**17** (* = diethyl ether).

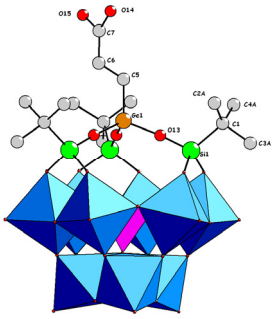

Figure 33. Mixed polyhedral and ball-and-stick representation of $[PW_9O_{34}(t\text{BuSiO})_3Ge(CH_2)_2CO_2H]^{3-}$(**14**).

Crystal structure of $(NBu_4)_3[PW_9O_{34}(t\text{-BuSiO})_3Ge(CH_2)_2CO_2H]\cdot H_2O$ was determined. Colorless crystals of $(NBu_4)_3$-**14**$\cdot H_2O$ were obtained upon slow evaporation of a solution of **14** in DMF in air at room temperature. They belong to the trigonal *R*3c space group. The asymmetric unit contains one tetrabutylammonium cation, one third of the anion, located at a C_3 axis, going through O(11), P(1), Ge(1) and C(5), and a water molecule H-bonded to the carboxylic acid function. A disorder model has been introduced for the $CH_2CH_2CO_2H$ and the *t*-butyl groups. The overall molecular structure of the anion (**Figure 33**) is similar to that of other derivatives of the type α-A-$[PW_9O_{34}(RSiO)_3(RSi)]^{3-}$. The W-O bond lengths fall in the range expected for terminal [1.711(11) to 1.744(11) Å], doubly- [1.871(11) to

1.965(12) Å] and triply-bridging oxo ligands [2.358(10) to 2.402(10) Å]. The Ge(1)-O(13) distance of 1.822(14) Å is consistently longer than the Si(1)-O(13) distance of 1.558(15) Å.

The monolacunary $\{PW_{11}\}$ derivatives react similarly with the $Cl_3Ge(CH_2)_2COOH$ compound to afford compounds **21** (Equation 8) and **22** (Equation 9), consequently.

$$\alpha\text{-}[PW_{11}O_{39}]^{7-} + Cl_3Ge(CH_2)_2COOH \rightarrow \alpha\text{-}[PW_{11}O_{39}\{Ge(CH_2)_2COOH\}]^{4-} + 3Cl^- \quad \text{Equation 8}$$

$$\alpha\text{-}[PW_{11}O_{39}\{Ge(CH_2)_2COOH\}]^{4-} + NH_2CH_2C{\equiv}CH \rightarrow \alpha\text{-}[PW_{11}O_{39}\{Ge(CH_2)_2CO(O)CH_2C{\equiv}CH\}]^{4-} \quad \text{Equation 9}$$

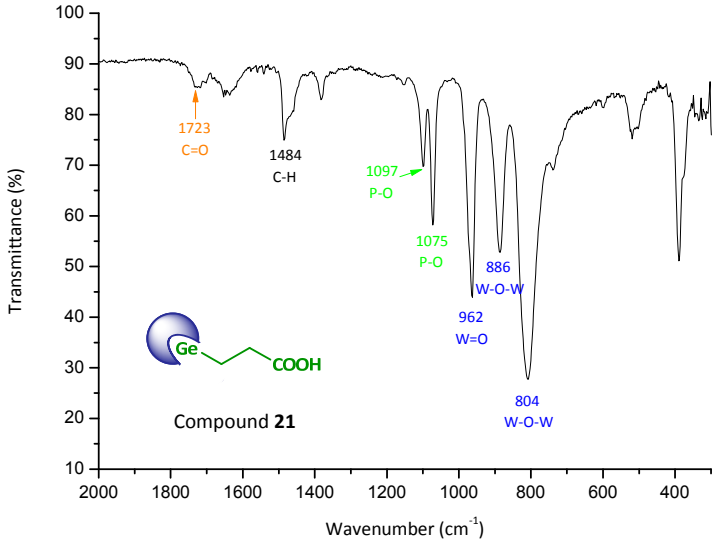

Figure 34. The IR spectrum of the $[PW_{11}O_{39}Ge(CH_2)_2CO_2H]^{4-}$ anion (**21**).

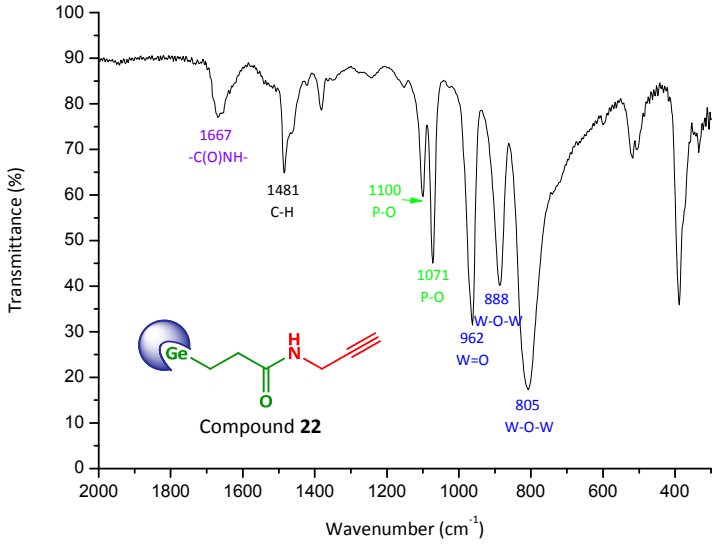

Figure 35. The IR spectrum of the $[PW_{11}O_{39}Ge(CH_2)_2CONHCH_2\text{-}C{\equiv}CH]^{4-}$ anion (**22**).

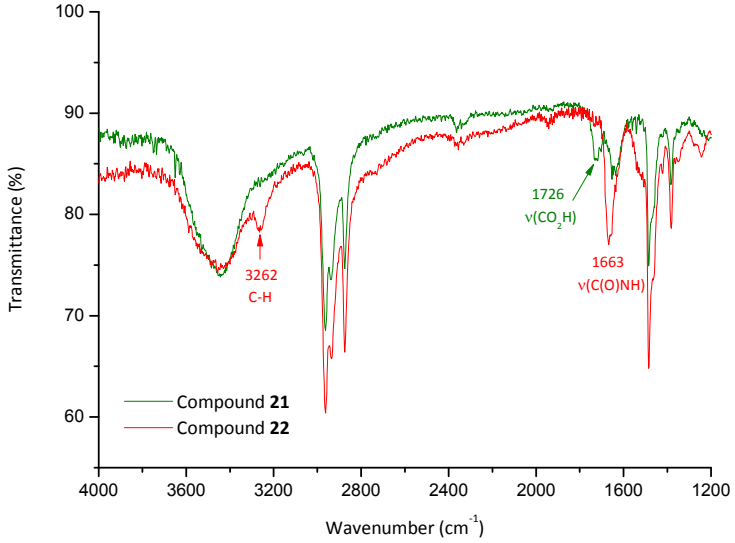

Figure 36. Fragment of the overlaid infrared spectra of compounds **21** and **22**.

Table 9. Infrared data (cm^{-1}) for the germyl compounds derived from $[PW_{11}O_{39}]^{7-}$ anion (**1**).

Compound	ν(≡C-H)	ν(CO-NH)	N(C=O)	ν(P-O)	ν(W=O)	ν(W-O-W)
1	-	-	-	1086m 1043m	952vs	903m 858s 810vs 730vs
21	-	-	1723w	1097m 1075m	962s	886m 804vs
22	3262w	1667w	-	1100m 1071m	962s	888m 805vs

2.3.2.2. Electrochemical Behavior in Solution at the Glassy Carbon Electrode

The electrochemical behavior of germyl derivatives was also investigated in acetonitrile solution at the glassy carbon electrode in comparison with their precursors. The characteristic voltammograms are displayed bellow (**Figure 37**, **Figure 38**, **Figure 39** and **Figure 40**) and their formal potentials of the redox waves are gathered in **Table 10**.

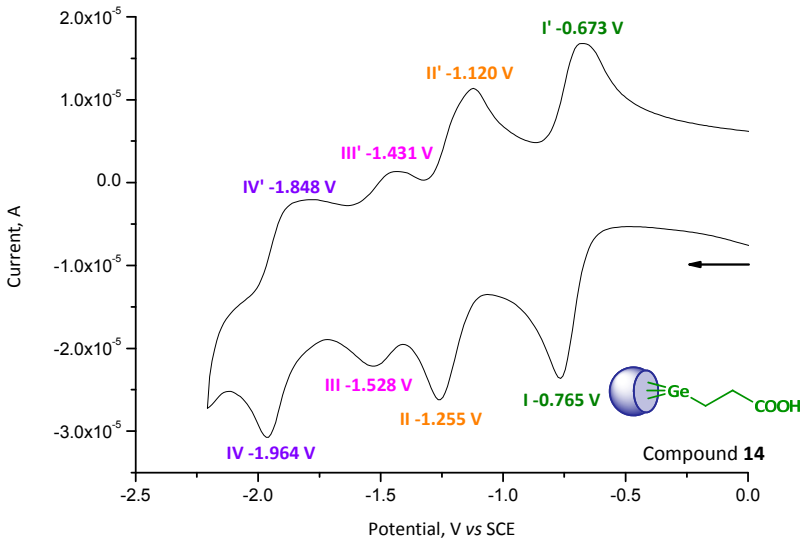

Figure 37. Cyclic voltammogram of compound **14** at glassy carbon electrode. [**14**] = 1 × 10^{-3} M in acetonitrile with 10^{-1} M Bu_4NBF_4 as supporting electrolyte. Scanning rate: 100 mV/s.

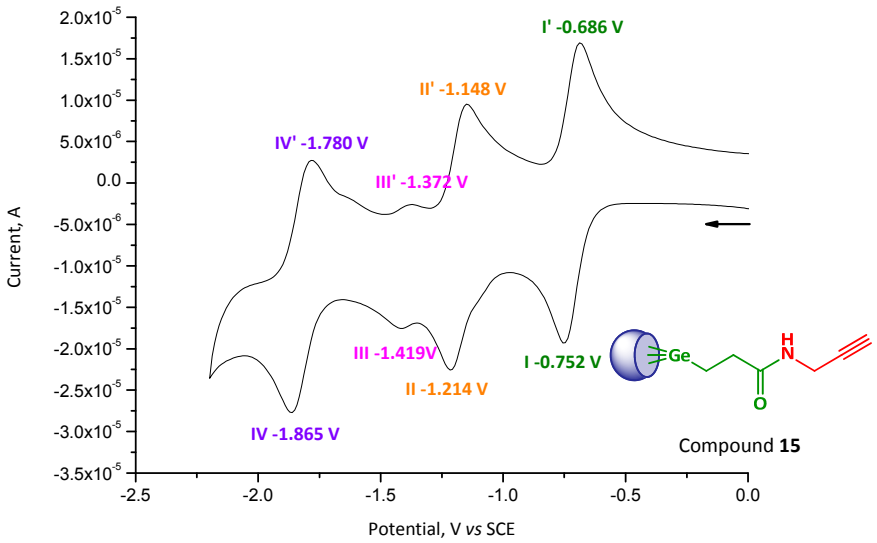

Figure 38. Cyclic voltammogram of compound **15** at glassy carbon electrode. [**15**] = 1 × 10^{-3} M in acetonitrile with 10^{-1} M Bu_4NBF_4 as supporting electrolyte. Scanning rate: 100 mV/s.

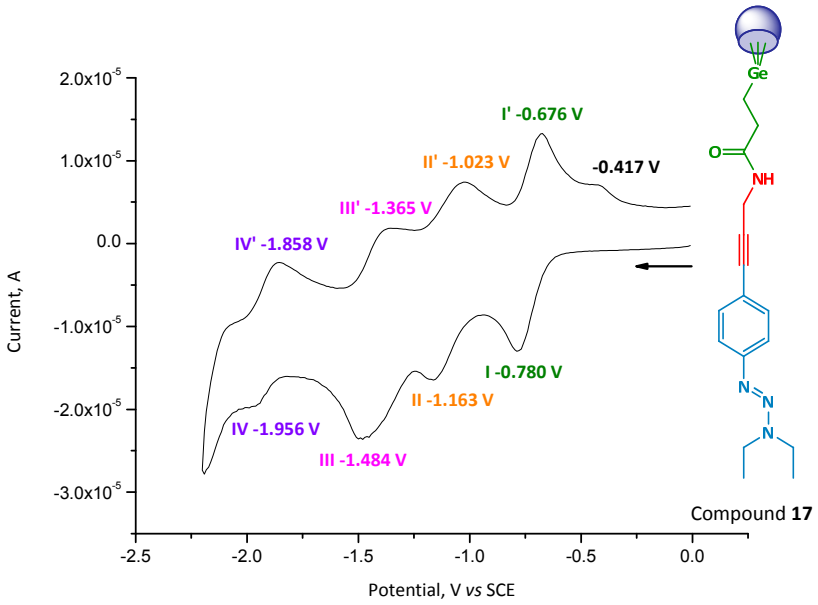

Figure 39. Cyclic voltammogram of compound **17** at glassy carbon electrode. [**17**] = 1 × 10^{-3} M in acetonitrile with 10^{-1} M Bu_4NBF_4 as supporting electrolyte. Scanning rate: 100 mV/s.

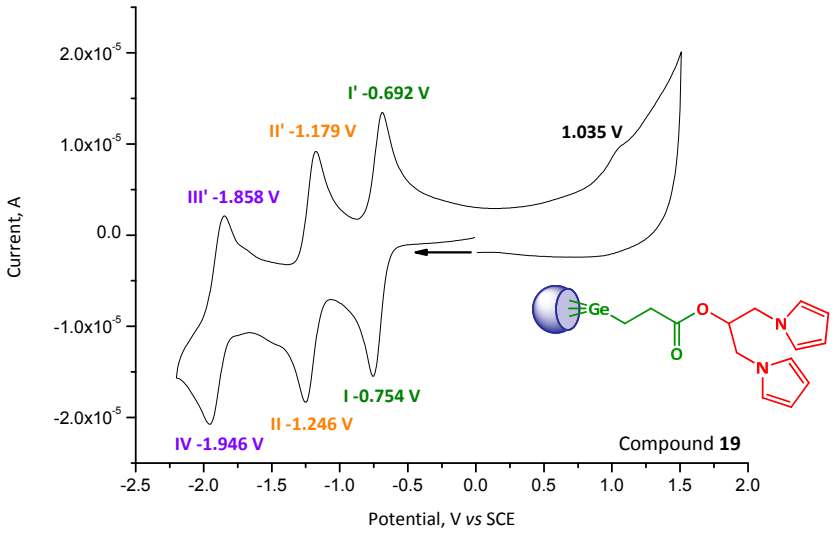

Figure 40. Cyclic voltammogram of compound **19** at glassy carbon electrode. [**19**] = 1 × 10^{-3} M in acetonitrile with 10^{-1} M Bu_4NBF_4 as supporting electrolyte. Scanning rate: 100 mV/s.

Table 10. Representative cyclic voltammetric data *vs* SCE electrode for compound **3**, **14**, **15**, **17** and **19**.

Compounds[a]	E(I)[b](ΔE(I))[c]	E(*II*)[b](ΔE(II))[c]	E(*III*)[b](ΔE(III))[c]	E(*IV*)[b](ΔE(IV))[c]
3	-0.645 V (65 mV)	-1.127 V (64 mV)	-	-1.806 V (65 mV)
14	-0.722 V (92 mV)	-1.189 V (135 mV)	-1.484 V (97 mV)	-1.906 V (116 mV)

15	-0.719 V (66 mV)	-1.181 V (66 mV)	-1.398 V (47 mV)	-1.822 V (85 mV)
17	-0.728 V (104 mV)	-1.093 V (140 mV)	-1.424 V (119 mV)	-1.908 V (98 mV)
19	-0.723 V (62 mV)	-1.212 V (67 mV)	-	-1.902 V (90 mV)

[a] [POM] = 1×10^{-3} M in acetonitrile with 10^{-1} M Bu_4NBF_4 as supporting electrolyte.
[b] $E(i) = 1/2\ (E(i)_{ox} + E(i)_{red})$
[c] $\Delta E(i) = E(i)_{ox} - E(i)_{red}$

Broadly speaking, a few remarks could be drawn from the cyclic voltammetric data: firstly, the germyl derivatives are slightly more difficult to reduce by comparison with the silyl derivatives and secondly, they exhibit four redox processes between 0 and -2.5 V, an additional redox couple appear at around -1.4 V. Contrary to the silylated compounds, no patterns could be extracted from the cyclic voltammetric data (**Table 10**), the first two redox couples (I-I' and II-II') are situated at very close potential values to each other, the position of the fourth redox couple (IV-IV') is influenced by the position of the third redox process (III-III'), the more negative potential values for the third redox couple the more negative potential values for the fourth redox process.

An interesting trend was highlighted for compounds **14** and **15** during the cycling of the glassy carbon electrode in a 10^{-3} M POMs deaerated acetonitrile solution (10^{-1} M Bu_4NBF_4), the intensity of the additional redox couple (III-III' $\sim$ -1.4 V) tends to decrease upon cycling until its complete disappearance by the end of the 30th cycle (**Figure 41**, A and **Figure 42**, A). The resulting cyclic voltammogram exhibits three one-electron redox processes (**Figure 41**, B and **Figure 42**, B) as for the silylated derivatives (*vide supra*). The cyclic voltammogram data for **14** and **15** for the first and 30th cycle are gathered in **Table 11**. A few conclusions can be drawn from these data: after cycling the potential values for the redox processes are slightly shifted towards more negative values, the III-III' redox process completely disappear leaving a voltammogram which exhibits three redox curves very stable and well defined. This trend is also valid at different scanning rates: 20, 50, 100, 200, and 500 $mV \cdot s^{-1}$ (*results not shown*).

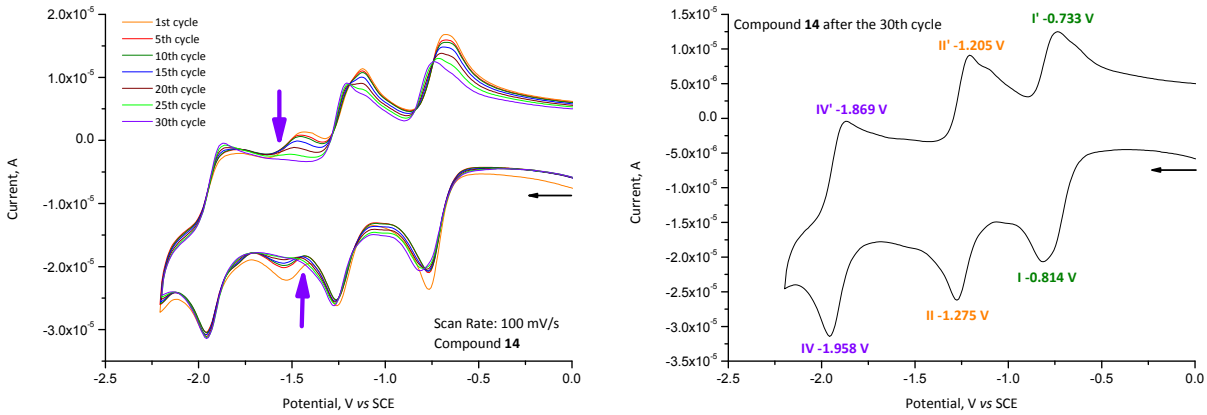

A B

Figure 41. Cyclic voltammogram of compound **14** at glassy carbon electrode. $[(NBu_4)_3$-**14**$]$ = 10^{-3} M in acetonitrile, 10^{-1} M NBu_4BF_4. (A) The electrode was cycled 30 times at scanning rate 100 mV·s^{-1}. (B) The 30th cyclic voltammogram.

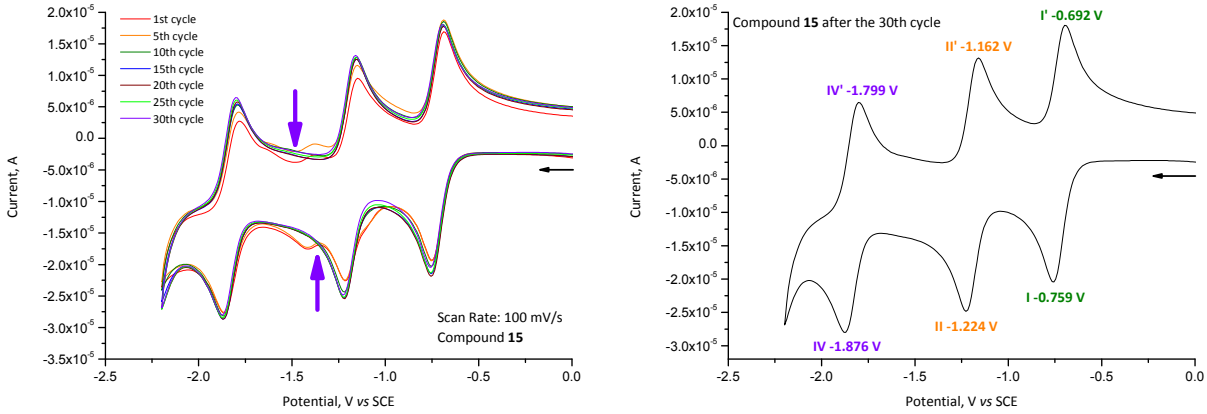

A B

Figure 42. Cyclic voltammogram of compound **15** at glassy carbon electrode. $[(NBu_4)_3$-**15**$]$ = 10^{-3} M in acetonitrile, 10^{-1} M NBu_4BF_4. (A) The electrode was cycled 30 times at scanning rate 100 mV·s^{-1}. (B) The 30th cyclic voltammogram.

Table 11. Representative cyclic voltammetric data *vs* SCE electrode for compound **3**, **14** and **15** after cycling.

Comp.[a]	*Scan No.*	E(I)[b](ΔE(I))[c]	E(*II*)[b](ΔE(II))[c]	E(*III*)[b](ΔE(III))[c]	E(*IV*)[b](ΔE(IV))[c]
14	*1st*	-0.722 V (92 mV)	-1.189 V (135 mV)	-1.484 V (97 mV)	-1.906 V (116 mV)
14	*30th*	-0.773 V (81 mV)	-1.240 V (70 mV)	-	-1.913 V (89 mV)
15	*1st*	-0.719 V (66 mV)	-1.181 V (66 mV)	-1.398 V (47 mV)	-1.822 V (85 mV)

15	*30th*	-0.725 V (67 mV)	-1.193 V (62 mV)	-	-1.837 V (77 mV)

[a] [POM] = 1×10^{-3} M in acetonitrile with 10^{-1} M Bu_4NBF_4 as supporting electrolyte.
[b] $E(i) = 1/2\ (E(i)_{ox} + E(i)_{red})$
[c] $\Delta E(i) = E(i)_{ox} - E(i)_{red}$

The disappearance of the additional redox couple was investigated in the glove box away from the oxygen influence. It was found that in the absence of oxygen the III-III' redox process is maintained even after the 90th cycle (**Figure 43**).

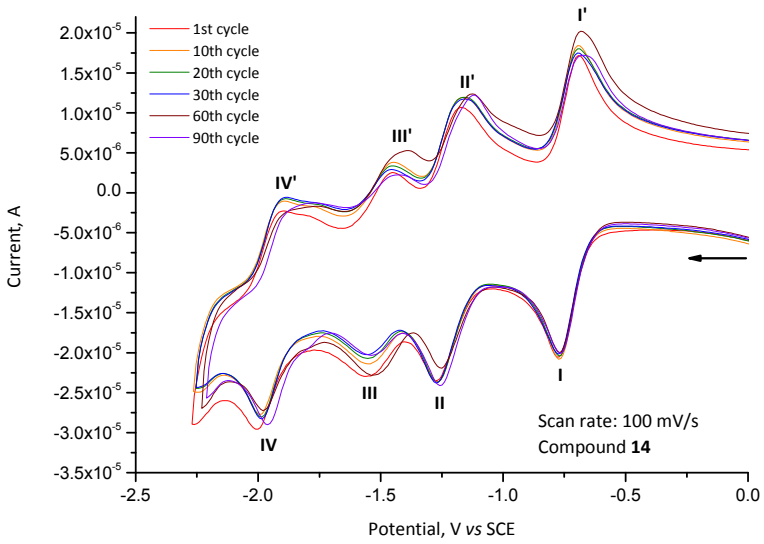

Figure 43. Cyclic voltammogram of compound **14** at glassy carbon electrode. $[(NBu_4)_3$-**14**$] = 10^{-3}$ M in acetonitrile, 10^{-1} M NBu_4BF_4. The electrode was cycled 90 times at scanning rate 100 mV·s^{-1} inside of the glove box.

2.3.3. Synthetic Routes for *Organostannyl Derivatives*

The incorporation of organic groups into polyoxometalate structures is easily achieved, for example by reaction of $RSnCl_3$ with a monolacunary anion. These reactions results in polyoxoanions in which $(O)_5WO^{4+}$ octahedron is replaced by $(O)_5SnR^{3+}$. The stability of the Sn-carbon bonds towards hydrolysis makes the resulting polyoxometalate derivatives particularly suitable for further derivatization.

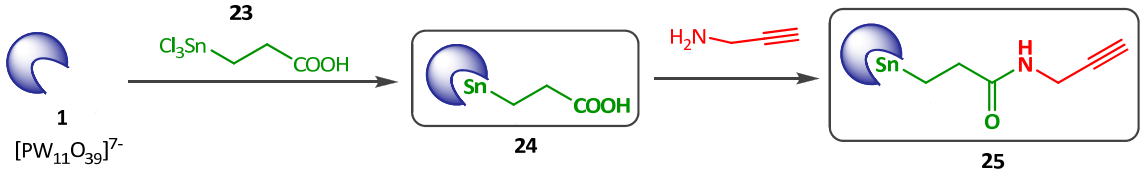

Scheme 7. Synthetic routes for organostannyl derivatives

2.3.3.1. Spectroscopic Characterization

The incorporation of organic group $Cl_3SnCH_2CH_2COOH$ into the lacunary anion α-{PW_{11}} was already reported by Pope et al.[14] Reaction of trichlorotin precursors with the monolacunary polyoxotungstate anions (**Equation 10**) proceeds smoothly in acetonitrile to give the desired derivative in good yield. The derivatization of the side chain with propargyl amine (**Equation 11**) was also described by the groups of Paris 6, Inorganic Chemistry and Molecular Materials and Organic Chemistry laboratories.[15]

$$\alpha\text{-}[PW_{11}O_{39}]^{7-} + Cl_3SnCH_2CH_2COOH \rightarrow \alpha\text{-}[PW_{11}O_{39}\{SnCH_2CH_2COOH\}]^{4-} + 3Cl^- \qquad \textbf{Equation 10}$$

$$\alpha\text{-}[PW_{11}O_{39}\{SnCH_2CH_2COOH\}]^{4-} + NH_2CH_2C{\equiv}CH \rightarrow \alpha\text{-}[PW_{11}O_{39}\{SnCH_2CH_2CO(O)CH_2C{\equiv}CH\}]^{4-} \qquad \textbf{Equation 11}$$

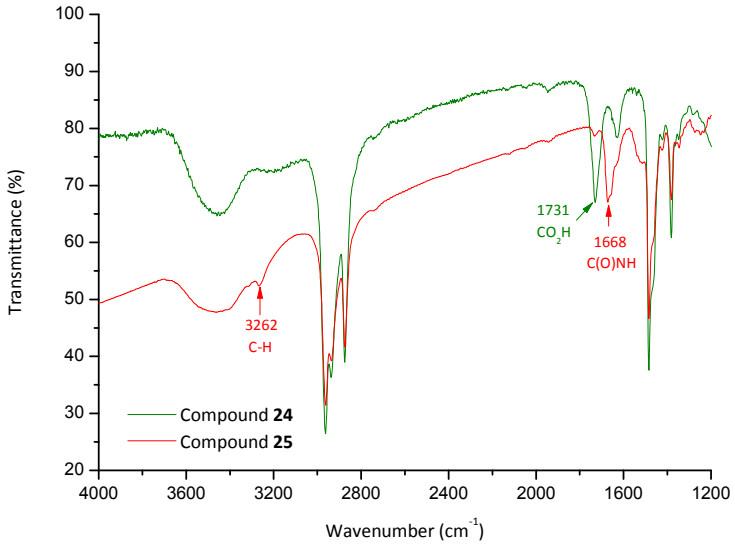

Figure 44. Fragment of the overlaid infrared spectra of compounds **24** and **25**.

The infrared spectrum of the compound displays the vibration bands slightly shifted to higher wavenumbers, with respect to {PW_{11}}, which confirms a partial saturation of the structure (**Table 12**)

[14] G. Sazani, M. T. Pope, Organotin and organogermanium linkers for simple, direct functionalization of polyoxotungstates, *Dalton Trans.* **2004**, 1989-1994.
[15] S. Bareyt, S. Piligkos, B. Hasenknopf, P. Gouzerh, E. Lacôte, S. Thorimbert, M. Malacria, Efficient Preparation of Functionalized Hybrid Organic/Inorganic Wells-Dawson-type Polyoxotungstates, *J. Am. Chem. Soc.* **2005**, *127*, 6788-6794.

and the infrared data are comparable with those reported in literature. Moreover, the IR spectra (Figure 44) show the disappearance of the ν(CO_2H) band at 1731 cm^{-1} and the appearance of two new bands at 1668 cm^{-1} and 3262 cm^{-1} assigned to the ν(C(O)NH) and ν(C≡H) vibration modes, respectively.

Table 12. Infrared data (cm^{-1}) for the stannyl compounds derived from $[PW_{11}O_{39}]^{7-}$ anion (**1**).

Compound	ν(≡C-H)	N(C=O)	ν(CO-NH)	ν(P-O)	ν(W=O)	ν(W-O-W)
1	-	-	-	1086m 1043m	952vs	903m 858s 810vs
24	-	1731w	-	1067s 1030w	962vs	730vs 887s 809vs
25	3262w	-	1668w	1067s 1029w	962vs	886s 810vs

The ^{31}P NMR spectrum for the compound exhibits one signal at δ = -10.8 ppm for compound **24** shifted to low frequencies with respect to {PW_{11}} δ = -10.3 ppm (Table 13), indicative for the presence of a single product. For compound **25** also one signal can be noticed in the ^{31}P NMR situated at almost the same value as for compound **24**, not surprisingly since the derivatization step takes place far away from the POMs skeleton. In addition, the occurrence of a pair of satellites flanking the single line in the ^{31}P NMR spectra, arising from unresolved coupling with ^{117}Sn and ^{119}Sn, is a strong evidence that the tin atom is bounded to the phosphate group (Figure 45 and Figure 46).

Table 13. ^{31}P NMR (300 MHz, acetone D6) data for the compounds **1**, **24** and **25**.

Compound	**1**	**24**	**25**
Chemical shift, δ ppm	-10.31	-10.89	-10.90

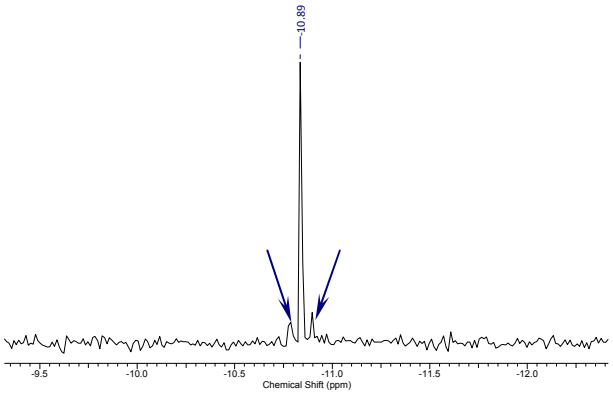

Figure 45. The ^{31}P NMR spectrum (161.97 MHz, acetone D6) of compound **24**.

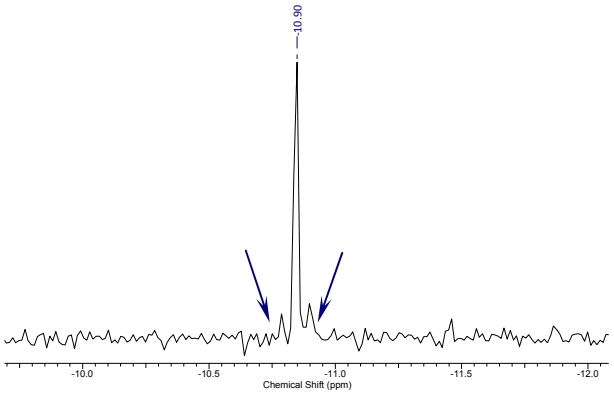

Figure 46. The ^{31}P NMR spectrum (161.97 MHz, acetone D6) of compound **25**.

The ^{1}H NMR (**Figure 47**, **Figure 48**) spectra confirms the presence of the side chain, thus showing unambiguously that the preparation of compound **24** and **25** succeeded in good yield. Apart the four multiplets from the ammonium cations, the spectrum of compound **24** exhibits (**Figure 47**) one complex multiplet centered 2.66 ppm assigned to the methylene group adjacent to the COOH moiety and another multiplet (methylene group close to Sn) at 1.36 ppm, partially hidden under the NBu_4 signal. In the ^{1}H NMR spectrum of compound **25** (**Figure 48**) the amide and ethynyl protons give rise to triplets 6.88 and 2.51 ppm, respectively, due to the coupling with the propargyl protons (doublets of doublets at 3.96 ppm). The signals of the methylene groups closed to CO and Sn (multiplets centered at 2.54 and 1.38 ppm) are slightly shifted to a lower frequency relative to that of **24**.

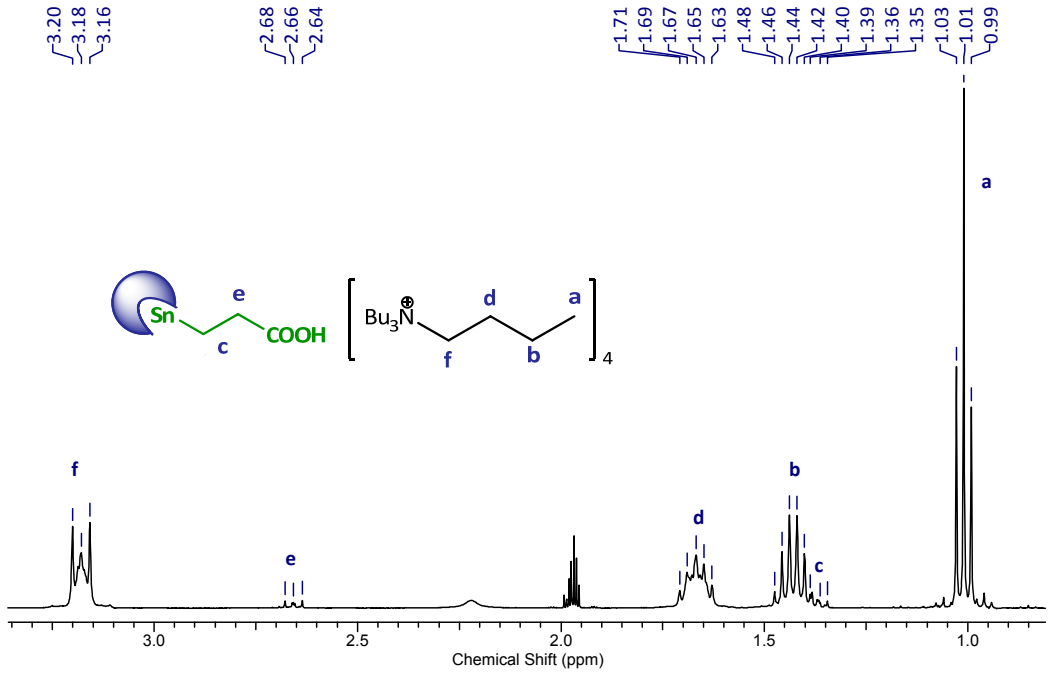

Figure 47. The ^{1}H NMR (400.13 MHz, CD_3CN) spectrum of compound $(NBu_4)_4$-**24**.

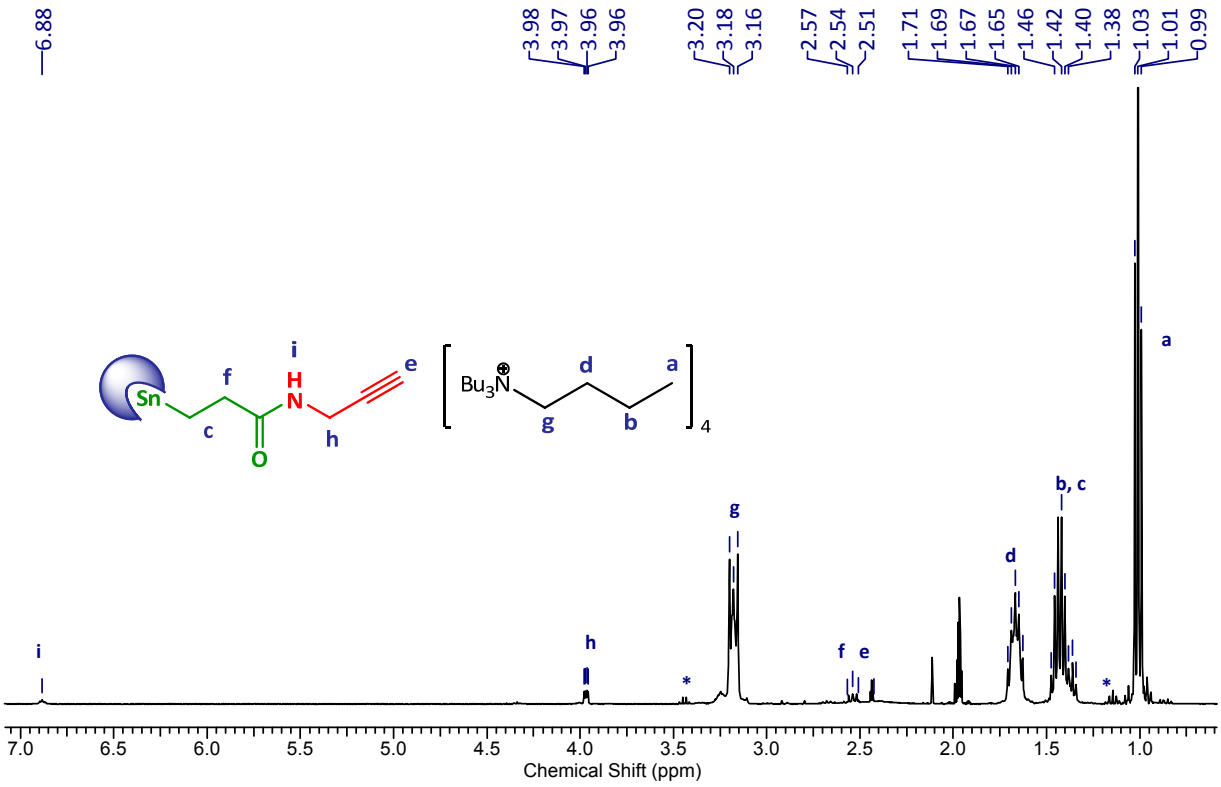

Figure 48. The ^{1}H NMR (400.13 MHz, CD_3CN) spectrum of compound $(NBu_4)_4$-**25** (* = diethyl ether).

2.3.4. Electrochemical Behavior in Solution at the Silicon Electrode

The properties of semiconductor electrodes, and their differences from those of metallic electrodes, can be understood by examining the electronic structures of these materials (**Figure 49**). Due to the essentially infinite number of atoms that must be considered, the electronic structure of these solids is typically discussed in terms of energy bands, which are made up of atomic orbitals of the individual atoms. It is the energy gap (the band gap) E_B, between the upper edge of the valence band and the lower edge of the conduction band that determines the properties of the material. For insulators, the band gap is sufficiently large that electrons cannot be promoted from the valence band to the conduction band. The promotion of electrons leaves a positively charged vacancy in the valence, which is referred to as a hole. These holes can be moved through space by the transfer of an electron to the vacancy; therefore holes are considered to be mobile.

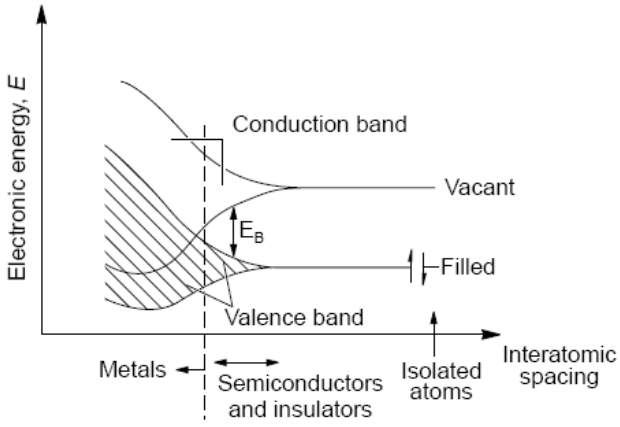

Figure 49. Generation of bands in solids from atomic orbitals of isolated atoms into a lattice.[16]

Electrons can be excited to the conduction band either thermically or photochemically. However, there is another method for generating charge carriers (*i.e.*, electrons or holes) within a semiconductor, referred to as doping. Undoped semiconductors are referred to as ***intrinsic semiconductors***. In addition, the energy diagrams of intrinsic silicon and two types of doped silicon are given (**Figure 50**, bottom). The difference between the energy level of the conduction and valence band is the band gap (E_g), which amounts 1.12 eV (~ 1107 nm) for silicon at 300 K. Doped semiconductors in which the dominant (or majority) charge carriers are electrons are referred to as ***n-type semiconductors***, whereas those in which holes are the majority charge carriers are referred to as ***p-type semiconductors***.

[16] A.W. Bott, Electrochemistry of Semiconductors, *Current Separations* **1998**, *17*, 87-91.

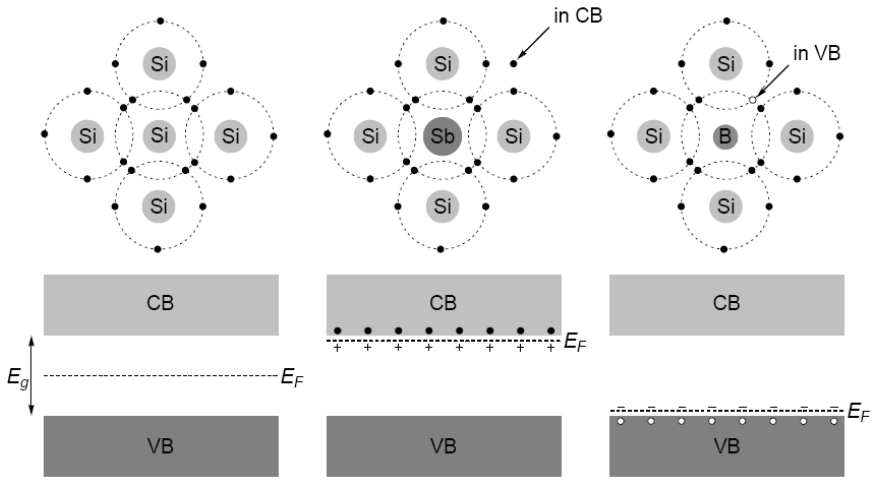

Figure 50. Schematic 2-dimensional representations of crystal lattices (top) and energy diagrams (bottom) of intrinsic silicon (left), *n*-type silicon (center) and *p*-type silicon (right). CB, VB, *EF*, and *Eg* are the conduction band, the valence band, the Fermi level, and the band gap, respectively. The dots and open circles represent electrons and holes, respectively. The positive and negative charges represent the fixed donor ions (Sb^+) and fixed acceptor ions (B^-), respectively.

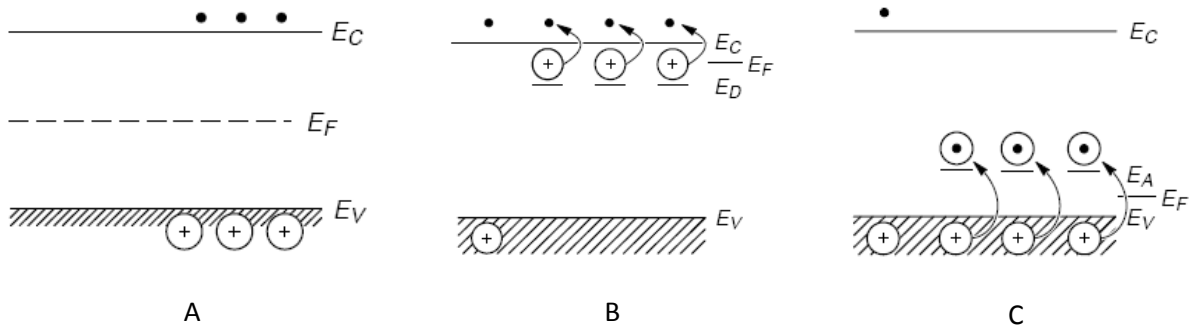

Figure 51. Schematic diagram of the energy levels of an: (A) intrinsic semiconductor, (B) *n*-type semiconductor and (C) *p*-type semiconductor. Notation: E_C – conduction band, E_V – valence band, E_F – Fermi level, E_D – energy level introduced by the dopant (donor atoms), E_A – energy level introduced by the dopant (acceptor atoms).[16]

Doping changes the distribution of electrons within the solid, and hence changes Fermi level. For a *n*-type semiconductor, the Fermi level lies just below the conduction band, whereas for a *p*-type semiconductor it lies just above the valence band (**Figure 51**). In addition, as with metal electrodes, ***the Fermi level of a semiconductor electrode varies with the applied potential***; for example, moving to more negative potentials will raise the Fermi level. In conclusion, electrons in the conduction band and holes in the valence band are introduced by the substitution of acceptor and donors atoms (dopants) in the semiconductor lattice to produce ***extrinsic semiconductors***. Thus an arsenic atom (a

Group V element) behaves as an electron donor when substituted into crystalline silicon (a Group IV element) and introduces an energy level at E_D, just bellow the bottom of the conduction band. At room temperature, most of the donor atoms are ionized, each yielding an electron in the conduction band and leaving behind an isolated positive site at the donor atom (*see* **Figure 51**, B). If an acceptor atom (*e.g.*, gallium, a Group III element) is substituted into the silcon, an energy level is introduced at E_A, just above the top of the valence band. In this case, electrons are thermally excited from the valence band into these acceptor sites, leaving mobile holes in the valence band and isolated, negatively charged acceptor sites (*see* **Figure 51**, C).[17]

The conductivity of semiconductors is usually reported in terms of resistivity, which is equal to the reciprocal of the conductivity. The resistivity of intrinsic silicon is 230 kΩcm. However, this is the theoretical limit. Upon the addition of dopants, the resistivity can decrease spectacularly. The resistivity does not only depend on the dopant concentration, but also on the type of dopant as the mobilities of electrons and holes are different. To give an example, the addition of only one phosphorous or boron atom to 5 × 1010 Si atoms reduces the resistivity of the semiconductor at 296 K with a factor of ~ 60 and ~ 18, respectively. In this thesis we used silicon substrates with resistivities of $8 \cdot 10^{-3}$ – $2.2 \cdot 10^{-2}$ Ω·cm and 14-22 Ω·cm, which are referred to as highly doped and lowly doped, respectively.

The electrochemical behavior of some selected silyl and germyl derivatives was investigated at a *n*-type silicon electrode in a acetonitrile solution, by using NBu_4BF_4 as the supporting electrolyte. The potential values are reported *vs* SCE electrode. For this study a single-crystal phosphorus doped *n*-type silicon wafer. After the removing of the oxide film by etching in 1% HF, the silicon electrode was immediately plunged into the acetonitrile solution which contained the POMs derivative and the cyclic voltammogram was registered. All the following measurements were performed under argon atmosphere, into a glove-box.

The electrochemical window was set between 0 and -1.5 V outside which, towards more negative values, passivation of the silicon electrode occurs associated with a pronounced increase in current intensity. Anyways, the silicon electrode remains very sensitive towards oxidation in the polyoxometalate solution. **Figure 52** shows the oxidation of the silicon electrode in the compounds **3** and **14** acetonitrile solution. Starting yet with the second cycle, the intensity of the electrochemical waves tends to decrease in intensity towards their almost complete disappearance at the end of the

[17] A.J. Bard, L.R. Faulkner, Electrochemical Methods Fundamentals and Applications, 2nd edition, Wiley, **2001**.

10th cycle. Also, it can be observed that the position reduction waves have the tendency to shift towards more negative values as the oxidation of the silicon electrode is more pronounced.

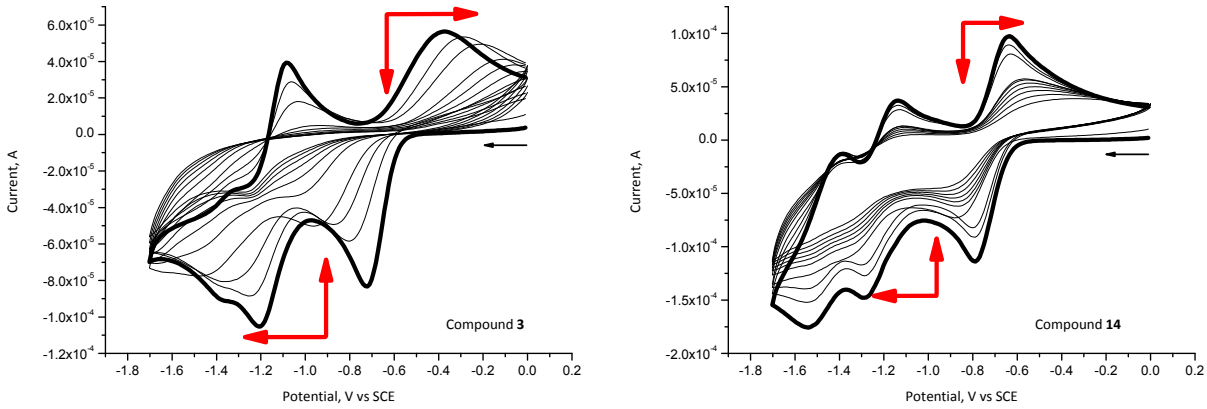

A B

Figure 52. Cyclic voltammograms of compounds **3** (A) and **14** (B) at silicon electrode. The electrode was cycled ten times at scanning rate 100 mV/s between 0 and -1.5 V. Ageing of the silicon electrode in an acetonitrile solution (0.1 M Bu4NBF4) containing 1×10^{-3} M compound **3** and **14**, respectively.

Generally speaking, between 0 and -1.5 V three reversible redox waves are distinguished for all the species studied. Compounds **6**, **7** and **19** exhibit relatively a peculiar pattern in comparison with the other compounds. Their first reduction potentials are situated at rather unusual high negative values: -0.843, 0.942 and 0.950 V relative to the rest of the species investigated. We suspect that this is due to the silicon electrode which was not completely oxide free at the beginning of the measurement or that they oxidize much quicker the silicon electrode. Their electrochemical data are highlighted in grey in **Table 14**.

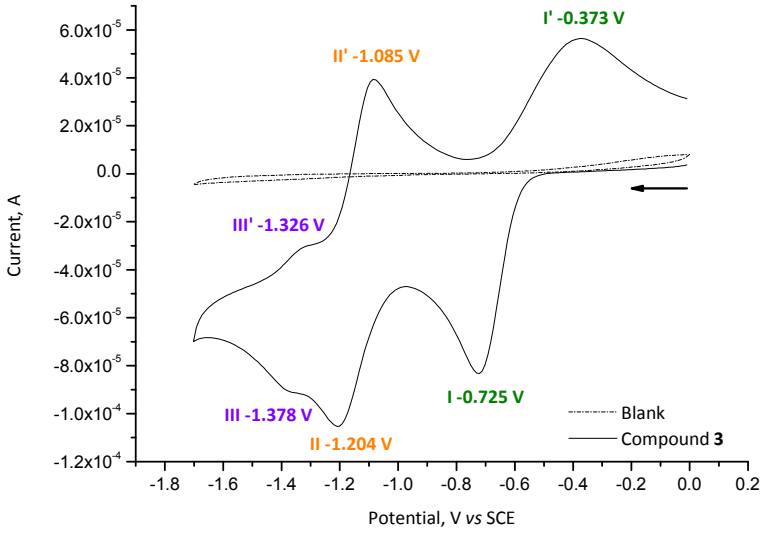

Figure 53. Cyclic voltammogram of compound **3** at silicon electrode. [**3**] = 1 × 10^{-3} M in acetonitrile with 10^{-1} M Bu_4NBF_4 as supporting electrolyte. Scanning rate: 100 mV/s.

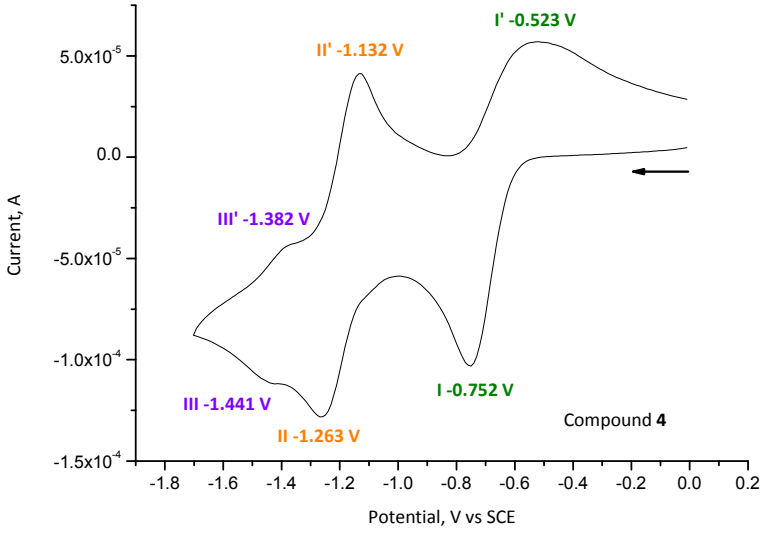

Figure 54. Cyclic voltammogram of compound **4** at silicon electrode. [**4**] = 1 × 10^{-3} M in acetonitrile with 10^{-1} M Bu_4NBF_4 as supporting electrolyte. Scanning rate: 100 mV/s.

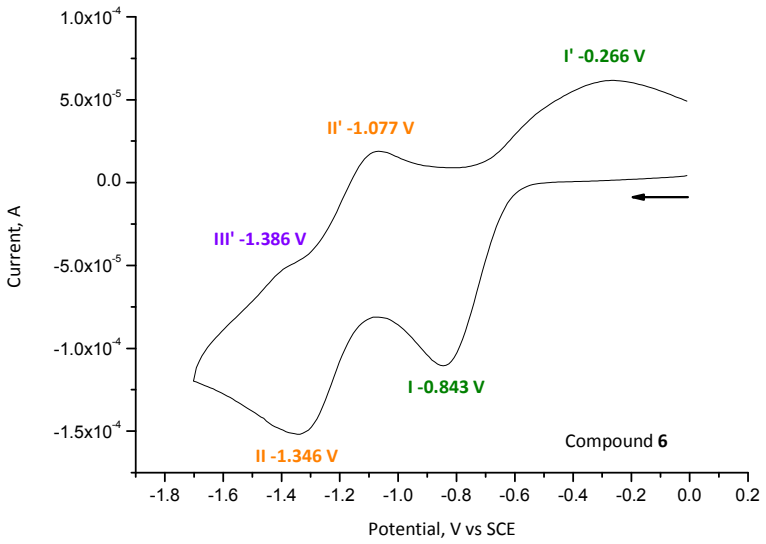

Figure 55. Cyclic voltammogram of compound **6** at silicon electrode. [**6**] = 1 × 10^{-3} M in acetonitrile with 10^{-1} M Bu_4NBF_4 as supporting electrolyte. Scanning rate: 100 mV/s.

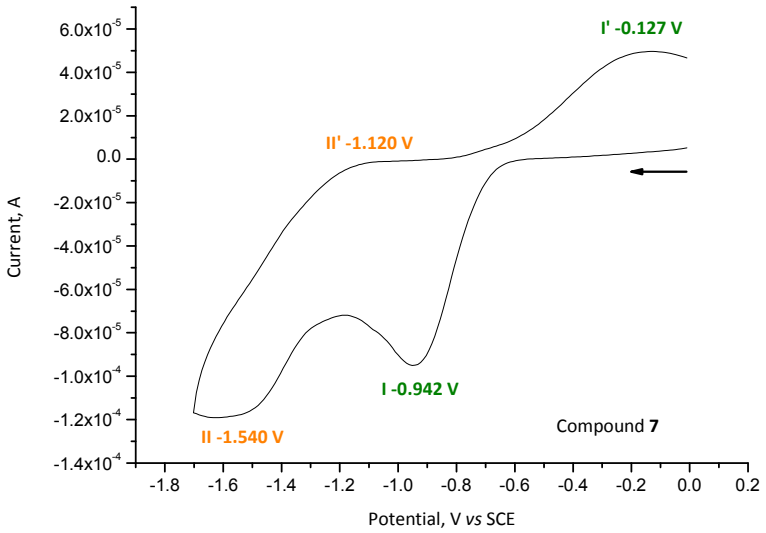

Figure 56. Cyclic voltammogram of compound **7** at silicon electrode. [**7**] = 1 × 10^{-3} M in acetonitrile with 10^{-1} M Bu_4NBF_4 as supporting electrolyte. Scanning rate: 100 mV/s.

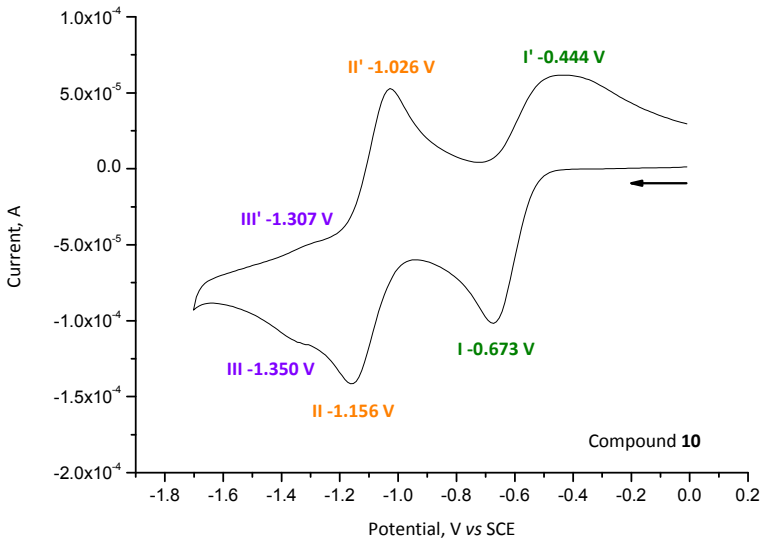

Figure 57. Cyclic voltammogram of compound **10** at silicon electrode. [**10**] = 1×10^{-3} M in acetonitrile with 10^{-1} M Bu_4NBF_4 as supporting electrolyte. Scanning rate: 100 mV/s.

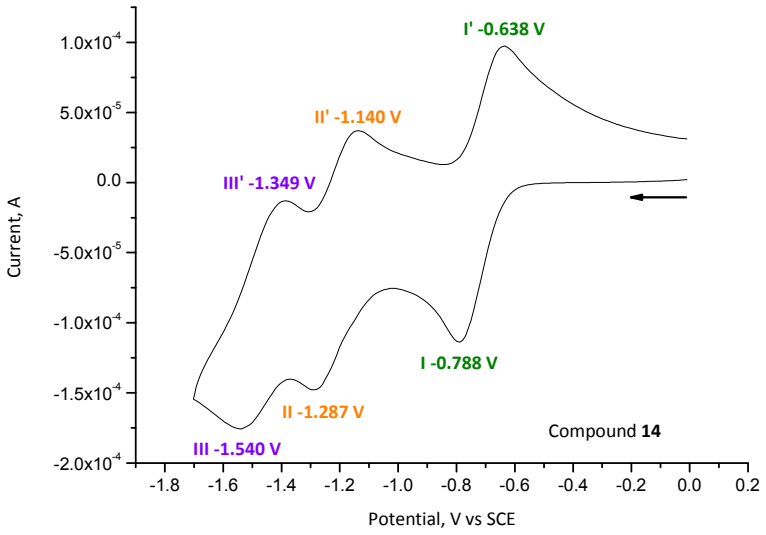

Figure 58. Cyclic voltammogram of compound **14** at silicon electrode. [**14**] = 1×10^{-3} M in acetonitrile with 10^{-1} M Bu_4NBF_4 as supporting electrolyte. Scanning rate: 100 mV/s.

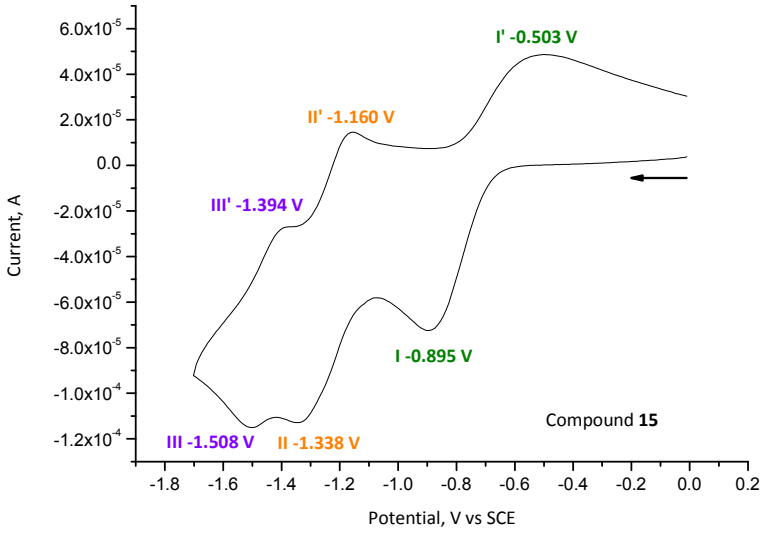

Figure 59. Cyclic voltammogram of compound **15** at silicon electrode. [**15**] = 1 × 10^{-3} M in acetonitrile with 10^{-1} M Bu_4NBF_4 as supporting electrolyte. Scanning rate: 100 mV/s.

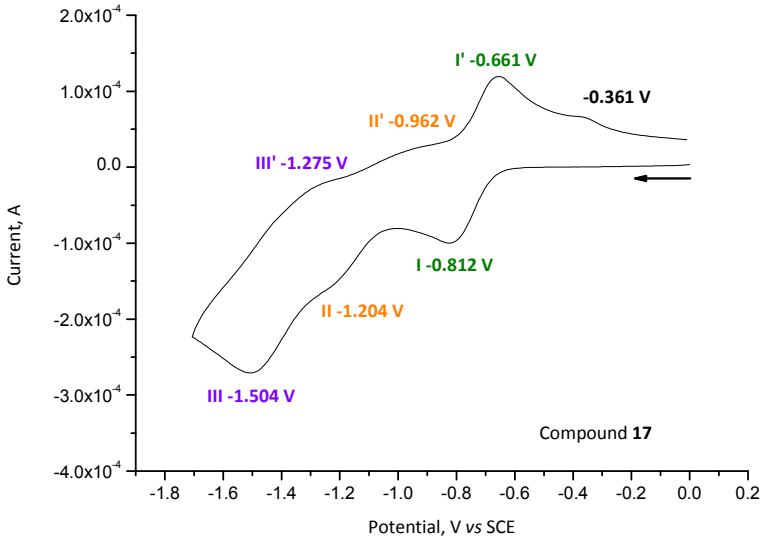

Figure 60. Cyclic voltammogram of compound **17** at silicon electrode. [**17**] = 1 × 10^{-3} M in acetonitrile with 10^{-1} M Bu_4NBF_4 as supporting electrolyte. Scanning rate: 100 mV/s.

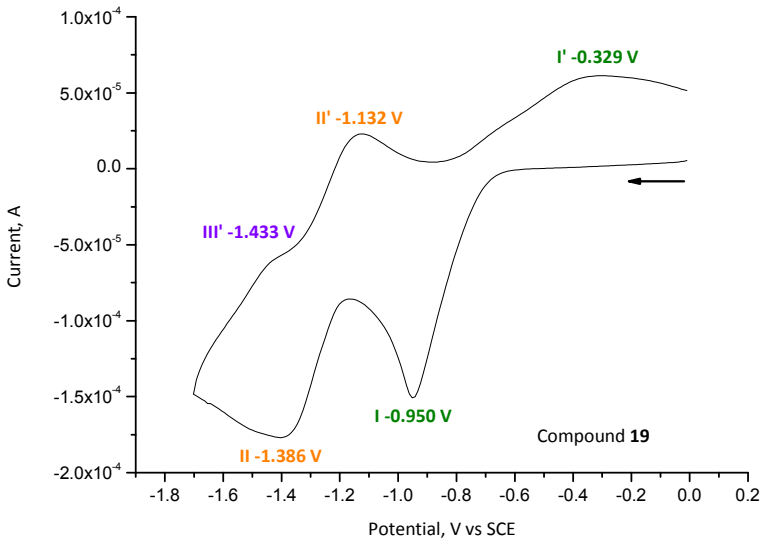

Figure 61. Cyclic voltammogram of compound **19** at silicon electrode. [**19**] = 1×10^{-3} M in acetonitrile with 10^{-1} M Bu_4NBF_4 as supporting electrolyte. Scanning rate: 100 mV/s.

Table 14. Representative cyclic voltammetric data *vs* SCE electrode for selected silyl and germyl compounds.

Compounds[a]	$E(I)^b(\Delta E(I))^c$	$E(II)^b(\Delta E(II))^c$	$E(III)^b(\Delta E(III))^c$
3	-0.549 V (352 mV)	-1.144 V (119 mV)	-1.352 V (52 mV)
4	-0.637 V (229 mV)	-1.197 V (131 mV)	-1.411 V (59 mV)
6	-0.554 V (577 mV)	-1.211 V (269 mV)	-1.386 V (irrev.)
7	-0.534 V (815 mV)	-1.330 V (420 mV)	-
10	-0.558 V (229 mV)	-1.091 V (130 mV)	-1.328 V (43 mV)
14	-0.713 V (150 mV)	-1.213 V (147 mV)	-1.444 V (191 mV)
15	-0.699 V (392 mV)	-1.249 V (178 mV)	-1.451 V (114 mV)
17	-0.736 V (151 mV)	-1.083 V (242 mV)	-1.389 V (229 mV)
19	-0.639 V (621 mV)	-1.259 V (254 mV)	-1.433 V (irrev.)

[a] [POM] = 1×10^{-3} M in acetonitrile with 10^{-1} M Bu_4NBF_4 as supporting electrolyte.
[b] $E(i) = 1/2\ (E(i)_{ox} + E(i)_{red})$
[c] $\Delta E(i) = E(i)_{ox} - E(i)_{red}$

2.4. CONCLUSIONS

Within this chapter 15 functionalized polyoxometalates able to covalently graft onto a silicon surface were synthesized. Among these derivatives 7 of them were for the first time described; they are compounds: **11**, **14**, **15**, **17**, **19**, **20** and **22**. In collaboration with the Inorganic Chemistry and Molecular Materials laboratory we succeded their purification and fully characterization, concretised in an article in the *Chemistry a European Journal*. Although, the synthesis procedures of compounds **19** and **20** were not completely adjusted by the end of my contract, I am confident that they can be obtained in pure state. They present interesting perspectives, compound **19** is especially mentioned, it was synthesized for a copolymerization in a pyrrole solution for a better attachment of the POMs in a polypyrrole film.

A comparative study of the electrochemical behavior in acetonitrile solution of functionalized polyoxometalates was performed also for the first time at the glassy carbon and *n*-type silicon electrode. They exhibit several reversible redox waves and this property can be exploited for construction of multilevel molecular memory devices.

Part 3

POLYOXOMETALATES MODIFIED ELECTRODES

3. Third Part – Polyoxometalates Modified Electrodes

Abstract – Within this chapter the attachment of polyoxometalate molecules onto the silicon surface is described. Towards this goal I was engaged in a program aimed at constructing devices that use the properties of POMs to store information. In a general approach, ***a redox-active molecule attached to a semiconductor surface serves as the active storage medium, and information is stored in the discrete redox states of the molecule*** (POMs).

Résumé – Dans ce chapitre la fixation des molécules de polyoxométallate sur la surface de silicium est décrite. Dans ce but, j'ai été engagé dans un programme visant à construire des dispositifs qui utilisent les propriétés des polyoxométallates (POM) pour stocker des informations. Dans une approche générale, ***une molécule redox-active fixée à une surface d'électrode de silicium sert de support de stockage actif, et l'information est stockée dans les états d'oxydo-réduction discrets de la molécule*** (POMs).

3.1. INTRODUCTION

The first part of this manuscript emphasizes that the covalently modified silicon surface is the key for molecular memory. An attractive perspective is the realization of multilevel molecular memory based on semiconducting nanowire field-effect transistors or hybrid molecular-silicon capacitors by using POMs as redox-active components. The objective of this research is ***to fabricate molecular memories using polyoxometalates (POMs) monolayer on silicon surface by different linkers to form uniform and dense active storage medium***. Application of POMs usually requires their immobilization onto an appropriate support or into an appropriate matrix. While most POM-based hybrid materials reported to date involve noncovalent interactions, for example, van der Waals contacts, hydrogen binding, and ionic interaction, a few hybrid polymers involve covalent linkage. Covalent grafting of POMs on

surface is even more rare. Yet, covalent grafting offers advantages in terms of stability and structure control, and it is the approach we have chosen.

3.2. FUNCTIONALIZATION METHODS

3.2.1. HYDROSILYLATION PROCESS

3.2.1.1. Hydrogen-terminated crystalline silicon

The most common surface orientation of silicon are the Si(100) and Si(111) facets. Upon exposure to air single-crystalline silicon surfaces readly oxidize, resulting in the formation of a thin native oxide layer. Oxide-free, hydrogen-terminated silicon surfaces can be obtained by the reaction of a clean surface with hydrogen atoms ultra-high vacuum conditions. A rapid and efficient alternative method involves the dissolution of the native oxide layer in fluoride-containing aqueous sources.[1,2] Interfacial Si atoms on the Si(100) surface are occupied with two hydrogen atoms (SiH_2), while the Si(111) surface is mainly occupied with Si-H groups (Figure 1).[3]

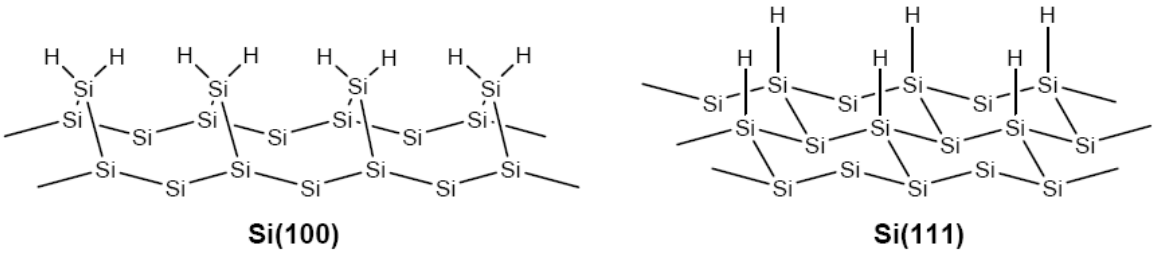

Figure 1. Schematic representation of the hydrogen-terminated Si(100) (left) and Si(111) (right) surface.

[1] Y. J. Chabal, G. S. Higashi, K. Raghavachari, V. A. Burrows, Infrared spectroscopy of Si(111) and Si(100) surfaces after HF treatement: Hydrogen termination and surface morphology, *J. Vac. Sci. Technol. A* **1989**, *7*, 2104-2109.
[2] G. S. Higashi, Y. J. Chabal, G. W. Trucks, K. Raghavachari, Ideal hydrogen termination of the Si(111) surface, *Appl. Phys. Lett.* **1990**, *56*, 656-658.
[3] D. D. M. Wayner, R. Wolkow, Organic modification of hydrogen terminated silicon surfaces, *J. Chem. Soc., Perkin Trans 2*, **2002**, 23-34.

3.2.1.2. Introduction

The full control over surface properties is a "Holy Grail" in material science. Organic monolayers are a strong candidate to achive this highly desired control and therefore have been investigated for many years. [4] Hydrosilylation involves insertion of an unsaturated bond into a silicon-hydride group. Alkyne and alkene hydrosilylation on Si-H terminated surfaces yield alkenyl and alkyl termination, respectively, resulting in Si-C bond formation as shown in **Figure 2**. The Si-C bond is both thermodynamically and kinetically stable due to the high bond strength and low polarity of the bond.

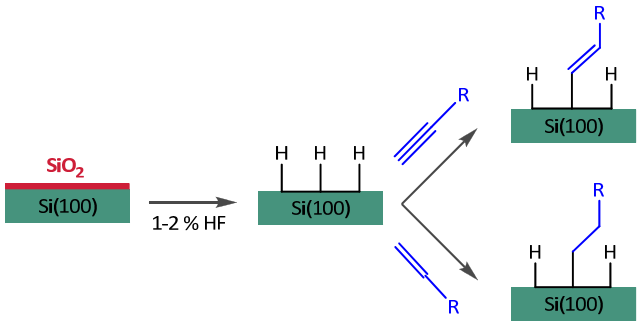

Figure 2. Schematic of hydrosilylation chemistry. The etching of a native oxide-covered silicon surface yielding an oxide-free hydrogen-terminated surface, followed by the reaction with 1-alkyne and 1- alkene, resulting in the formation of a Si-C linked monolayer.

The first example of hydrosilylation on a Si(100) and Si(111) surfaces was carried out in 1993 by Lindford and Chidsey. [5,6] They have reported the preparation of densely packed alkyl monolayers covalently bound to Si(111) and Si(100) surfaces by pyrolysis of diacyl peroxides in the presence of hydrogen-terminated silicon. Hydrosilylation can involve a radical initiator, can be thermally or photochemically induced. *Hydrosilylation involving a radical initiator*, the diacyl peroxide, which undergoes homolytic cleavage to form two acyloxy radicals which decompose to carbon dioxide and an alkyl radical. The alkyl radical can then abstract H• from a surface Si-H group to produce a silicon radical. Because silyl radicals are known to react rapidly with olefins, formation of a silicon carbon

[4] J. M. Buriak, Organometallic Chemistry on Silicon and Germanium Surfaces, *Chem. Rev.* **2002**, *102*, 1271-1308.
[5] M. R. Lindford, C. E.D. Chidsey, Alkyl Monolayers Covalently Bonded to Silicon Surfaces, *J. Am. Chem. Soc.* **1993**, *115*, 12631-12632.
[6] M. R. Lindford, P. Fenter, P. M. Eisenberger, C. E. D. Chidsey, Alkyl Monolayers on Silicon Prepared from 1-Alkenes and Hydrogen-Terminated Silicon, *J. Am. Chem. Soc.* **1995**, *117*, 3145-3155.

bond is the next probable step.[7] The carbon-based radical can then abstract a hydrogen atom either from a neighboring Si-H group or from the allylic position of an unreacted olefin. *Hydrosilylation could occur in the absence of diaclyperoxide initiator at high temperatures* (≥ 150°C), almost certainly through homolytic Si-H cleavage, Si-H → Si• + H•. This yields the silicon surface-based radical (dangling bond) who can then react via the mechanism outlined in **Figure 3**.

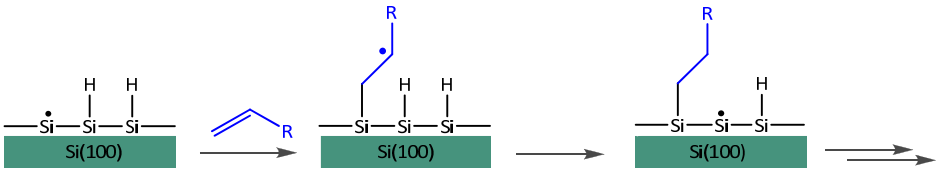

Figure 3. Mechanism for radical-based hydrosilylation.

UV irradiation can also promote hydrosilylation of unsaturated compounds due to homolytic cleavage of Si-H bonds, as is the case with thermal induction. UV photoinduction,[8] however, takes place at room temperature and thus provides a way to avoid thermal input that could be harmful to delicate or small features on a silicon chip.

3.2.2. SILANIZATION PROCESS

The formation of self-assembled organic monolayers on oxidized silicon surface from the solution of alkyltrichlorosilane was introduced by Bigelow et al.[9] and developed further by Maoz and Sagiv.[10] The native oxide layer usually contains a high density of traps therefore, it is desirable to remove the native oxide layer and grow an ultra-thin (1–1.5 nm) thermal oxide layer of better electrical quality. On a silicon oxide surface, three classes of molecules, namely, silanes ($RSiX_3$, with X = Cl, OMe, OEt), organometallics (RLi or RMgX), and alcohols (ROH) are widely used for the formation of self assembled monolayers. Thorough cleaning of the substrate is a prerequisite for obtaining a clean

[7] C. Chatgilialoglu, Organosilanes as Radical-Based Reducing Agents in Synthesis, *Acc. Chem. Res.* **1992**, *25*, 188-194.
[8] R. L. Cicero, M. R. Linford, C. E. D. Chidsey, Photoreactivity of Unsaturated Compounds with Hydrogen-Terminated Silicon(111), *Langmuir* **2000**, *16*, 5688-5695.
[9] W. C. Bigelow, D. L. Pickett, W. A. Zisman, Oleophobic monolayers: I. Films adsorbed from solution in non-polar liquids, *J. Colloid Sci.* **1946**, *1*, 513-538.
[10] R. Maoz, J. Sagiv, On the formation and structure of self-assembling monolayers. I. A comparative atr-wettability study of Langmuir-Blodgett and adsorbed films on flat substrates and glass microbeads, *J. Colloid Interf. Sci.* **1984**, *100*, 465-496.

oxide layer with high density of silanol groups (Si–OH) on the surface. These silanol groups, which provide a highly hydrophilic surface (allowing molecules to diffuse on the physisorbed ultra-thin water layer), are either used as anchoring sites for silanization reactions or converted into more reactive functions (i.e. Si–Cl or Si–NEt_2) suitable for alkylation or alkoxylation reactions (**Figure 4**).

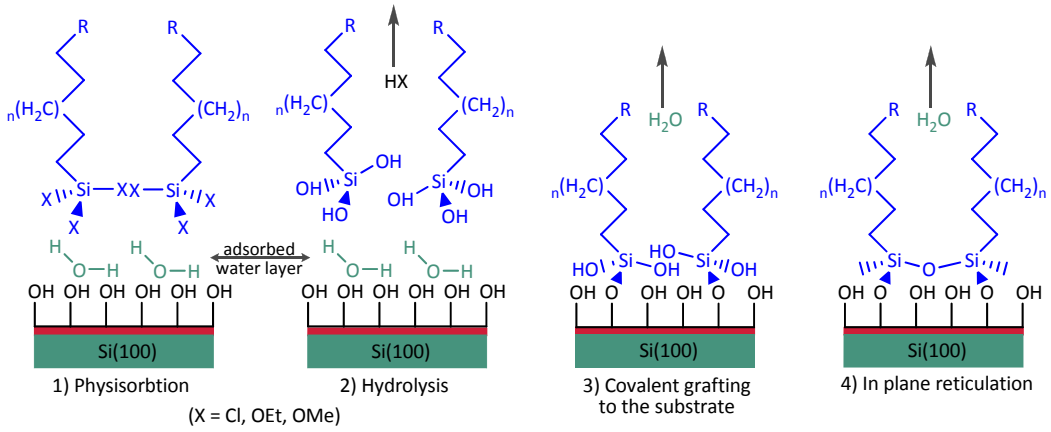

Figure 4. Schematic representation showing different steps involved in the mechanism of SAM formation on a hydrated silicon surface.[11]

3.2.3. MULTI-STEPS IMMOBILIZATION PROCEDURES

Because many of the surfaces prepared through wet chemical techniques have proven themselves to be very robust with respect to demanding chemical and oxidative conditions, further chemistry has been carried out on these interfaces to prepare more sophisticated surfaces for a variety of applications.

3.2.4. ELECTROCHEMICAL METHODS

3.2.4.1. Terminal ethynyl (C≡C) as reactant

Buriak *et al.*[12] have reported a cathodic electrografting process that directly attaches alkynes to the porous Si surface (**Scheme 1**). The electrografting was carried out using a solution of alkyne mixed with the electrolyte solution. A current then is applied for a period of time. It has been proposed that

[11] D. K. Aswal, S. Lenfant, D. Guerin, J. V. Yakhmi, D. Vuillaume, Self assembled monolayers on silicon for molecular electronics, *Anal. Chim. Acta* **2006**, *569*, 84-108.
[12] H. C. Choi, J. M. Buriak, Effects of Organic Monolayer formation on Electrochemiluminescence Behavior of Porous Silicon, *Chem. Mater.* **2000**, *12*, 2151-2156.

the cathodic electrografting reaction of alkynes proceeds via a silyl anion intermediate formed by reduction of surface Si-H bonds. The subsequent in situ generation of a carbanion from deprotonation of the weakly acidic alkyne leads directly to nucleophilic Si-Si bond attack.[13] Moreover, it is worth to recall that during cathodic electrografting silicon is normally protected against oxide (SiO_2) growth, which is instead enhanced in photochemical and mostly in thermal processes.

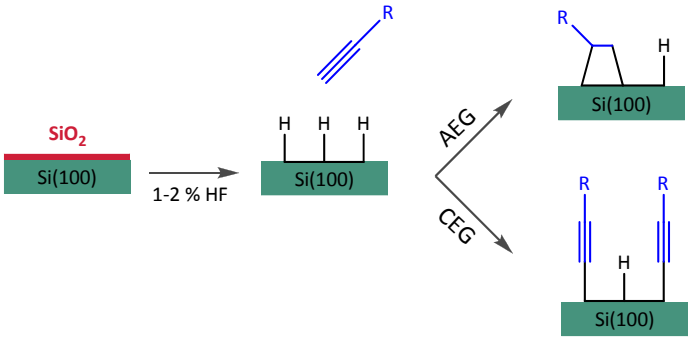

Scheme 1. Outline of cathodic (CEG) and anodic (AEG) electrografting of hydride-terminated silicon surface.

3.2.4.2. Diazonium chemistry

3.2.4.2.1. Diazonium salts

The grafting of organic molecule to Si surface using electrochemical reduction of diazonium is a very simple process.[14,15] A diazonium salt (BF_4^- ^+N_2ArR, where Ar and R represent benzene ring and a functional group, respectively) of typical concentration 1-10 mM is dissolved in an aprotic medium with a supporting electrolyte (ACN + 0.1 M NBu_4BF_4) or in acidic aqueous medium (for example H_2SO_4 0.1 M). The diazonium salt is then reduced using H-terminated Si as a cathode, which results in the grafting of ArR molecules to Si surface. The grafting can be carried out in CV mode or by applying a constant potential (determined from the voltammetric reduction peak of the diazonium) for a variable period of time, typically few tens of seconds. The H-terminated Si is then rinsed in an ultrasonic bath in order to remove physisorbed molecules. This approach, apart from Si, has been used to graft molecules on different substrates, such as, carbon (GC, HOPG, pyrolized photoresists,

[13] E. G. Robins, M. P. Stewart, J. M. Buriak, Anodic and cathodic electrografting of alkynes on porous silicon, *J. Chem. Soc., Chem. Commun.* **1999**, 2479-2480.
[14] C. Henry de Villeneuve, J. Pinson, M. C. Bernard, P. Allongue, Electrochemical Formation of Close-Packed Phenyl Layers on Si(111), *J. Phys. Chem. B* **1997**, *101*, 2415-2420.
[15] P. Allongue, C. Henry de Villeneuve, J. Pinson, F. Ozanam, J. N. Chazalviel, X. Wallart, Organic monolayers on Si(111) by electrochemical method, *Electrochim. Acta* **1998**, *43*, 2791-2798.

pyrolized Teflon, carbon fibers, carbon blacks, carbon nanotubes, diamond), semiconductors (GaAs) and metals (Au, Cu, Fe, Ni, Pt, Pd).

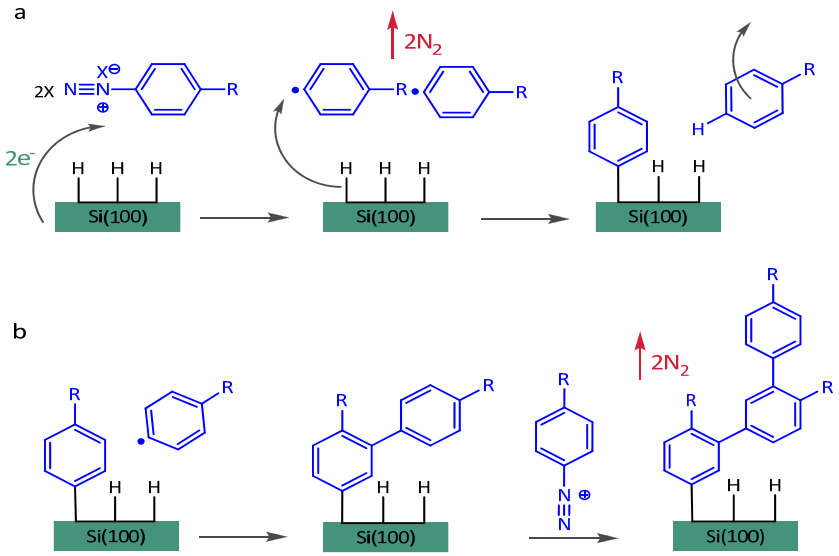

Figure 5. The possible formation mechanism of (a) monolayer and (b) multilayers on H-terminated Si surface using the electrochemical reduction of the diazonium salts.[16]

The monolayer formation process is schematically demonstrated in **Figure 5** (a). The phenyl radical is produced directly "on the electrode" through an electrode transfer concerted with the cleavage of dinitrogen to give the phenyl radical. The aryl radical then causes abstraction of the hydrogen from the Si surface and moves away from the surface. The silyl radical then reacts with a second aryl radical, which results in the formation of a ≡Si–ArR bond, and hence formation of the first monolayer. However, other aryl radical might attack the grafted aromatic group of the monolayer, as schematically shown in **Figure 5** (b), to form a bilayer. Repetition of this reaction would lead to the formation of the multilayers. Since the attachment of subsequent molecules occurs randomly, the multilayers grown in this way are expected to be inhomogeneous in thickness.

3.2.4.2.2. Triazenes

The chemistry of diazonium salts provides tremendous opportunities for immobilization on solid support. Triazenes, which are protected diazonium ions, have much to offer. Some diazonium salts are not stable to oxygen; hence the reaction must be conducted in a glove box, under a nitrogen

[16] D. K. Aswal, S. P. Koiry, B. Jousselme, S. K. Gupta, S. Palacin, J. V. Yakhmi, Hybrid molecule-on-silicon nanoelectronics: Electrochemical processes for grafting and printing monolayers, *Physica E* **2009**, *41*, 325-344.

atmosphere. Furthermore, some diazonium species are not stable to isolation; therefore, their direct reaction with Si-H cannot be carried out. There are also potential safety hazards involved with the production and storage of some diazonium salts. The use of organic triazenes overcomes these limitations by offering an air-stable compound that can be converted *in situ* to the corresponding diazonium salt with the use of an appropriate acid,[17] as shown in **Scheme 2**. When the diazonium salt is generated by acid treatment in the presence of a hydride passivated silicon surface, a covalently bound organic layer is formed.[18]

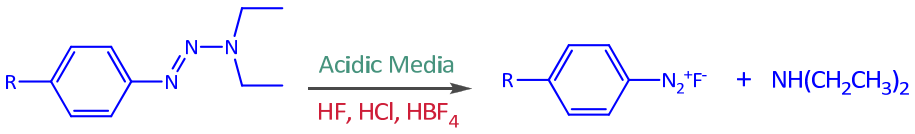

Scheme 2.

In 2005, the group of Tour [19] successfully bounded functionalized SWNTs (single-walled carbon nanotubes) to the monolayers derived from an aryldiazonium intermediate grafted onto a Si(111) surface, producing nonmetallic molecular junctions for electronic devices. They have developed a convenient *in situ* film assembly using organic triazenes for the formation of Si-molecule assemblies under ambient conditions. Dilute aqueous HF serves as the reagent necessary for the organic conversion (triazene to diazonium) and concomitantly acts as *in situ* etchant for Si-O to Si-H conversion, thereby making the reactions possible in air.

3.2.4.3. Immobilization into conducting polymers

3.2.4.3.1. Introduction

An important class of polymers is conducting polymers (CPs) which have the ability to conduct electrical current. They are also known as conjugated polymers because of the extended π-conjugation along the polymer backbone. Representative examples of CPs are given in **Figure 6**.

---

[17] S. Bräse, The Virtue of the Multifunctional Triazene Linkers in the Efficient Solid-Phase Synthesis of Heterocycle Libraries, *Acc. Chem. Res.* **2004**, *37*, 805-816.
[18] A. K. Flatt, B. Chen, J. M. Tour, Fabrication of Carbon Nanotube-Molecule-Silicon Junctions, *J. Am. Chem. Soc.* **2005**, *127*, 8918-8919.
[19] B. Chen, A. K. Flatt, H. Jian, J. L. Hudson, J. M. Tour, Molecular Grafting to Silicon Surface in Air Using Organic Triazenes as Stable Diazonium Sources and HF as a Constant Hydride-Passivation Source, *Chem. Mater.* **2005**, *17*, 4832-4836.

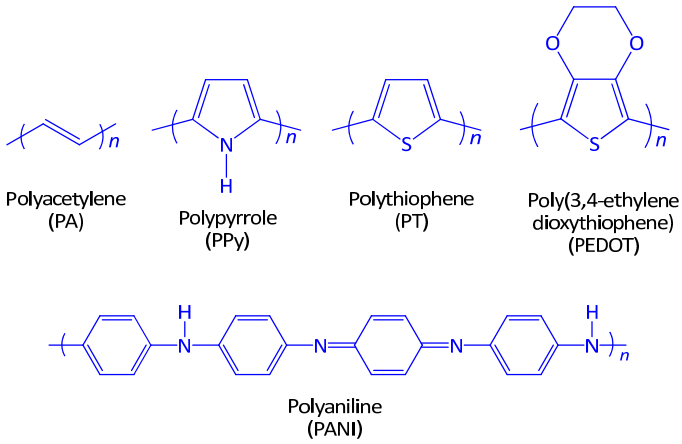

Figure 6. Representative examples of common conducting polymers.

The first conjugated polymer, polythiazyl $(SN)_x$, was discovered in 1975.[20] However, the idea of using polymers for their electrical conducting properties first appeared in 1977 when Shirakawa *et al.*[21] reported a 10 million-fold increase in the conductivity of polyacetylene doped with iodine. It exhibited a conductivity of 10^3 $S \cdot cm^{-1}$. Since then, an active interest in synthesizing other organic polymers possessing this property has been initiated.

3.2.4.3.2. POMs Incorporation into Polymeric Matrices

The synthesis of electrodes modified by POMs entrapped in polymer films has attracted the attention of many electrochemists. The interaction between the polymers and the POMs is stronger than the interaction between the polymers and the small counteranions such as sulphate, chloride or perchlorate. Therefore, POMs are efficiently immobilized in the polymer matrix and do not exchange with these small anions. [22] The POMs can be entrapped into a polymer matrix by a two-step or one-step method. Using the two-step method POMs are electrostatically incorporated into a polymer which is already formed on the electrode surface. In the case of one-step method, POMs are immobilized simultaneously during the electropolymerization procedure. For POMs immobilization, several polymeric matrices have been used, such as conducting polymers (i.e. polypyrrole, poly-N-methylpyrrole, polyaniline) and polyimidazole and polyvinylpyridine films.

---

[20] R. L. Greene, G. B. Street, L. J. Suter, Superconductivity in Polysulfur Nitride $(SN)_x$, *Phys. Rev. Lett.* **1975**, *34*, 577-579.
[21] H. Shirakawa, E. J. Louis, A. G. MacDiarmid, C. K. Chiang, A. J. Heeger, Synthesis of Electrically Conducting Organic Polymers: Halogen Derivatives of Polyacetylene, $(CH)_x$, *J. Chem. Soc., Chem. Commun,* **1977**, 578-580.
[22] D. E. Katsoulis, A Survey of Applications of Polyoxometalates, *Chem. Rev.* **1998**, *98*, 359-387.

Utilities of these doped materials have been proposed in the area of catalysis, due to the ease of separation of the POM catalyst from the reaction mixture when it is embedded in a polymer matrix. The incorporation process involves the chemical or electrochemical oxidation of a polymerizable monomer to form a polymer in the presence of POM solution. The more commonly used electrochemical oxidation of the monomer takes advantage of the POMs as the electrolyte. Upon the application of the suitable oxidation potential, the conductive polymer is deposited on the working electrodes (usually carbon or graphite) doped with the anions of heteropolyoxometalate. The POM-doped membrane modified electrodes are sought as electrochemical catalysts, *e.g.* electrocatalytic reduction of O_2, [23] electrocatalytic reduction of NO. [24,25,26,27]

Polypyrrole doped with POMs (*i.e.* $SiW_{12}O_{40}^{4-}$ and $P_2W_{18}O_{62}^{6-}$) via electrochemical polymerization exhibited redox properties inherent to the POMs and to the polypyrrole moiety. The anions were retained in the polymer matrix without being ion-exchanged after repeated potential cycles in electrolyte solutions containing no POMs. Charge compensation on reduction was accomplished by cation insertion instead of anion release.

3.3. RESULTS AND DISCUSSION

3.3.1. HYDROSILYLATION PROCESS (Method A)

The presence of a tunnelling barrier between the molecules and the surfaces can alter the charge-storage time. In this work, our approach was the evaluation of POM-containing molecules attached via linkers to silicon substrate. The linkers, who lie between the redox-active molecular component

[23] G. Bidan, E.M. Genies, M. Lapkowski, Modification of Polyaniline Films with Heteropolyanions: Electrocatalytic Reduction of Oxygen and Protons, J. Chem. Soc., Chem. Commun. **1988**, 533-535.
[24] B. Fabre, G. Bidan, Electrocatalytic behaviour of an electrode coated with a nitrite-sensitive layer based upon an iron-substituted heteropolytungstate doped poly(*N*-methylpyrrole), *J. Chem. Soc.,Faraday Trans.* **1997**, *93*, 591-601.
[25] B. Fabre, G. Bidan, M. Lapkowski, Poly(*N*-methylpyrrole) Films Doped with Iron-substituted Heteropolytungstates: A New Sensitive Layer for the Amperometric Detection of Nitrite Ions, *J. Chem. Soc., Chem. Commun.* **1994**, 1509-1511.
[26] B. Fabre, G. Bidan, Electrosynthesis of different electronic conducting polymer films doped with an iron-substituted heteropolytungstate: choice of the immobilization matrix the most suitable for electrocatalytic reduction of nitrite ions, *Electrochim. Acta* **1997**, *42*, 2587-2590.
[27] T. McCormac, D. Farrell, D. Drennan, G. Bidan, Immobilization of a Series of Dawson Type Heteropolyanions, *Electroanalysis* **2001**, *13*, 836-842.

and the silicon electrode, act as tunneling barriers and can be optimized by variation in structure and connectivity to obtain the desired tunneling probability. Tuning the tunnelling probability will have a direct impact on the charge retention time of the molecule. For this purpose functionalized POMs with different linker lengths were synthesised.

The hydrosilylation process route for the selected alkenes- and alkynes-substituted POMs derivatives is shown in Scheme 3. Monolayers were prepared by thermally induced hydrosilylation reaction between hydrogenated Si(100) (substrate **A**) and the corresponding POM derivative to afford substrates **Si-A5**-**A7**, **Si-A10**, **Si-A11**, **Si-A15**, **Si-A22**, and **Si-A25**, respectively. As usual for organic salts of POMs, all compounds synthesized in Part 2 are very soluble in polar solvents such as acetone, acetonitrile, DMF or DMSO and insoluble in apolar (pentane, diethyl ether) and protic solvents (water, ethanol). Therefore, for the wet hydrosilylation approach, which implies the dissolution of the starting reactants in a solvent, our choice was limited to the polar, aprotic solvents with a high boiling point, since the thermally induced hydrosilylation takes place at temperatures higher than 180°C. Although we are limited by the dissolution of functionalized POM, the neat method was considered, since it does not involve the use of a solvent.

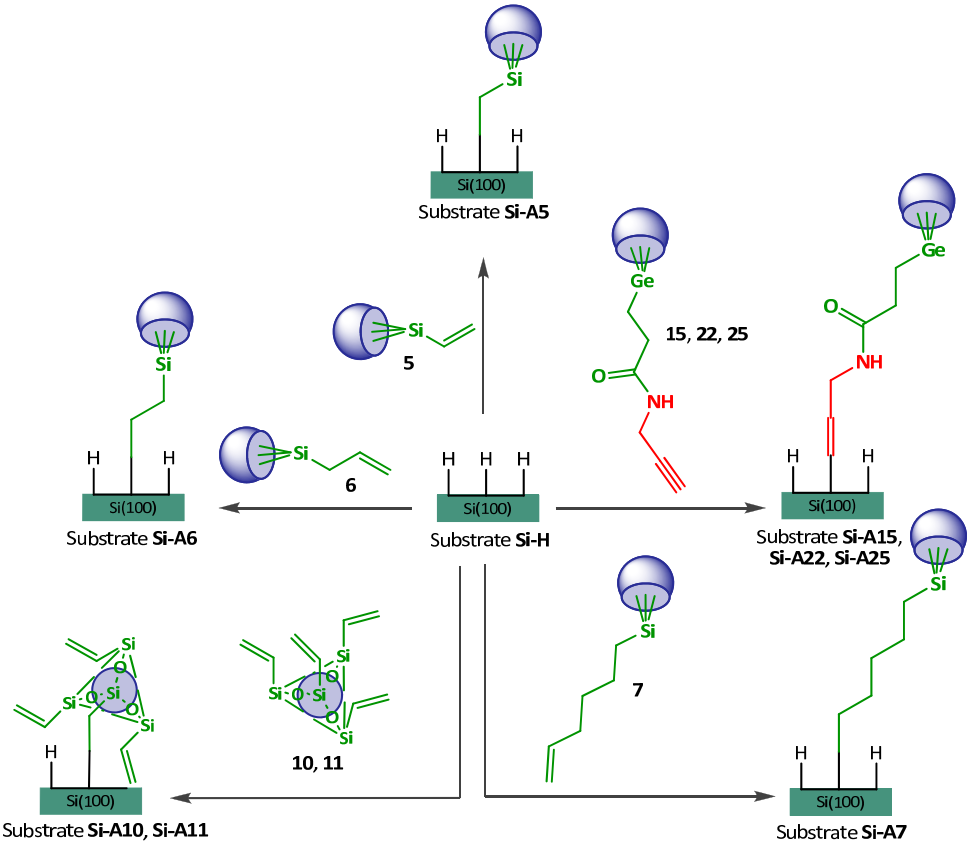

Scheme 3. Synthetic routes for the hydrosilylation method.

The substrates formed by hydrosilylation were investigated by means of cyclic voltammetry at scan rates ranging from 5 to 100 $mV \cdot s^{-1}$. The potential window ranged from 0 to -2.5 V. The electrochemical measurements were made mainly in acetonitrile/ 10^{-1} M Bu_4NBF_4 solution, the electrolyte solution was degassed with argon before using. In all cases the characteristic redox waves of the polyoxometalates could not been observed. To enlarge the electrochemical window, ionic liquids were investigated for the study of Si-POMs derivatized surfaces. A few representative voltammograms for the Si-POMs modified substrate are shown bellow, although for all substrates presented in **Scheme 3** the cyclic voltammograms were registered however they did not exhibit the electrochemically signature of the POMs derivative (*see* **Figures 7-10**). After the hydrosilylation the substrates were washed with copious amounts of acetonitrile and ultrasonicated in acetonitrile three times (× 5 minutes) to ensure that are not physisorbed species at the silicon surface. For the substrates **Si-A10** and **Si-A15** a broad reduction wave can be noticed around -2 and -2.3 V, respectively.

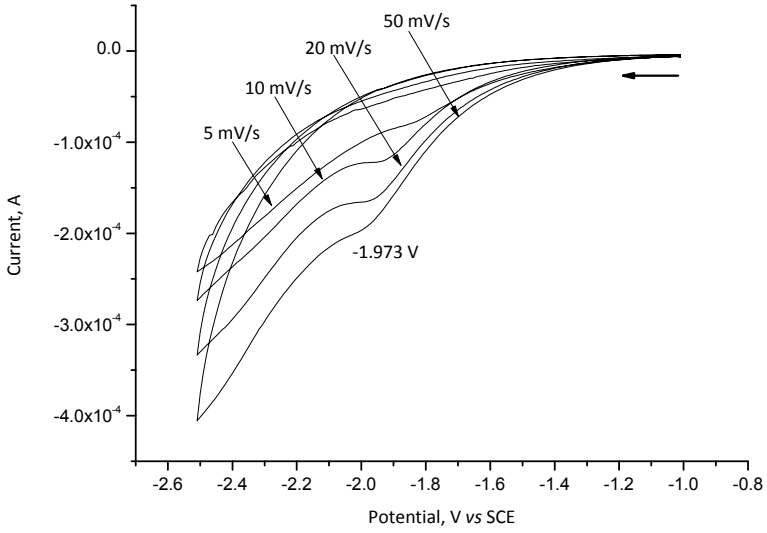

Figure 7. Cyclic voltammetry recorded for **Si-A10** (10^{-1}M Bu_4NBF_4 in acetonitrile). Different scan rate: 5, 10, 20, 50 $mV \cdot s^{-1}$. Conditions: DMF/180°C/2hrs. Electrode surface: 0.75 cm^2 exposing 0.55 cm^2 area.

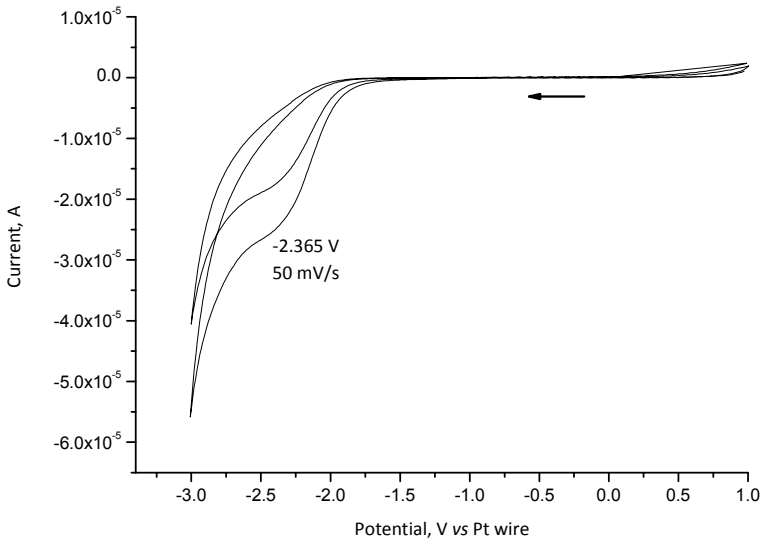

Figure 8. Cyclic voltammetry recorded for **Si-A15** (ionic liquid). Scan rate: 50 $mV \cdot s^{-1}$. Conditions: neat/180°C/2hrs. Electrode surface: 0.75 cm^2 exposing 0.55 cm^2 area.

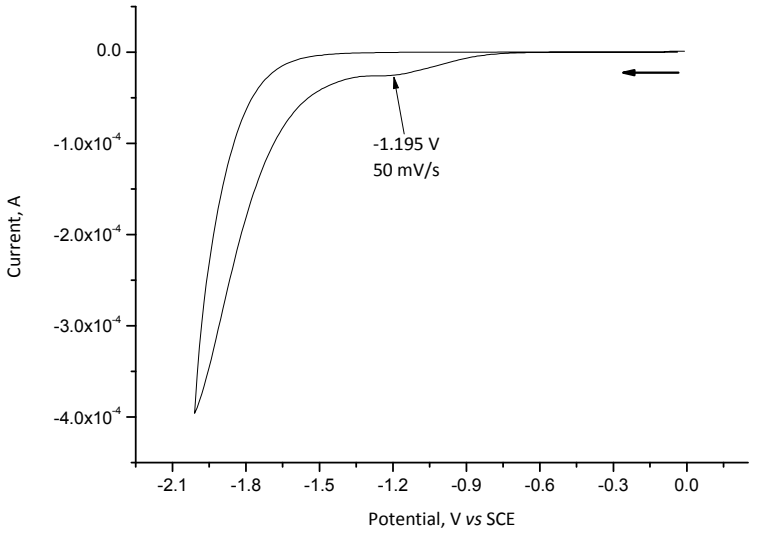

Figure 9. Cyclic voltammetry recorded for **Si-A15** (10^{-1}M Bu_4NBF_4 in acetonitrile). Scan rate: 50 $mV \cdot s^{-1}$. Conditions: neat/180°C/2hrs. Electrode surface: 0.75 cm^2 exposing 0.55 cm^2 area.

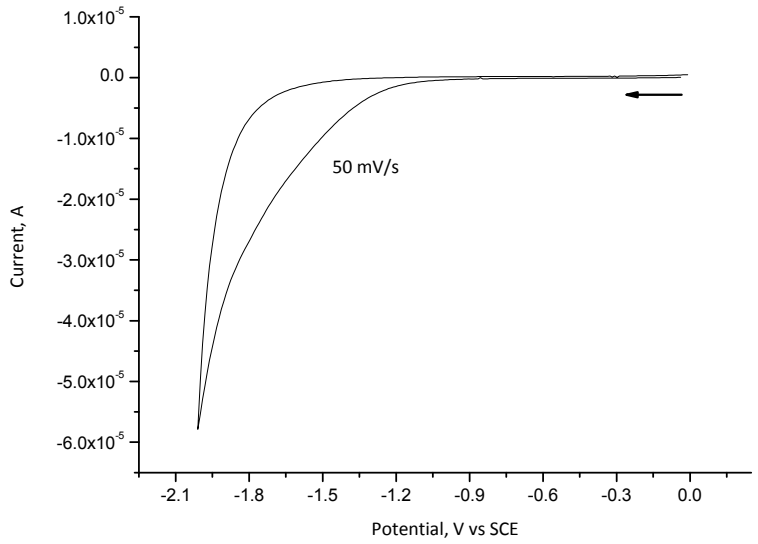

Figure 10. Cyclic voltammetry recorded for **Si-A22** (10^{-1}M Bu_4NBF_4 in acetonitrile). Scan rate: 50 mV·s^{-1}. Conditions: neat/180°C/2hrs. Electrode surface: 0.75 cm^2 exposing 0.55 cm^2 area.

X-ray photoelectron spectroscopy (XPS) analysis of the substrates **Si-A15** (Figure 11), **Si-A22** (Figure 12), **Si-A5-A7** (Figure 13, Figure 14, Figure 15), **Si-A10** (*not shown*), and **Si-A11** (*not shown*) confirms the presence of W and Ge/P at the silicon surface. The W $4f_{7/2}$ and $4f_{5/2}$ binding energies around 36 and 38 eV, the Ge 3d binding energy of 33 eV and the P 2p binding energy of 134 eV are comparable with those reported in the literature and undoubtedly must result from the POM derivative. Also, a high degree of oxidation of the silicon surface is noticeable from the Si 2p core-level spectrum (Si-O, around 103 eV) indicating the POM oxidized silicon surface upon thermal hydrosilylation.

Undoubtedly, the W 4f, Ge 3d and P 2p XPS signals have the only origin of the POM derivative. In the binding energy window between 98 and 106 eV, a well-resolved Si 2p signal appears at *ca.* 103 eV characteristic of SiO_2. In addition, the W 4f signal is always present in doublet shape with binding energy located at around 36 and 38 eV for W $4f_{7/2}$ and $4f_{5/2}$ levels, which are closely similar to the reported data of 35.5 and 37.4 eV for the $K_4SiW_{12}O_{40}$ powder. These binding energy values are consistent with the spin orbit splitting of the W 4f level in oxidation state of +6.[28]

[28] J. Wang, Z. Wu, H. Zhang, Z. Zhao, X. Wang, Q. Wei, *Chem. J. Chin. Univ.* **1992**, *13*, 1428.

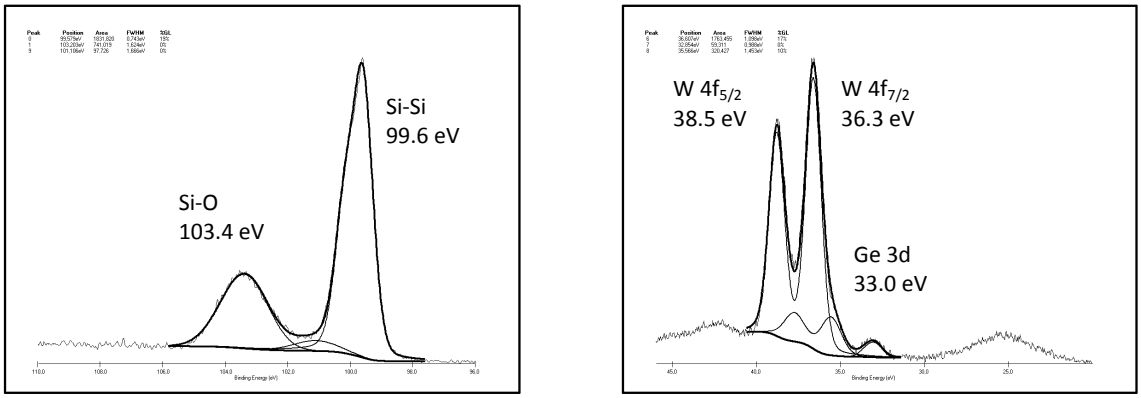

Figure 11. The Si 2p, W 4f and Ge 3d core-level spectrum of substrate **Si-A15** formed by neat hydrosilylation.

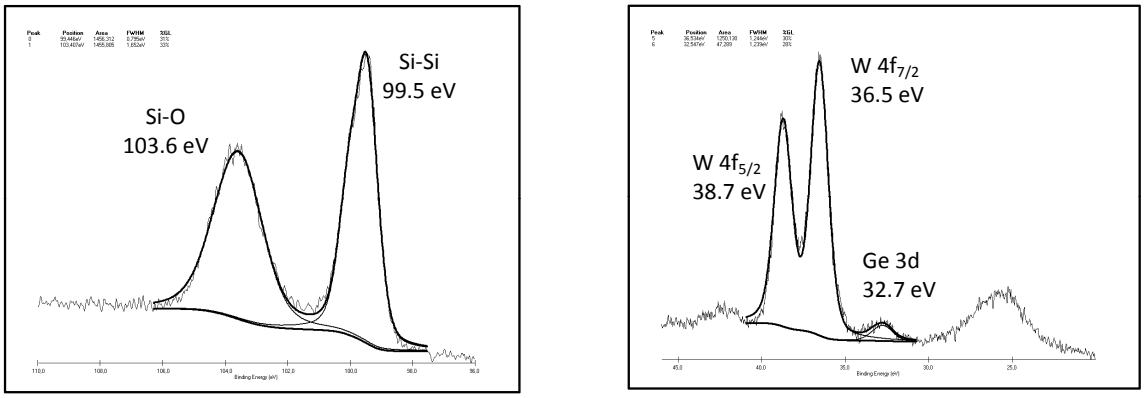

Figure 12. The Si 2p, W 4f and Ge 3d core-level spectrum of substrate **Si-A22** formed by neat hydrosilylation.

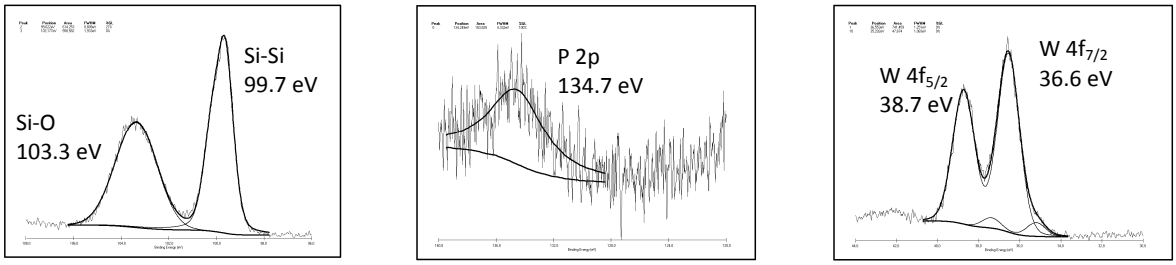

Figure 13. The Si2p, P 2p and W 4f core-level spectrum of substrate **Si-A5** formed by neat hydrosilylation.

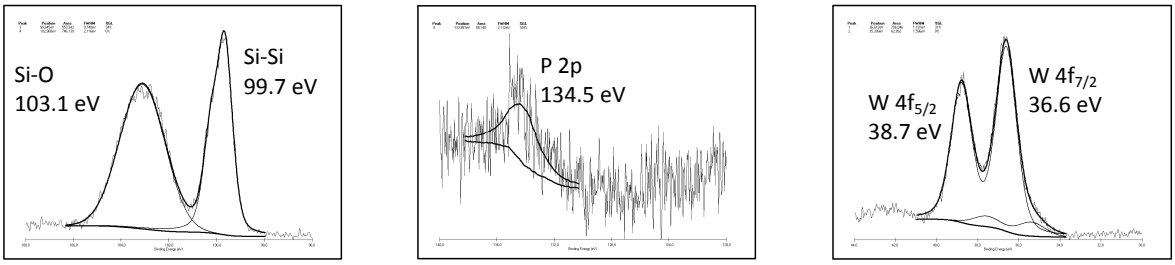

Figure 14. The Si2p, P 2p and W 4f core-level spectrum of substrate **Si-A6** formed by neat hydrosilylation.

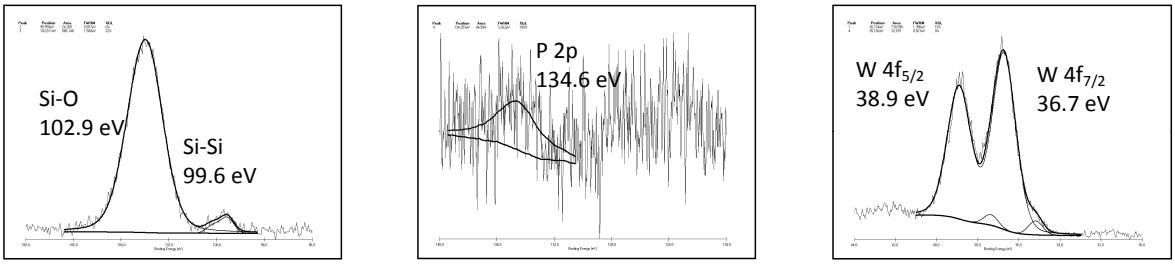

Figure 15. The Si2p, P 2p and W 4f core-level spectrum of substrate **Si-A7** formed by neat hydrosilylation.

For all the samples investigated by means of cyclic voltammetry the redox waves characteristic of the POMs do not appear, probably due to a charge transfer impediment between the silicon substrate and the POMs grafted onto it. Also, the oxidation of the silicon substrate during the thermally activated process needs to be considered. Although, we are confident that the hydrosilylation process took place, we believe that this procedure does not allow the formation of a dense redox-active layer of POMs.

3.3.2. MULTI-STEPS GRAFTING PROCEDURES

3.3.2.1. Hydrosilylation (Method B)

The grafting process was carried out using a two-steps procedure (**Scheme 5**). Substrate **Si-B26** was formed by exposing the freshly etched samples (silicon macroelectrodes) to a 0.5 mM solution of the diazonium salt (compound **27**, *see* **Scheme 4**) in anhydrous acetonitrile under an inert atmosphere during 5 hours. After the grafting the sample ware ultrasonicated in acetonitrile to remove the residual diazonium salt and the physisorbed materials, and then dried with an argon

flow.[29] Substrate **Si-B26** was plunged in a compound **4** DMF solution and refluxed several hours to afford substrate **Si-B4**.

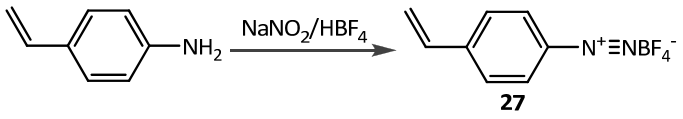

Scheme 4. The synthesis of the diazonium compound **27**.

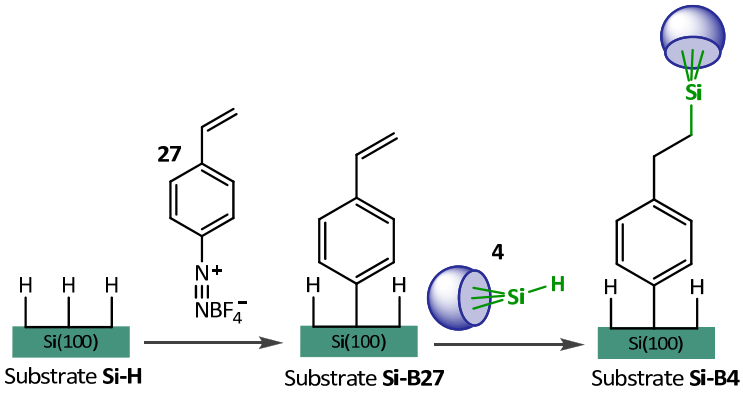

Scheme 5. Schematic representation of the multi-step hydrosilylation process.

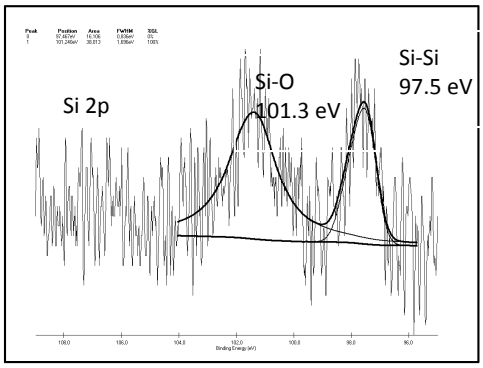

Figure 16. The Si 2p core-level spectrum of substrate **Si-B26**.

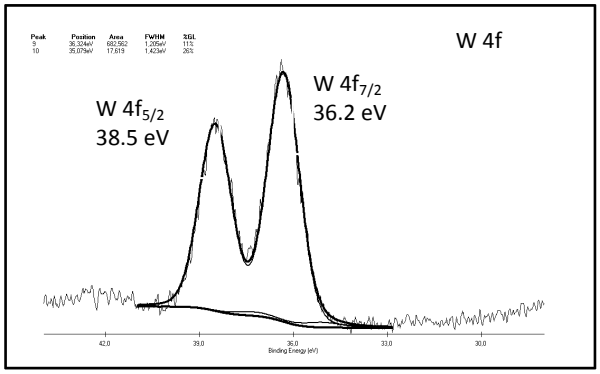

Figure 17. The W 4f core-level spectrum of substrate **Si-B4**.

The XPS measurements recorded for the **Si-B26** substrate (Figure 16), showed that the signals attributable to the Si 2p (binding energies 101.4 eV and 97.6 eV corresponding to the SiO_2 and Si-Si, respectively) are considerably diminished, indicating a good surface coverage. The representative W

[29] T. He, J. He, M. Lu, B. Chen, H. Pang, W.F. Reus, W.M. Nolte, D.P. Nackashi, P.D. Franzon, J.M. Tour, Controlled Modulation of Conductance in Silicon Devices by Molecular Monolayers, *J. Am. Chem. Soc.* **2006**, *128*, 14537-14541.

4f XPS spectrum for the substrate **Si-B4** is shown in Figure 17, indicating for the presence of POMs at the silicon surface. Substrate **Si-B4** was also investigated by means of cyclic voltammetry. The characteristic redox waves of the POMs were not observed (*results not shown*).

3.3.2.2. Peptidic bond formation *via* silanization (Method C)

In this study, POM derivatives of type **14** and **21** are used to form covalently bonded layers onto a silicon dioxide surface (growth chemically) previously derivatized with aminopropyl triethoxysilane *via* a silanization method. The oxide layer acts as a tunneling barrier for the electrons and its thickness can be optimized to obtain desired redox potentials and also to tune the charge retention times.[30]

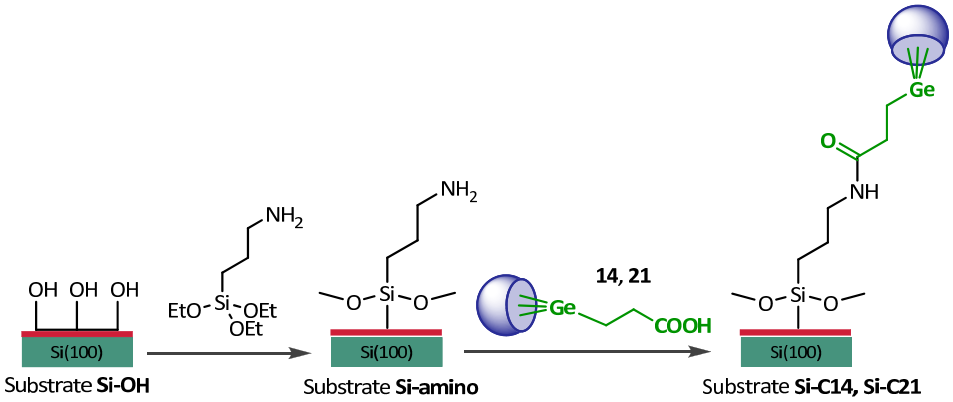

Scheme 6. Schematic representation of the silanization method.

For the formation of substrates **Si-C14** and **Si-C21** a two step procedure is envisaged (Scheme 6). To generate an amino function-terminated monolayer on the silicon dioxide surface (substrate **Si-amino**), the triethoxy propylamine was reacted with the silicon oxide surface (substrate **Si-OH**) in toluene at 80°C in the presence of triethylamine. The intermediary substrate **Si-amino** was first investigated by means of XPS measurement, to ensure that the derivatization process was successful. The full spectrum of substrate **Si-amino** shows the presence of all expected elements: Si, C and N (Figure 18). The high resolution of N 1s signal (Figure 19, right) shows the presence of one peak situated at 400.0 eV, indicating that the amino-terminated monolayer has been formed. Moreover,

[30] G. Mathur, S. Gowda, Q. Li, S. Surthi, Q. Zhao, V. Misra, Properties of Functionalized Redox-Active Monolayers on Thin Silicon Dioxide – A Study of the Dependence of Retention Time on Oxide Thickness, *IEEE Trans. Nanotechnol.* **2005**, *4*, 278-283.

the Si 2p signal (**Figure 19**, left) is also visible at 102.3 eV which is the binding energy characteristic of SiO_2.

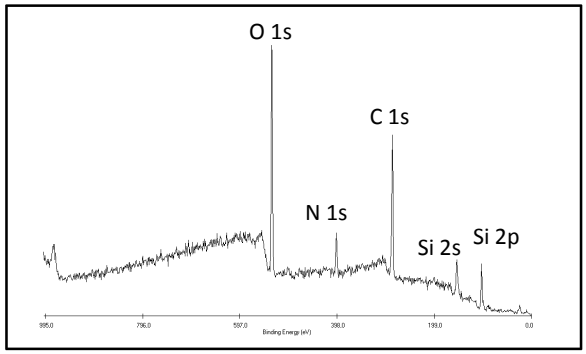

Figure 18. Full XPS spectrum recorded for substrate **Si-amino**.

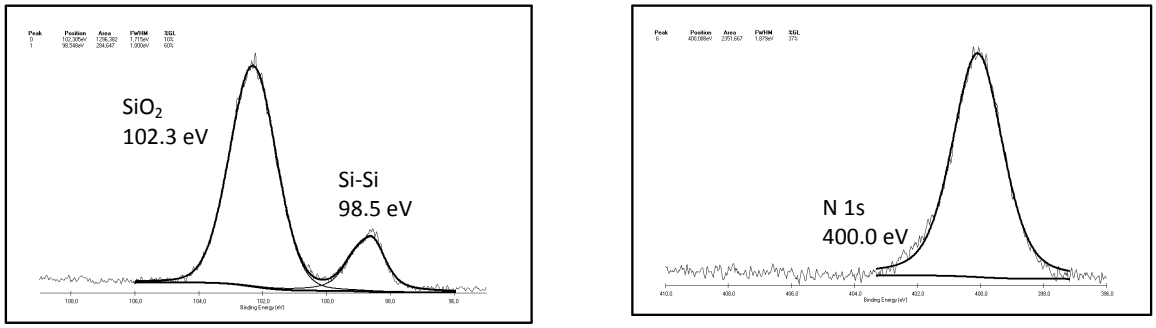

Figure 19. The Si 2p and N 1s core-level spectrum of substrate **Si-amino**.

The coupling between the substrate **Si-amino** and the carboxylic function of the derivatives **14** and **21** were performed in acetonitrile in the presence of triethylamine and isobutyl chloroformiate, as coupling agent, to afford substrates **Si-C14** and **Si-C21**, respectively. Their XPS analysis confirms the presence of W and Ge at the silicon surface. The W $4f_{7/2}$ and $4f_{5/2}$ binding energies of 37.4 and 39.6 eV attributable to the W-O bond are comparable with those reported in the literature (**Figure 20**, left). Although very complicated, the N 1s core-level spectrum, at about 400 eV (**Figure 20**, right), can be curve-fitted with two peak components, the one at 401.4 eV attributable to unreacted NH_2 species and the other one at about 403 eV attributable to the $[Bu_4N]^+$ couterion from the POM molecule. Due to the abundance of nitrogen atoms at the surface the N-C binding energy from the peptidic bond is too unsure to ascertain. The XPS spectra for C 1s and O 1s levels corresponding to substrates **Si-amino** and **Si-C14**, respectively, are not discussed in detail due to their complex origins and less characteristic features.

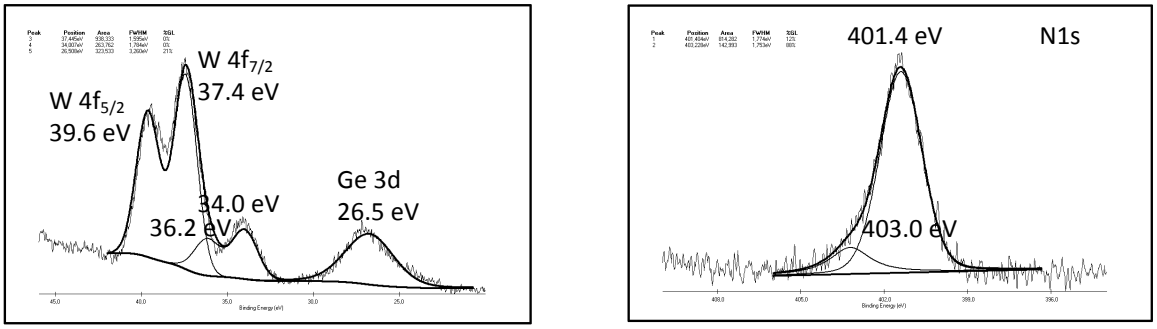

Figure 20. The W 4f, Ge 3d and N 1s core-level spectrum of **Si-C14**.

The SAMs of POMs formed by silanization/coupling method were investigated by cyclic voltammetry in acetonitrile using tetrabutylammonium tetrafluoroborate as supporting electrolyte (**Figure 21**, **Figure 22**). The specific redox waves of the POMs, grafted onto the silicon dioxide surface, can not be seen in these voltammograms.

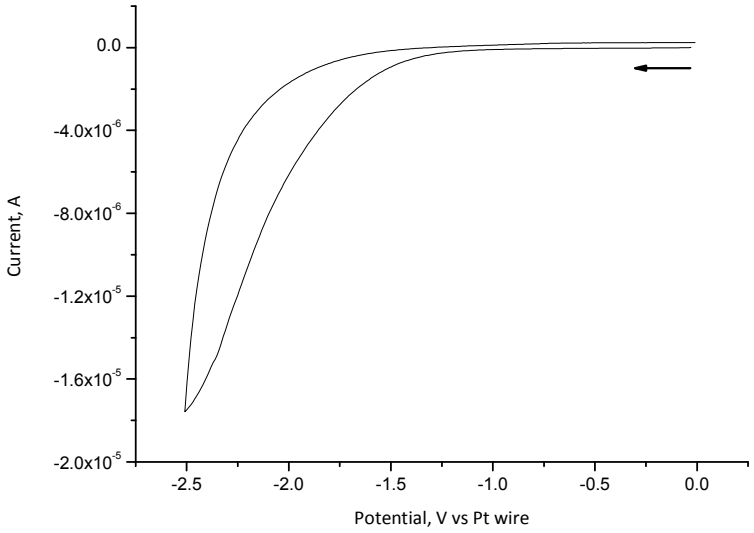

Figure 21. Cyclic voltammetry recorded for **Si-C14** (10^{-1}M Bu_4NBF_4 in acetonitrile). Scan rate: 20 $mV \cdot s^{-1}$. Electrode surface: 0.75 cm^2 exposing 0.55 cm^2 area.

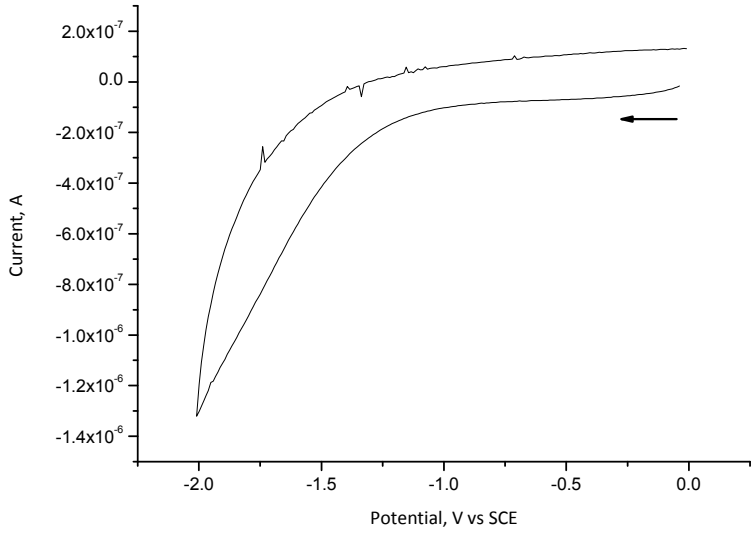

Figure 22. Cyclic voltammetry recorded for **Si-C21** (10^{-1}M Bu_4NBF_4 in acetonitrile). Scan rate: 50 mV·s^{-1}. Electrode surface: 0.75 cm^2 exposing 0.55 cm^2 area.

We can conclude that the grafting method described in this part has succeeded, even if it is in small yield, the XPS results showed the presence of the W and Ge on these samples. Anyway, other methods of surface characterization are needed, in order to assure the integrity of the POMs molecule on the silicon substrate. Even if the presence of the POMs at the surface is very poor, we can conclude that the coupling reaction took place in a small yield.

3.3.2.3. "Click" Chemistry (Method D)

Huisgen 1,3-dipolar cycloaddition are exergonic fusion processes that unite two unsaturated reactants and provide fast access to an enormous variety of five-membered heterocycles. The cycloaddition of azides and alkynes to give triazoles is irreversible and usually quantitative. There are many advantages for Sharpless "click" chemistry. For example: (i) azides and alkynes are convenient to introduce, do not react among themselves, and show extraordinary tolerance for other functionality; (ii) the coupling reaction gives a high yield and proceeds under very mild conditions; (iii) regioselective copper (I) catalyst system used in this reaction is surprisingly indifferent to solvent and pH. So, the advantages of Sharpless "click" chemistry provides a new access to prepare monolayer on different surface and many groups have report SAMs on surface using "click" chemistry.

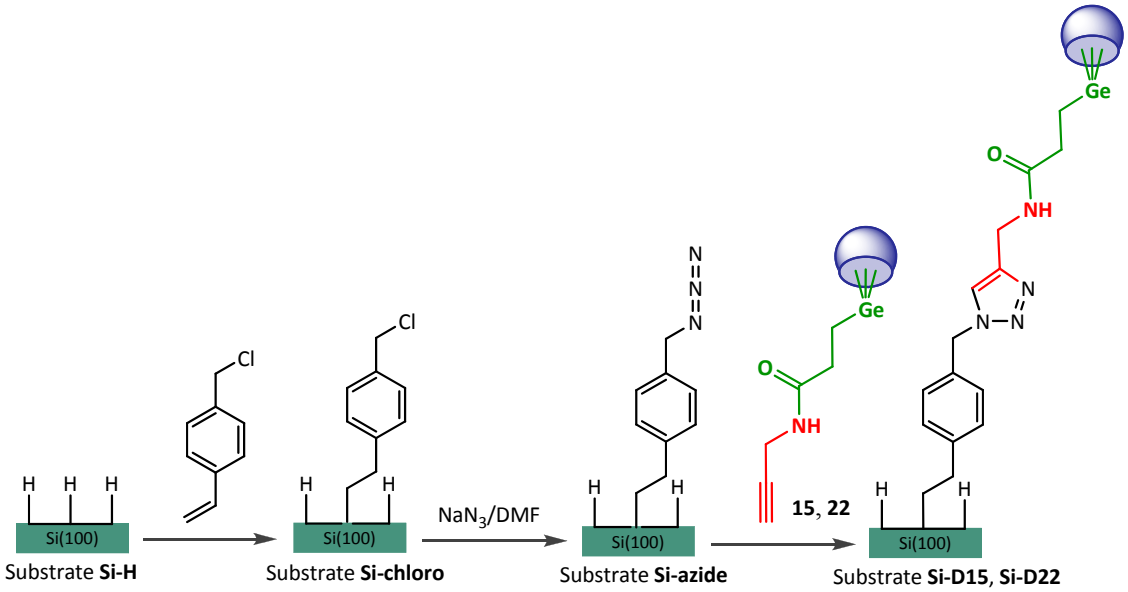

Scheme 7. Schematic representation for the "click" chemistry process.

The functionalization of azide-terminated monolayer on Si(100) using "click" chemistry, specifically, the reaction of POMs-alkynes (**15**, **22**) with surface bond azides, is described as follow. Covalently immobilized, structurally well-defined azide-terminated organic monolayer was prepared from a Si-H surface (freshly prepared) and 4-vinylbenzyl chloride using a hydrosilylation procedure; the Si-C_6H_4-CH_2Cl surface was then introduced in a saturated solution NaN_3/DMF for 18 hours at 80°C to afford the azide-terminated monolayer, Si-C_6H_4-CH_2N_3 (**Scheme 7**).

The full-scan XPS spectrum of substrates **Si-chloro** and **Si-azide** show the presence of all expected elements (*not shown*): Si, O, C, Cl and Si, O, C, N, respectively. **Figure 23** displays one peak clearly noticeable at *ca.* 270 eV which corresponds to the Cl 2s photoelectrons. On the high-resolution spectrum of substrate **Si-azide** (**Figure 24**) it is clearly visible that the Cl 2s signal has almost disappeared.

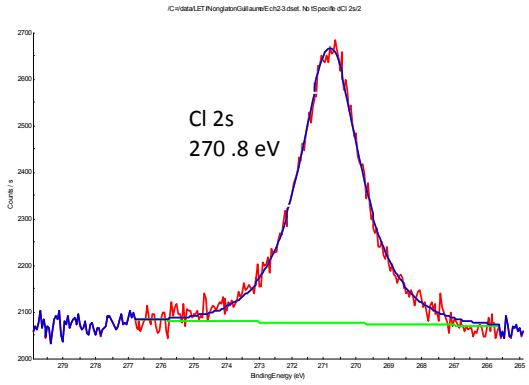

Figure 23. High-resolution XPS spectrum of Cl 2s signal of **Si-chloro** substrate.

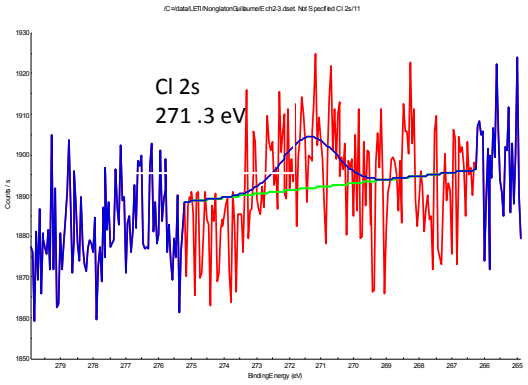

Figure 24. High-resolution XPS spectrum of Cl 2s signal of **Si-azide** substrate.

As shown in **Scheme 7**, two molecules, $(NBu_4)_3[PW_9O_{34}(t\text{BuSiO})_3Ge(CH_2)_2C(O)NHCH_2C{\equiv}CH]$ **15** and $(NBu_4)_4[PW_{11}O_{39}Ge(CH_2)_2C(O)NHCH_2C{\equiv}CH]$ **22**, were especially design to attach on the Si surface via "click" chemistry, and to form a SAM of POMs. To bind these molecules onto the surface by 1,3-dipolar cycloaddition reactions (Sharpless "click" reactions), the azide-terminated surface was completely submerged in a solution of the POMs-alkynes (**15** or **22**) and copper (II) sulphate pentahydrate in DMF. A solution of sodium ascorbate in water was added, and the turbid solution was homogenized and stirred at 25 °C for 48 h (all solutions were degassed with argon to prevent dimerization of the alkyne or oxidation of the Cu(I); the sodium ascorbate acts as a reducing agent, thus generating the catalytically active Cu(I) species *in situ*). Final washing of the SAMs (sonicated in acetonitrile, three times, each for 5 min) and blow drying with nitrogen furnished the final, modified SAMs.

Substrate **Si-D15** was characterized by XPS measurements. The characteristic signals in the W 4f and Ge 3d region are shown in **Figure 25**. By curve fitting we retrieve the characteristic peaks of W 4f and Ge 3d situated at binding energies of 37.6 eV, 39.8 eV and 34.0 ev, respectively.

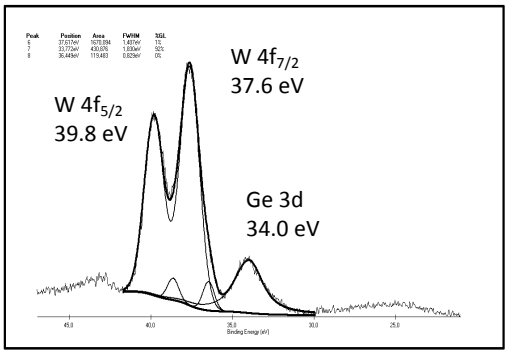

Figure 25. The W 4f and Ge 3d core-level spectrum of substrate **Si-D15**.

The XPS data allowed the elemental analysis of the surface, but complementary ATR-FTIR measurements were performed to identify the types of chemical functionality present on the surface. In the Si-H bond-vibration region of the hydrogenated silicon surface (after 1% HF etching) (**Figure 26**, (A) black curve), two sharp bands can be observed at 2104 and 2134 cm^{-1} corresponding to Si-H and SiH_2, respectively. On the ATR-FTIR spectrum of substrate **Si-chloro**, these two bands completely disappear (**Figure 26**, (A) red curve). In the 2000-2400 cm^{-1} region of substrate **Si-azide** (**Figure 26**, (B)), after Cl/N_3 exchange, a new sharp band is observed at 2100 cm^{-1} and was assigned to the azide group. This band cannot be mistaken for the Si-H vibration as it is sharper, more intense, and does not possess another component (*i.e.* SiH_2 in the case of Si-H).

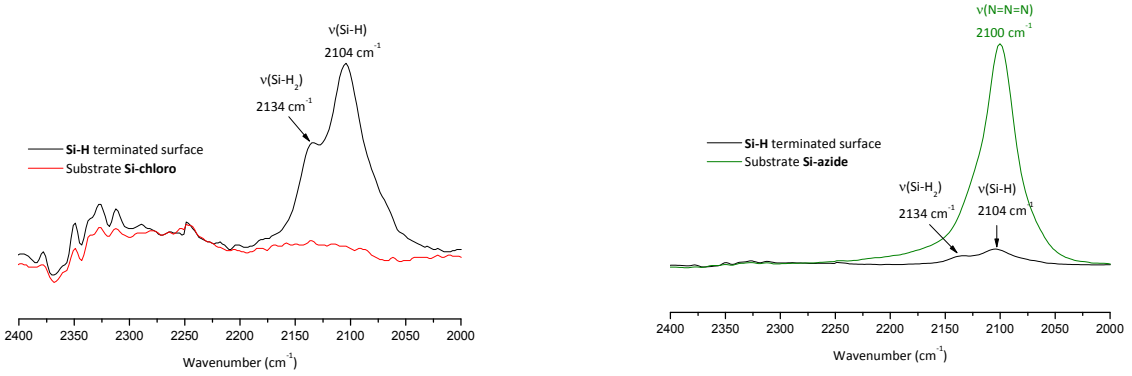

Figure 26. Fragment of the ATR-FTIR spectra of substrate **Si-chloro** (A) and **Si-azide** (B) in comparison with the **Si-H** terminated surface.

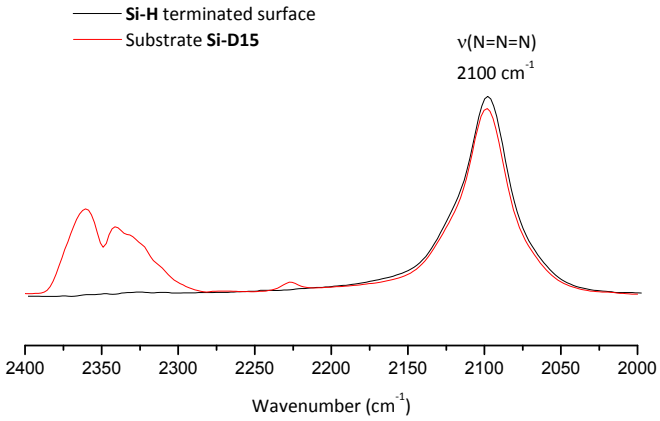

Figure 27. Fragment of the ATR-FTIR spectra of substrate **Si-D15** (red line) in comparison with the substrate **Si-azide** (black line).

The ATR-FTIR of the POMs modified surface (**Figure 27**), substrate **Si-D15**, shows that the sharp band of the azide group at 2100 cm^{-1} does not disappear entirely. However, its intensity is slightly decreased and one can conclude that the reaction between the ethynyl ended POM (compound **15**) and the **Si-azide** surface took place in very small yield and that we did not obtained a dense layer of POMs at the surface. The cyclic voltammetry measurements confirm this supposition seeing as the characteristic redox waves of compound **15** were not retrievable in the CV of substrate **Si-D15** (**Figure 28**).

The substrates formed by "click chemistry" were investigated by cyclic voltammetry in acetonitrile, using Bu_4NBF_4 as supporting electrolyte. One irreversible broad reduction wave can be observed around -1.5 V for the substrate **Si-D22 (Figure 29)**.

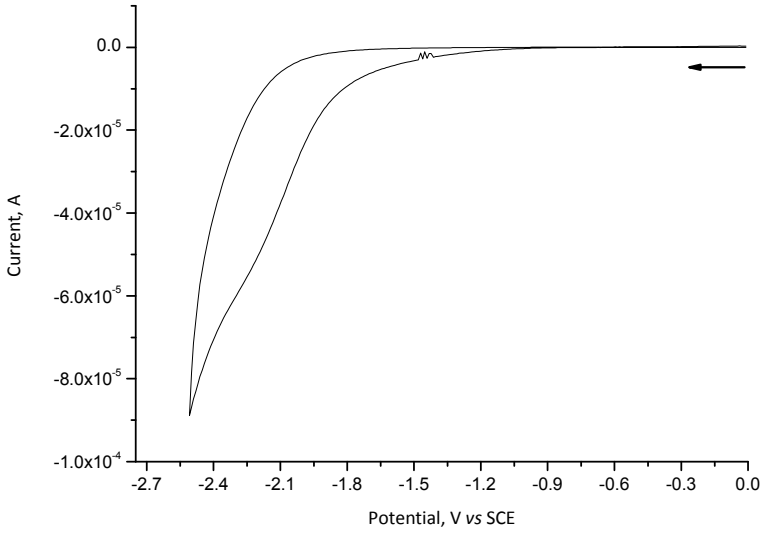

Figure 28. Cyclic voltammetry recorded for substrate **Si-D15** (10^{-1}M Bu_4NBF_4 in acetonitrile). Scan rate: 50 mV·s^{-1}. Electrode surface: 0.75 cm^2 exposing 0.55 cm^2 area.

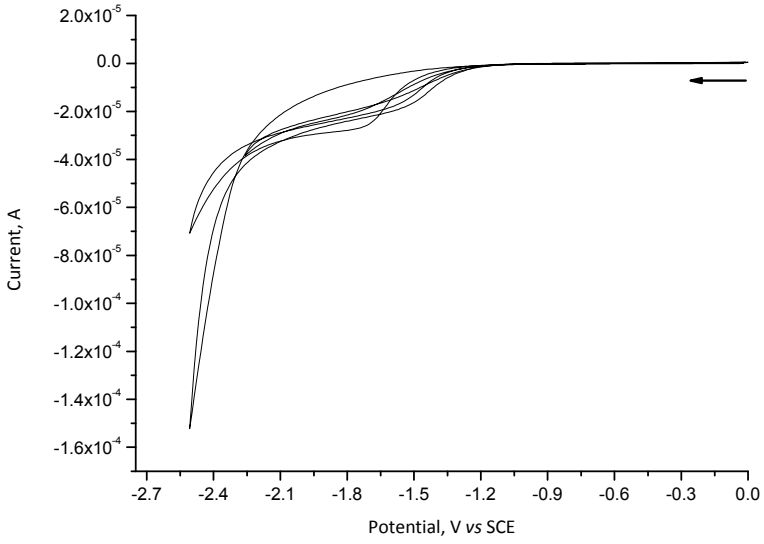

Figure 29. Cyclic voltammetry recorded for substrate **Si-D22** (10^{-1}M Bu_4NBF_4 in acetonitrile). Scan rate: 50 mV·s^{-1}. Electrode surface: 0.75 cm^2 exposing 0.55 cm^2 area.

3.3.3. ELECTROCHEMICAL METHODS

3.3.3.1. Terminal ethynyl (C≡C) as reactant (Method E)

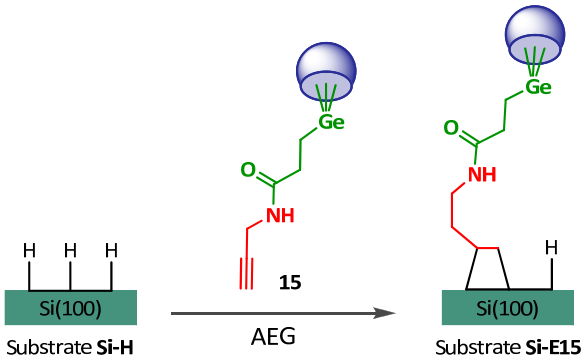

Scheme 8. Schematic representation of the anodic electrografting procedure.

The electrografting procedure (**Scheme 8**), derived partially from the literature, was performed by passing an anodic current through the compound **15** solution at the *n*-type highly doped silicon electrode. Within the potential range of -1.5 to 0 V, three reversible redox couples can be observed by cyclic voltammetry (**Figure 30**) at the silicon-POMs bonded electrode (substrate **Si-E15**). The formal potentials of these redox waves, at the scanning rate 100mV/s, are respectively pointed at -0.51 V for the redox couple I-I', -0.93 V for the redox couple II-II' and -1.38 V for redox couple III-III'. Surprisingly, the redox waves are not very well defined compared with those of compound **15** in solution. The electrode potential was scanned from the lower to higher limit and back at scan rates varying from 20 to 1500 mV/s. The second cathodic and anodic peak current (II-II') exhibits a linear dependence on the scan rate, as a strong indication that POMs are indeed surface-confined. The linear dependency of peak current on scan rate is shown in the **Figure 31**. These electrochemical results indicate that the POM-modified silicon is electrochemically active.

By comparison, the covalent grafting of the functionalized hexamolybdates on an electron-deficient *p*-type Si surface, described by Tour, showed two reversible redox waves for the surface-bonded hexamolybdates (*see* Part 1, page 33, Figure 25). Since the hexamolybdate cluster exhibits one reversible redox couple in acetonitrile solution in this potential range, the additional redox couple, which was found under constant cathodic peak currents, was attributed to the limited electron transfer between the hexamolybdates clusters and the p-type Si substrate. In our case, the POM-modified silicon electrode is electrochemically accessible to three reversible redox states, which

can be assigned to the three redox couples of the polyoxotungstic skeleton. In addition, it exhibits the same electrochemical behavior in propylene carbonate (results not shown here).

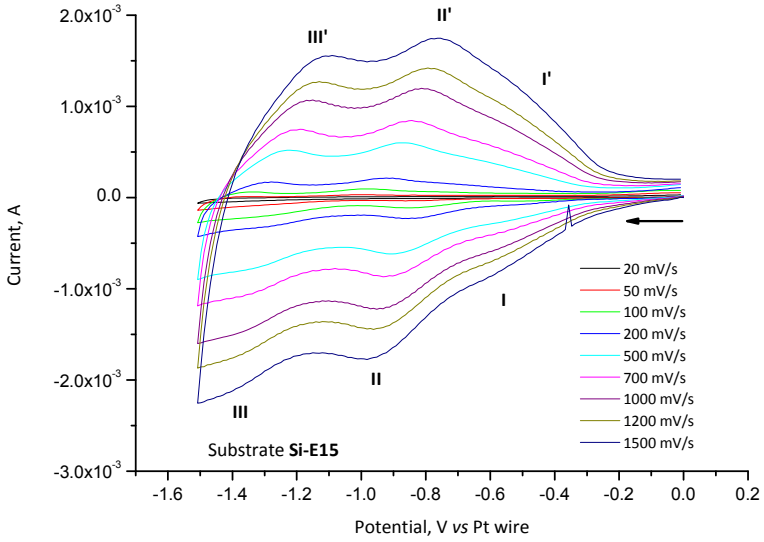

Figure 30. Cyclic voltammograms of **Si-E15** substrate at different scan rates: 20, 50, 100, 200, 500, 700, 1000, 1200, 1500 $mV \cdot s^{-1}$. The experiments were performed in acetonitrile/0.1 M Bu_4NBF_4 using Pt as the reference and counter electrode. Electrode surface: 0.75 cm^2 exposing 0.45 cm^2 area.

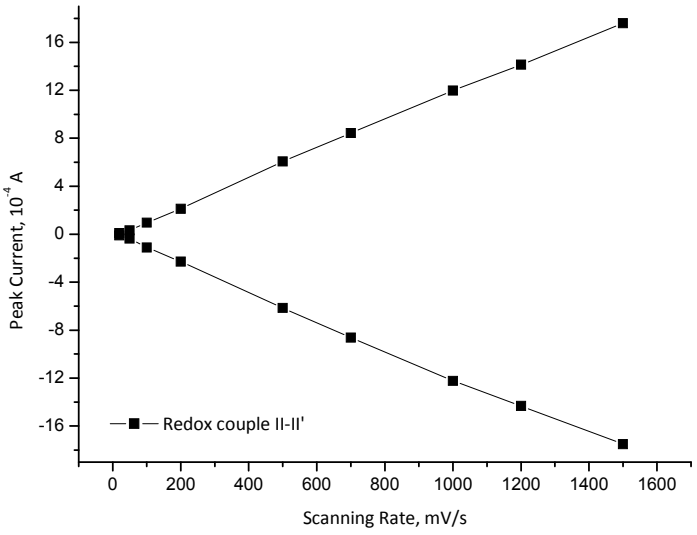

Figure 31. The linear dependency of peak current on scan rate for the second cathodic and anodic peaks (II-II').

The AFM images of substrate **Si-E15** were taken to provide information about the surface morphology and homogeneity of the deposited films. Figure 32 shows tapping mode AFM images of 10 µm × 10 µm of an unmodified silicon sample and a POM-modified silicon sample. These profiles illustrate the varying *z*-axis topography of each surface. The root-mean-square (rms) roughness was 0.800 and 0.435 nm for the unmodified and POM-modified surfaces, respectively.

A B

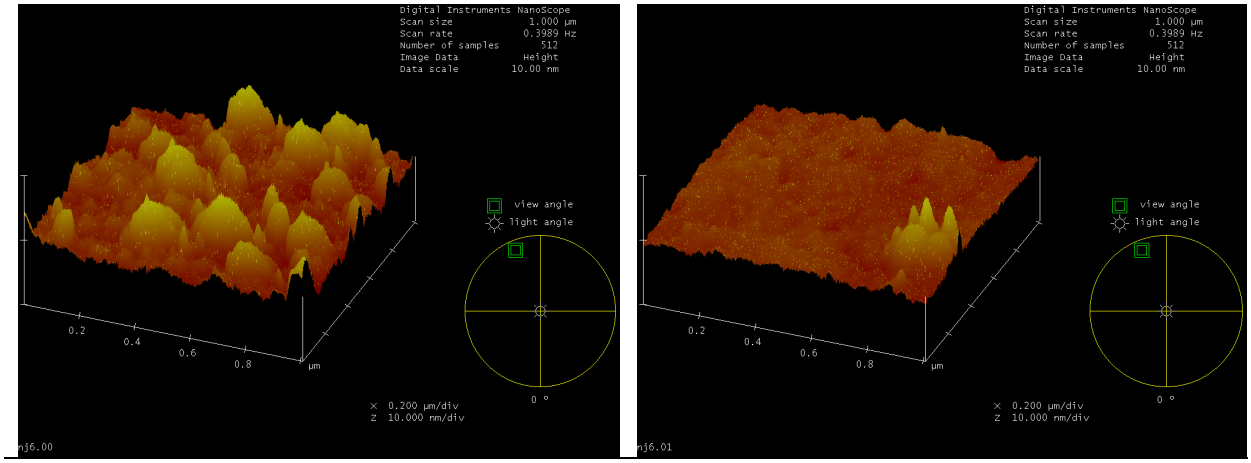

RMS = 0.800 nm RMS = 0.435 nm

Figure 32. Typical AFM images of 10×10 µm areas of (A) unmodified substrate and (B) substrate **Si-E15**.

The AFM measurement showed that the **Si-E15** substrate was deeply modified upon anodic electrografting. However, no important conclusion could be extract from these measurements, and other analyses are imposed, like SEM (Scanning Electron Microscopy).

3.3.3.2. Diazonium chemistry (Method F)

The direct covalent grafting of aryl-POM molecules onto hydride passivated silicon surface via the reaction of aryldiazonium salts is a challenge of great importance for this project. We choose to covalently graft the POM-triazene derivative (compound **17**) onto a hydride-terminated Si(100) surfaces by *in situ* conversion of aryldiethyltriazene into diazonium salts using aqueous HBF_4. For the optimization of the electrografting reaction conditions onto the *n*-silicon electrode, glassy carbon electrode was used at first.

Upon addition of 1 equivalent of HBF_4 to the compound **17** acetonitrile solution, the initial yellow pale solution becomes orange. The overlaid infrared spectrum of those two species (Figure 33), reveals the disappearance of the ν(N-N) stretching modes at 1238 cm^{-1} assigned to the triazene -N=N-

N- moiety. Moreover, the $\{PW_9\}$ backbone is retained upon acidification and we retrieve the W-O stretchings of the polyanionic structure. The ν(N≡N) stretching vibration was not evidentiate in the infrared spectrum.

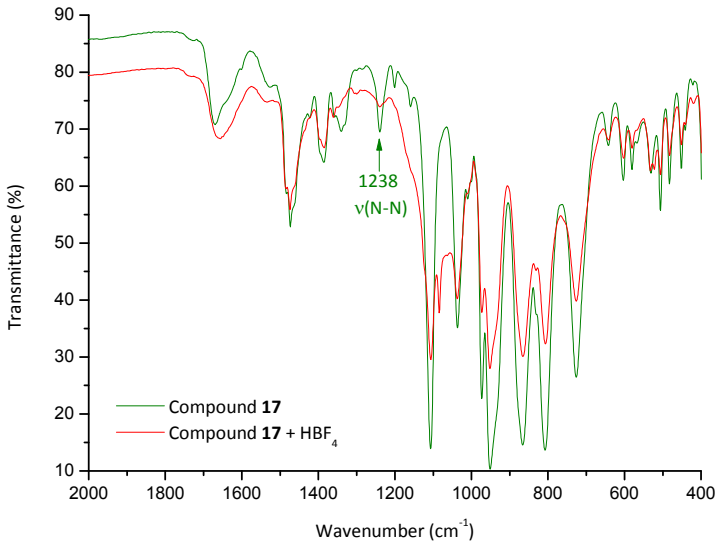

Figure 33. Overlay IR spectrum of the compound **17** and compound **17** upon addition of 1 equivalent HBF_4.

In the following section one-step method for covalently grafting POMs on an electrode surface is described. The electrochemically assisted (method FE) and spontaneous (method FS) grafting procedures of **17** onto glassy carbon and silicon electrode are comparatively studied. Attachment conditions are optimized for a better electroactivity of the electrode surface, including different imposed potential values for various reaction attachment times. Using this method, organically functionalized POMs **17** were grafted onto Si(100) and glassy carbon electrodes through a linker by diazonium chemistry.

3.3.3.2.1. Electrochemically assisted surface grafting (Method FE)

The surface grafting of compound **17** onto the glassy carbon and *n*-type Si(100) was achieved by applying an imposed potential at the working electrode, which was found to be -1.7 V *vs* Pt wire. The electrografting solution typically contained 1 mM of **17** dissolved in a deaerated acetonitrile solution (0.1 M Bu_4NBF_4) and 1 equivalent of HBF_4. Upon acid addition, the compound **17** is converted to the

corresponding diazonium salt, which is attached to the electrode surface by applying a voltage of -1.7 V for various reaction times.

Electrografting at the glassy carbon electrode

Figure 34 displays the overlaid CVs at the glassy carbon electrode in acetonitrile (0.1 M Bu_4NBF_4) of compound **17** before and after the HBF_4 addition. In the CV of compound **17**, besides the four reversible redox waves characteristic to the tungsten-centered single electron processes, an additional peak can be observed at -0.298 V *vs* SCE which can be attributed to the triazene oxidation (**Figure 34**, black curve). Upon HBF_4 addition and the formation of the corresponding diazonium salt, the CV displays an irreversible reduction peak at -1.563 V vs SCE attributable to the reduction of diazonium (**Figure 34**, red curve) giving nitrogen and radicals that react with the carbon electrode surface.

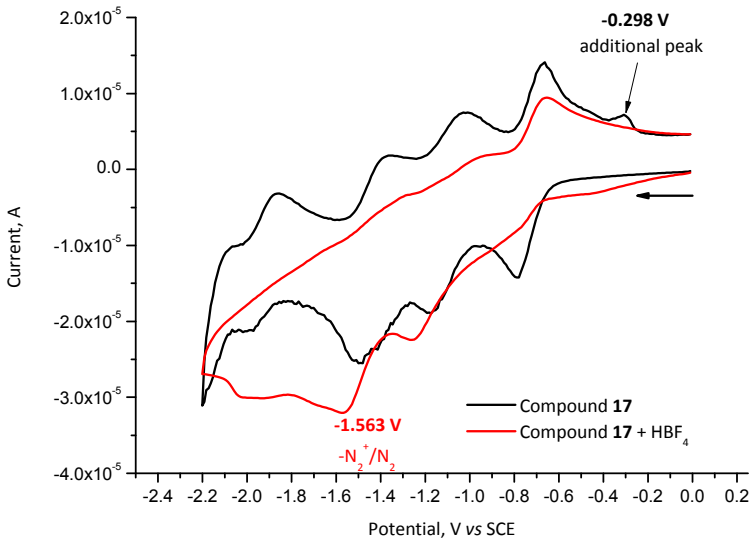

Figure 34. Overlaid CV of **17** in acetonitrile (0.1 M Bu_4NBF_4) (black line) and acetonitrile (0.1 M Bu_4NBF_4)/1 eq. HBF_4 solution (red line) at the glassy carbon electrode. Electrode surface: 0.07 cm^2 area.

The clean glassy carbon electrode was plunged in an acetonitrile solution containing 1 mM **17** and 1 eq. HBF_4 dissolved in acetonitrile (0.1 M Bu_4NBF4). Upon HBF_4 addition the solution, initially yellow-pale, becomes orange almost instantaneously indicative of the diazonium salt formation. A voltage of -1.7 V *vs* Pt wire was then applied for 30, 60 and 120 seconds, respectively. Following the completion of the reaction, the POMs-modified electrode **GC-FE17** (**Scheme 9**) was rinsed with copious amounts

of acetonitrile, ultrasonicated in acetonitrile 3 minutes (× 3), to remove the physisorbed species and dried under a flow of argon. The **GC-FE17** substrate was characterized by cycling voltammetry by using a solution of 0.1 M Bu_4NBF_4 in acetonitrile and 1.0 M Bu_4NPF_6 in propylene carbonate.

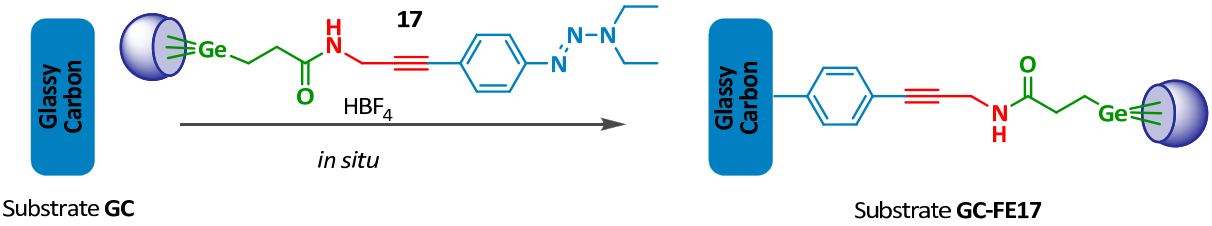

Scheme 9. Schematic representation of the electrografting procedure electrochemically assisted at the glassy carbon electrode.

A scan rate study was performed on the **GC-FE17** substrate in acetonitrile (0.1 M Bu_4NBF_4). The characteristic CVs are shown in **Figure 35**, **Figure 36** and **Figure 37** for the **GC-FE17** formed at an imposed potential of -1.7 V *vs* Pt wire by controlling the reaction times: 30, 60 and 120 seconds, respectively. In all cases the POMs-modified electrode proved to be electrochemically active. Even if the CV of compound **17** in solution manifests four reversible redox waves within the potential range of -2 to 0 V, the **GC-FE17** modified substrate exhibits two distinct reversible redox waves, well defined and stable.

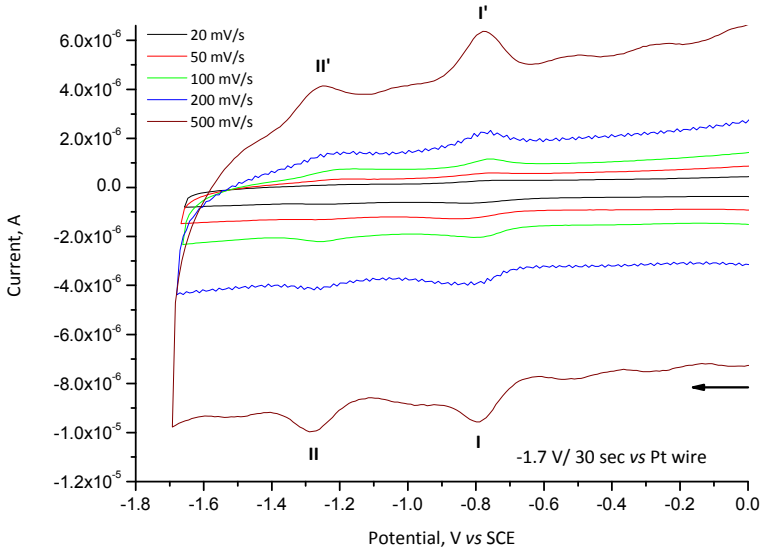

Figure 35. Cyclic voltammetric curves of substrate **GC-FE17** at different scan rates in acetonitrile (0.1 M Bu_4NBF_4). The **GC-FE17** substrate was formed by potentiostatic electrografting at -1.7 V *vs* Pt wire for 30 seconds in acetonitrile (0.1 M Bu_4NBF_4). Electrode surface: 0.07 cm^2 area.

Consequently, it was found that the optimal treatment time was 60 seconds for the best electroactivity of the **GC-FE17** substrate, as a result the discussion will refer to this particular case. According to the peak potentials shown in **Figure 36** (A), the formal potentials of these two redox waves were estimated to be -0.769 and -1.244 V *vs* SCE at a scanning rate of 100 mV/s (**Table 1**), which were assigned to successive reduction of tungsten centers. They are shifted with 41 and 151 mV, respectively towards more negative values in comparison with the firsts two redox waves of compound **17** in solution. This phenomenon can be explained by the fact that the electron transfer is no longer governed by a diffusion mechanism and the redox center is kept at a linker length from the electrode, which could lead to a shift of the redox potential towards more negative values.

The redox acitivity of **GC-FE17** substrate was recorded at different scan rates. As represented in **Figure 36** (B), the cathodic and anodic currents for both redox waves increases linearly with increasing scan rate, thus implying that the POMs entities are surface-confined electroactive molecules. These linear relationships also confirms that the **GC-FE17** substrate is stable and that the electrochemical processes observed at the electrode are only due to the surface-bound species.

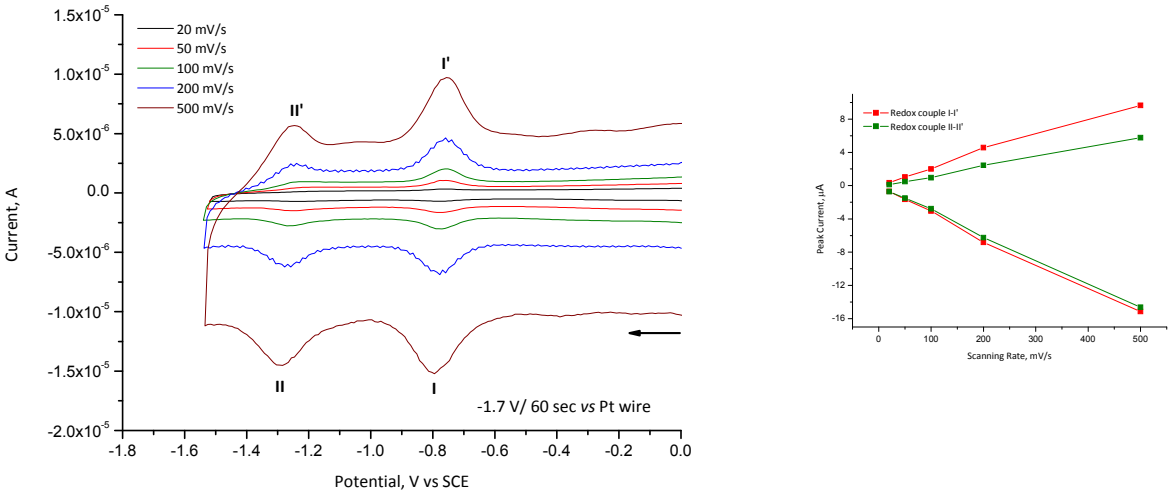

A B

Figure 36. (A) Cyclic voltammetric curves of substrate **GC-FE17** at different scan rates in acetonitrile (0.1 M Bu_4NBF_4). The **GC-FE17** substrate was formed by potentiostatic electrografting at -1.7 V *vs* Pt wire for 60 seconds in acetonitrile (0.1 M Bu_4NBF_4). (B) Linear dependence of peak current on scan rate. Electrode surface: 0.07 cm^2 area.

Table 1. Cyclic voltammetry results for **GC-FE17** substrate in acetonitrile (0.1 M Bu_4NBF_4), formed by potentiostatic electrografting at -1.7 V *vs* Pt wire for 60 seconds in acetonitrile (0.1 M Bu_4NBF_4).

Scan Rate (mV/s)	$E(I)^a(\Delta E(I))^b$	$E(II)^a(\Delta E(II))^b$
20	-0.770 V (17 mV)	-1.213 V (61 mV)
50	-0.769 V (14 mV)	-1.225 V (51 mV)
100	-0.769 V (20 mV)	-1.244 V (40 mV)
200	-0.767 V (24 mV)	-1.254 V (27 mV)
500	-0.775 V (41 mV)	-1.268 V (48 mV)

[a] $E(i) = 1/2\ (E(i)_{ox} + E(i)_{red})$
[b] $\Delta E(i) = E(i)_{ox} - E(i)_{red}$

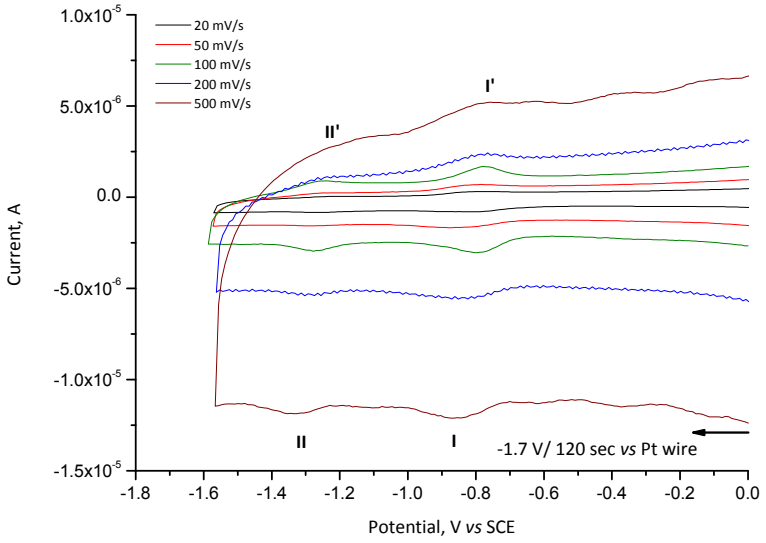

Figure 37. Cyclic voltammetric curves of substrate **GC-FE17** at different scan rates in acetonitrile (0.1 M Bu_4NBF_4). The **GC-FE17** substrate was formed by potentiostatic electrografting at -1.7 V *vs* Pt wire for 120 seconds in acetonitrile (0.1 M Bu_4NBF_4). Electrode surface: 0.07 cm^2 area.

The **GC-FE17** substrate was also investigated in propylene carbonate (1.0 M Bu_4NPF_6) and the representative cyclic voltammograms is shown in **Figure 38** (A). The measured redox potentials are reported in **Table 2**. The reversible redox processes are observed with formal potentials of -0.675 and -1.139 V *vs* SCE at the scanning rate 100 $mV \cdot s^{-1}$, slightly shifted towards less negative values by comparison with the analysis of the same substrate in acetonitrile. The peak currents also show a linear dependence on the scan rate, which indicates that, the electroactive species are indeed surface-confined (**Figure 38**, (B)).

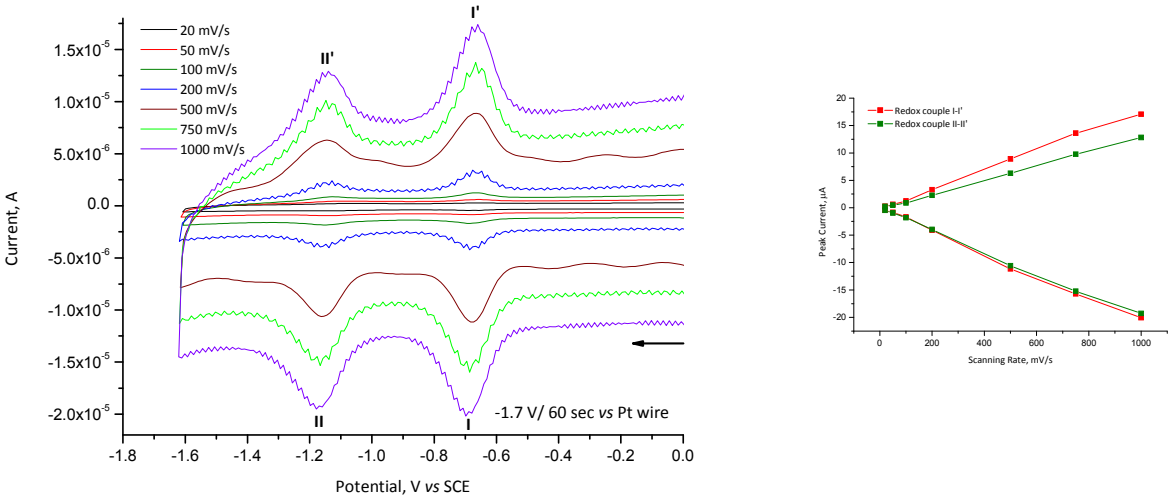

A B

Figure 38. (A) Cyclic voltammetric curves of substrate **GC-FE17** at different scan rates in propylene carbonate (1.0 M Bu_4NPF_6). The **GC-FE17** substrate was formed by potentiostatic electrografting at -1.7 V *vs* Pt wire for 60 seconds in acetonitrile (0.1 M Bu_4NBF_4). (B) Linear dependence of peak current on scan rate. Electrode surface: 0.07 cm^2 area.

Table 2. Cyclic voltammetry results for **GC-FE17** substrate in propylene carbonate (1 M Bu_4NPF_6), formed by potentiostatic electrografting at -1.7 V *vs* Pt wire for 60 seconds in acetonitrile (0.1 M Bu_4NBF_4) (*after* **Figure 38**, A).

Scan Rate (mV/s)	$E(I)^a(\Delta E(I))^b$	$E(II)^a(\Delta E(II))^b$
20	-0.665 V (17 mV)	-1.110 V (58 mV)
50	-0.667 V (20 mV)	-1.120 V (30 mV)
100	-0.675 V (17 mV)	-1.139 V (20 mV)
200	-0.674 V (20 mV)	-1.145 V (21 mV)
500	-0.670 V (13 mV)	-1.150 V (17 mV)
750	-0.676 V (24 mV)	-1.154 V (24 mV)
1000	-0.679 V (24 mV)	-1.157 V (31 mV)

[a] $E(i) = 1/2\ (E(i)_{ox} + E(i)_{red})$
[b] $\Delta E(i) = E(i)_{ox} - E(i)_{red}$

Thus far, the electrografting procedures were undertaken at -1.7 *vs* the Pt wire a quasi-reference electrode, therefore another objective of this section was to find the precise voltage for the

electrografting technique measured *vs* SCE. As it can be seen in **Figure 39**, a **GC-FE17** substrate was formed by applying a voltage of -1.7 V *vs* SCE for 60 seconds and investigated in acetonitrile solution (0.1 M Bu_4NBF_4). We retrieve both redox waves in the same position only not so intense. It seems that the -1.7 V potential value *vs* SCE does not afford the best surface coverage for **GC-FE17** substrate. Unfortunately, this work remained unfinished.

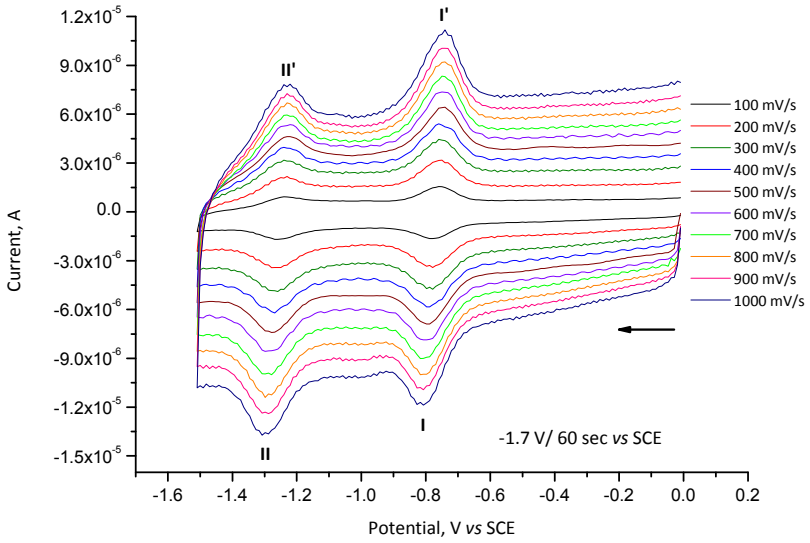

Figure 39. Cyclic voltammetric curves of substrate **GC-FE17** at different scan rates in acetonitrile (0.1 M Bu_4NBF_4). The **GC-FE17** substrate was formed by potentiostatic electrografting at -1.7 V *vs* SCE for 60 seconds in acetonitrile (0.1 M Bu_4NBF_4). Electrode surface: 0.07 cm^2 area.

Electrografting at the n-silicon electrode

The reactive diazonium species need not be isolated and the entire electrografting procedure is conducted in the glove-box to avoid the oxidation of the silicon substrate. The grafting was carried out by chronoamperometry. In the presence of an externally applied cathodic potential and for various time periods we succeeded the formation of substrate **Si-FE17** (**Scheme 10**), which was washed with plenty of acetonitrile and ultrasonicated in acetonitrile three times (× 3 minutes) to ensure that are not physisorbed species at the surface. Than, the substrates were dried under argon and investigated by means of cyclic voltammetry in acetonitrile (0.1 M Bu_4NBF_4) or propylene carbonate (1.0 M Bu_4NPF_6) solution. One important advantage in the constant applied potential mode is that in the cathodic process, the surface electron riches during the reaction, which renders it less susceptible to nucleophilic attack by water, suppressing oxidation.

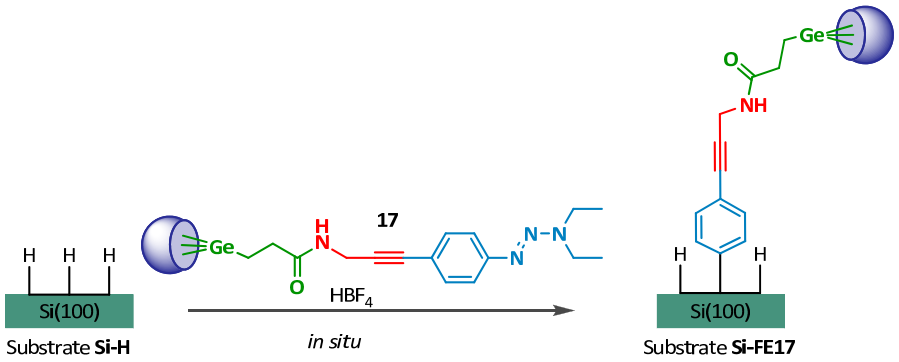

Scheme 10. Schematic representation of the electrografting procedure electrochemically assisted.

Cyclic voltammetry (CV) of compound **17** on *n*-silicon electrode was carried out in acetonitrile using Bu_4NBF_4 (0.1 M) as supporting electrolyte. The CV of **17** in **Figure 40** (A) presents three reversible redox couple not very well defined with the exception of the first one (I-I'). Upon scanning, the intensity of the redox peaks decreases probably due to the oxidation of the silicon surface. Furthermore, the CV of **17** with 1 equivalent HBF_4 (**Figure 40** (B)) shows an additional irreversible peak at -1.279 V corresponding to the reduction of diazonium giving nitrogen and radicals which react with the silicon surface.

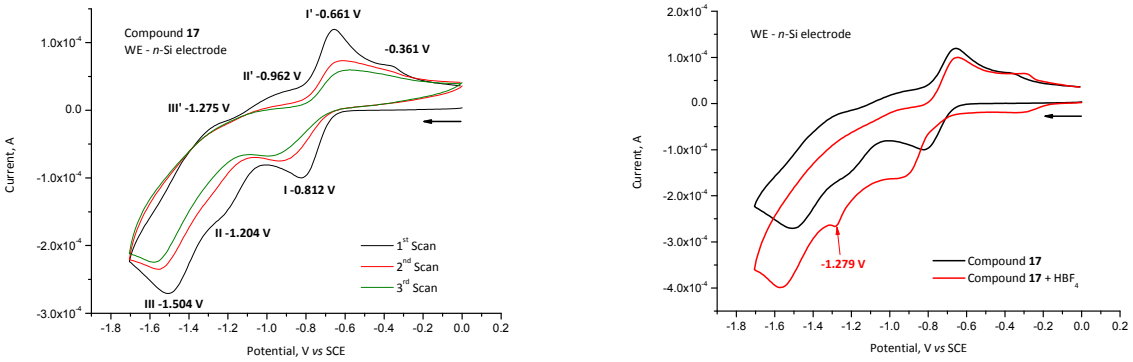

A B

Figure 40. (A) Electrochemical behavior of compound **17** in acetonitrile solution (0.1 M Bu_4NBF_4) at the *n*-Si electrode (scan rate 100 mV/s). (B) Overlaid CyV of **17** in acetonitrile (0.1 M Bu_4NBF_4) (black line) and acetonitrile (0.1 M Bu_4NBF_4)/1 eq. HBF_4 solution (red line) at the *n*-silicon electrode. Electrode surface: 0.60 cm^2 exposing 0.36 cm^2 area.

The electrografting procedure was carried out in a 1 mM compound **17** in acetonitrile (0.1 M Bu_4NBF_4) solution and 1 eq. HBF_4 at a constant potential of -1.7 V *vs* Pt wire electrode. The POM-

functionalized substrate **Si-FE17** was then investigated in a solution of tetrabutylammonium hexafluorophosphate in propylene carbonate (1.0 M Bu_4NBF_4) with Pt reference and counter electrode.

The CV characteristics of substrate **Si-FE17** are shown in Figure 41 (A), Figure 42 (A) and Figure 43 (A) formed by application of a potential of -1.7 V *vs* Pt wire for 30, 60 and 90 seconds, respectively. Between 0 and -1.9 V two redox waves are observed, attributable to the POMs reduction. A linear dependence on the scan rate is indicative that the electroactive species are indeed surface-confined (Figures 41-43, (B)).

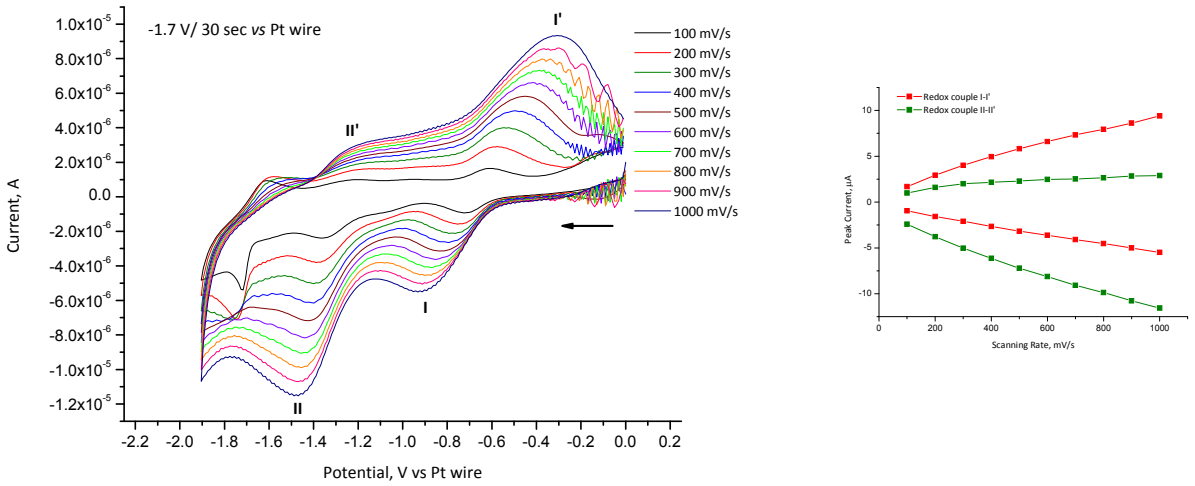

A B

Figure 41. (A) Cyclic voltammetric curves of substrate **Si-FE17** at different scan rates in propylene carbonate (1.0 M Bu_4NPF_6). The **Si-FE17** substrate was formed by potentiostatic electrografting at -1.7 V *vs* SCE for 30 seconds in acetonitrile (0.1 M Bu_4NBF_4). (B) Linear dependence of peak current on scan rate. Electrode surface: 0.60 cm^2 exposing 0.36 cm^2 area.

The redox activities of POMs layer **Si-FE17** were recorded in propylene carbonate (1.0 M Bu_4NPF_6) at different scan rates (Figure 42, A). As represented in Figure 42, B the anodic and cathodic current increases linearly with increasing scan rate, thus implying that the POMs entities are surface-confined electroactive molecules. These linear relationships also confirm that **Si-FE17** layer is stable and that the electrochemical processes observed at the electrode are only due to the surface-bound species.

It can also be seen from the Table 3 that the separation between the oxidation and reduction potentials (ΔE) increases as the scan rate increases. This scan rate dependence of the peak separation can be explained by a slower electron-transfer rate from the redox centre to the silicon substrate

through the long linker. The presence of the linker hampers the electron transfer and when the scan rate is increased, it becomes too fast for the electrons to overcome the linker tunnel barrier and therefore higher potentials are required for electron transfer to occur. A large surface-modification effect can be observed from the Δ*E* value, which increases from 103 to 561 mV and from 38 to 179 mV for the redox process I-I' and II-II', respectively, as the scan rate increases from 100 to 1000 $mV \cdot s^{-1}$. Such behaviour has already been observed by Chidsey *et al*.[31]

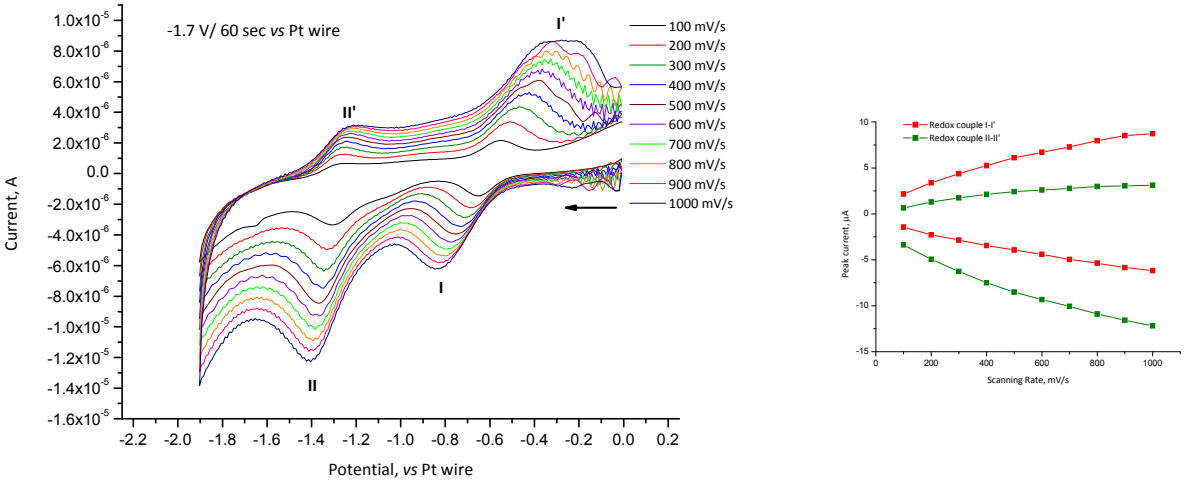

A B

Figure 42. (A) Cyclic voltammetric curves of substrate **Si-FE17** at different scan rates in propylene carbonate (1.0 M Bu_4NPF_6). The **Si-FE17** substrate was formed by potentiostatic electrografting at -1.7 V *vs* SCE for 60 seconds in acetonitrile (0.1 M Bu_4NBF_4). (B) Linear dependence of peak current on scan rate. Electrode surface: 0.60 cm^2 exposing 0.36 cm^2 area.

Table 3. Cyclic voltammetry results for **Si-FE17** substrate in propylene carbonate (1 M Bu_4NPF_6), formed by potentiostatic electrografting at -1.7 V *vs* Pt wire for 60 seconds in acetonitrile (0.1 M Bu_4NBF_4) (*after* **Figure 42**, A)

Scan Rate (mV/s)	$E(I)^a(\Delta E(I))^b$	$E(II)^a(\Delta E(II))^b$
100	-0.601 V (103 mV)	-1.285 V (38 mV)
200	-0.594 V (175 mV)	-1.294 V (66 mV)
300	-0.587 V (245 mV)	-1.299 V (84 mV)
400	-0.580 V (306 mV)	-1.299 V (104 mV)
500	-0.568 V (368 mV)	-1.306 V (128 mV)

[31] N.K. Devaraj, R.A. Decreau, W. Ebina, J.P. Collman, C.E.D. Chidsey, Rate of Interfacial Electron Transfer through the 1,2,3-Triazole Linkage, *J. Phys. Chem. B* **2006**, *110*, 15955-15962.

600	-0.570 V (401 mV)	-1.306 V (146 mV)
700	-0.570 V (447 mV)	-1.308 V (151 mV)
800	-0.566 V (486 mV)	-1.308 V (169 mV)
900	-0.573 V (509 mV)	-1.306 V (184 mV)
1000	-0.561 V (561 mV)	-1.317 V (179 mV)

[a] $E(i) = 1/2\ (E(i)_{ox} + E(i)_{red})$
[b] $\Delta E(i) = E(i)_{ox} - E(i)_{red}$

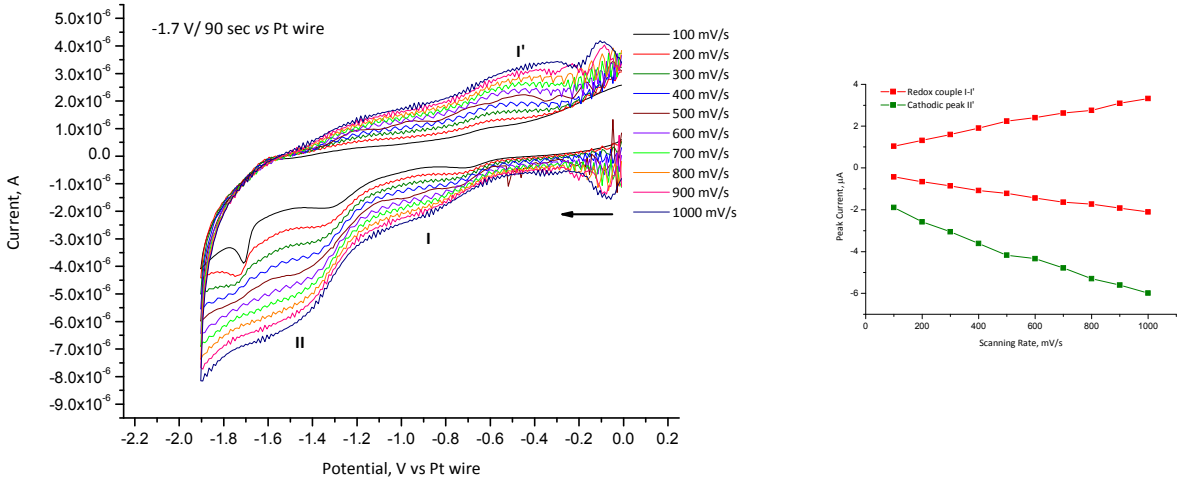

A B

Figure 43. (A) Cyclic voltammetric curves of substrate **Si-FE17** at different scan rates in propylene carbonate (1.0 M Bu_4NPF_6). The **Si-FE17** substrate was formed by potentiostatic electrografting at -1.7 V *vs* SCE for 90 seconds in acetonitrile (0.1 M Bu_4NBF_4). (B) Linear dependence of peak current on scan rate. Electrode surface: 0.60 cm^2 exposing 0.36 cm^2 area.

As in the case of glassy carbon electrode, the best results for the electrografting procedure on a Si-H ended surface were obtained at an imposed potential of -1.7 V *vs* Pt wire for 60 seconds (*see* **Figure 44**, red curve). The stability test showed the constancy of the redox peaks during ten cycles. A significant decrease in the second reduction peak intensity is noticeable from the **Figure 45**.

As the first redox couple presents a better stability towards cycling it was further investigated. It was found that the best results were obtained by applying a potential of -1.5 V vs SCE for 60 seconds. The CV (**Figure 46**, A) results are summarized in **Table 4**. The dependencies of the scan rate on the intensity of the peak current of reduction and oxidation peaks for substrate Si-FE17 is displayed in **Figure 46**, B. Linear relationships can also be observed, which is in agreement with surface-confined species.

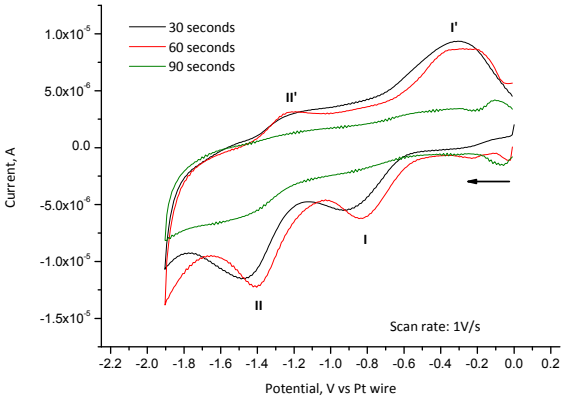

Figure 44. Overlaid CV of substrate **Si-FE17** in propylene carbonate (1.0 M Bu_4NPF_6), at an imposed potential of -1.7 V *vs* Pt wire for 30, 60 and 90 seconds, respectively.

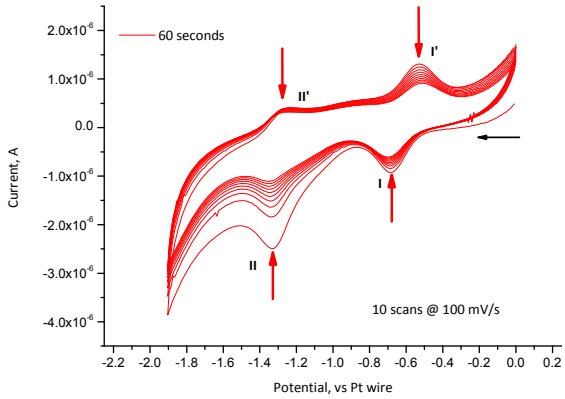

Figure 45. Stability test of the substrate **Si-FE17** towards cycling in propylene carbonate (1.0 M Bu_4NPF_6).

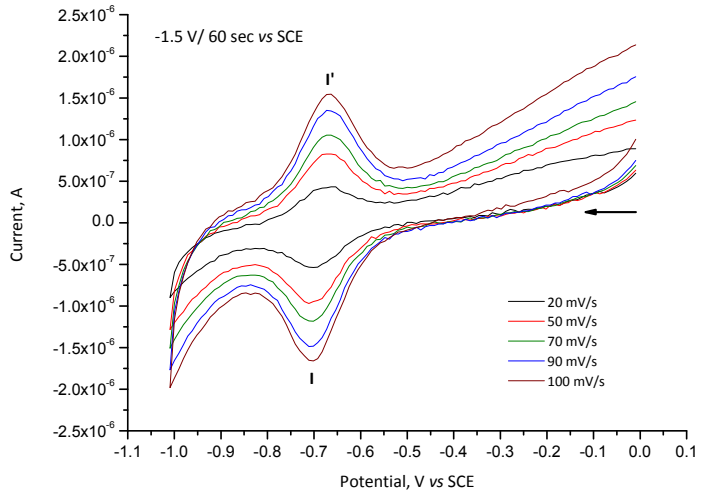

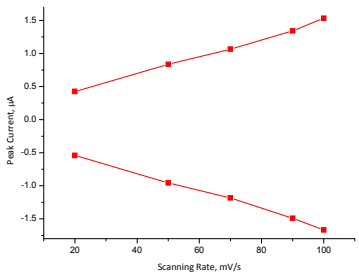

A B

Figure 46. (A) Cyclic voltammetric curves of substrate **Si-FE17** at different scan rates in propylene carbonate (1.0 M Bu_4NPF_6). The **Si-FE17** substrate was formed by potentiostatic electrografting at -1.5 V *vs* SCE for 60 seconds in acetonitrile (0.1 M Bu_4NBF_4). (B) Linear dependence of peak current on scan rate. Electrode surface: 0.60 cm^2 exposing 0.36 cm^2 area.

Table 4. Cyclic voltammetry results for **Si-FE17** substrate in propylene carbonate (1 M Bu_4NPF_6), formed by potentiostatic electrografting at -1.5 V *vs* SCE for 60 seconds in acetonitrile (0.1 M Bu_4NBF_4).

Scan Rate (mV/s)	$E(I)^a(\Delta E(I))^b$
20	-0.684 V (36 mV)
50	-0.687 V (39 mV)
70	-0.687 V (39 mV)
90	-0.688 V (41 mV)
100	-0.686 V (36 mV)

[a] $E(i) = 1/2\ (E(i)_{ox} + E(i)_{red})$
[b] $\Delta E(i) = E(i)_{ox} - E(i)_{red}$

The voltammetric response of substrate **Si-FE17** during cycling is shown in **Figure 47**. As shown, substrate **Si-FE17** manifests stability towards cycling, the intensity of the peak current remains almost the same without any significant loss of electroactivity.

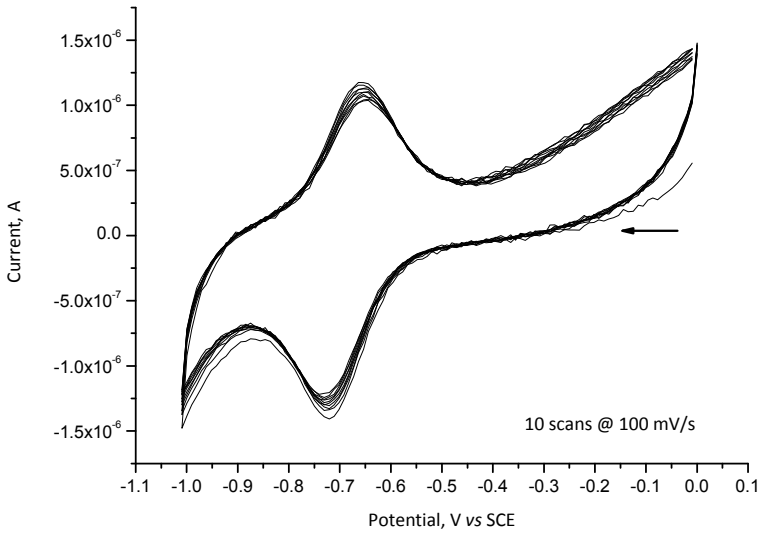

Figure 47. Stability test of the substrate **Si-FE17** towards cycling in propylene carbonate (1.0 M Bu_4NPF_6). The **Si-FE17** substrate was formed by potentiostatic electrografting at -1.5 V *vs* SCE for 60 seconds in acetonitrile (0.1 M Bu_4NBF_4).

The **Si-FE17** substrate was examined by XPS, the high rezolution spectra of Si 2p, W 4f and P 2p are shown in **Figure 48**. The small intensity of the SiO_2 peak at 103.6 eV is indicative that the

oxidation of the silicon surface is minimal and the presence of W 4f and P 2p at the **Si-FE17** surface is confirmed.

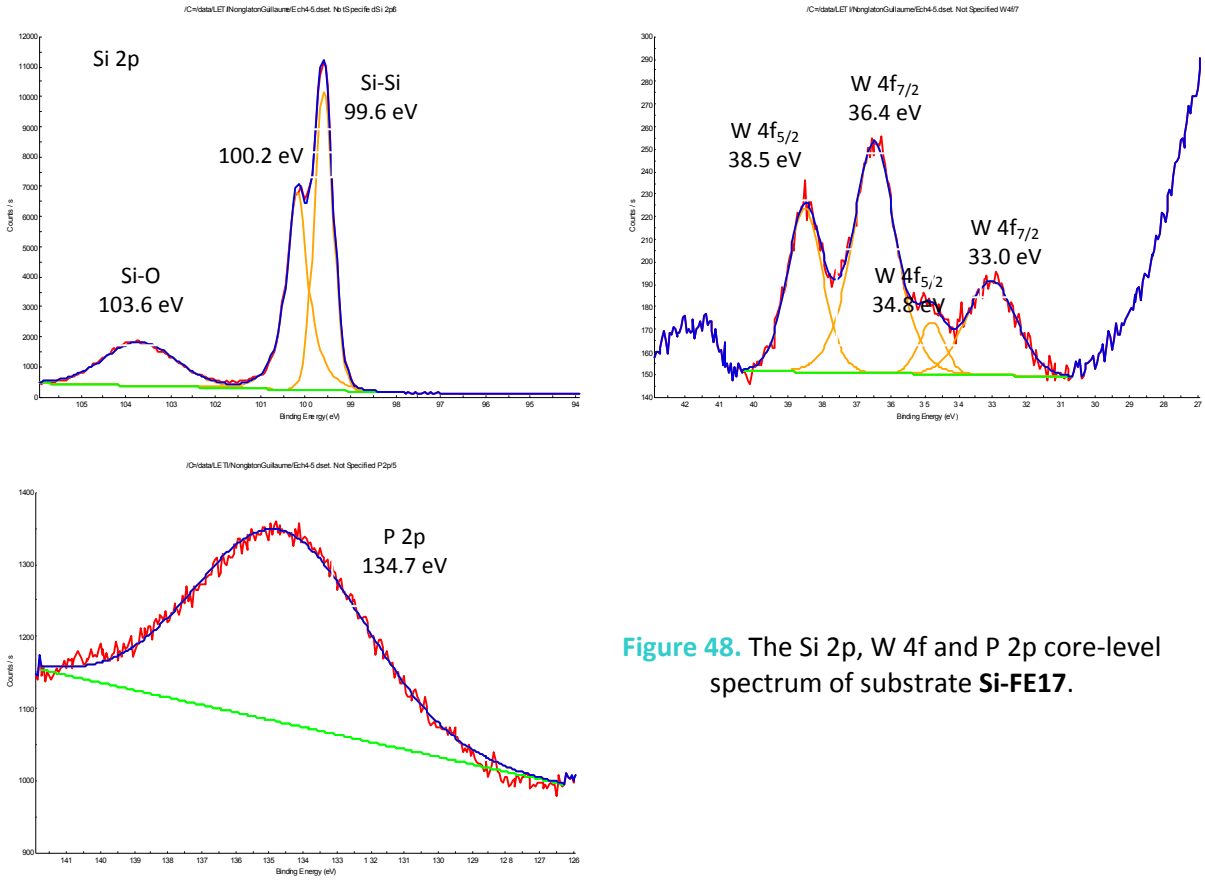

Figure 48. The Si 2p, W 4f and P 2p core-level spectrum of substrate **Si-FE17**.

3.3.3.2.2. Spontaneous surface grafting (Method FS)

The surface grafting of **17** onto the glassy carbon and silicon surfaces was achieved by using a known protocol for the surface grafting of aryl diazonium salts. Freshly clean glassy carbon and H-passivated *n*-type Si(100) electrodes were immersed in the 1 mM compound **17** and 1 equivalent HBF_4 deaerated acetonitrile solution for different reaction times (**Scheme 11** and **Scheme 12**).

Spontaneous grafting at the glassy carbon electrode

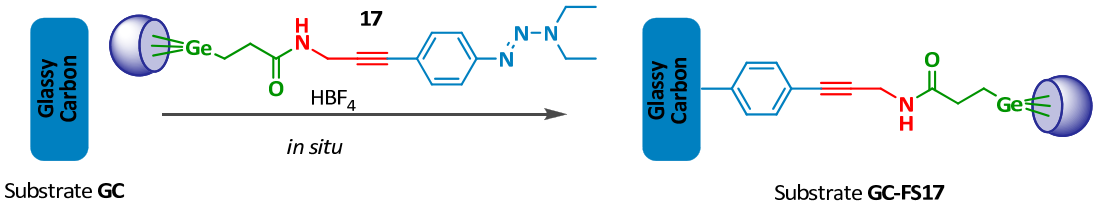

Scheme 11. Schematic representation of the spontaneous electrografting procedure.

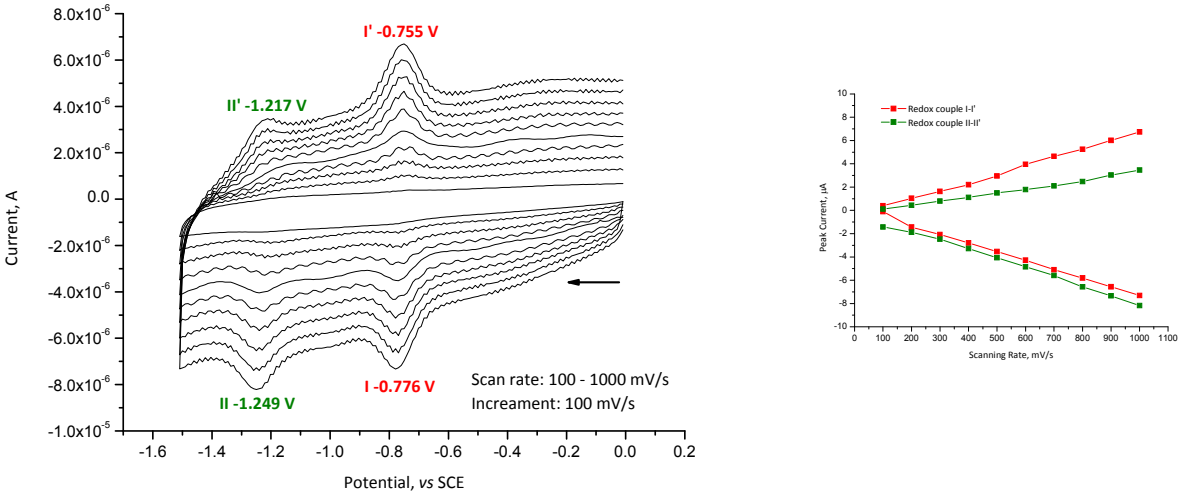

A B

Figure 49. (A) Cyclic voltammetric curves of substrate **GC-FS17** at different scan rates in acetonitrile (0.1 M Bu_4NBF_4). The **GC-FS17** substrate was formed by spontaneous electrografting for 30 minutes. (B) Linear dependence of peak current on scan rate. Electrode surface: 0.07 cm^2 area.

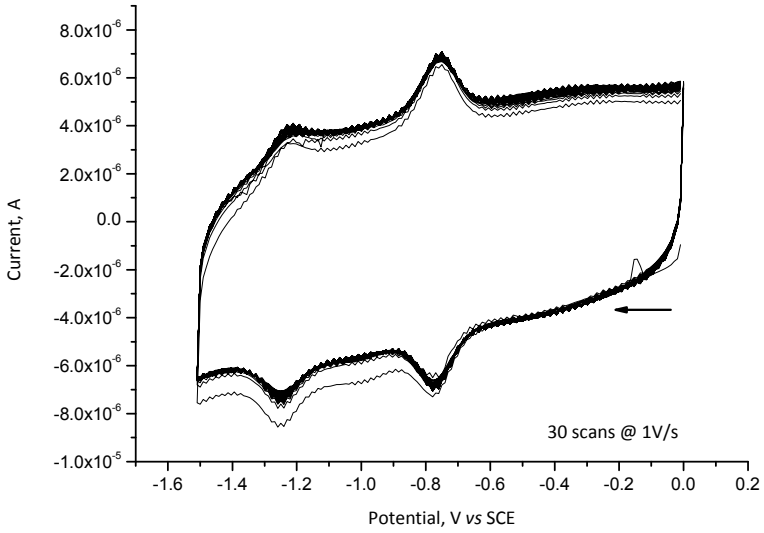

Figure 50. Stability test of the substrate **GC-FS17** towards cycling in acetonitrile (0.1 M Bu_4NBF_4). The **GC-FS17** substrate is formed by spontaneous grafting for 30 minutes. Electrode surface: 0.07 cm^2 area.

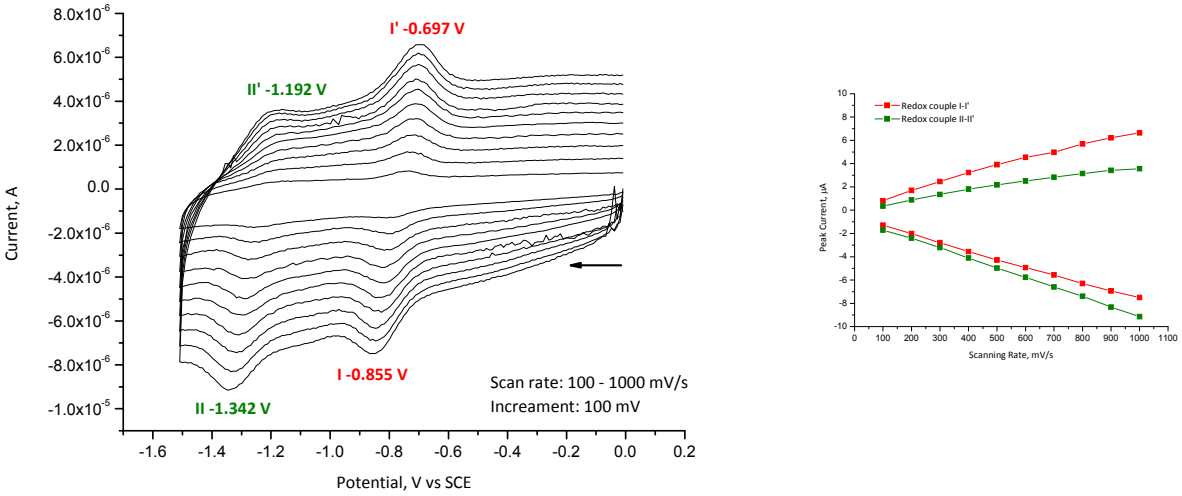

A B

Figure 51. (A) Cyclic voltammetric curves of substrate **GC-FS17** at different scan rates in acetonitrile (0.1 M Bu_4NBF_4). The **GC-FS17** substrate was formed by spontaneous electrografting for 60 minutes. (B) Linear dependence of peak current on scan rate. Electrode surface: 0.07 cm^2 area.

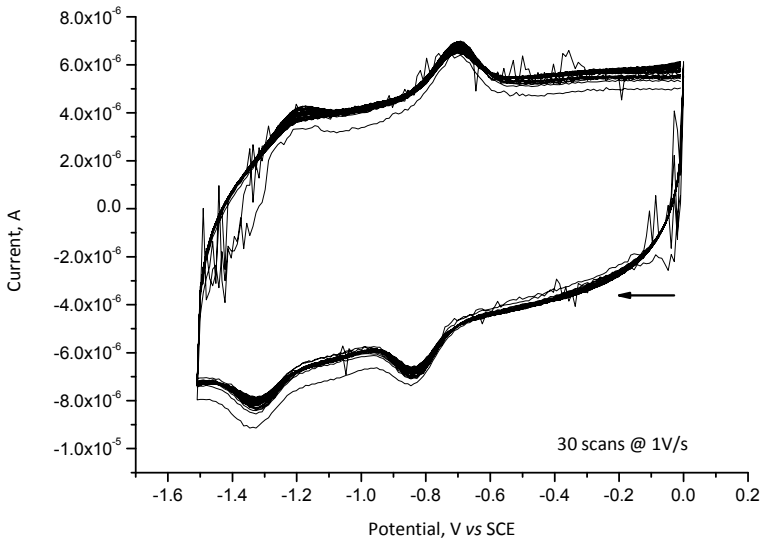

Figure 52. Stability test of the substrate **GC-FS17** towards cycling in acetonitrile (0.1 M Bu_4NBF_4). The **GC-FS17** substrate is formed by spontaneous grafting for 60 minutes.

For the spontaneous grafting (**Figure 49** (A) and **Figure 51** (A)) we retrieve the two redox couples, obtained by electrochemically assisted grafting, at the same formal potential values (*see* **Figure 36**), indicating that the same type of species are grafted at the **GC-FE17** and **GC-FS17** surfaces.

Spontaneous grafting at the n-silicon electrode

For the assembling procedure (**Scheme 12**), a freshly etched Si-H surface is exposed to a solution of compound **17** in anhydrous acetonitrile, previously treated with 1 equivalent HBF_4. In a typical experiment, the diazonium salt was allow to react for the desired reaction time (*vide infra*) in a nitrogen-filled glovebox. Following the completion of reaction time, the substrate was removed from the glovebox, washed with copious amounts of acetonitrile, ultrasonicated in acetonitrile three times ($\times$ 3 minutes) and dried under a flow of argon. Cyclic voltammetry was used to characterize the thus prepared **Si-FS17** substrate in a propylene carbonate solution (1.0 M Bu_4NPF_6) (**Figure 53**).

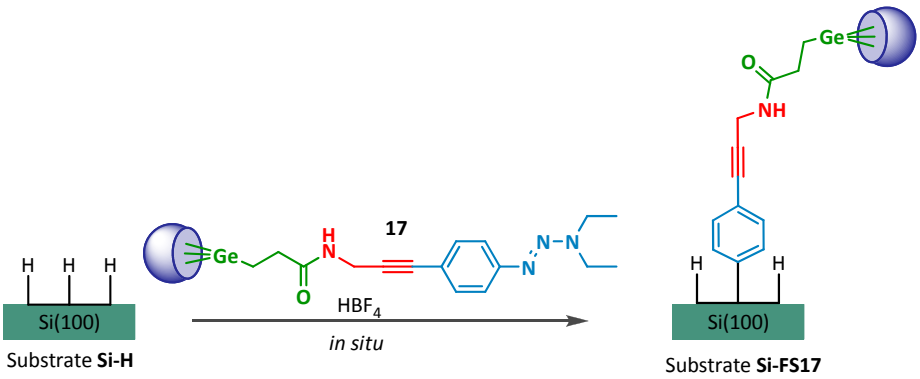

Scheme 12. Schematic representation of the spontaneous electrografting procedure.

The overlaid CVs of substrate **Si-FS17** formed by spontaneous grafting for various periods of time is represented below (**Figure 53**). The results are not very promising; a redox couple can be observed around -1.2 V *vs* SCE of weak intensity. No other attempts were made for this experiment, for example the use of HF instead of HBF_4 for the diazonium generation.

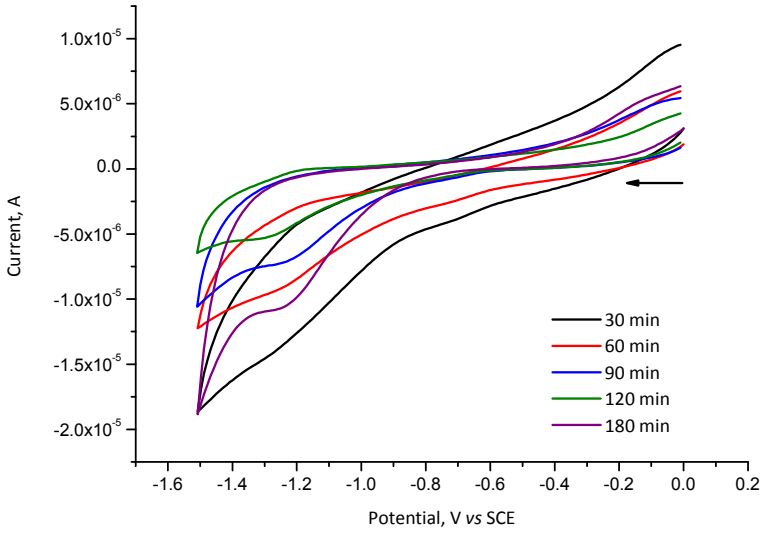

Figure 53. Overlaid cyclic voltammetric curves of substrate **Si-FS17** for spontaneous electrografting for 30, 60, 90, 120, and 180 minutes. CVs registered in propylene carbonate (1.0 M Bu_4NPF_6) at scanning rate 100 mV/s. Electrode surface: 0.60 cm^2 exposing 0.48 cm^2 area.

Apparently, the presence of HF is necessary to ensure a fresh hydrogen-terminated silicon surface in the presence of the water (from the acid) and atmospheric oxygen. Dilute aqueous HF acts both as

an acid for the triazene-to-diazonium conversion as well as an etching agent for the continuous silicon-oxide to Si-H conversion.[32]

3.3.3.3. Immobillization into conducting polymers (Method G)

Within this part, the immobilization method was investigated, namely the incorporation into polypyrrole film using $[SiW_{12}O_{40}]^{4-}$ (SiW_{12}). The objective here is to anchor the conducting polymer polypyrrole doped with polyoxometalates to the silicon surface. This method involves covalent cross-linking of the growing polypyrrole film to an allyl-pyrrole modified surface. The behavior of a polypyrrole film, doped with POMs, deposited at a silicon surface has never been studied before.

Formation of doped polypyrrole films was based on a previous method described by Lapkowski *et al*. [33] Polypyrrole (PPy) was prepared by electrochemical oxidation at a constant potential of the appropriate monomers (Py and SiW_{12}) in acetonitrile and water solutions. The ***conducting polymer films with polyoxometalates were prepared by a one-step method, which is based on electrochemical doping with anions during the electrodeposition of the polymer***. By using the one-step method, film electrodes with good stability and electrochemical behavior can be obtained. Furthermore, it is possible to monitor the amount of POMs in the film. The films were grown on a glassy carbon, platinum or modified silicon working electrode with platinum counter electrode and $Ag/(10^{-2}$ M$)Ag^+$ reference electrode. Once grown, the films were thoroughly rinsed with the solution that the film was going to be electrochemically investigated in. The solutions used for the preparation of films typically contained 10^{-3} M of pyrrole monomer with 10^{-1} M SiW_{12} in acetonitrile and 10^{-1} M of pyrrole monomer with 5×10^{-3} M SiW_{12} in water.

The voltammograms obtained after the electrodeposition of the PPy/SiW_{12} to the electrode surface, displayed the redox waves due to the presence of POMs into the polymer matrix. During the first cycle the redox waves are broaden and slightly shifted in respect with the other ones who follow during the next cycle. According to Otero *et all*.[34] this is a consequence of the fact that the PPy film

---

[32] B. Chen, A. K. Flatt, H. Jian, J. L. Hudson, J. M. Tour, Molecular Grafting to Silicon Surfaces in Air Using Organic Triazenes as Stable Diazonium Sources and HF as a Constant Hydride-Passivation Source, *Chem. Mater.* **2005**, *17*, 4832-4836.

[33] M. Lapkowski, G. Bidan, M. Fournier, Synthesis of polypyrrole and polythiophene in aqueous solution of Keggin-type structure heteropolyanions, *Synth. Met.* **1991**, *41*, 407-410.

[34] T.F. Otero, S.A. Cheng, D. Alonso, F. Huerta, Hybrid Materials Polypyrrole/$PW_{12}O_{40}^{3-}$. 2. Physical, Spectroscopic and Electrochemical Characterization, *J. Phys. Chem. B* **2000**, *104*, 10528-10533.

consists of two distinct components: a soluble part, which is dissoluted during the first cycle, and a insoluble part, which is exposed to the electrolyte after the soluble part leaves.

The glassy carbon and platinum electrodes were used at first in order to optimize the electropolymerization procedure.

Immobilization of POMs into polypyrrole film deposited at the glassy carbon electrode

Polypyrrole was the first conducting polymer film used to try and immobilize the POMs (**Scheme 13**). The reason for this was due to the fact that polypyrrole is by far the most studied of all the conducting polymers. Films with varying thickness were grown by holding the potential of the electrode in an acetonitrile solution of pyrrole and $H_4SiW_{12}O_{40}$. It was found that by passing an average charge of 2 mC at +0.9 V the film exhibit the best electroactivity.

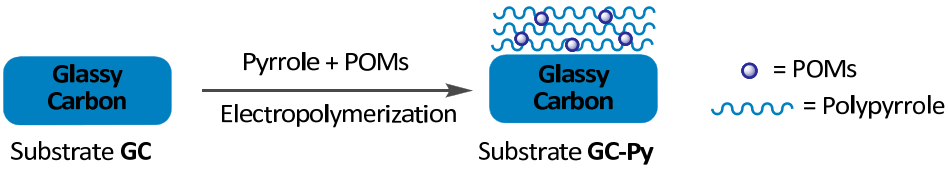

Scheme 13. Schematic representation of the electropolymerization process at the glassy carbon electrode.

Figure 54 and **Figure 55** show the series of cyclic voltammograms obtained for the SiW_{12} doped polypyrrole film in 10^{-1} M CF_3LiO_3S acetonitrile solution and $2{\cdot}10^{-1}$M Na_2SO_4 in water, respectively. Within the potential range +0.3 to -1.7 V (**Figure 54**) three redox waves appear with E_p values of -0.158 V (irreversible), -0.738 V, -1.133 V and one additional irreversible peak situated at -0.629 V who disappear after the first cycle whose presence we can not be explained. These redox peaks correspond to the reduction and oxidation of the tungsten skeleton. The irreversible one (-0.158 V) can be attributed to the oxidation of the polypyrrole film. However, it can be seen that the electroactivity of the POMs doped polypyrrole film decreases upon cycling, probably due to the fact the POMs are released into solution during the film analysis.

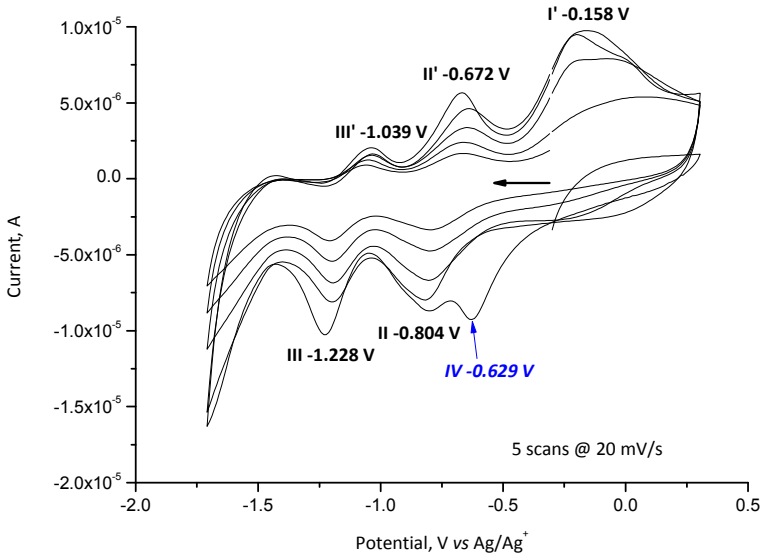

Figure 54. Cyclic voltammetry recorded for **GC-Py** hybrid film (10^{-1} M CF_3LiO_3S in acetonitrile). Scan rate 20 mV·s^{-1}. The film was deposited at +0.9 V with a deposition of charge of 2 mC at the GC electrode. Conditions of electropolymerization: 10^{-3} M of pyrrole monomer with 10^{-1} M SiW_{12} in acetonitrile. Surface electrode: 0.07 cm^2 area.

The **GC-Py** hybrid film was analyzed into a $2 \cdot 10^{-1}$ M Na_2SO_4 water solution (**Figure 55**) to observe the differences in the electroactivity of the POMs doped polypyrrole film. Between 0 and -0.8 V at the first cycle two redox waves are observed situated at -0.340 (I-I') and -0.532 (II-II'). Nevertheless, starting with the next cycle, when the film probably became more stable, the two redox peaks are slightly shifted and they can be observed at -0.329 and -0.554 V, respectively. The **GC-Py** film shows a good stability in the $2 \cdot 10^{-1}$ M Na_2SO_4 water solution compared with 10^{-1} M CF_3LiO_3S in acetonitrile (*vide supra*). By comparing **Figure 55** with **Figure 56**, it was found that the electrochemical behaviour of the SiW_{12} in the polypyrrole film is similar with that in the solution concerning the first two redox waves. However, the third redox couple could not be retrieved in the **GC-Py** voltammogram.

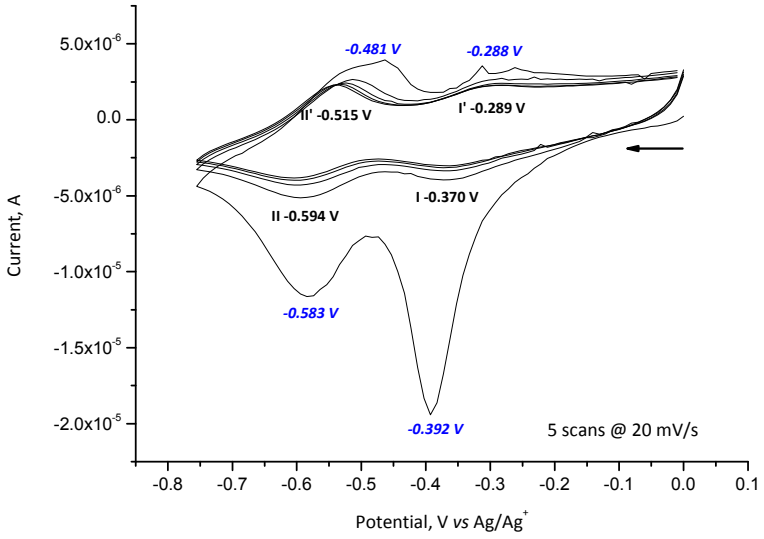

Figure 55. Cyclic voltammetry recorded for **GC-Py** hybrid film ($2 \cdot 10^{-1}$ M Na_2SO_4 in water). Scan rate 20 $mV \cdot s^{-1}$. The film was deposited at +0.9 V with a deposition of charge of 2 mC at the GC electrode. Conditions of electropolymerization: 10^{-3} M of pyrrole monomer with 10^{-1} M SiW_{12} in acetonitrile. Surface electrode: 0.07 cm^2 area.

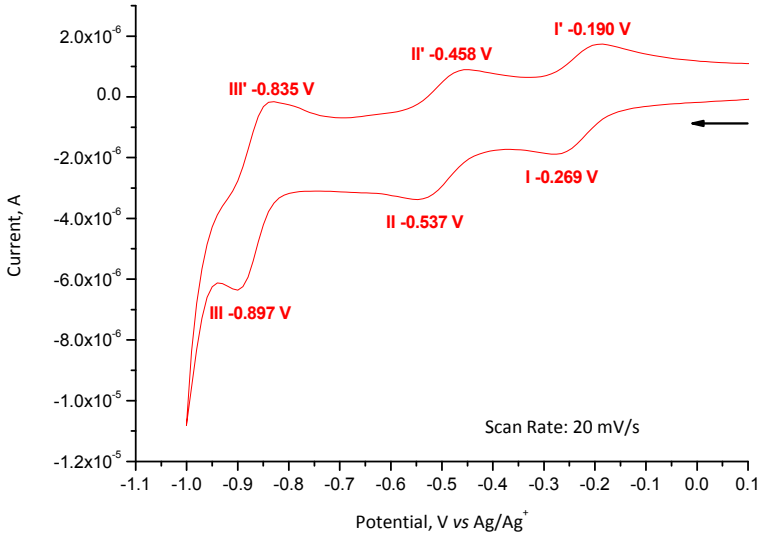

Figure 56. Cyclic voltammogram of $H_4SiW_{12}O_{40}$ (10^{-3} M) in $2 \cdot 10^{-1}$ M Na_2SO_4 water solution at the glassy carbon electrode. Scanning rate 20 mV/s *vs* Ag/Ag^+ electrode, Pt counter electrode. Surface electrode: 0.07 cm^2 area.

Cyclic voltammogram at 20 mV/s of the SiW_{12} doped polypyrrole film, made at constant potential of +0.65 V in water solution, at glassy carbon electrode in buffer solution pH 4, is shown in **Figure 57**.

These voltammograms display the redox couple of the POMs at -0.364 (I-I'), -0.611 (II-II') and -0.842 (III-III'), respectively (Table 5). Furthermore, at cathodic potentials they undergo several electronic transfers which are well defined. The film was found to be extremely stable within the potential limits 0 and -1 V with no significant loss in the global activity after 10 scans at 20 mV·s^{-1}.

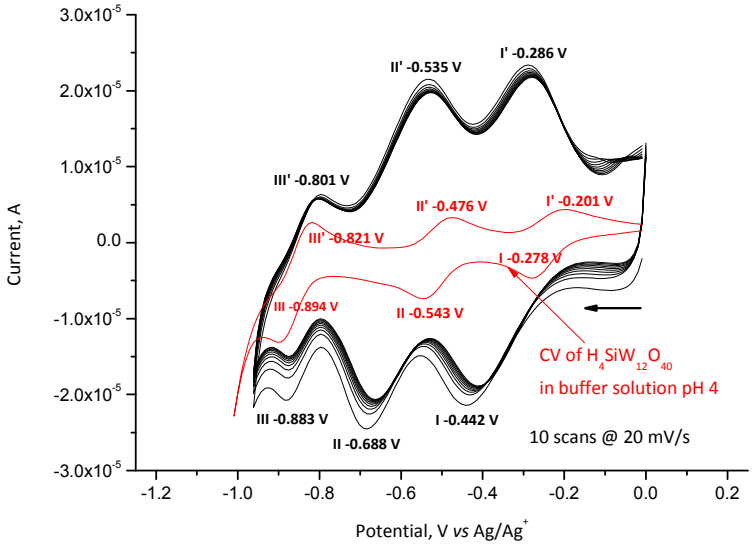

Figure 57. Cyclic voltammetry recorded for **GC-Py** hybrid film (buffer solution pH 4). Scan rate 20 mV·s^{-1}. The film was deposited at +0.65 V with a deposition of charge of 5 mC at the GC electrode. Conditions of electropolymerization: 10^{-1} M of pyrrole monomer with 5 mM SiW_{12} in water. Surface electrode: 0.07 cm^2 area.

Table 5. Representative cyclic voltammetric data *vs* Ag/Ag$^+$ electrode for substrate **GC-Py** and bare GC electrode in a $H_4SiW_{12}O_{40}$ in buffer solution pH 4 (*after* Figure 57).

Substrate	$E(I)^b(\Delta E(I))^c$	$E(II)^b(\Delta E(II))^c$	$E(IV)^b(\Delta E(IV))^c$
GC-Py	-0.364 V (156 mV)	-0.611 V (153 mV)	-0.842 V (82 mV)
bare GC[a]	-0.239 V (77 mV)	-0.509 V (67 mV)	-0.857 V (73 mV)

[a] [POM] = 1 × 10^{-3} M in buffer solution at pH 4.
[b] $E(i) = 1/2\ (E(i)_{ox} + E(i)_{red})$
[c] $\Delta E(i) = E(i)_{ox} - E(i)_{red}$

The redox properties of the conducting polymers are of main interest in this section, because most of the important applications are associated with switching the electroactive polymer films from the neutral (reduced) state to the doped (oxidized) state. Polymerization of pyrrole produces the

highly conducting, oxidized (doped) form of the polypyrrole. A loss in electrochemical activity and a decrease in conductivity of film are caused by applying anodic potentials over +0.8 – +1.0 V. At positive potentials an overoxidation of PPy can occur which leads to a lowering of PPy conductivity and makes leakage of anionic molecules easier if they were included in the polymeric backbone.[35] The stability of the **GC-Py** in the buffer solution pH 4 was tested. Because of their large size, POMs cannot be expelled during the reduction of the polymer or during the overoxidation of the PPY. However, a slight decrease in the electroactivity of the film was highlighted (**Figure 58**). In this case these voltammograms display the conducting polymer redox couples (IV-IV') with the additional electrochemical response of the immobilized POMs inside the polymer matrix (I-I', II-II' and III-III').

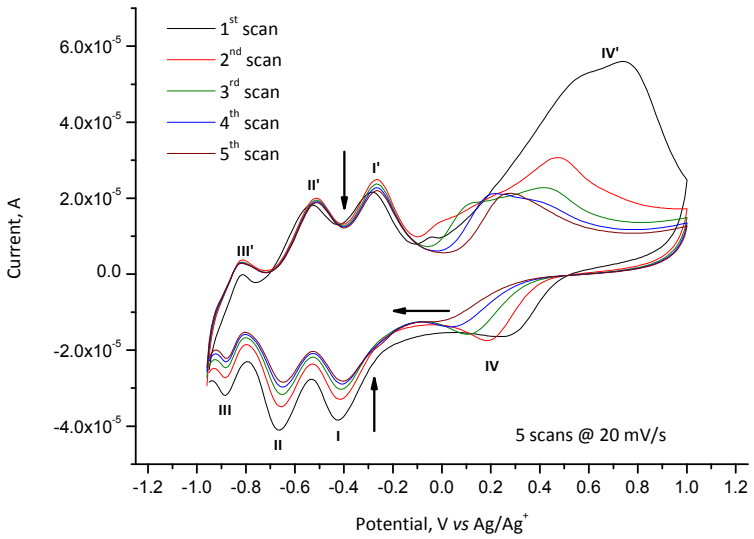

Figure 58. Overoxidation of the polypyrrole film in buffer solution pH 4.

Immobilization of POMs into polypyrrole film deposited at the platinum electrode

In order to check the electrochemical properties of the hybrid materials Pt-Py, the POMs doped films were electrogenerated by flow of 12 mC, at a constant potential of +0.9 V, through acetonitrile solution containing 10^{-3} M of pyrrole monomer with 10^{-1} M SiW_{12} at the platinum electrode (**Scheme 14**). The electrogenerated films were then analyzed by cyclic voltammetry in 10^{-1} M CF_3LiO_3S in acetonitrile (**Figure 59**) and $2\cdot10^{-1}$M Na_2SO_4 in water (**Figure 60**).

[35] A. Ramanavičius, A. Ramanavičiene, A. Malinauskas, Electrochemical sensors based on conducting polymer – polypyrrole, *Electrochim. Acta* **200**6, *51*, 6025-6037.

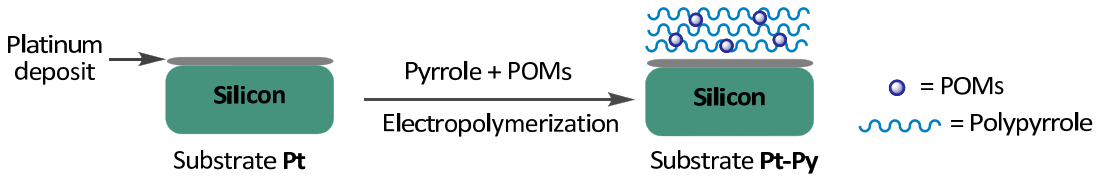

Scheme 14. Schematic representation of the electropolymerization process at the platinum electrode.

The consecutive cyclic voltammograms for the freshly synthesized **Pt-Py** POMs doped hybrid materials are shown below. The CV of the **Pt-Py** substrate in 10^{-1} M CF_3LiO_3S acetonitrile solution (**Figure 59**) exhibits an irreversible wave at -0.066 V (*vs* Ag/Ag^+) and two redox couples at -0.772 V and 1.152 V, associated to the oxidation of the polypyrrole film and to the SiW_{12} redox systems, respectively. Still, the film shows a significant loss of electroactivity starting with the second cycle.

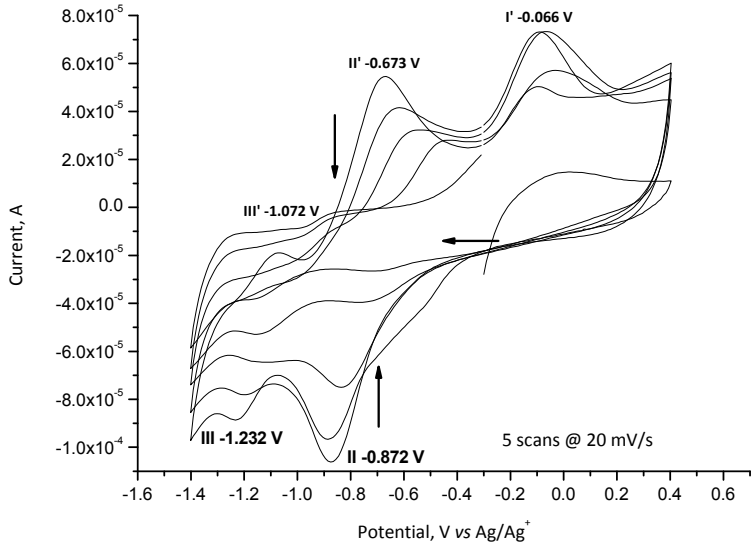

Figure 59. Cyclic voltammetry recorded for **Pt-Py** hybrid film (10^{-1} M CF_3LiO_3S in acetonitrile). Scan rate 20 $mV \cdot s^{-1}$. The film was deposited at +0.9 V with a deposition of charge of 12 mC at the platinum electrode. Conditions of electropolymerization: 10^{-3} M of pyrrole monomer with 10^{-1} M SiW_{12} in acetonitrile. Electrode surface: 0.60 cm^2 exposing 0.36 cm^2 area.

In $2 \cdot 10^{-1}$M Na_2SO_4 in water solution the **Pt-Py** substrate manifests an improved stability towards cycling. After the first potential cycle, the hybrid film presents similar responses to the consecutive cyclic voltammograms. **Figure 60**, A shows two well defined redox waves at -0.221 and -0.479 V, respectively. These redox systems can be undoubtedly associated with the POMs reduction as it can

be seen in **Figure 60**, B. During the first cathodic sweep from -0.1 to -0.8 V, the **Pt-Py** hybrid material shows two cathodic peaks shifted with about 126 and 36 mV, respectively, by comparing them with the next that follow. It has been observed previously that a substantial loss of film weight appears during the first cycle, associated with the release of POMs from the film.[36]

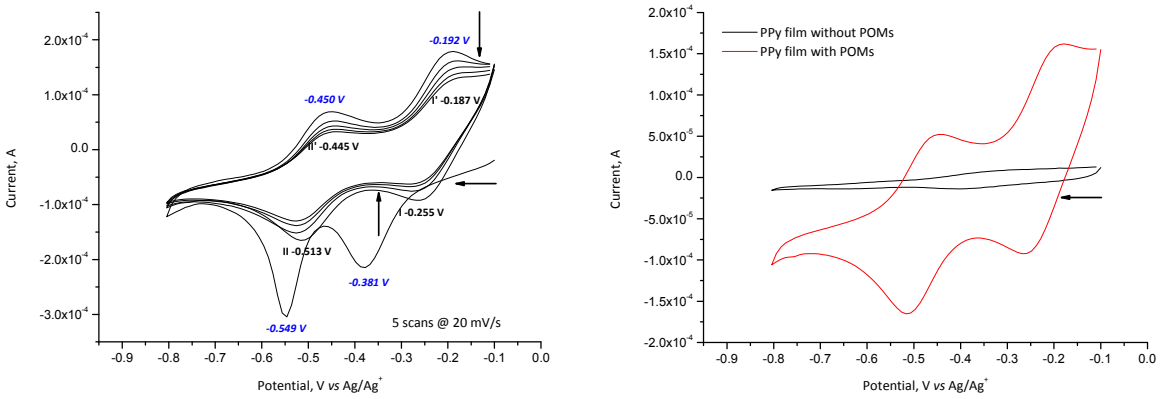

Figure 60. (A) Cyclic voltammetry recorded for **Pt-Py** hybrid film ($2 \cdot 10^{-1}$M Na_2SO_4 in water). (B) Overlaid CVs of the polypyrrole film without POMs (black line) and polypyrrole film with POMs (red line). Scan rate 20 $mV \cdot s^{-1}$. The film was deposited at +0.9 V with a deposition of charge of 12 mC at the platinum electrode. Conditions of electropolymerization: 10^{-3} M of pyrrole monomer with 10^{-1} M SiW_{12} in acetonitrile. Electrode surface: 0.60 cm^2 exposing 0.36 cm^2 area.

The electroactivity of the **Pt-Py** film electrogenerated in water solution was also investigated. By passing 10 mC of charge at a constant potential of +0.9 V in a 10^{-1} M of pyrrole monomer with 5 mM SiW_{12} water solution, we afforded the **Pt-Py** substrates. Two reversible redox waves appear for the **Pt-Py** film in its cyclic voltammetry analysis as it is shown in **Figure 61**. Between 0 and -0.6 V the redox couples are situated at -0.188 V (I-I') and -0.450 V (II-II') very well defined and very stable. The redox transition is very rapid, as is shown by the fact the peak potential separation at the scanning rate 20 $mV \cdot s^{-1}$ is 12 and 14 mV, respectively. The stability of the film was investigated by cycling the **Pt-Py** POMs doped electrode 10 times at 20 $mV \cdot s^{-1}$. The stability test shows no significant loss of electroactivity towards cycling indicating that the POMs are immobilized in the polypyrrole film and that their redox properties is maintained in the immobilized state. By comparing the CV of the **Pt-Py** (**Figure 61**, black line) with the CV of the SiW_{12} at the Pt electrode (**Figure 61**, red line), an additional

[36] S.A. Cheng, T.F. Otero, Electrogeneration and electrochemical properties of hybrid materials: polypyrrole doped with polyoxometalates $PW_{12-x}Mo_xO_{40}^{3-}$ (x = 0, 3, 6, 12), *Synth. Met.* **2002**, *129*, 53-59.

redox couple appear for the **Pt-Py** substrate, indicating that the redox properties of the POMs are better highlighted in the polypyrrole film.

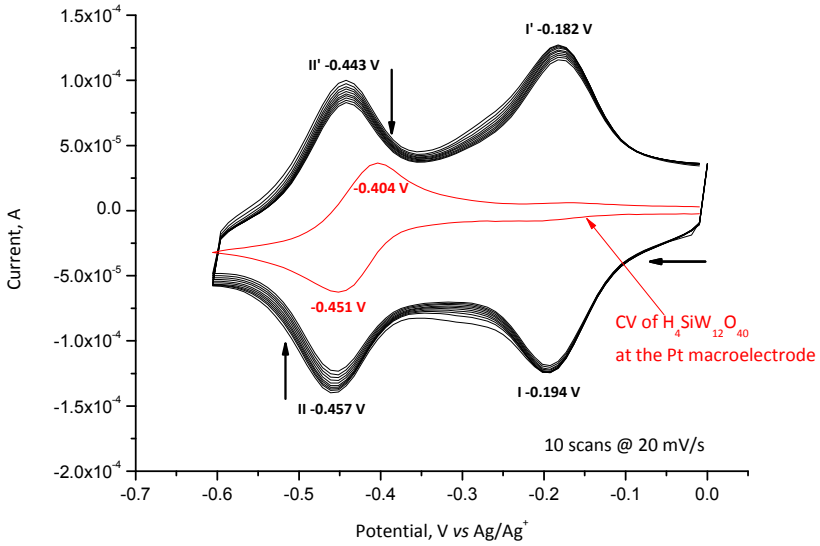

Figure 61. Cyclic voltammetry recorded for **Pt-Py** hybrid film ($2 \cdot 10^{-1}$ M Na_2SO_4 in water). Scan rate 20 $mV \cdot s^{-1}$. The film was deposited at +0.9 V with a deposition of charge of 10 mC at the platinum electrode. Conditions of electropolymerization: 10^{-1} M of pyrrole monomer with 5 mM SiW_{12} in water. Electrode surface: 0.60 cm^2 exposing 0.36 cm^2 area.

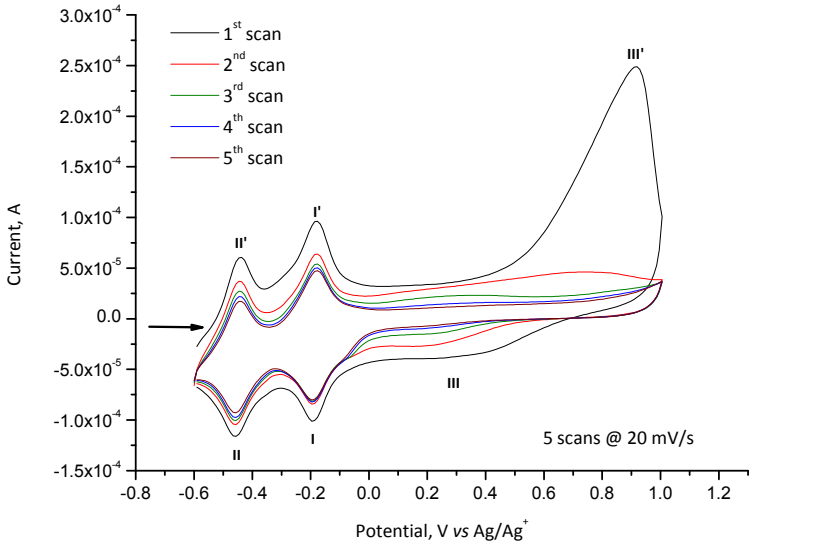

Figure 62. Overoxidation of the polypyrrole film in $2 \cdot 10^{-1}$ M Na_2SO_4 in water solution.

Upon overoxidation of the polypyrrole film, by cycling the **Pt-Py** substrate between -0.6 and 1 V, the electroactivity of the hybrid film is maintained indicating the firm entrapment of the POMs anions into the polymer matrix (**Figure 62**).

The XPS analysis of the **Pt-Py** hybrid film reveals the characteristic peaks from the $SiW_{12}O_{40}^{4-}$ anion, indicating that the POMs are confined in the polymer matrix. The high-resolution Si 2p and W 4f peaks corresponding to the SiO_4 tetrahedron and the tungsten framework are represented in **Figure 63**.

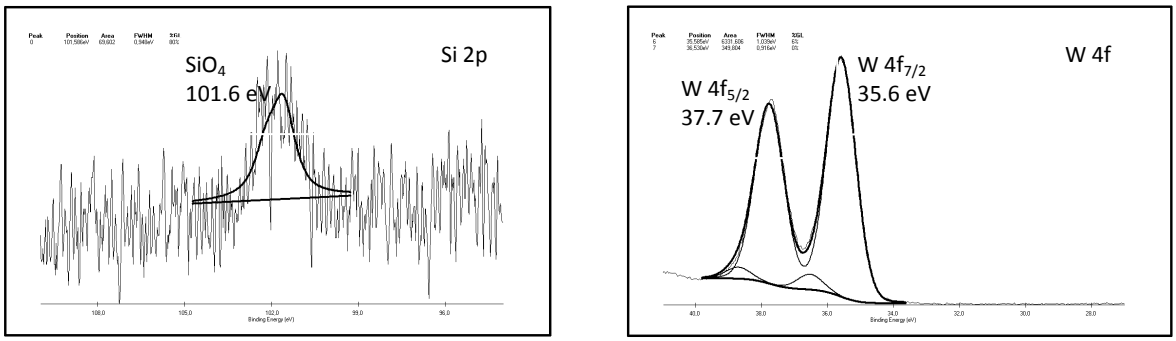

Figure 63. The Si 2p and W 4f core-level spectrum of the hybrid film **Pt-Py** deposited at the platinum electrode.

These experimental results show that the electropolymerization of pyrrole on the electrode surface is accompanied by the immobilization of the SiW_{12} anion on the electrode surface. These results also show that the ***conducting polymers appear to be a good support for the immobilization of the Keggin-type polyoxometalates***.

Immobilization of POMs into polypyrrole film deposited at the n-silicon electrode

In order to perform the polymerization of the pyrrole onto a silicon surface, an additional step is needed to ensure the attachment of the polypyrrole film to the surface. The additional step implies a hydrosilylation reaction performed at reflux under argon in *ca.* 0.02 M toluene solution of N-allyl pyrrole (**Scheme 15**) (compound **26**). The reaction was protected from light by wrapping the reaction vessel in aluminum foil.[37] The electropolymerization conditions were optimize first for the platinum or glassy carbon electrodes before applying to the modified silicon electrode.

[37] A. R. Pike, S. N. Patole, N. C. Murray, T. Ilyas, B. A. Connolly, B. R. Horrocks, A. Houlton, Covalent and Non-covalent Attachment and Patterning of Polypyrrole at Silicon Surfaces, *Adv. Mater.* **2003**, *15*, 254-257.

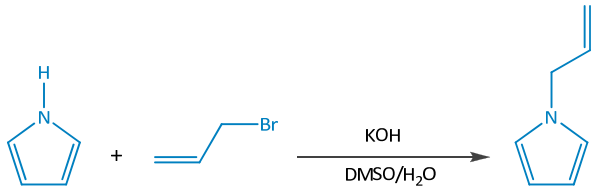

Scheme 15. Schematic representation of the N-allyl pyrrole (compound **26**) synthesis.

As it was shown previously, the best POMs ($\{SiW_{12}\}$) doped polypyrrole films, from the electroactivity point of view, were generated in water solution. However, these conditions are not suitable for the silicon electrodes, consequently the **Si-G26-Py** substrates were fabricated in acetonitrile following the **Scheme 16** route.

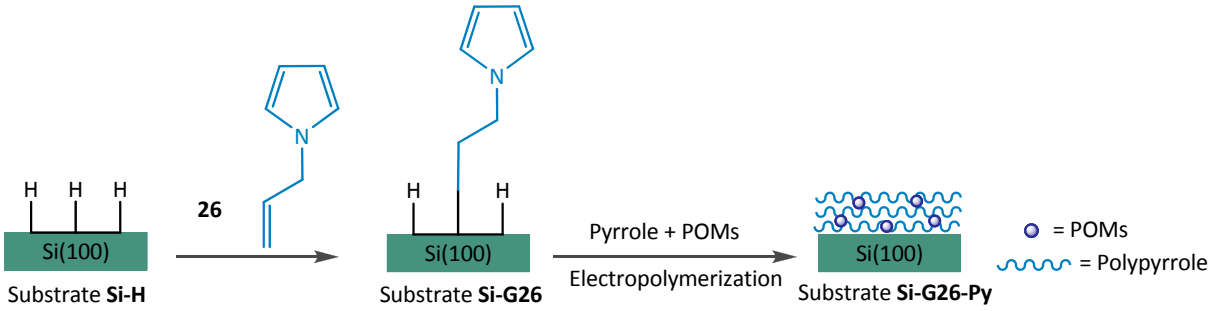

Scheme 16. The preparation of the modified silicon electrode.

The XPS analysis of the allypyrrole terminated substrate **Si-G26** discloses characteristic peaks from the silicon substrate itself and from the N 1s and C 1s core levels of the attached organic molecule (**Figure 64**). The Si 2p spectrum, reveals the formation of some SiO_2 (peak situated at 103.2 eV) in small yields, anyways a good coverage was obtained following the hydrosilylation step. As for the N 1s spectrum, the main peak at 400.7 eV is characteristic to the aromatic nitrogen of the pyrrole unit. The high-resolution C 1s peak shows several components at 285.4, 286.8 and 288.9 eV which can be reasonably assigned to the C-C, C-N and Si-C, respectively.

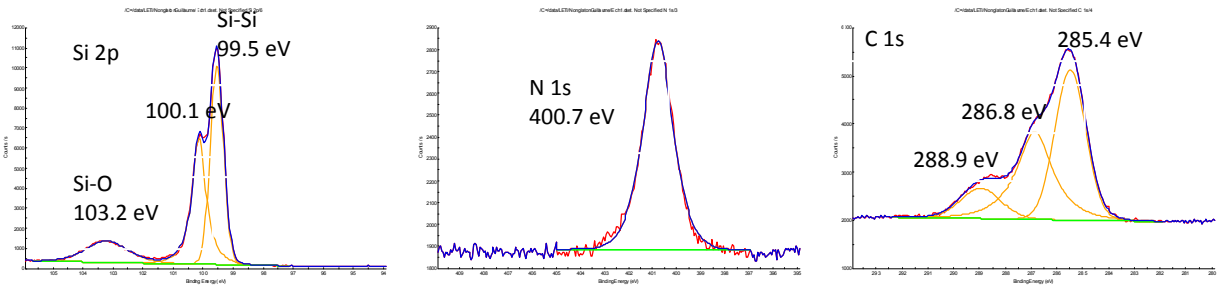

Figure 64. The Si 2p, N 1s and C 1s core-level spectrum of substrate **Si-G26**.

Alkylation was confirmed by ATR-FTIR of the **Si-G26** and compared with the Si-H substrate (**Figure 65**). Bands corresponding to the pyrrole C-H strech (3015 cm^{-1}) can be seen.

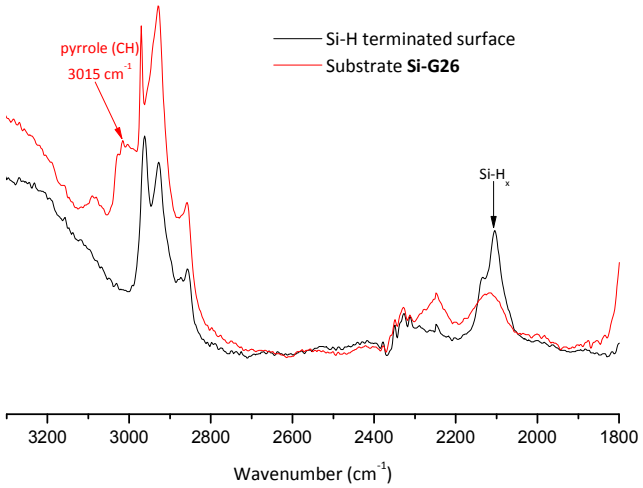

Figure 65. Comparison of the ATR-FTIR spectra of Si-H terminated surface and substrate **Si-G26**.

The pyrrole modified **Si-G26** substrate was used as working electrodes to deposit the POMs doped polypyrrole films. This was done by applying a controlled potential of +1.05 V by passing a charge of 12 mC through an acetonitrile solution containing 10^{-3} M of pyrrole monomer and 10^{-1} M SiW_{12} in a three electrode equipped electrochemical cell. After the electrodeposition of the hybrid film, the substrate **Si-G26-Py** was washed in 10^{-1} M CF_3LiO_3S in acetonitrile solution, dried under argon and investigated by means of cyclic voltammetry in the same acetonitrile solution. Several redox waves are evidentiate in the voltammogram of substrate **Si-G26-Py** (**Figure 66**) associated with

the oxidation and reduction of the tungsten centers and the polypyrrole film (-0.017 V). Nonetheless, they are asymmetric and completely disappear after the fifth cycle. This is probably due to the poor quality of the polypyrrole film and as a consequence the $SiW_{12}O_{40}^{4-}$ anions are released into the solution. To overcome this problem compound **19** was synthesized, a PW_9 unit decorated with two pyrrole units (*see* Part 3, Organogermyl derivatives), for a copolymerization at the pyrrole modified silicon surface (**Si-G26**) towards a stabilization of the POM into the polymer matrix. Unfortunately, the first attempts with the unpurified compound **19** din not give the expected results. Nevertheless, this is the first example of an electroactive hybrid POMs/polypyrrole film deposited at a silicon surface.

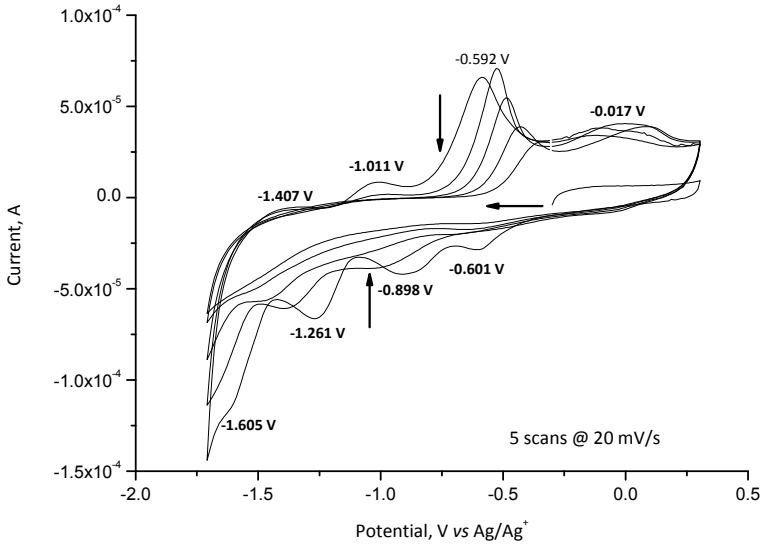

Figure 66. Cyclic voltammetry recorded for **Si-G26-Py** hybrid film (10^{-1} M CF_3LiO_3S in acetonitrile). Scan rate 20 mV·s^{-1}. The film was deposited at +1.05 V with a deposition of charge of 12 mC at the modified silicon electrode. Conditions of electropolymerization: 10^{-3} M of pyrrole monomer with 10^{-1} M SiW_{12} in acetonitrile. Electrode surface: 0.75 cm^2 exposing 0.45 cm^2 area.

The **Si-G26-Py** substrate was also investigated by XPS means. The core-level spectrum of the Si 2p and W 4f confirms the presence of the $SiW_{12}O_{40}^{4-}$ anion into the polymer matrix (**Figure 67**).

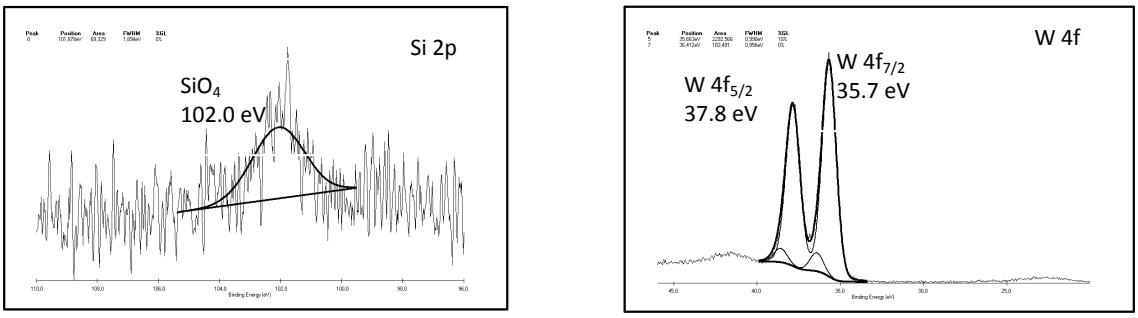

Figure 67. The Si 2p and W 4f core-level spectrum of the hybrid film **Si-G26-Py** deposited at the modified silicon electrode.

Even if, the research linked to the copolymerization of compound **19** and pyrrole monomer in an acetonitrile solution at silicon surface remained unfinished, ***the perspectives are very interesting towards construction of new polyoxometalates based materials with interesting redox properties***.

3.4. CONCLUSIONS

Several grafting procedures for functionalized polyoxometalates attachment onto a surface were explored in this part. Generally speaking, the electrochemical methods proved to be the most effective. The ethynyl POM derivative (compound **15**) is able the react with the Si-H ended surface *via* an anodic electrografting. The ***POM-modified silicon electrode is electrochemically accessible to three reversible redox states***, which can be assigned to the three redox couples of the polyoxotungstic skeleton.

The optimal conditions for the electrochemically assisted and spontaneous grafting of triazene POM derivative (compound **17**) onto glassy carbon and Si electrode were both studied in this part. Important results were obtained in this section. ***Two distinct reversible redox waves were highlighted on the glassy carbon and silicon POMs modified electrodes*** attributable to the POMs reduction. The ***redox couples are well defined and show stability towards cycling without significant loss of electroactivity***.

Part 4

ELECTRICAL INVESTIGATION OF THE POLYOXOMETALATES MODIFIED CAPACITORS

4. Fourth Part – Electrical Investigation of the Polyoxometalates Modified Capacitors

Abstract – Characterization by conventional capacitance and conductance techniques showed very high capacitance and conductance peaks associated with charging and discharging of electrons into and from discrete levels in the monolayer owing to the presence of the redox-active polyoxometalates. Implementation of such a molecular-based charge-trapping layer as the dielectric of a metal-oxide-semiconductor (MOS) structure can lead to a memory device. Due to the molecular stability and low-power operation, molecular-silicon hybrid devices may be strong candidates for next-generation of electronic devices.

Résumé – La caractérisation par des techniques classiques de capacitance et de conductance ont montré des pics de capacité et de conductance très élevés associés à la charge et la décharge d'électrons dans et à partir de niveaux discrets dans la monocouche en raison de la présence des polyoxométalates redox-actifs. La mise en œuvre d'une telle couche de piégeage de charge à base moléculaire comme diélectrique d'une structure métal-oxyde-semiconducteur (MOS) peut conduire à un dispositif de type mémoire. En raison de la stabilité moléculaire et du fonctionnement à faible puissance, des appareils hybrides moléculaires et silicium peuvent être de bons candidats pour la prochaine génération de dispositifs électroniques.

4.1. INTRODUCTION

The electrical characterization of ferrocene and porphyrin monolayers on a silicon surface in microelectrode devices, such as electrode-molecule-silicon (EMS) capacitors, has already been reported by Bocian *et al.* [1, 2, 3]

[1] Q. Li, S. Surthi, G. Mathur, S. Gowda, Q. Zhao, T. A. Sorenson, R. C. Tenent, K. Muthukumaran, J. S. Lindsey, V. Misra, Multiple-bit, storage properties of porphyrin monolayers on SiO_2, *Appl. Phys. Lett.* **2004**, *85*, 1829-1831.
[2] Q. Li, G. Mathur, S. Gowda, S. Surthi, Q. Zhao, L. Yu, J. S. Lindsey, D. F. Bocian, V. Misra, Multibit Memory Using Self-Assembly of Mixed Ferrocene/ Porphyrin Monolayers on Silicon, *Adv. Mater.* **2004**, *16*, 133-137.

Characterization of an EMS capacitor can provide critical information on the feasibility of using charge-trapping molecules in memory devices. For example, the hysteresis and charge-retention information obtained from capacitance-voltage (*C-V*) and conduction-voltage (*G-V*) methods can assist in modification of the silicon substrate. The test structure of the EMS capacitor and its simplified equivalent circuit are shown in **Figure 1** (a). The capacitance contributed from the electrolyte, overlap silicon oxide, molecular SAM, or the silicon substrate is labeled as C_E, C_{OL}, C_M, and C_S, respectively.

In 2002, Bocian *et al.*[4] reported conventional *C-V* and *G-V* analysis on redox-active compound 4-ferrocenylbenzyl alcohol attached to silicon surface *via* the oxygen atom of the alcohol. For comparison purposes, a SAM containing the nonredox-active analog 4-biphenylmethanol was also studied (**Figure 1** (b)). They shown that the SAM of ferrocene covalently attached to the silicon surface exhibits capacitance and conductance peaks associated with trapping and detrapping of the charge in the molecules. **Figure 2** shows the cyclic voltammetry of the ferrocene modified EMS capacitor obtained with different scan rates. The gate voltage refers to the top electrode/electrolyte contact.[3] The cyclic voltammogram of the nonredox-active biphenylmethanol modified EMS capacitor did not indicate the presence of any redox behavior.

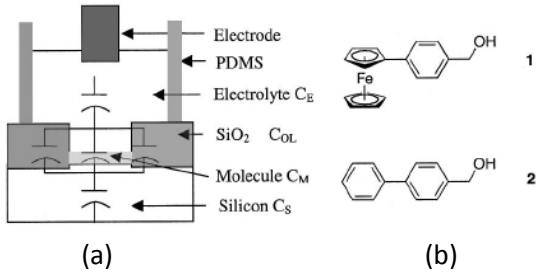

Figure 1. (a) Schematic representation of the electrolyte-molecule-silicon capacitor with a simplified equivalent circuit. (b) The structure of the Ferrocene derivative (1) and the nonredox-active analog (2). In each case, SAM formation affords a covalent attachment between the oxygen of the linker and the silicon surface. [4]

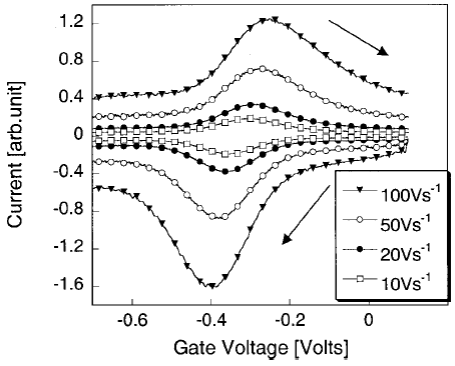

Figure 2. Cyclic voltammetry of the EMS capacitor with Ferrocene containing monolayers with voltage scanning rates: 10, 20, 50, and 100 V·s^{-1} (Ag wire counter electrode).[4]

[3] N.B. – The sign of the potentials is negative because the voltage is applied to the gate rather than the working electrode; accordingly, the potential at the working electrode (which is at virtual ground) is positive relative to the gate electrode.

[4] Q. Li, G. Mathur, M. Homsi, S. Surthi, V. Misra, V. Malinovski, K.-H. Schweikart, L. Yu, J. S. Lindsey, Z. Liu, R. B. Dabke, A. Yasseri, D. F. Bocian, W. G. Kuhr, Capacitance and conductance characterization of ferrocene-

Figure 3 and **Figure 4** show the peaks related to the oxidation and reduction processes observed for the ferrocene-based monolayers. In the *C-V* plots (**Figure 3**), these peaks are especially pronounced at lower frequencies but are reduced in amplitude as the measurement frequency increases. On the other hand, in the *G-V* plots (**Figure 4**) the increase in frequency determines an increase in the amplitude of the peaks. The same behavior was observed for a monolayer of ferrocene directly grafted onto the silicon surface *via* a Si-C bond.[5] In order to assure that the origin of the peaks was indeed the redox-active ferrocene and not due to defects at Si interface,[6] capacitance and conductance measurements were also performed on 4-biphenylmethanol modified capacitors. As shown in the inset of **Figure 3** and inset (b) of **Figure 4**, no peaks in *C-V* and *G-V* methods were observed in these nonredox monolayers, thereby confirming that the origin of the peaks arise from the redox-active monolayer.

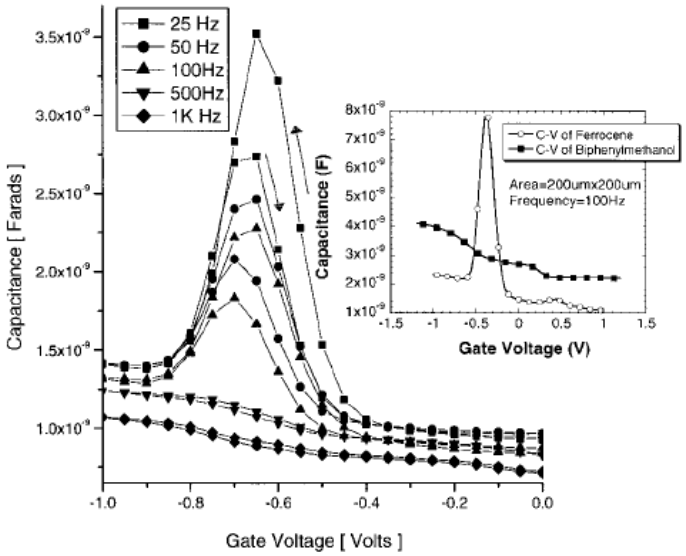

Figure 3. *C-V* characteristics of the EMS capacitor with redox-active ferrocene monolayers measured at 25, 50, 100, 500, and 1000 Hz. Inset shows the lack of *C-V* peaks in the nonredox-active monolayers measured at 100 Hz.[4]

---

containing self-assembled monolayers on silicon surfaces for memory applications, *Appl. Phys. Lett.* **2002**, *81*, 1494-1496;

[5] T. Pro, J. Buckley, K. Huang, A. Calborean, M. Gély, G. Delapierre, G. Ghibaudo, F. Duclairoir, J.-C. Marchon, E. Jalaguier, P. Maldivi, B. De Salvo, S. Deleonibus, Investigation of Hybrid Molecular/Silicon Memories With Redox-Active Molecules Acting As Storage Media, *IEEE Trans. Nanotechnol.* **2009**, *8*, 204-213.

[6] S. Kar, C. Miramond, D. Vuillaume, Properties of electronic traps at silicon/1-octadecene interfaces, *Appl. Phys. Lett.* **2001**, *78*, 1288-1290.

The position of the peaks in the *C-V* and *G-V* plots was measured around -0.6 V, shifted in comparison with the peak positions obtained in cyclic voltammetry (-0.4 V) (**Figure 3**). This shift is attributed to use of different electrodes: silver for cyclic voltammetry and tungsten for *C-V* and *G-V* measurements. The voltage drops occurring at the electrolyte/electrode interface may be the source of these differences. The upper inset of **Figure 4** shows the differences in the peak position and amplitude for silver and tungsten electrodes. A smaller oxidation voltage of -0.5 V was found when a silver electrode was used during the *C-V* and *G-V* measurements.

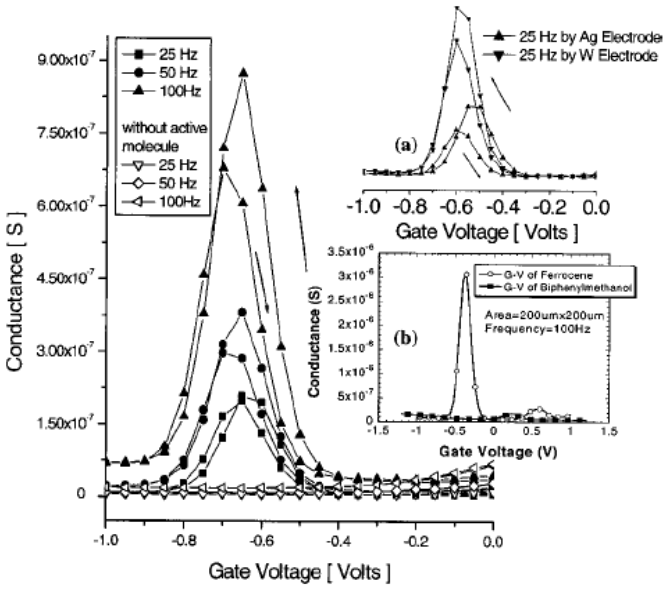

Figure 4. *G-V* characteristics of the EMS capacitor with redox-active ferrocene monolayers measured at 25, 50, and 100 Hz. Inset (a) shows a smaller oxidation/reduction voltage by using a Ag counter electrode. Inset (b) shows the lack of *G-V* peaks in the non-redox-active monolayers (100 Hz).[4]

The use of such hybrid electrode-molecules-silicon EMS capacitors in the characterization of a molecular SAM verifies that these types of assembling could be used for memory application.

4.2. RESULTS AND DISCUSSIONS

Cyclic voltammetry has been widely used to characterize the redox properties of self-assembled monolayers (SAMs). The present chapter of this manuscript reports on impedance spectroscopy (capacitance and conductance) of self-assembled layers that contain low voltage redox-active centers of polyoxometalate type. Such analysis can be very useful in designing molecular devices comprised

of these molecules. ***To the best of our knowledge, no reports of such polyoxometalate modified EMS capacitors have been reported so far in the literature***.

Compound **17** have been incorporated into capacitive devices such as the structure presented in **Figure 5**. These study cells are made of a well with walls in SiO_2 (~10 µm) and a bottom in silicon (*n*-type). After grafting of the POMs at the bottom of this well, the electrochemical capacitive cell is completed with an electrolyte droplet (1M NBu_4PF_6 in propylene carbonate). A silver wire used as a pseudo-counter electrode is precisely positioned inside the droplet. Electrical properties of POMs/Si systems were studied through capacitance-voltage *C-V* and conductance-voltage *G-V* measurements. The experiments were performed using an Agilent 4284 A tool in a nitrogen atmosphere. The gate voltage was applied to a silver electrode (*see* the experimental setup in **Figure 5**). The molecular layer was prepared according to the method **FE**, applied to compound **17** on the silicon substrate, presented in the third part of this manuscript (*see* Scheme 10, page 139). The layer of POMs attached to the silicon provided the basis for EMS capacitors.

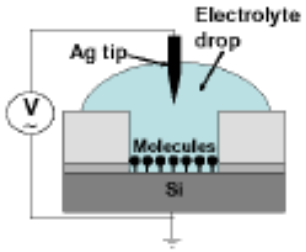

Figure 5. Schematic representation of the experimental setup for the impedance measurements.

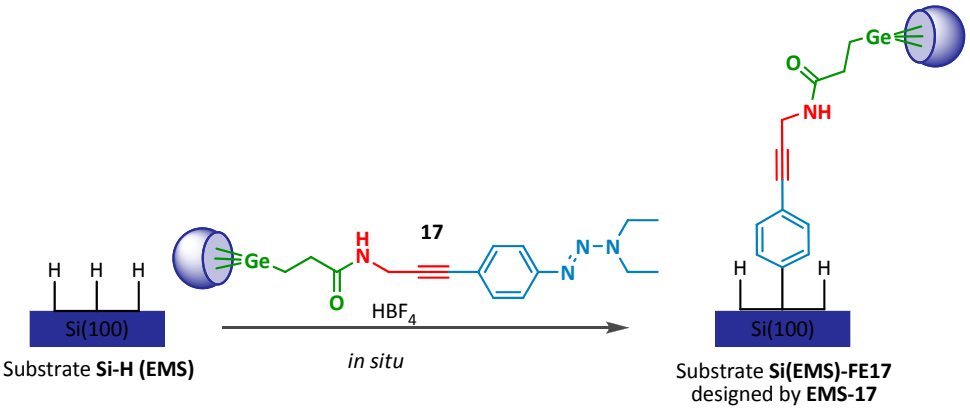

Scheme 1. Schematic representation of the electrografting procedure electrochemically assisted.

The cyclic voltammogram characteristics of substrate **Si-FE17** at various scan rates are shown in Part 3 of this manuscript (*see* Part 3, page 143, Figure 46). The POMs layer exhibits an average reduction peak at -0.70 V and an oxidation one at -0.66 V over the entire range of the scan rate. The linear dependence confirms that the redox process is related to species grafted on the electrode.

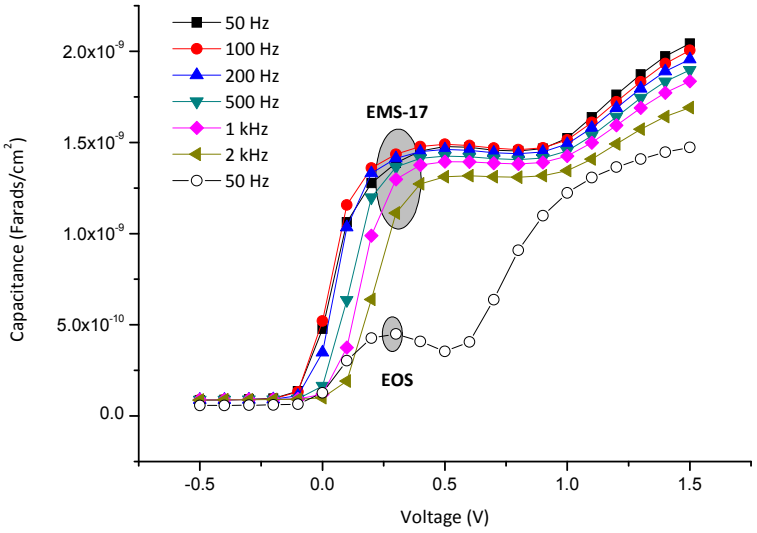

Figure 6. *C-V* plot of the **EMS-17** capacitor containing **17** and the **EOS** capacitor (lacking POMs) at different frequencies for **EMS-17**.

The *C-V* measurements obtained on POMs modified capacitors are presented in **Figure 6**. The measurements were performed between 1.75 and -0.75 V at frequencies comprised between 50 and 2 kHz. The plots in show *C-V* curves **EMS-17** capacitor cell in comparison with an electrolyte-oxide-silicon (**EOS**) capacitor (lacking POMs) (N.B. – the oxide layer in the **EOS** capacitor is a naturally grown oxide onto a silicon surface by exposure to air). The *C-V* curve of the POMs cell shows a peak around 0.30 V. These peaks are especially pronounced at lower frequencies but are reduced in amplitude as the measurement frequency is increased. In the case of redox-inert cell one can observe the presence of a small peak associated with the silicon/oxide interface states.

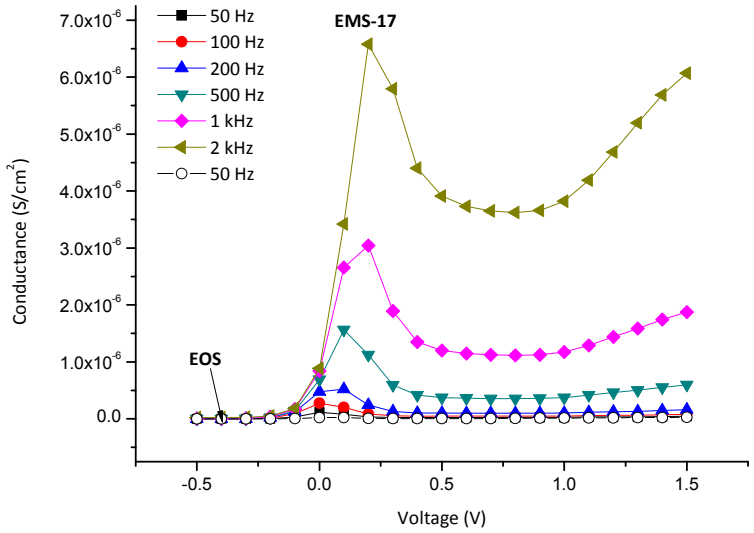

Figure 7. *G-V* plot of the **EMS-17** capacitor containing **17** and the **EOS** capacitor (lacking POMs) at different frequencies for **EMS-17**.

Identical results were obtained from *G-V* curves measured during the same tests that show a peak at around 0.20 V (**Figure 7**). We also studied the POM/Si electron transfer rate behavior by varying the measurement frequency from 50 Hz to 2 kHz. An attenuation of the peak intensity of the *C-V* curve is observed with increasing frequencies, while the *G-V* peak intensity increases. This result can be explained by the fact that at low frequencies, the charge movement can occur at a rate comparable to the measurement signal and is reflected by the presence of the peak; while at high frequencies, the electron transfer process becomes gradually rate-limited until a threshold frequency is achieved at which no peak occurs.

The *C-V* and *G-V* measurements at 100 Hz are shown in **Figure 8** and **Figure 9**, respectively. For comparison purposes, the *C-V* and *G-V* curves of the **EMS-17** capacitor are plotted against the curves of an **EOS** capacitor (lacking POMs). The *C-V* curve of the **EMS-17** capacitor exhibits a peak at 0.3 V at 100 Hz. This peak can be attributed to the charging/discharging transient currents associated with the oxidation/reduction of polyoxometalate molecule. The *G-V* curve of the same **EMS-17** capacitor also exhibits a peak at around 0 V at 100 Hz. The peak position difference in the *C-V*, *G-C* curves and in the cyclic voltammetry curve (*see* Part 3, page 143, Figure 46) is attributed to use of different electrodes: silver for *C-V* and *G-V* measurements and SCE for cyclic voltammetry.

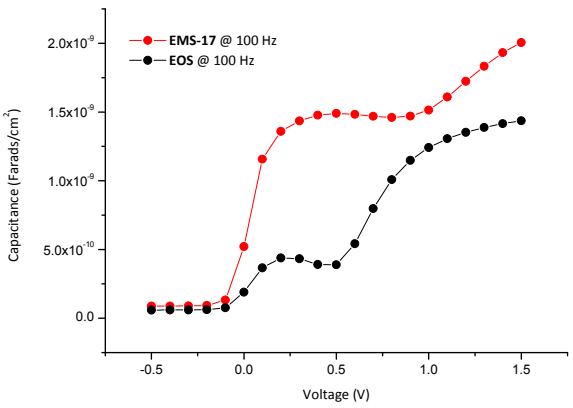

Figure 8. *C-V* curve of the **EMS-17** capacitor (red line) plotted against the **EOS** capacitor (black line) at 100 Hz.

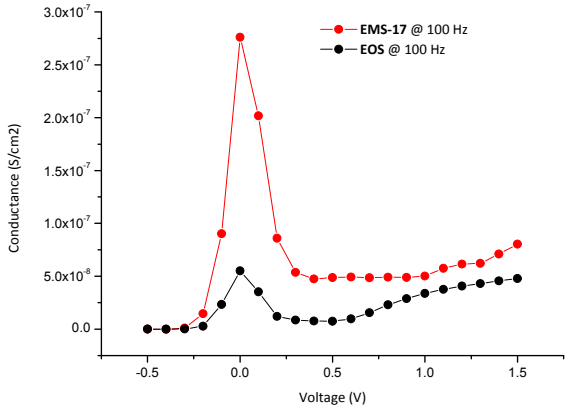

Figure 9. *G-V* curve of the **EMS-17** capacitor (red line) plotted against the **EOS** capacitor (black line) at 100 Hz.

As it can be observed from Figure 8 and Figure 9 for the **EOS** capacitor exhibits also a peak at around the same values as for the **EMS-17** capacitor, however, the higher intensity peaks noticeable for the POMs modified capacitors made us believe that they can be attributable to the polyoxometalate redox layer.

4.3. CONCLUSIONS

In this chapter, the capacitance-voltage and conductance-voltage measurements on a redox-active layer attached to a silicon surface were performed. The ***EMS capacitor exhibits distinct capacitance and conductance peaks which can be associated with the charged state of the POM molecule***.

The *C-V* and *G-V* measurements on an **EMS-17** are reproducible, they were performed several times on two different samples and the same curve pattern was noticed.

This is the ***first example of characterization by conventional capacitance and conductance techniques demonstrated on a redox-active layer of POMs covalently attached onto a silicon surface***. These results suggest their potential application in memory devices.

The fact that the EMS capacitor operates at low applied voltage is an advantage of the device and suggests possible applications in FLASH memory. The relatively low write and erase voltages of the EMS devices are attractive compared to traditional FLASH devices wherein the operating gate voltages are much higher.

Considering the fact that these are the first electrical measurements performed on a POMs-modified capacitor, supplementary measurements are required to ascertain that the *C*-*V* and *G*-*V* peaks observed are indeed due to the POMs. Unfortunately this work remains incomplete.

GENERAL CONCLUSIONS

In this thesis, various subjects of a plural disciplinary domain were approached, promising results were obtained and interesting perspectives were envisaged.

The focus of our research has been on integrating redox-active molecules into Si-based structures, to understand the properties of molecules, to generate a new class of hybrid CMOS/molecular devices for memory applications and open new routes for developing molecular-only devices. This thesis has concentrated on the fabrication and characterization of hybrid silicon-molecular devices. The major findings of this work are summarized as follows.

15 functionalized polyoxometalates able to covalently graft onto a silicon surface were synthesized. The functionalized POMs display terminal vinyl, ethynyl, carboxylic, triazene functions. Among these derivatives 7 of them were for the first time described. In collaboration with the Inorganic Chemistry and Molecular Materials laboratory we succeded their purification and fully characterization.

Specific procedures have been developed for the attachment of POMs on Si and SiO_2 surfaces. Attachment conditions have been optimized for tightly-bonded, well-packed molecular layers including attachment time, attachment temperature, and inert environment. Two procedures reveal successful in terms of electroactivity onto silicon surface.

Hybrid silicon-molecular devices have been characterized using traditional cyclic voltammetry, capacitance-voltage/conductance-voltage measurements. The redox properties of molecules have been studied through these characterization techniques.

Finally, we have been able to perform preliminary capacitance-voltage/conductance-voltage measurements in an integrated microelectronic device.

CONCLUSIONS GÉNÉRALES

Dans cette thèse, divers aspects d'un domaine pluridisciplinaire ont été abordés, des résultats encourageants ont été obtenus et des perspectives intéressantes ont été envisagées.

L'objectif de notre recherche concerne l'intégration de molécules redox-actives dans les structures à base de Si. Pour ce faire, il s'est agit de générer une nouvelle classe des dispositifs hybrides CMOS/moléculaires pour des applications de mémoire, comprendre les propriétés des molécules et d'ouvrir des nouvelles voies pour le développement de dispositifs moléculaires. Cette thèse s'est concentrée sur la fabrication et la caractérisation des dispositifs moléculaires hybrides basés sur silicium. Les principales conclusions de ce travail sont résumées comme suit.

15 polyoxométallates fonctionnalisés capables de se greffer de manière covalente sur une surface de silicium ont été synthétisés. Les POMs fonctionnalisés présentent les fonctions terminales vinyle, éthynyle, carboxyliques, triazène. Parmi ces dérivés 7 d'entre eux ont été décrits pour la première fois. En collaboration avec le Laboratoire de Chimie Inorganique et Matériaux Moléculaires, nous avons réussi leur purification et leur caractérisation complète.

Des procédures spécifiques ont été développées pour la fixation des POMs sur les surfaces Si et SiO_2. Les conditions d'attachement ont été optimisées pour bien lier et bien densifier les couches moléculaires, y compris la durée de fixation, la température de fixation, et la nature de l'environnement inerte. Deux procédures révèlent une réussite en termes d'électroactivité sur surface de silicium.

La nature et les propriétés redox des molécules ont été caractérisées par spectroscopie IRTF, ^{1}H et ^{31}P RMN et par voltammétrie cyclique. Les assemblages hybrides de silicium/molecule ont été caractérisés par analyse XPS et l'électroactivité par voltammétrie cyclique.

Enfin, nous avons été en mesure d'effectuer des mesures préliminaires capacitance-voltage/conductance-voltage dans un dispositif intégré de microélectronique.

Part 5

EXPERIMENTAL PART

5. Fifth Part – Experimental

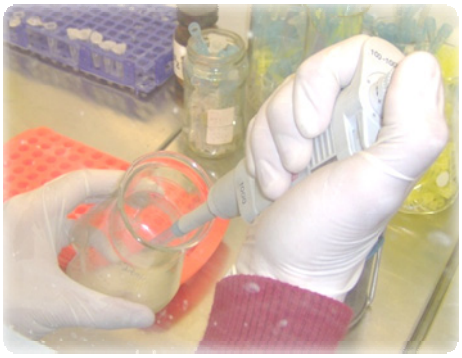

5.1. FUNCTIONALIZED POLYOXOMETALATES PREPARATION

Chemicals and Solvents

Unless otherwise noted, chemicals were purchased from commercial suppliers and used without further purification. All solvents were distilled prior to use.

NMR Spectroscopy

NMR spectra were recorded from $CDCN_3$, $(CD_3)_2CO$ or D_2O solutions on a Bruker AC 200 (^1H 200.13 MHz) or on a Bruker Avance II 300 (^1H 300.13 MHz, ^{31}P 121.49 MHz) spectrometer at room temperature in 5 mm o.d. tubes and chemical shifts are reported in ppm.

IR Spectroscopy

IR spectra were obtained as KBr pellets on a Bio-Rad Win-IR FTS 165 FTIR spectrophotometer.

Electrochemical Measurements

All electrochemical measurements were performed under an argon atmosphere at room temperature in a standard three-electrode cell connected to an Autolab PGSTAT100 potentiostat (from Eco Chemie BV) equipped with general-purpose electrochemical system software.

Elemental analysis

Elemental analyses were performed by the Service de Microanalyses (Université Pierre et Marie Curie) and the Laboratoire Central d'Analyse of the CNRS (Vernaison and Solaize, France).

General Procedures

General Procedure I for Si Surface Preparation

The single-crystal phosphorous-doped *n*-type Si(100) wafers were polished and sliced into rectangular strips of about 0.4×1.5 cm^2 in size. A 0.4×0.3 cm^2 Ti top contact layer (thickness: 488 nm) was deposited on the silicon substrate electrode for cyclic voltammetry measurements. *n*-Si(100) (phosphorous-doped, one side polished, ~1×10^{-3} Ω·cm resistivity) electrodes were used for the experiments. To remove the organic residue on the surface, the Si(100) wafers were ultrasonicated in "Brown solution" for 30 minutes. After rinsing with copious amounts of water, the Si(100) wafers were blow-dried with purified argon and then immersed in 1% HF for 1 minute to remove the oxide film and leave behind a hydrogen-ended wafer.

General Procedure II for Si Surface Preparation

The single-crystal phosphorous-doped *n*-type Si(100) wafers were polished and sliced into rectangular strips at about 0.5×1.5 cm^2 in size. A 0.4×0.5 cm^2 Cr/Au top contact layer (thickness: 25 nm/500 nm) was deposited on the silicon substrate electrode for cyclic voltammetry measurements. *n*-Si(100) (phosphorous-doped, one side or two-sides polished, 8×10^{-3}–2.2×10^{-2} Ω·cm resistivity) electrodes were used for the experiments. To remove the organic residues on the surface, the Si(100) wafers were immersed in a 96 wt. % mixture of concentrated 70 % H_2SO_4 and 30 % H_2O_2 (piranha solution) for about 30 seconds. After rinsing with copious amounts of water, the Si(100) wafers were blow-dried with purified argon and then immersed in 1 % HF for 1 min to remove the oxide film and to leave behind a hydrogen-ended wafer.

GP III: General procedure for preparation of compounds 4, 5, 6, and 7

To a solution of 0.5 g (0.150 mmol) of **3** in 5mL deoxygenated DMF was added dropwise $RSiCl_3$ (0.45 mmol) at room temperature. After one day of stirring, the solution was filtrated then precipitated by

ethanol/ether mixture. The white powder obtained was redissolved in DMF and precipitated again several times, in order to remove the excess of hydrolysed silane. Compounds were isolated as a white powder. Slow evaporation at room temperature of the resulting DMF solution gave crystals in a few days.

GP IV: General procedure for the preparation of compound 10, 11, and 12

The compounds A, α-$K_9PW_9O_{34}\cdot16H_2O$ (2.869 g, 1 mmol) and *n*Bu_4NBr (0.967 g, 3 mmol) were suspended in DMF (15 mL); RSiCl3 (4 mmol) was added dropwise under vigorous stirring. The mixture was stirred 3 hours at room temperature. After separation of the white solid (NaCl, NaBr, traces of $K_9PW_9O_{34}\cdot16H_2O$, colorless crystals were formed by slow evaporation of the resulting solution at room temperature.

5.1.1. Preparation of α-$K_{7-x}Na_xPW_{11}O_{39}\cdot14H_2O$ [1] (Compound **1**)

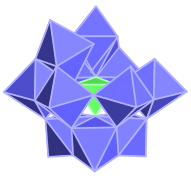

To a solution of $Na_2WO_4\cdot2H_2O$ (181.5 g, 0.550 mol) in 300 mL water were added 50 mL of H_3PO_4 1M and 88 mL of glacial CH_3COOH. The solution was refluxed during one hour, then KCl (60 g, 0.805 mol) were added; the white precipitate which appeared was filtered, washed with water and dried in air to afford the compound **1** (Yield: 104.4 g, 58 %).

Appearance	White solid
^{31}P NMR (D_2O)	^{31}P NMR (121.49 MHz) δ ppm: -10.31
Chemical formula	$H_{28}K_{6.4}Na_{0.6}O_{53}PW_{11}$
Exact mass	3186.99 g/mol
IR (KBr pellets)	IR (KBr pellets) ν cm^{-1}: 1086 (P-O), 1043 (P-O), 952 (W=O), 903 (W-O-

[1] R. Contant, Relation entre les tungstophophates apparentés à l'anion $PW_{12}O_{40}^{3-}$. Synthèse et propriétés d'un nouveau polyoxotungstophosphate lacunaire $K_{10}P_2W_{20}O_{70}\cdot24H_20$, *Can. J. Chem.* **1987**, *65*, 568-573.

	W), 858 (W-O-W), 810 (W-O-W), 730 (W-O-W), 360 (α isomer signature)
Elemental analysis	Calcd. (%): H 0.89, H 7.36, Na 0.72, P 0.97 Found (%): H 0.75, K 6.15, Na 2.36, P 0.85
Compound No.	**1**

5.1.2. Preparation of A, α-$K_9PW_9O_{34}\cdot16H_2O$ [1] (Compound **2**)

To a solution of 64 g of α-$K_{7-x}Na_xPW_{11}O_{39}\cdot14H_2O$ in 200 mL of water, 60 mL of K_2CO_3 2M were added; the white precipitate which appeared was filtered, washed with alcohol and dried in air to afford compound **2** (Yield: 46.4 g, 80 %).

Appearance	White solid
Chemical formula	$K_9H_{32}PO_{50}W_9$
Exact mass	2869.64 g/mol
IR (KBr pellets)	IR (KBr pellets) ν cm^{-1}: 1054 (P-O), 1003 (P-O), 929 (W=O), 909 (W=O), 821 (W-O-W), 733 (W-O-W), 367 and 315 (α isomer signature)
Compound No.	**2**

5.1.3. Preparation of α-A-(nBu$_4$N)$_3$[PW$_9$O$_{34}$(tBuSiOH)$_3$]·0.5MeCN [2] (Compound **3**)

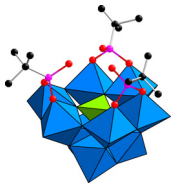

To a well-stirred suspension of α-A-K$_9$[PW$_9$O$_{34}$]·16H$_2$O (10 g, 3.48 mmol) in dry MeCN (200 mL) under argon were added solid nBu$_4$NBr (6 g, 18.6 mmol) and then tBuSiCl$_3$ (2.1 g, 10.1 mmol): the mixture was stirred overnight at 0°C. After separation of the white solid (KCl + KBr), white crystals of (nBu$_4$N)$_3$[PW$_9$O$_{34}$(tBuSiOH)$_3$] formed upon slow evaporation of the resulting solution in an open vessel at room temperature to afford compound **3** (Yield: 6.7 g, 59 %).

Appearance	Colorless crystals
^{1}H NMR (*CD_3CN*)	^{1}H NMR (200.13 MHz) δ ppm: 1.03 (s, 27H, tBu), 1.05 (t, 36H, NCH$_2$CH$_2$CH$_2$C***H$_3$***), 1.42 (m, 24H, NCH$_2$CH$_2$C***H$_2$***CH$_3$), 1.64 (m, 24H, NCH$_2$C***H$_2$***CH$_2$CH$_3$), 3.17 (m, 24H, NC***H$_2$***CH$_2$CH$_2$CH$_3$), 5.01 (s, 3H, O***H***)
^{31}P NMR (*$(CD_3)_2CO$*)	^{31}P NMR (121.49 MHz) δ ppm: -15.76
Chemical formula	C$_{61}$H$_{139.5}$N$_{3.5}$PO$_{37}$Si$_3$W$_9$
Exact mass	3276.54 g/mol
IR (KBr pellets)	IR (KBr pellets) ν cm^{-1}: 1487 (C-C), 1100 (P-O), 1034 (P-O), 1003 (W=O), 969 (W=O), 940 (W=O), 864 (W-O-W), 835 (W-O-W), 727 (W-O-W), 389 and 345 (α isomer signature)
Elemental analysis	Calcd. (%): C 22.36, H 4.27, N 1.28, P 0.94 Found (%): C 23.15, H 4.23, N 1.46, P 0.83
Compound No.	**3**

[2] A. Mazeaud, N. Ammani, F. Robert, R. Thovenot, Coordination Chemistry of Polyoxometalates: Rational Synthesis of the Mixed Organosilyl Derivatives of Trivacant Polyoxotungstates α-A-[PW$_9$O$_{34}$(tBuSiO)$_3$(RSi)]$^{3-}$ and α-B-[AsW$_9$O$_{33}$(tBuSiO)$_3$(HSi)]$^{3-}$, *Angew. Chem., Int. Ed. Engl.* **1996**, *35*, 1961-1964.

5.1.4. Preparation of α-A-(nBu$_4$N)$_3$[PW$_9$O$_{34}$(tBuSiO)$_3$(His)] [2] (Compound **4**)

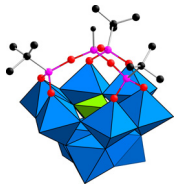

Following the **GP III**, upon addition of 0.45 mmol of $HsiCl_3$, compound **4** was isolated as colorless crystals (Yield: 0.3 g, 59 %).

Appearance	Colorless crystals
^{1}H NMR (*CD_3CN*)	^{1}H NMR (200.13 MHz) δ ppm: 0.99 (s, 27H, *t*Bu), 1.02 (t, 36H, $NCH_2CH_2CH_2C\boldsymbol{H_3}$), 1.42 (m, 24H, $NCH_2CH_2C\boldsymbol{H_2}CH_3$), 1.68 (m, 24H, $NCH_2C\boldsymbol{H_2}CH_2CH_3$), 3.17 (m, 24H, $NC\boldsymbol{H_2}CH_2CH_2CH_3$), 4.36 (s, 1H, Si***H***)
^{31}P NMR (*CD_3CN*)	^{31}P NMR (121.49 MHz) δ ppm: -16.64
Chemical formula	$C_{60}H_{136}N_3PO_{37}Si_4W_9$
Exact mass	3289.59 g/mol
IR (KBr pellets)	IR (KBr pellets) ν cm^{-1}: 2200 (Si-H), 1127 (Si-O-Si), 1095 (P-O), 1040 (P-O), 1000 (W=O), 976 (W=O), 957 (W=O), 893 (W-O-W), 874 (W-O-W), 834 (W-O-W), 802 (W-O-W)
Elemental analysis	Calcd. (%): C 21.90, H 4.16, N 1.27, P 0.94 Found (%): C 22.29, H 4.12, N 1.36, P 0.88
Compound No.	**4**

5.1.5. Preparation of α-A-(nBu$_4$N)$_3$[PW$_9$O$_{34}$(tBuSiO)$_3$(Si-CH=CH$_2$)] [3] (Compound **5**)

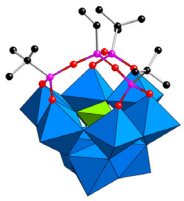

Following the **GP III**, upon addition of 0.45 mmol of CH_2=$CHSiCl_3$, compound **5** was isolated as colorless crystals (Yield: 0.4 g, 79 %).

Appearance	Colorless crystals
^{1}H NMR (*CD_3CN*)	^{1}H NMR (200.13 MHz) δ ppm: 1.02 (s, 27H, *t*Bu), 1.01 (t, 36H, $NCH_2CH_2CH_2C\boldsymbol{H_3}$), 1.41 (m, 24H, $NCH_2CH_2C\boldsymbol{H_2}CH_3$), 1.67 (m, 24H, $NCH_2C\boldsymbol{H_2}CH_2CH_3$), 3.16 (m, 24H, $NC\boldsymbol{H_2}CH_2CH_2CH_3$), 5.7-6.2 (m, 3H, $C\boldsymbol{H}$=$C\boldsymbol{H_2}$)
^{31}P NMR (*$(CD_3)_2CO$*)	^{31}P NMR (121.49 MHz) δ ppm: -16.44
Chemical formula	$C_{62}H_{138}N_3PO_{37}Si_4W_9$
Exact mass	3315.63 g/mol
IR (KBr pellets)	IR (KBr pellets) ν cm^{-1}: 1603 (C=C), 1278 (Si-C), 1120 (Si-O-Si), 1086 (P-O), 1037 (P-O), 1000 (W=O), 975 (W=O), 955 (W=O), 864 (W-O-W), 810 (W-O-W), 730 (W-O-W), 392 and 341 (α isomer signature)
Compound No.	**5**

5.1.6. Preparation of α-A-(nBu$_4$N)$_3$[PW$_9$O$_{34}$(tBuSiO)$_3$(Si-CH$_2$-CH=CH$_2$)] [3] (Compound **6**)

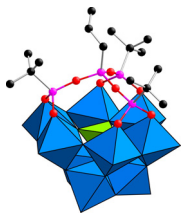

[3] D. Agustin, C. Coelho, A. Mazeaud, P. Herson, A. Proust, R. Thouvenot, Organic-Inorganic Hybrids based on Polyoxometalates. Part 8. Synthesis and Spectroscopic Characterization of the Heterosilylated Anions [PW$_9$O$_{34}$(^{t}BuSiO)$_3$(SiR)]$^{3-}$ (R = -CH$_3$, -CH=CH$_2$, -CH$_2$-CH=CH$_2$, -(CH$_2$)$_4$-CH=CH$_2$) – X-ray Crystal Structure of [^{n}Bu$_4$N]$_3$[PW$_9$O$_{34}$(^{t}BuSiO)$_3$(SiCH$_2$-CH=CH$_2$)], *Z. Anorg. Allg. Chem.* **2004**, *630*, 2049-2053.

Following the **GP III**, upon addition of 0.45 mmol of CH_2=CH-CH_2SiCl_3, compound **6** was isolated as colorless crystals (Yield: 0.4 g, 78 %).

Appearance	Colorless crystals
^{1}H NMR (*CD_3CN*)	^{1}H NMR (300.13 MHz) δ ppm: 0.97 (s, 27H, *t*Bu), 1.00 (t, 36H, $NCH_2CH_2CH_2C\boldsymbol{H_3}$), 1.39 (m, 24H, $NCH_2CH_2C\boldsymbol{H_2}CH_3$), 1.62 (m, 24H, $NCH_2C\boldsymbol{H_2}CH_2CH_3$), 1.80 (m, 2H, $C\boldsymbol{H_2}CH=CH_2$), 3.11 (m, 24H, $NC\boldsymbol{H_2}CH_2CH_2CH_3$), 4.9-6.0 (m, 3H, $CH_2C\boldsymbol{H}=C\boldsymbol{H_2}$)
^{31}P NMR (*$(CD_3)_2CO$*)	^{31}P NMR (121.49 MHz) δ ppm: -16.45
Chemical formula	$C_{63}H_{140}N_3PO_{37}Si_4W_9$
Exact mass	3329.65 g/mol
IR (KBr pellets)	IR (KBr pellets) ν cm^{-1}: 1634 (C=C), 1256 (Si-C), 1118 (Si-O-Si), 1092 (P-O), 1037 (P-O), 1000 (W=O), 975 (W=O), 958 (W=O), 864 (W-O-W), 813 (W-O-W), 764 (W-O-W), 727 (W-O-W), 392 and 341 (α-isomer signature)
Elemental analysis	Calcd. (%): C 22.71, H 4.24, N 1.27, P 0.93 Found (%): C 22.42, H 4.16, N 1.42, P 0.82
Compound No.	**6**

5.1.7. Preparation of α-A-(nBu$_4$N)$_3$[PW$_9$O$_{34}$(tBuSiO)$_3$(Si-(CH$_2$)$_4$-CH=CH$_2$)] [3] (Compound **7**)

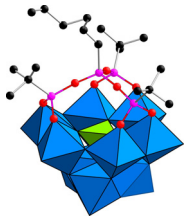

Following the **GP III**, upon addition of 0.45 mmol of CH_2=CH-$(CH_2)_4SiCl_3$, compound **7** was isolated as colorless crystals (Yield: 0.3 g, 52 %).

Appearance	Colorless crystals

^{1}H NMR (*CD_3CN*)	^{1}H NMR (300.13 MHz) δ ppm: 0.70 (m, 2H, $(CH_2)_3C\boldsymbol{H_2}Si$), 0.97 (s, 27H, *t*Bu), 1.00 (t, 36H, $NCH_2CH_2CH_2C\boldsymbol{H_3}$), 1.40 (m, 24H, $NCH_2CH_2C\boldsymbol{H_2}CH_3$), 1.3-1.9 (m, 6H, $(C\boldsymbol{H_2})_3CH_2Si$), 1.63 (m, 24H, $NCH_2C\boldsymbol{H_2}CH_2CH_3$), 3.12 (m, 24H, $NC\boldsymbol{H_2}CH_2CH_2CH_3$), 4.7-6.1 (m, 3H, $C\boldsymbol{H}=C\boldsymbol{H_2}$).
^{31}P NMR (*$(CD_3)_2CO$*)	^{31}P NMR (121.49 MHz) δ ppm: -16.51
Chemical formula	$C_{66}H_{146}N_3PO_{37}Si_4W_9$
Exact mass	3371.73 g/mol
IR (KBr pellets)	IR (KBr pellets) ν cm^{-1}: 1641 (C=C), 1228 (Si-C), 1117 (Si-O-Si), 1082 (P-O), 1040 (P-O), 1000 (W=O), 975 (W=O), 955 (W=O), 867 (W-O-W), 813 (W-O-W), 727 (W-O-W), 392 and 340 (α isomer signature)
Compound No.	**7**

5.1.8. Preparation of α-A-(*n*Bu_4N)$_3$[PW_9O_{34}(*t*BuSiO)$_3$(Si-$(CH_2)_9$-CH=CH_2)] (Compound **8**)

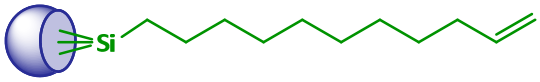

Following the **GP III**, upon addition of 0.45 mmol of CH_2=CH-$(CH_2)_9Si(CH_3O)_3$, compound **8** could not be isolated.

Compound No. **8**

5.1.9. Preparation of α-A-(*n*Bu_4N)$_3$[PW_9O_{34}(*t*BuSiO)$_3$(Si-C_6H_4-NH_2)] (Compound **9**)

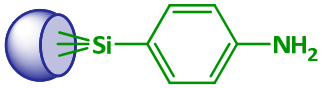

Following the **GP III**, upon addition of 0.45 mmol of *p*-NH_2-C_6H_4-$Si(CH_3O)_3$, compound **9** could not be isolated.

Compound No. **9**

5.1.10. Preparation of $(Bu_4N)_3[PW_9O_{34}(CH_2=CHSiO)_3(Si\text{-}CH=CH_2)]$ (Compound **10**)

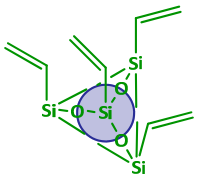

Following the **GP IV**, upon addition of 4 mmol of CH_2=$CHSiCl_3$, compound **10** was isolated as colorless crystals (Yield: 1.7 g, 52 %).

Appearance	Colorless crystals
^{31}P NMR ($(CD_3)_2CO$)	^{31}P NMR (121.49 MHz) δ ppm: -16.38
Chemical formula	$C_{56}H_{120}N_3PO_{37}Si_4W_9$
Exact mass	3225.42 g/mol
IR (KBr pellets)	IR (KBr pellets) ν cm^{-1}: 1600 (C=C), 1276 (Si-C), 1125 (Si-O-Si), 1097 (P-O), 1037 (P-O), 1006 (W=O), 975 (W=O), 960 (W=O), 867 (W-O-W), 818 (W-O-W), 730 (W-O-W), 389 and 334 (α isomer signature)
Elemental analysis	Calcd. (%): C 20.85, H 3.75, N 1.30, P 0.96 Found (%): C 21.13, H 3.77, N 1.27, P 0.90
Compound No.	**10**

5.1.11. Preparation of $(Bu_4N)_3[PW_9O_{34}(CH_2=CH\text{-}CH_2\text{-}SiO)_3(Si\text{-}CH_2\text{-}CH=CH_2)]$ (Compound **11**)

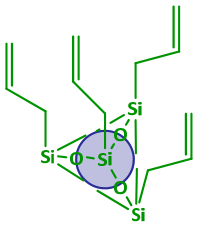

Following the **GP IV**, upon addition of 4 mmol of CH_2=$CH\text{-}CH_2SiCl_3$, compound **11** was isolated as colorless crystals (Yield: 1.1 g, 33 %).

Appearance	Colorless crystals
^{31}P NMR ($(CD_3)_2CO$)	^{31}P NMR (121.49 MHz) δ ppm: -16.12

Chemical formula	$C_{60}H_{128}N_3PO_{37}Si_4W_9$
Exact mass	3281.53 g/mol
IR (KBr pellets)	IR (KBr pellets) ν cm^{-1}: 1634 (C=C), 1256 (Si-C), 1123 (Si-O-Si), 1098 (P-O), 1036 (P-O), 1001 (W=O), 975 (W=O), 960 (W=O), 868 (W-O-W), 817 (W-O-W), 725 (W-O-W), 389 and 343 (α isomer signature)
Compound No.	**11**

5.1.12. Preparation of $(Bu_4N)_3[PW_9O_{34}(CH_3\text{-}CH_2SiO)_3(Si\text{-}CH_2\text{-}CH_3)]$ (Compound **12**)

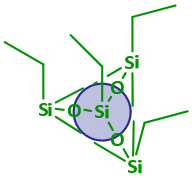

Following the **GP IV**, upon addition of 4 mmol of $CH_3\text{-}CH_2SiCl_3$, compound **12** was isolated as colorless crystals.

Appearance	Colorless crystals
^{31}P NMR ($(CD_3)_2CO$)	^{31}P NMR (121.49 MHz) δ ppm: -16.72
Chemical formula	$C_{56}H_{128}N_3PO_{37}Si_4W_9$
Exact mass	3233.48 g/mol
Compound No.	**12**

5.1.13. Preparation of $Cl_3Ge(CH_2)_2COOH$ [4] (Compound **13**)

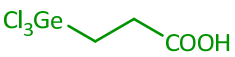

Germanium tetrachloride (8.0 mL, 0.069 mol) was dissolved in 40 mL of absolute ether in a round bottom two-necked flask, equipped with a reflux condenser and a septum inlet, which had been previously flushed with dry nitrogen. A mineral oil bubbler was used in order to keep air out of the reaction flask. Tetramethyldisiloxane (12.0 mL, 0.069 mol) was added and the homogenous solution was stirred at room temperature for ~ 4-5 hours. (In order to speed up the reaction vessel can be

[4] G. Sazani, M. T. Pope, Organotin and organogermanium linkers for simple, direct functionalization of polyoxotungstates, *Dalton Trans.* **2004**, 1989-1994.

immersed in a water-bath at ~ 40°C). After completion, the reaction mixture separated into two layers. The upper layer (excess ether) was removed by means of a syringe through the septum and the lower greenish-yellow oily layer containing the etherate complex $HgeCl_3 \cdot 2(C_2H_5)_2O$ was used immediately for further reaction. Acrylic acid (6.0 mL, 0.086 mol) was added dropwise to 2.6 g (0.069 mol) $HgeCl_3 \cdot 2(C_2H_5)_2O$ complex cooled to 0°C in an ice-water bath. The reaction mixture was stirred for ~ 12 hours. The excess ether and acrylic acid were removed by rotary evaporation. The residue was extracted with chloroform which was later removed in a rotary evaporator (Yield: 11.9 g, 55 %).

Appearance	White powder
^{1}H NMR (*CD_3CN*)	^{1}H NMR (300.13 MHz) δ ppm: 2.13 (t, 2H, C***H_2***COOH), 2.87 (t, 2H, GeC***H_2***), 7.20 (s, 1H, COO***H***)
Chemical formula	$C_3H_5O_2GeCl_3$
Exact mass	252.07 g/mol
Compound No.	**13**

5.1.14. Preparation of $(Nbu_4)_3[PW_9O_{34}(t\text{BuSiO})_3Ge(CH_2)_2COOH]$ (Compound **14**) (*See Appendix*)

An excess of **13** (0.801 g, 3.170 mmol) was added to a solution of **3** (2.016 g, 0.633 mmol) in dry acetonitrile (80 mL). The reaction mixture was kept overnight at room temperature, then the solvent was removed in vacuo after checking for completion of the reaction by ^{31}P NMR spectroscopy. The residue was dissolved in acetone (10 mL) and compound **14** was precipitated by the addition of a mixture of diethyl ether and ethanol (10:1), filtered off, and dried in air (1.8 g, 83 %). Colorless crystals of **14**·H2O, suitable for single-crystal X-ray crystallography, were grown from a DMF solution by slow evaporation in air at room temperature.

Appearance	Colorless crystals
^{1}H NMR (*CD_3CN*)	^{1}H NMR (300.13 MHz) δ ppm: 0.98 (t, 36H, $NCH_2CH_2CH_2CH_3$), 0.99 (s, 27H, *t*Bu), 1.40 (sextet, 24H, $NCH_2CH_2CH_2CH_3$), 1.55 (m, 2H, $GeCH_2CH_2COOH$), 1.63 (m, 24H, $NCH_2CH_2CH_2CH_3$), 2.57 (m, 2H,

	$GeCH_2C\boldsymbol{H_2}COOH$), 3.13 (m, 24H, $NC\boldsymbol{H_2}CH_2CH_2CH_3$).
^{31}P NMR (CD_3CN)	^{31}P NMR (121.49 MHz) δ ppm: -16.34
Chemical formula	$C_{63}H_{140}GeN_3PO_{39}Si_3W_9$
Exact mass	3406.28 g/mol
IR (KBr pellets)	IR (KBr pellets) ν cm^{-1}: 2963 (m), 2935 (m), 2876 (w), 2860 (w), 1732 (w), 1677 (w), 1487 (m), 1475 (s), 1384 (w), 1107 (s), 1036 (m), 974 (s), 951 (s), 866 (s), 806 (s), 726 (m), 603 (w), 580 (w), 530 (w), 505 (w), 482 (w), 425 (w), 391 (m), 363 (m)
Elemental analysis	Calcd. (%): C 22.21, H 4.14, Ge 2.13, N 1.23, P 0.91, Si 2.47, W 48.58 Found (%): C 22.37, H 3.96, Ge 1.66, N 1.30, P 0.95, Si 2.44, W 46.77
Compound No.	**14**

5.1.15. Preparation of $(Nbu_4)_3[PW_9O_{34}(t\text{BuSiO})_3Ge(CH_2)_2C(O)NHCH_2C{\equiv}CH]$ (Compound **15**) (*See Appendix*)

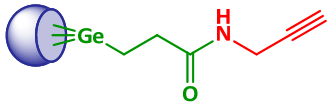

Triethylamine (43 µL, 0.307 mmol), isobutylchloroformiate (40 µL, 0.307 mmol), and after 25 min, propargylamine (36 µL, 0.521 mmol) were added successively to a solution of **14** (0.888 g, 0.261 mmol) in dry acetonitrile (10 mL). The solution was stirred overnight and then evaporated to dryness. The residue was dissolved in acetone (10 mL) and compound **15** was precipitated by the addition of a mixture of diethyl ether and ethanol (10:1), filtered off, and dried in air (0.67 g, 74 %).

Appearance	White powder
^{1}H NMR (CD_3CN)	^{1}H NMR (300.13 MHz) δ ppm: 0.98 (t, 36H, $NCH_2CH_2CH_2C\boldsymbol{H_3}$), 1.02 (s, 27H, *t*Bu), 1.39 (sextet, 24H, $NCH_2CH_2C\boldsymbol{H_2}CH_3$), 1.55 (m, 2H, $GeC\boldsymbol{H_2}CH_2C(O)NHCH_2C{\equiv}CH$), 1.63 (m, 24H, $NCH_2C\boldsymbol{H_2}CH_2CH_3$), 2.42 (t, 1H, $GeCH_2CH_2C(O)NHCH_2C{\equiv}C\boldsymbol{H}$), 2.45 (m, 2H, $GeCH_2C\boldsymbol{H_2}C(O)NHCH_2C{\equiv}CH$), 3.13 (m, 24H, $NC\boldsymbol{H_2}CH_2CH_2CH_3$), 3.91 (dd, 2H, $GeCH_2CH_2C(O)NHC\boldsymbol{H_2}C{\equiv}CH$), 6.69 (brt, 1H, $GeCH_2CH_2C(O)N\boldsymbol{H}CH_2C{\equiv}CH$).

^{31}P NMR (*CD_3CN*)	^{31}P NMR (121.49 MHz) δ ppm: -16.35
Chemical formula	$C_{66}H_{143}GeN_4PO_{38}Si_3W_9$
Exact mass	3443.35 g/mol
IR (KBr pellets)	IR (KBr pellets) ν cm^{-1}: 2963 (m), 2935 (m), 2877 (w), 2860 (w), 1674 (w), 1485 (m), 1474 (s), 1384 (w), 1107 (s), 1037 (m), 973 (s), 951 (s), 865 (s), 807 (s), 726 (m), 603 (w), 580 (w), 530 (w), 506 (w), 482 (w), 425 (w), 392 (m), 364 (m)
Elemental analysis	Calcd. (%): C 23.02, H 4.19, Ge 2.11, N 1.63, Si 2.45, W 48.05 Found (%): C 22.60, H 4.27, Ge 1.94, N 1.65, Si 2.93, W 48.25
Compound No.	**15**

5.1.16. Preparation of 1-(4-Iodophenyl)-3,3-diethyltriazene [5] (Compound **16**)

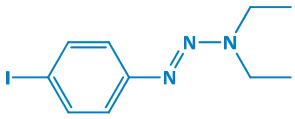

4-Iodoaniline (5.00 g, 22.83 mmol) was added to a 250 mL round bottom flask. THF (25 mL) was added and the reaction was cooled to -30 °C. Borontrifluoride diethyletherate (11.57 mL, 91.32 mmol) was added dropwise followed by the dropwise addition of *t*-butylnitrite (9.50 mL, 79.91 mmol). The reaction was warmed to room temperature and Et_2O (150 mL) was added. The mixture was vacuum filtered and washed with Et_2O to afford the aryl diazonium salt which was dissolved in CH_3CN (80 mL) and cooled to 0 °C. A solution of H_2O (40 mL), K_2CO_3 (8.34 g, 60.41 mmol), and diethylamine (4.20 mL, 40.27 mmol) was added to the reaction which turned up deep red. The mixture was allowed in H_2O and extracted (3×) with CH_2Cl_2, dried using anhydrous $MgSO_4$ and concentrated *in vacuo*. Column chromatography, silica gel (3:1 CH2Cl2/hexane) afforded **16** as a viscous red oil.

Appearance	Red oil
^{1}H NMR (*CD_3CN*)	^{1}H NMR (200.13 MHz) δ ppm: 1.26 (s, 6H, $(CH_2C\boldsymbol{H_3})_2$), 3.77 (q, 4H, $(C\boldsymbol{H_2}CH_3)_2$), 7.17 (d, 2H, ArH), 7.66 (d, 2H, ArH)

[5] A.K. Flatt, B. Chen, J.M. Tour, Fabrication of Carbon Nanotube-Molecule-Silicon Junctions, *J. Am. Chem. Soc.* **2005**, *127*, 8918-8919.

Chemical formula	$C_{10}H_{14}N_3I$
Exact mass	303.14 g/mol
Compound No.	**16**

5.1.17. Preparation of $(Nbu_4)_3[PW_9O_{34}(t\text{BuSiO})_3Ge(CH_2)_2C(O)NHCH_2C{\equiv}CC_6H_4N_3Et_2]$ (Compound **17**)

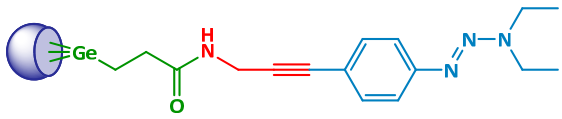

A mixture of **15** (0.80, 0.232 mmol), 4-iodophenyldiethyltriazene (91.55 mg, 0.302 mmol), $Pd(PPh_3)_2Cl_2$ (7 mg, 0.01 mmol), CuI (3 mg, 0.02 mmol), triethylamine (42 µL, 0.302 mmol) and acetonitrile (10 mL) was stirred at room temperature overnight under argon. The resulting yellow solution was filtered. The filtrate was concentrated to about 3 mL and a solid was precipitated by adding diethyl ether. The yellow precipitate was filtered to afford **17** as a yellow product (Yield: 0.655 g, 78 %).

Appearance	Yellow powder
^{1}H NMR (*CD_3CN*)	^{1}H NMR (300.13 MHz) δ ppm: 0.98 (t, 36H, $NCH_2CH_2CH_2C\boldsymbol{H_3}$), 1.00 (s, 27H, *t*Bu), 1.38 (m, 24H, , $NCH_2CH_2C\boldsymbol{H_2}CH_3$), 1.64 (m, 24H, $NCH_2C\boldsymbol{H_2}CH_2CH_3$), 2.49 (m, 2H, $GeCH_2C\boldsymbol{H_2}$), 3.12 (m, 24H, $NC\boldsymbol{H_2}CH_2CH_2CH_3$), 3.78 (q, 4H, $(C\boldsymbol{H_2}CH_3)_2$), 4.13 (d, 2H, $NHC\boldsymbol{H_2}$), 6.77 (t, 1H, CON***H***), 7.33 (d, 4H, ArH)
^{31}P NMR (*CD_3CN*)	^{31}P NMR (121.49 MHz) δ ppm: -16.35
Chemical formula	$C_{76}H_{156}N_7PO_{38}Si_3W_9Ge$
Exact mass	3618.50 g/mol
IR (KBr pellets)	IR (KBr pellets) ν cm^{-1}: 1669 (CONH), 1238 (N-N), 1107 (P-O), 1036 (P-O), 1008 (W=O), 973 (W=O), 949 (W=O), 866 (W-O-W), 806 (W-O-W), 727 (W-O-W)
Elemental analysis	Calcd. (%): C 25.22, H 4.34, N 2.70, P 0.85, Ge 2.00 Found (%): C 25.22, H 4.31, N 2.73, P 0.70, Ge 1.80
Compound No.	**17**

5.1.18. Preparation of HO-CH$(CH_2)_2Py_2$ (Compound **18**) (*Synthesize in Inorganic Chemistry and Molecular Materials laboratory, Paris 6*)

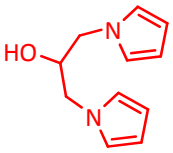

Compound No.	**18**

5.1.19. Preparation of $(NBu_4)_3[PW_9O_{34}(tBuSiO)_3Ge(CH_2)_2COOCH(CH_2)_2Py_2]$ (Compound **19**)

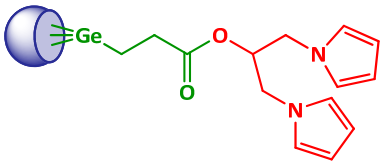

Compound **14** (340 mg, 0.1 mmol) was added to a solution of EEDQ (37 mg, 0.15 mmol) at 80 °C in acetonitrile (10 mL). After 15 minutes compound **18** (38 mg, 0.2 mmol) was added to the refluxing solution. The mixture was stirred for 48 hours. After completion, the remaining solid was filtered off. Concentration of the solvent *in vacuo* afforded a pale yellow oil which was crystallized (Acetone/Et_2O, 1:10) to give the desired ester **19**.

Appearance	White powder
Chemical formula	$C_{74}H_{152}N_5PO_{39}Si_3W_9Ge$
Exact mass	3578.45 g/mol
Elemental analysis	Calcd. (%): C 24.83, H 4.28, N 1.95, P 0.86, Ge 2.03
	Found (%): C 23.23, H 4.10, N 1.28, P 0.61, Ge 2.08
Compound No.	**19**

5.1.20. Preparation of $(NBu_4)_3[PW_9O_{34}(tBuSiO)_3Ge(CH_2)_2C(O)NHCH_2C{\equiv}CC_6H_4NH_2]$ (Compound **20**)

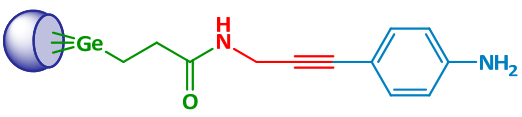

A mixture of **15** (0.80, 0.232 mmol), 4-iodoaniline (66.14 mg, 0.302 mmol), $Pd(PPh_3)_2Cl_2$ (7 mg, 0.01 mmol), CuI (3 mg, 0.02 mmol), triethylamine (42 µL, 0.302 mmol) and acetonitrile (10 mL) was stirred at room temperature overnight under argon. The resulting yellow solution was filtered. The filtrate was concentrated to about 3 mL and a solid was precipitated by adding diethyl ether. The yellow precipitate was filtered to afford **17** as a yellow product.

Compound No. **20**

5.1.21. Preparation of $(NBu_4)_4[PW_{11}O_{39}Ge(CH_2)_2COOH]$ (Compound **21**) (*See Appendix*)

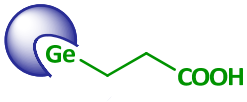

Compound **13** (0.250 g, 0.992 mmol) and triethylamine (210 µL, 1.505 mmol) were added successively to a solution of $(NBu_4)_4[H_3PW_{11}O_{39}]$ (was prepared as described in the literature[6]) (4 g, 1.096 mmol) in dry acetonitrile (160 mL). The solution was stirred for 5 h and evaporated to dryness. The residue was dissolved in acetone (10 mL). The white product that precipitated by addition of a mixture of diethyl ether and ethanol (10:1) was filtered off and dried in air (3.9 g). It proved to be a mixed NEt_3H^+/NBu_4^+ salt on the basis of ^1H and ^{13}C NMR spectroscopic analyses. Analytically pure NBu_4^+ salt (**21**) was obtained by recrystallization in DMF.

Appearance	White powder
^1H NMR (CD_3CN)	^1H NMR (300.13 MHz) δ ppm: 0.99 (t, 48H, $NCH_2CH_2CH_2C\boldsymbol{H_3}$), 1.40 (m, 34H, $NCH_2CH_2C\boldsymbol{H_2}CH_3$+$GeC\boldsymbol{H_2}CH_2COOH$), 1.65 (m, 32H, $NCH_2C\boldsymbol{H_2}CH_2CH_3$), 2.62 (m, 2H, $GeCH_2C\boldsymbol{H_2}COOH$), 3.15 (m, 32H, $NC\boldsymbol{H_2}CH_2CH_2CH_3$).
^{31}P NMR (CD_3CN)	^{31}P NMR (121.49 MHz) δ ppm: -13.48
Chemical formula	$C_{67}H_{149}GeN_4PO_{41}W_{11}$
Exact mass	3792.85 g/mol
IR (KBr pellets)	IR (KBr pellets) ν cm^{-1}: 2963 (m), 2935 (m), 2875 (w), 1654 (w), 1485

[6] E. Radkov, R. H. Beer, High yield synthesis of mixed-metal keggin polyoxoanions in non-aqueous solvents: Preparation of $(n\text{-}Bu_4N)_4[PMW_{11}O_{40}]$ (M = V, Nb, Ta), *Polyhedron* **1995**, *14*, 2139-2143.

	(m), 1382 (w), 1099 (m), 1072 (s), 963 (s), 886 (s), 808 (s), 738 (sh), 519 (w), 389 (s)
Elemental analysis	Calcd. (%): C 21.22, H 3.96, Ge 1.91, N 1.48, P 0.82, W 53.32
	Found (%): C 21.14, H 3.67, Ge 1.46, N 1.67, P 0.96, W 52.45
Compound No.	**21**

5.1.22. Preparation of $(NBu_4)_4[PW_{11}O_{39}Ge(CH_2)_2C(O)NHCH_2C{\equiv}CH]$ (Compound **22**) (*See Appendix*)

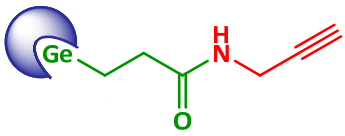

Triethylamine (81 µL, 0.630 mmol), isobutylchloroformiate (87 µL, 0.630 mmol), and after 25 min, propargylamine (72 µL, 1.050 mmol) were added successively to a solution of **21** (2 g, 0.530 mmol) in dry acetonitrile (20 mL). The solution was stirred overnight, filtered, and then evaporated to dryness. The residue was redissolved in acetone (10 mL) and compound **22** was precipitated by the addition of a mixture of diethyl ether and ethanol (10:1), filtered off, and dried in air (1.8 g, 89 %).

Appearance	White powder
^{1}H NMR (*CD_3CN*)	^{1}H NMR (300.13 MHz) δ ppm: 0.99 (t, 48H, $NCH_2CH_2CH_2C\boldsymbol{H_3}$), 1.41 (sextet, 32H, $NCH_2CH_2C\boldsymbol{H_2}CH_3$), 1.35 (m, 2H, $GeC\boldsymbol{H_2}CH_2C(O)NHCH_2C{\equiv}CH$), 1.65 (m, 32H, $NCH_2C\boldsymbol{H_2}CH_2CH_3$), 2.39 (t, 1H, $GeCH_2CH_2C(O)NHCH_2C{\equiv}C\boldsymbol{H}$), 2.48 (m, 2H, $GeCH_2C\boldsymbol{H_2}C(O)NHCH_2C{\equiv}CH$), 3.17 (m, 32H, $NC\boldsymbol{H_2}CH_2CH_2CH_3$), 3.92 (dd, 2H, $GeCH_2CH_2C(O)NHC\boldsymbol{H_2}C{\equiv}CH$), 6.84 (brt, 1H, $GeCH_2CH_2C(O)N\boldsymbol{H}CH_2C{\equiv}CH$).
^{31}P NMR (*CD_3CN*)	^{31}P NMR (121.49 MHz) δ ppm: -13.50
Chemical formula	$C_{70}H_{152}GeN_5PO_{40}W_{11}$
Exact mass	3829.91 g/mol
IR (KBr pellets)	IR (KBr pellets) ν cm^{-1}: 2963 (m), 2937 (m), 2875 (w), 1668 (w), 1485 (m), 1485 (m), 1382 (w), 1100 (m), 1072 (s), 963 (s), 886 (s), 807 (s), 518 (w), 506 (sh), 388 (s)

Elemental analysis	Calcd. (%): C 21.95, H 4.00, Ge 1.90, N 1.83, P 0.81, W 52.80
	Found (%): C 21.18, H 3.56, Ge 1.66, N 1.87, P 0.91, W 52.35
Compound No.	**22**

5.1.23. Preparation of $Cl_3Sn(CH_2)_2COOH$ (Compound **23**) (*Synthesize in Inorganic Chemistry and Molecular Materials laboratory, Paris 6*)

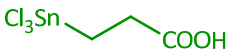

No. **23**

5.1.24. Preparation of $(NBu_4)_4[PW_{11}O_{39}\{SnCH_2CH_2COOH\}]$ [7] (Compound **24**)

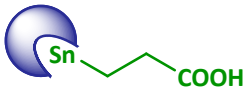

$Cl_3SnCH_2CH_2COOH$ (0.782 g, 2.625 mmol) was added at room temperature to a solution of NBu_4Br (3.22 g, 10 mmol) and α-$K_{7-x}Na_xPW_{11}O_{39}\cdot 14H_2O$ (**1**) (8.008 g, 2.5 mmol) in acetonitrile (250 mL). The reaction mixture was stirred at room temperature for the period of 5 hours. The remaining solid was filtered off and the clear filtrate was concentrated under vacuum in a rotavapory until a yellow oil remains. The yellow oil was then dissolved in minimum of acetone and precipitated (EtOH/Et_2O 1:10) to give the desired compound **24** (Yield: 8.1 g, 84 %).

Appearance	Yellow powder
^{1}H NMR (*CD_3CN*)	^{1}H NMR (400.13 MHz) δ ppm: 1.01 (t, 48H, $NCH_2CH_2CH_2C\boldsymbol{H_3}$), 1.36 (m, 2H, $SnC\boldsymbol{H_2}$) 1.42 (m, 32H, $NCH_2CH_2C\boldsymbol{H_2}CH_3$), 1.67 (m, 32H, $NCH_2C\boldsymbol{H_2}CH_2CH_3$), 2.66 (m, 2H, $SnCH_2C\boldsymbol{H_2}COOH$), 3.18 (m, 32H, $NC\boldsymbol{H_2}CH_2CH_2CH_3$)
^{31}P NMR (*CD_3CN*)	^{31}P NMR (161.97 MHz) δ ppm: -10.89
Chemical formula	$C_{67}H_{149}N_4PO_{41}W_{11}Sn$
Exact mass	3838.82 g/mol

[7] Cécile Boglio PhD Thesis

IR (KBr pellets)	IR (KBr pellets) ν cm^{-1}: 1731 (C=O), 1067 (P-O), 1030 (P-O), 962 (W=O), 887 (W-O-W), 809 (W-O-W)
Compound No.	**24**

5.1.25. Preparation of$(NBu_4)_4[PW_{11}O_{39}\{SnCH_2CH_2CONHCH_2C{\equiv}CH\}]$ [6] (Compound **25**)

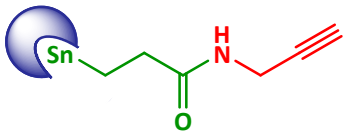

Triethylamine (34 µL, 0.248 mmol), isobutylchloroformiate (32 µL, 0.248 mmol), and, after 25 minutes, propargylamine (26 µl, 0.208 mmol) were added successively to a solution of **24** (800 mg, 0.104 mmol) in dry acetonitrile (10 mL). The solution was stirred overnight and then evaporated to dryness. The residue was dissolved in acetone (8 mL) and compound **25** was precipitated by the addition of a mixture of diethyl ether and ethanol (10:1), filtered off, and dried in air (Yield: 0.4 g, 52 %).

Appearance	Yellow powder
^{1}H NMR (CD_3CN)	^{1}H NMR (400.13 MHz) δ ppm: 1.01 (t, 48H, $NCH_2CH_2CH_2CH_3$), 1.38 (m, 2H, $SnCH_2$) 1.42 (m, 32H, $NCH_2CH_2CH_2CH_3$), 1.67 (m, 32H, $NCH_2CH_2CH_2CH_3$), 2.51 (t, 1H, C≡CH), 2.54 (m, 2H, $SnCH_2CH_2COOH$), 3.18 (m, 32H, $NCH_2CH_2CH_2CH_3$), 3.96 (dd, 2H, $NHCH_2C{\equiv}CH$), 6.88 (t, 1H, $CONHCH_2$)
^{31}P NMR (CD_3CN)	^{31}P NMR (161.97 MHz) δ ppm: -10.90
Chemical formula	$C_{70}H_{152}N_5PO_{40}W_{11}Sn$
Exact mass	3875.88 g/mol
IR (KBr pellets)	IR (KBr pellets) ν cm^{-1}: 3262 (≡C-H), 1668 (CONH), 1067 (P-O), 1029 (P-O), 962 (W=O), 886 (W-O-W), 810 (W-O-W)
Compound No.	**25**

5.1.26. Crystal data for $(NBu_4)_3[PW_9O_{34}(t\text{BuSiO})_3Ge(CH_2)_2CO_2H]\cdot H_2O$ (Compound **14**·H_2O)

Crystal data for $(NBu_4)_3[PW_9O_{34}(t\text{BuSiO})_3Ge(CH_2)_2CO_2H]\cdot H_2O$ (**14**·H_2O): $C_{63}H_{140}GeN_3PO_{39}Si_3W_9$; M = 3424.28; colorless crystals; trigonal; space group = $R3c$; $a = b$ = 22.284(4), c = 36.880(6) Å; $\alpha = \beta$ = 90, γ

= 120°; U = 15860(5) Å^3; Z = 6; T = 200(2) K; μ = 10.15 mm^{-1}; 23428 reflections measured, 7333 independent (R_{int} = 0.046), 5525 observed with I >= 2σ(I), 375 variables refined, final R indices R_1 [I >2σ(I)] = 0.0386 and wR_2 (all data) = 0.1161; GOF on F^2 = 1.21; max/min residual electron density = 2.819/-3.025 e Å^{-3}. Measurements were performed with a Bruker-Nonius Kappa-CDD diffractometer by using graphite-monochromated Mo_{Ka} radiation. Unit-cell parameter termination, data collection strategy, and integration were carried out with the Nonius EVAL-14 suite of programs. The data were corrected from absorption by a multiscan method. The structure was solved by direct method by using the SHELXS-97 program and refined anisotropically by full-matrix least-squares on F^3 by using the SHELXL-97 software package. Graphics were carried out by using DIAMOND. All non-H atoms, except those of the pending $CH_2CH_2CO_2H$ on the anion, were refined anisotropically. Hydrogen atoms of the cation were introduced at calculated positions and refined isotropically. $CH_2CH_2CO_2H$ is disordered due to the three-fold axis: its geometry was restrained and isotropic displacement parameters of the oxygen atoms were fixed at 0.18, slightly above that of the carbon atom to which they are attached (0.17). The three terminal methyl groups of the *t*Bu group are also disordered over two equally occupied positions. The displacement parameters of related carbon atoms have consequently been fixed to be equal. The crystallographic data can be obtained free of charge from The Cambridge Crystallographic Data Centre *via* www.ccdc.cam.ac.uk/data_request/cif.

Empirical formula	$C_{63}H_{142}GeN_3O_{40}Psi_3W_9$	
Formula weight	3424.28	
Temperature	200(2) K	
Wavelength	0.71073 Å	
Crystal system	Trigonal	
Space group	R3c	
Unit cell dimensions	a = 22.284(4) Å	α = 90°
	b = 22.284(4) Å	β = 90°
	c = 36.880(6) Å	γ = 120°
Volume	15860(5) Å^3	
Z	6	
ρ_{cacd}	2.151 Mg/m^3	
Absorption coefficient	10.150 mm^{-1}	
F(000)	9696	

Crystal size	0.35 x 0.14 x 0.14 mm^3
θ range	2.47 to 30.01° .
Index ranges	−31<=h<=28, −22<=k<=22, −28<=l<=51
Reflections collected	23428
Independent reflections	7333 [R(int) = 0.0462]
Completeness to theta = 30.01°	98.4 %
Absorption correction	Semi−empirical from equivalents
Max. and min. transmission	0.241 and 0.121
Refinement method	Full−matrix least−squares on F^2
Data / restraints / parameters	7333 / 29 / 375
GOF on F^2	1.214
Final R indices [I>2sigma(I)]	R_1 = 0.0386, wR_2 = 0.0867
R indices (all data)	R_1 = 0.0867, wR_2 = 0.1161
Absolute structure parameter	0.08(2)
Largest diff. peak and hole	2.819 and −3.025 e $Å^{-3}$

5.2. POLYOXOMETALATES MODIFIED ELECTRODE PREPARATION

Chemicals and Solvents

Unless otherwise noted, all the chemical compounds and reagents were purchased from Aldrich. Sulphuric acid (H_2SO_4, 98%), hydrogen peroxide (H_2O_2, 30% vol), 4-vinylbenzyl chloride (90%), sodium azide (NaN_3), copper (II) sulfate pentahydrate ($CuSO_4 \cdot 5H_2O$, 99.995%), triethyamine (99.5%), 3-aminopropyltriethoxysilane (99%), isobutyl chloroformiate (98%) were used as received. Hydrofluoric acid (HF, 1%), toluene, water, N,N-dimethylformamide (DMF, anhydrous, 99.8%), acetonitrile were deoxygenated using argon. Acetonitrile (Purex Analytical Grade) was distilled over CaH_2 under argon just before used. Dichloromethane, acetone, ethanol were used as received.

ATR-FTIR Spectroscopy

The ATR set up consist of a germanium prism pressed against the silicon sample as shown in **Figure 1**. A pressure tip mounted on a micrometric screw allows a tight contact between the prism and the wafer. This enable a reproducibility better than +/- 10%. A P polarized IR beam coming from a Bruker

IFS55 FTIR spectrometer is directed onto the prism base with an angle of 65° which ensures a total reflection on the germanium prism dioptre. After one reflection on the prism base, the IR light is focused onto a liquid N_2 cooled HgCdTe detector. The sensitivity of ATR measurement is due to the enhancement of the E_{pz} electric field component, orthogonal to the sample surface. The E_{pz} component can be increased by a factor 50 under total reflection in the air gap which is present between the germanium prism and the polarization that is not sensitive enough to detect such thin layers. Moreover, theoretical development shows that P polarization ATR spectra gives an image of the energy loss function $\varepsilon_f''/ |\varepsilon_f|^2$ of the absorbing thin film on silicon substrate. Sample spectrum is referenced to the spectrum obtain when no sample is coupled to the prism. Infrared data are acquired between 600 and 4500 cm^{-1}, but ATR lost its sensitivity with increasing wavenumber due to the penetration depth decrease. So ATR spectra are exploited between 600 and 2000 cm^{-1}.[8]

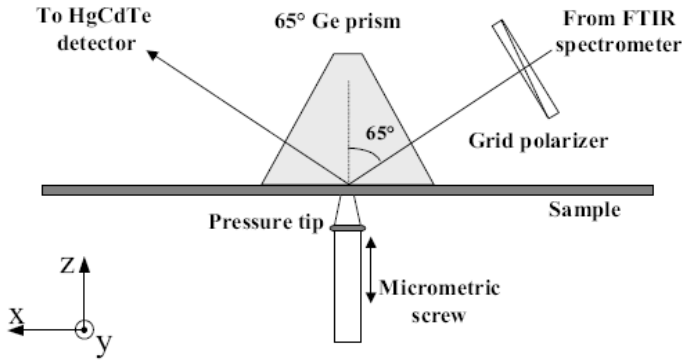

Figure 1. Schematic representation of ATR set up.[8]

Electrochemical Measurements

Electrochemical measurements were performed under an argon atmosphere on devices connected to an Autolab PGSTAT100 potentiostat (from Eco Chemie BV) equipped with general-purpose electrochemical system software, in a standard three-electrode cell.

X-Ray Photoelectron Spectroscopy

The XPS measurements were performed on a S-Probe spectrometer from SSI using a monochromatic Al Kα X-ray source (1486.6 eV photons) at a constant dwell time of 100 ms and pass energy of 50 eV.

[8] N. Rochat, K. Dabertrand, V. Cosnier, S. Zoll, P. Besson, U. Weber, Infrared spectroscopy of high k thin layer by multiple internal refletion and attenuated total reflection, *Phys. Stat. Sol.* **2003**, *8*, 2961-2965.

The core-level signals were obtained at a photoelectron takeoff angle (θ, measured with respect to the sample surface) of 35°. The pressure in the analysis chamber was maintained at 10^{-9} Torr or lower during each measurement. All binding energies (BE's) were referenced to the Au 4f peak at 84 eV. No charging effect was observed as checked on the C 1s hydrocarbon peak at 284.6 eV. Photoelectrons were detected using a hemispherical analyzer, with an angular acceptance of 30° and an energy resolution of 850 meV.

General Procedures

General Procedure I for Si Surface Preparation (*Vide Supra*)

General Procedure II for Si Surface Preparation (*Vide Supra*)

GP V: General procedure for the preparation of Si-AX substrates (X = compound number)

The Si-H (0.75 cm^2 exposing 0.55 cm^2 area) terminated surface was prepared following **GPII**. Neat reactant (just enough compound X was added to cover the silicon wafer) was placed in a stoppered tube under argon with a Si-H terminated Si(100) wafer, heated above 180 °C and allowed to react at this temperature for 2 hours. After functionalization, all samples were subjected to the same cleaning procedure, consisting of several washes with copious amounts of CH_3CN, followed by four sonication cycles, 5 minutes each, in CH_3CN and dried in a stream of argon.

GP VI: General procedure for the preparation of Si-CX substrates (X = compound number)

The **Si-amino** (0.75 cm^2 exposing 0.55 cm^2 area) substrate was plunged in 10 mL anhydrous degassed acetonitrile solution which contains the carboxylic derivative (0.0132 mmol), triethylamine (0.0157 mmol, 2.2 µL) and isobutyl chloroformiate (0.0264 mmol, 3.5 µL). The resulting solution was stirred overnight at room temperature under argon. Afterward, the Si-CX substrate was removed from the acetonitrile solution, washed with CH_3CN, sonicated 3 times (× 3 min) in CH_3CN and then dried under a flow of argon. Subsequently, the resulting POM-modified silicon wafers were investigated by means of cyclic voltammetry.

GP VII: General procedure for the preparation of Si-DX substrates (X = compound number)

The "click" chemistry reaction was performed after an adapted procedure already reported in the literature. [9] To the reaction vial containing the **Si-azide** (0.75 cm^2 exposing 0.55 cm^2 area) substrates were added the alkyne derivative (0.04 mmol) in 5 mL degassed acetonitrile freshly distilled. A solution of $CuSO_4 \cdot 5H_2O$ (0.04 mmol, 1 equiv., 10 mg) in water (1 mL) and a solution of sodium ascorbate (1.6 mmol, 40 equiv., 316 mg) in water (1 mL) were then added. The mixture was stirred at room temperature for 24 hours. The **Si-DX** substrates were removed from the flask washed with plenty of CH_3CN and sonicated 3 times ($\times$ 3 min) in CH_3CN and then dried under a flow of argon. Subsequently, the resulting POM-modified silicon wafers were investigated by means of cyclic voltammetry.

GP VIII: General procedure for the CG electrode cleaning

The working electrode (GC, A = 0.07 cm^2) was polished successively with 1.0, 0.3 and 0.05 µm alumina powder. The electrode was rinsed with ethanol between each polishing step and sonicated 5 min in ethanol.

5.2.1. HYDROSILYLATION PROCESS (Method A)

5.2.1.1. Preparation of substrates Si-AX *via* method A

Substrates **Si-A5** – **Si-A7**, **Si-A10**, **Si-A11**, **Si-A15**, **Si-A22**, and **Si-A25** were prepared according to the **GP V**.

5.2.2. MULTI-STEPS GRAFTING PROCEDURES

5.2.2.1. Hydrosilylation (Method B)

5.2.2.1.1. Preparation of 4-vinylphenyldiazonium tetrafluoroborate (Compound **27**)

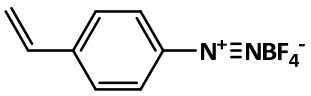

The synthesis was carried out after a similar procedure reported in literature. [10] 4-Aminoaniline (100 mg, 0.839 mmol) was weight into a three-necked 50 mL round-bottom flask; then 5 mL of 50 %

[9] K. Micoine, B. Hasenknopf, S. Thorimbert, E. Lacôte, M. Malacria, A General Strategy for Ligation of Organic and Biological Molecules to Dawson and Keggin Polyoxotungstates, *Org. Lett.* **2007**, *9*, 3981-3984.
[10] A.O. Solak, L.R. Eichorst, W.J. Clark, R.L. McCreery, Modified Carbon Surfaces as "Organic Electrodes" That Exhibit Conductance Switching, *Anal. Chem.* **2003**, *75*, 296-305.

fluoroboric acid was added and the resultant mixture stirred with a magnetic stirring bar. A 3:1 molar ratio of $NaNO_2$ (relative to the amino precursor) (147 mg, 2.517 mmol) was weighed into a separate container, just enough water was added to dissolve the $NaNO_2$ at room temperature, and the solution was cooled to 0 °C. A thermometer was inserted in the three-necked flask, and the precursor solution was cooled to 0 °C in the ice bath. The cold $NaNO_2$ solution was added dropwise, and the temperature was always kept below 4 °C during the reaction. Following the complete addition of $NaNO_2$, the mixture was stirred ~30 min in the ice bath. The insoluble diazonium salt was filtered in a Buchner funnel, and anhydrous ether was used to remove the remaining sediments from the round-bottom flask. The product was recrystallized by dissolving in cold (0 °C) acetonitrile followed by slow addition of cold anhydrous ether to recover compound **27**.

Appearance	Dark brown product
Chemical formula	$C_8H_7N_2BF_4$
Exact mass	217.96 g/mol
Compound No.	**27**

5.2.2.1.2. Preparation of substrate Si-B27

The substrate **Si-B27** preparation was carried out after a similar procedure reported in literature. [11] The Si-H terminated surface (0.75 cm^2 exposing 0.55 cm^2 area) was prepared following **GP II**. The grafting process was carried out by exposing the freshly etched Si-H wafers to a 0.5 mM solution of the diazonium salt **27** in anhydrous acetonitrile under inert atmosphere for 5 hours. After the molecular grafting, the **Si-B27** substrates were rinsed thoroughly with CH_3CN to remove the residual diazonium salt and the physisorbed materials, and then dried with an argon flow.

5.2.2.1.3. Preparation of substrate Si-B4

Substrate **Si-B27** was immersed in a 60 mM DMF solution of compound **4**, heated at 130 °C for 2 hours to afford substrate **Si-B4**. After the completion of the hydrosilylation reaction, the **Si-B4**

[11] T. He, J. He, M. Lu, B. Chen, H. Pang, W.F. Reus, W.M. Nolte, D.P. Nackashi, P.D. Franzon, J.M. Tour, Controlled Modulation of Conductance in Silicon Devices by Molecular Monolayers, *J. Am. Chem. Soc.* **2006**, *128*, 14537-14541.

substrate was washed in DMF, sonicated four times (× 5 min) in acetonitrile and dried under a flow of argon.

5.2.2.2. Peptidic bond formation *via* silanization (Method C)

5.2.2.2.1. Preparation of substrate Si-OH

The Si-H terminated surface (0.75 cm^2 exposing 0.55 cm^2 area) was prepared following **GP II**. The silicon wafers were plunged in a 0.1 N "Brown" solution (140 mg NaOH, 20 mL EtOH, 15 mL EDI water), ultrasonicated for 30 min, washed with plenty amounts of EDI water and then dried under a flow of argon to afford the **Si-OH** substrates.

5.2.2.2.2. Preparation of substrate Si-amino

To afford the **Si-amino** substrates, the **Si-OH** (0.75 cm^2 exposing 0.55 cm^2 area) wafers were reacted with a 5 mM toluene solution of 3-aminopropyl-triethoxysilane and 0.2 M triethylamine for 16 h at 80 °C under argon. Subsequently, the **Si-amino** substrates were withdrawn from the solution and washed with toluene. After further 3 sonication cycles in CH_3CN for 3 min each, the **Si-amino** substrates were dried under a stream of argon.

5.2.2.2.3. Preparation of substrate Si-C14

The **Si-C14** sample was prepared following the **GP VI**, upon addition of 45 mg of carboxylic derivative **14**.

5.2.2.2.4. Preparation of substrate Si-C21

The **Si-C21** sample was prepared following the **GP VI**, upon addition of 50 mg of carboxylic derivative **21**.

5.2.2.3. "Click" chemistry (Method D)

5.2.2.3.1. Preparation of substrate Si-chloro

The freshly prepared Si-H surface (0.75 cm^2 exposing 0.55 cm^2 area) (**GP II**) was introduced in a 0.8 M mesitylene solution of 4-vinylbenzyl chloride in a three-necked flask that was degassed previously with argon. The mixture was refluxed for 2 hours under argon. The **Si-chloro** substrate was separated from the flask and sonicated in dichloromethane three times (× 3 min) to remove the residual physisorbed compounds.

5.2.2.3.2. Preparation of substrate Si-azide

The **Si-chloro** substrate was introduced in a three-necked flask containing a saturated solution of NaN_3 in DMF previously degassed with argon. This assembly was heated at 80 °C for 18 h under argon atmosphere. The **Si-azide** substrate was separated from the flask and sonicated successively in water, acetone, and dichloromethane to remove the residual compounds.

5.2.2.3.3. Preparation of substrate Si-D15

The **Si-D15** sample was prepared following the **GP VII**, upon addition of 137 mg of ethynyl derivative **15**.

5.2.2.3.4. Preparation of substrate Si-D22

The **Si-D22** sample was prepared following the **GP VII**, upon addition of 153 mg of ethynyl derivative **22**.

5.2.3. ELECTROCHEMICAL METHODS

5.2.3.1. Terminal ethynyl (C≡C) as reactant (Method E)

5.2.3.1.1. Preparation of substrate Si-E15

The electrografting procedure on the surface-activated samples were carried out in a N_2(g)-purged dry-box (Plas Labs). The working electrode was a hydrogenated n-Si wafer with an area of 0.75 cm^2, exposing a 0.45 cm^2 area (for both sides a total area of 0.9 cm^2), in a solution of the reactant (compound **15**, 0.1 mM) and the supporting electrolyte (Bu_4NBF_4, 0.1 M) in CH_3CN with a platinum reference electrode and a platinum counter electrode. The electrografting preparation route was carried out at a constant anodic-current density of 4.5 $mA \cdot cm^{-2}$ for 1000 seconds, in the three electrodes electrochemical cell, placed inside the dry-box.

For the electrochemical characterization of the substrate **Si-E15**, a solution of Bu_4NBF_4 in acetonitrile (0.1 M) was used as supporting electrolyte, with a platinum reference electrode, a platinum counter electrode, and the functionalized silicon surface as the working electrode with an active area of 0.4 cm^2. All electrochemical measurements were carried out at room temperature under an inert atmosphere.

5.2.3.2. Diazonium chemistry (Method F)

5.2.3.2.1. Preparation of substrate GC-FE17

The clean glassy carbon electrode (A = 0.07 cm^2) was plunged in an acetonitrile solution containing 10^{-3} M of **17** and 1 eq. HBF_4 dissolved in acetonitrile (0.1 M Bu_4NBF4). Upon HBF_4 addition the solution, initially yellow-pale, becomes orange almost instantaneously indicative of the diazonium salt formation. A voltage of -1.7 V *vs* Pt wire was then applied for 30, 60 and 120 seconds, respectively. Following the completion of the reaction, the POMs-modified electrode **GC-FE17** was rinsed with copious amounts of acetonitrile, ultrasonicated in acetonitrile 3 minutes (× 3), to remove the physisorbed species and dried under a flow of argon. The **GC-FE17** substrate was characterized by cycling voltammetry by using a solution of 10^{-1} M Bu_4NBF_4 in acetonitrile and 1.0 M Bu_4NPF_6 in propylene carbonate.

5.2.3.2.2. Preparation of substrate Si-FE17

Into an argon-atmosphere glovebox, the Si-H surface (0.60 cm^2 exposing 0.36 cm^2 area) (**GP I**) was freshly prepared. The grafting was carried out by chronoamperometry into an argon-atmosphere glovebox. The freshly prepared *n*-type silicon electrode was plunged in a solution containing 10^{-3} M of **17** and 1 eq. HBF_4 dissolved in acetonitrile (0.1 M Bu_4NBF4). In the presence of an externally applied cathodic potential of -1.7 V and for various time periods substrate **Si-FE17** was formed. Consequently, **Si-FE17** was washed with plenty of acetonitrile and ultrasonicated in acetonitrile three times (× 3 minutes) to ensure that are not physisorbed species at the surface. Than, the substrates were dried under argon and investigated by means of cyclic voltammetry in acetonitrile (10^{-1} M Bu_4NBF_4) or propylene carbonate (1.0 M Bu_4NPF_6) solution.

5.2.3.2.3. Preparation of substrate GC-FS17

The freshly clean glassy carbon electrode (A = 0.07 cm^2) was brought into an argon-atmosphere glovebox. Inside the glovebox an acetonitrile solution of **17** (10^{-3} M) and 1 eq. HBF_4 was prepared, providing enough volume to cover the electrode inside a reaction container. The glassy carbon electrode was then immersed in the acetonitrile solution, sealed to prevent evaporation, and kept for various reaction times. After the reaction, the **GC-FS17** modified electrode was brought out of the glovebox, rinsed with CH_3CN, sonicated three times (× 3 min) in acetonitrile, dried with a stream of argon and investigated by means of cyclic voltammetry.

5.2.3.2.4. Preparation of substrate Si-FS17

Into an argon-atmosphere glovebox, the Si-H surface (0.60 cm^2 exposing 0.36 cm^2 area) (**GP I**) was freshly prepared. Inside the glovebox an acetonitrile solution of **17** (10^{-3} M) and 1 eq. HBF_4 was prepared, providing enough volume to cover the entire sample inside a reaction container. The substrates were then immersed in the acetonitrile solution, sealed to prevent evaporation, and kept for various reaction times. After the reaction, the substrates were brought out of the glovebox, rinsed with CH_3CN, sonicated three times ($\times$ 3 min) in acetonitrile, dried with a stream of argon and investigated by means of cyclic voltammetry.

5.2.3.3. Immobilization into conducting polymers (Method G)

5.2.3.3.1. Preparation of substrate GC-Py in acetonitrile

The **GC-Py** substrate was formed at controlled potential of +0.9 V on a freshly clean glassy carbon electrode (A = 0.07 cm^2) (**GP VIII**) by passing 2 mC of charge through a one-compartment electrochemical cell. A platinum and an Ag/10^{-2} M Ag^+ counter and reference electrode, respectively, were used for this procedure. The solution used for the preparation of the film contains 10^{-3} M of pyrrole monomer with 10^{-1} M of tungstosilicic acid hydrate $H_4SiW_{12}O_{40}{\cdot}xH_2O$ as electrolyte, in acetonitrile. The acetonitrile was used directly without further purification and the solution was degassed previously with argon. Once grown, the film was thoroughly rinsed with acetonitrile and transferred to an acetonitrile solution containing 10^{-1} M CF_3LiO_3S or a water solution with $2{\cdot}10^{-1}$ M Na_2SO_4 as electrolyte.

5.2.3.3.2. Preparation of substrate GC-Py in water

Formation of doped polypyrrole film in water was based on a previous method described by McCormac *et al*. SiW_{12} doped conducting films were electrochemically grown by potentiostatic method from a solution containing 10^{-1} M pyrrole monomer and $5{\cdot}10^{-3}$ M SiW_{12}. The electropolymerization procedure took place at a constant potential of +0.65 V until 5 mC of charge had been passed. Once the polymer film was grown, the **GC-Py** substrate (A = 0.07 cm^2) was removed from the solution and washed in the buffer solution pH 4 that the film was going to be electrochemically investigated in. A platinum counter electrode and an Ag/10^{-2} M Ag^+ reference electrode were used for this experiment.

5.2.3.3.3. Preparation of substrate Pt-Py in acetonitrile

The working electrode was a Si wafer, covered with a platinum layer (0.60 cm^2 exposing 0.36 cm^2 area). The **Pt-Py** substrate was formed at controlled potential of +0.9 V on the working electrode (exposing area aprox. 0.4 cm^2) with a platinum counter electrode and an $Ag/10^{-2}$ M Ag^+ reference electrode. The solution used for the preparation of the film contains 10^{-3} M of pyrrole monomer with 10^{-1} M of tungstosilicic acid hydrate $H_4SiW_{12}O_{40}{\cdot}xH_2O$ as electrolyte, in acetonitrile. The acetonitrile was used directly without further purification and the solution was degassed previously with argon. Once grown, the film was thoroughly rinsed with acetonitrile and transferred to an acetonitrile solution containing 10^{-1} M CF_3LiO_3S or a water solution with $2{\cdot}10^{-1}$ M Na_2SO_4 as electrolyte.

5.2.3.3.4. Preparation of substrate Pt-Py in water

The working electrode was a Si wafer, covered with a platinum layer (0.60 cm^2 exposing 0.36 cm^2 area). The **Pt-Py** substrate was formed at controlled potential of +0.9 V on the working electrode (exposing area aprox. 0.4 cm^2). Formation of doped polypyrrole film in water was based on a previous method described by McCormac *et al*. SiW_{12} doped conducting films were electrochemically grown by potentiostatic method from a solution containing 10^{-1} M pyrrole monomer and $5{\cdot}10^{-3}$ M SiW_{12}. Once the polymer film was grown, the **Pt-Py** substrate was removed from the solution and washed in $5{\cdot}10^{-3}$ Na_2SO_4 water solution that the film was going to be electrochemically investigated in.

5.2.3.3.5. Preparation of N-allylpyrrole [12] (Compound **26**)

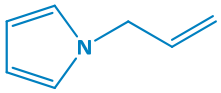

Dry DMSO (120 mL) was added to potassium hydroxide (13.2 g, 235 mmol) and the mixture was stirred for 5 min. Pyrrole (4.0 mL, 58 mmol) was then added and the mixture was stirred for 45 min. 3-Bromo-1-propene (6.5 mL, 75 mmol) was added and the mixture was stirred for a further 30 min before water (250 mL) was added. The mixture was extracted with ether and each extract was washed with water. The combined ether layers were dried (Na_2SO_4) and the solvent and the excess of 3-bromo-1-propene were removed by distillation at atmospheric pressure. The residue was distilled giving compound **26** as a colorless liquid.

Appearance	Colorless liquid

[12] R. Lazzaroni, R. Settambolo, A. Caiazzo, L. Pontorno, Rhodium-catalyzed hydroformylation of 1-allypyrrole as an unexpected way to 5,6-dihydroindolizine synthesis, *J. Organomet. Chem.* **2000**, *601*, 320-323.

^{1}H NMR (*CD_3CN*)	^{1}H NMR (200.13 MHz) δ ppm: 4.52 (m, 2H, NC***H_2***CH=CH_2), 5.18 (m, 2H, NCH_2CH=C***H_2***), 6.03 (m, 1H, NCH_2CH=CH_2), 6.10 (t, 2H), 6.70 (t, 2H)
Chemical formula	C_7H_9N
Exact mass	107.15 g/mol
Compound No.	**26**

5.2.3.3.6. Preparation of substrate Si-G26 [13]

Alkylation reactions were performed at reflux under argon in 0.02 M toluene solution of the compound **26** for 2 hours under argon atmosphere. Alkenyl-pyrrole reactions were protected from light by wrapping the reaction vessel in aluminium foil. After the completion of reaction the **Si-G26** (0.75 cm^2 exposing 0.45 cm^2 area) substrate was removed from the reaction vessel, washed with plenty of toluene, sonicated in CH_3CN three times (×3 min) and dried under a flow of argon.

5.2.3.3.7. Preparation of substrate Si-G26-Py in acetonitrile

The **Si-G26-Py** substrate (0.75 cm^2 exposing 0.45 cm^2 area) was formed at controlled potential of +1.05 V on a freshly prepared **Si-G26** substrate by passing 12 mC of charge through a one-compartment electrochemical cell. A platinum and an Ag/10^{-2} M Ag^+ counter and reference electrode, respectively, were used for this procedure. The solution used for the preparation of the film contains 10^{-3} M of pyrrole monomer with 10^{-1} M of tungstosilicic acid hydrate $H_4SiW_{12}O_{40}{\cdot}xH_2O$ as electrolyte, in acetonitrile. The acetonitrile was used directly without further purification and the solution was degassed previously with argon. Once grown, the film was thoroughly rinsed with acetonitrile and transferred to an acetonitrile solution containing 10^{-1} M CF_3LiO_3S to perform the cyclic voltammetry.

5.3. POLYOXOMETALATES MODIFIED CAPACITORS

Electrical measurements

The capacitance-voltage (*C*-*V*) and conductance-voltage (*G*-*V*) properties of the compound **17** modified silicon capacitors were investigated with an HP Agilent 4284A instrument in a nitrogen

[13] A.R. Pike, S.N. Patole, N.C. Murray, T. Ilyas, B.A. Connolly, B.R. Horrocks, A. Houlton, Covalent and Non-covalent Attachment and Patterning, of Polypyrrole at Silicon Surfaces, *Adv. Mater.* **2003**, *15*, 254-257.

atmosphere. Propylene carbonate (1.0 M Bu_4NPF_6) was used as a conducting gate with a silver electrode for contacting the molecular layer. The gate voltage was applied to the silver electrode.

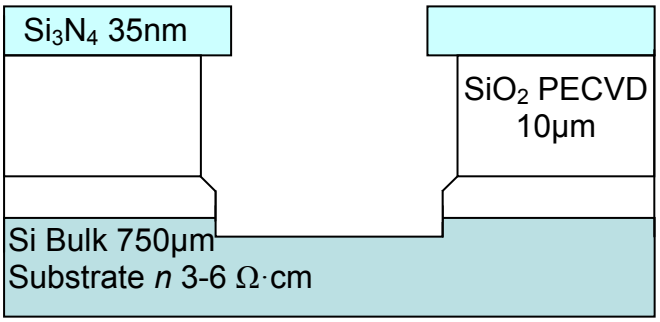

Figure 2. Schematic representation of a silicon capacitor used in this work. (PECVD – Plasma-Enhanced Chemical Vapor Deposition)

5.3.1. Preparation of substrate EMS-17

The EMS substrate freshly prepared, inside of an argon-atmosphere glovebox, following the **GPII**. The EMS electrode was immersed in an acetonitrile solution containing 10^{-3} M of **17** and 1 eq. HBF_4 dissolved in acetonitrile (0.1 M Bu_4NBF4). A voltage of -1.7 V vs Pt wire was then applied for 60 seconds. Following the completion of the reaction, the POMs-modified electrode **EMS-17** was rinsed with copious amounts of acetonitrile, ultrasonicated in acetonitrile 3 minutes ($\times$ 3), to remove the physisorbed species and dried under a flow of argon. The **EMS-17** substrate was characterized by capacitance-voltage (*C*-*V*) and conductance-voltage (*G*-*V*) by using a solution of 1.0 M Bu_4NPF_6 in propylene carbonate.

Appendix

DOI: 10.1002/chem.200903336

VIP

Organosilyl/-germyl Polyoxotungstate Hybrids for Covalent Grafting onto Silicon Surfaces: Towards Molecular Memories

Nicoleta Joo,[a] Séverine Renaudineau,[b] Guillaume Delapierre,[a] Gérard Bidan,*[c] Lise-Marie Chamoreau,[b] René Thouvenot,*[b] Pierre Gouzerh,[b] and Anna Proust*[b, d]

Abstract: Organosilyl/-germyl polyoxotungstate hybrids $[PW_9O_{34}(t\text{BuSiO})_3Ge(CH_2)_2CO_2H]^{3-}$ (**1a**), $[PW_9O_{34}(t\text{BuSiO})_3Ge(CH_2)_2CONHCH_2C{\equiv}CH]^{3-}$ (**2a**), $[PW_{11}O_{39}Ge(CH_2)_2CO_2H]^{4-}$ (**3a**), and $[PW_{11}O_{39}Ge(CH_2)_2CONHCH_2C{\equiv}CH]^{4-}$ (**4a**) have been prepared as tetrabutylammonium salts and characterized in solution by multinuclear NMR spectroscopy. The crystal structure of $(NBu_4)_3$**1a**$\cdot H_2O$ has been determined and the electrochemical behavior of **1a** and **2a** has been investigated by cyclic voltammetry. Covalent grafting of **2a** onto an n-type silicon wafer has been achieved and the electrochemical behavior of the grafted clusters has been investigated. This represents the first example of covalent grafting of Keggin-type clusters onto a Si surface and a step towards the realization of POM-based multilevel memory devices.

Keywords: molecular memories · NMR spectroscopy · organic–inorganic hybrid composites · polyoxometalates · silicon · surface chemistry

Introduction

Polyoxometalates (POMs) are molecular nanosized transition-metal oxide clusters with a large variety of structures, properties, and applications in fundamental and applied science.[1] One of their most significant properties is the ability of type-I POMs according to Pope classification[2] to accept and release specific numbers of electrons with minimal structural change,[1–4] which makes them attractive candidates for the catalysis of redox reactions.[4–7] As soluble analogues of transition-metal oxides, POMs are also promising components for the design of advanced materials and functional devices.[8–9] Indeed POM-based hybrid materials have the potential for applications in sensors,[10–12] electro- and photochromic devices,[13,14] fuel cells,[15] photovoltaic cells,[16] energy storage,[17] and molecular electronics.[18] An attractive perspective is the realization of multilevel molecular memories based on semiconducting nanowire field effect transistors[19] or hybrid molecular-silicon capacitors[20] by using POMs as redox-active components.[21] The feasibility of such a project is supported by recent results from the groups of Glezos[18a,22] and Tour[23] on electron transport or charge confinement in POM-based molecular devices.

Applications of POMs usually require their immobilization onto an appropriate support or into an appropriate matrix. With regard to attachment of POMs onto electrodes, various methods can be used, for example, 1) spontaneous adsorption on electrode surfaces,[5,24,25] 2) electrodeposition under constant potential,[5] 3) entrapment in polymeric matrices,[25–30] and 4) layer-by-layer self-assembly of alternating layers of POMs and positively charged species.[7,31] The latter technique is especially attractive as it provides control of the structure of POM-based films at the nanometer scale. While most POM-based hybrid materials reported to date involve noncovalent interactions, for example, van der Waals contacts, hydrogen bonding, and ionic interactions, a few hybrid polymers involve covalent linking.[16,30a,32–35] Covalent grafting of POMs on surfaces is even more rare (vide

[a] N. Joo, Dr. G. Delapierre
CEA-LETI-DTBS Minatec, 17 rue des Martyrs
38054 Grenoble Cedex 9 (France)

[b] S. Renaudineau, L.-M. Chamoreau, Dr. R. Thouvenot, Prof. Dr. P. Gouzerh, Prof. Dr. A. Proust
Institut Parisien de Chimie Moléculaire
UMR CNRS 7201, UPMC Univ Paris 06
4 Place Jussieu, Case courrier 42
75252 Paris Cedex 05 (France)
Fax: (+33) 144273841
E-mail: anna.proust@upmc.fr

[c] Dr. G. Bidan
INAC/DIR CEA-Grenoble, 17 rue des Martyrs
38054 Grenoble Cedex 9 (France)
Fax: (+33) 4 38785691
E-mail: gerard.bidan@cea.fr

[d] Prof. Dr. A. Proust
Institut Universitaire de France

Supporting information for this article is available on the WWW under http://dx.doi.org/10.1002/chem.200903336.

infra). Yet, covalent grafting offers advantages in terms of stability and structure control, and it is the approach we have chosen.

Choice of POM and that of grafting protocol are both central to the implementation of POM-based memories. The functionalization of Lindqvist-type POMs is still the most documented among the different families of POMs.[8] Thus bromo- and iodo-arylimido derivatives of $[Mo_6O_{19}]^{2-}$[36a] can be further derivatized by palladium-catalyzed Sonogashira[36b] or Heck[37] coupling reactions and a diazonium salt of a hybrid prepared in this way has been grafted onto silicon surfaces.[23,38] Another example is the covalent immobilization of a {TiW_5}-POM through alcoholysis of the Ti–OMe bond in $[MeOTiW_5O_{18}]^{3-}$ with alkanol-derivatized silicon surfaces.[39] Also surface micropatterning by a functionalized Anderson-type POM was very recently reported.[40]

Since redox properties of Keggin-type POMs are more tunable than those of Lindqvist-type species, we chose to functionalize Keggin-type POMs for covalent grafting on silicon surfaces. We thus report here the synthesis and characterization of $(NBu_4)_3[PW_9O_{34}(t\text{BuSiO})_3Ge(CH_2)_2CO_2H] \equiv (NBu_4)_3$**1a** (**1**), $(NBu_4)_3[PW_9O_{34}(t\text{BuSiO})_3Ge(CH_2)_2CONHCH_2C{\equiv}CH] \equiv (NBu_4)_3$**2a** (**2**), $(NBu_4)_4[PW_{11}O_{39}Ge(CH_2)_2CO_2H] \equiv (NBu_4)_4$**3a** (**3**), and $(NBu_4)_4[PW_{11}O_{39}Ge(CH_2)_2CONHCH_2C{\equiv}CH] \equiv (NBu_4)_4$**4a** (**4**), as well as preliminary results on their electrochemical behavior in solution and after grafting onto silicon surfaces. To our knowledge, no example of covalent grafting of Keggin-type POMs onto electrodes had been previously reported.

Results and Discussion

Synthesis: Direct functionalization of complete Keggin-type POMs is difficult, unlike their Lindqvist counterparts.[41] However lacunary species allow convenient synthesis of various functionalized Keggin-type POMs. In particular, lacunary Keggin-type polyoxotungstates react with organosilanes, -germanes, and -stannanes to afford a variety of hybrids containing one or several functional groups.[8] As we were primarily interested in compounds containing a single functional group, we chose to start from mono- and trivacant heteropolyoxotungstates. Whereas most trichlorosilanes react with $Na_8H[\beta\text{-A-}PW_9O_{34}]\cdot 24H_2O$ under phase-transfer conditions to give compounds of the type $(NBu_4)_3[\alpha\text{-A-}PW_9O_{34}(RSiO)_3(RSi)]$, the corresponding reaction with *t*BuSiCl$_3$ yields $(NBu_4)_3[\alpha\text{-A-}PW_9O_{34}(t\text{BuSiOH})_3]$, which then reacts cleanly with RECl$_3$ (E = Si, Ge) to give $(NBu_4)_3[\alpha\text{-A-}PW_9O_{34}(t\text{BuSiO})_3(RE)]$, in which R may be a reactive function.[42] Compound **1**, $(NBu_4)_3[PW_9O_{34}(t\text{BuSiO})_3Ge(CH_2)_2CO_2H]$, has been obtained by using this two-step procedure and subsequent coupling with propargylamine afforded $(NBu_4)_3[PW_9O_{34}(t\text{BuSiO})_3Ge(CH_2)_2CONHCH_2C{\equiv}CH]$ (**2**). Whereas trichlorosilanes react with monovacant POMs $[\alpha\text{-}XW_{11}O_{39}]^{n-}$ to yield disubstituted hybrid anions of the type $[\alpha\text{-}XW_{11}O_{39}\{O(SiR)_2\}]^{(n-4)-}$,[8] the corresponding reactions with trichloro-germanes/stannanes give monosubstituted derivatives of the type $[\alpha\text{-}XW_{11}O_{39}(ER)]^{(n-3)-}$ (E = Ge,[43,44] Sn[43]). We focused on organogermyl derivatives and prepared $(NBu_4)_4[PW_{11}O_{39}Ge(CH_2)_2CO_2H]$ (**3**) by reaction of $(NBu_4)_4[H_3PW_{11}O_{39}]$ with $Cl_3Ge(CH_2)_2CO_2H$ in homogeneous conditions, and then $(NBu_4)_4[PW_{11}O_{39}Ge(CH_2)_2CONHCH_2C{\equiv}CH]$ (**4**) by subsequent coupling with propargylamine. The tetramethylammonium salt of $[PW_{11}O_{39}Ge(CH_2)_2CO_2H]^{4-}$ has been recently reported; it was obtained from $K_7[PW_{11}O_{39}]\cdot 13H_2O$.[44]

Multinuclear (^{1}H, ^{13}C, ^{29}Si, ^{31}P, and ^{183}W) NMR spectroscopic characterization

*$(NBu_4)_3[PW_9O_{34}(t\text{BuSiO})_3Ge(CH_2)_2CO_2H]$ (**1**)*: The formation of $[PW_9O_{34}(t\text{BuSiO})_3Ge(CH_2)_2CO_2H]^{3-}$ (**1a**) by reaction of $[PW_9O_{34}(t\text{BuSiOH})_3]^{3-}$ with $Cl_3Ge(CH_2)_2CO_2H$ is conveniently monitored by ^{31}P NMR spectroscopy: the signal of **1a** ($\delta = -16.34$ ppm) is shifted to a lower frequency by approximately $\delta = 0.5$ ppm relative to that of the open-structure platform $[PW_9O_{34}(t\text{BuSiOH})_3]^{3-}$ ($\delta = -15.9$ ppm), which is consistent with a closed, that is, capped, structure.[42a] This conclusion is corroborated by {^{1}H}^{29}Si NMR spectroscopy which shows that the resonance of **1a** at $\delta = -58.34$ ppm (with tungsten satellites, ^2J(W-Si)≅8 Hz, see the Supporting Information, Figure S1) is shifted by more than $\delta = 10$ ppm relative to $[PW_9O_{34}(t\text{BuSiOH})_3]^{3-}$ ($\delta = -46.42$ ppm). Moreover, the observation of a single ^{29}Si NMR spectroscopic resonance points to equivalence of the three *t*BuSi groups.

The ^{1}H NMR spectrum of **1** (see the Supporting Information, Figure S2) exhibits the four multiplets from the tetrabutylammonium cations and three signals of the hybrid anion, that is, one singlet at $\delta = 0.99$ ppm (*t*Bu) and two AA′XX′ complex multiplets[45] centered at $\delta = 2.57$ and 1.55 ppm, which are assigned to the methylene groups adjacent to CO_2H and Ge, respectively. Note that because of overlapping with the strong NBu_4 multiplet centered at $\delta = 1.63$ ppm (24 H), observation and quantification of the last AA′XX′ system requires selective gated irradiation (homodecoupling experiment) at $\delta = 3.13$ ppm (see Figure S2c in the Supporting Information). Relative integration of the various multiplets agrees with the chemical formula, that is, three NBu_4^+ cations for one hybrid anion.

The {^{1}H}^{13}C NMR spectrum of **1a** displays five peaks at $\delta = 174.06$ (CO_2H), 27.07 (Me group of *t*Bu), 19.51 (C_Q of *t*Bu), 28.05, and 13.89 ppm (methylenic C). Consistently with the ^{1}H NMR spectra, the last signal, assigned to a CH_2 adjacent to Ge, is significantly shifted to a lower frequency with respect to $Cl_3Ge(CH_2)_2CO_2H$ ($\delta = 27.3$ ppm).

Finally, the ^{183}W NMR spectrum of **1a** displays two resonances in the intensity ratio 1:2 at $\delta = -79.4$ and -156.0 ppm, respectively (Figure 1). These chemical shift values and the homo- and heteronuclear coupling constants (^2J(W-W) = 22.4; ^2J(W-P) = ~0.8 and 1.4 Hz) do not differ markedly from the corresponding values for the open-structure platform $[PW_9O_{34}(t\text{BuSiO})_3]^{3-}$; this demonstrates again the relative rigidity of this platform. All together the NMR

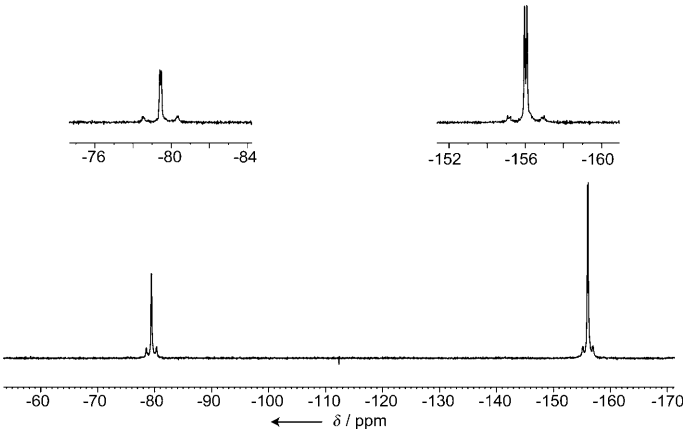

Figure 1. ^{183}W NMR spectrum of $[PW_9O_{34}(t\text{BuSiO})_3Ge(CH_2)_2CO_2H]^{3-}$ (**1a**) in DMF/CD_3COCD_3.

spectroscopic data show that in solution **1a** retains the ternary symmetry of the precursor (C_{3v}), which is consistent with the solid-state structure (vide infra).

*$(NBu_4)_3[PW_9O_{34}(t\text{BuSiO})_3Ge(CH_2)_2CONHCH_2C{\equiv}CH]$ (**2**)*: Whereas conversion of **1a** into **2a** does not shift the ^{31}P NMR spectroscopic signal ($\delta = -16.35$ ppm), the completion of the amide-coupling reaction can be demonstrated by ^{1}H NMR spectroscopy (Figure 2). Note that due to partial

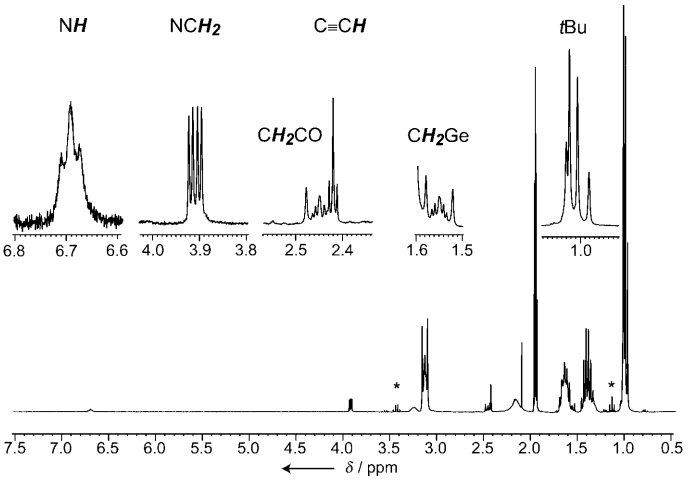

Figure 2. ^{1}H NMR spectrum of $(NBu_4)_3[PW_9O_{34}(t\text{BuSiO})_3Ge(CH_2)_2$-$CONHCH_2C{\equiv}CH]$ (**2**) in CD_3CN, with computer expansion of the hybrid anion resonances; expansion of the $\delta = 1.55$ ppm multiplet (CH_2 close to Ge) is part of a homodecoupled spectrum obtained with irradiation at $\delta = 3.13$ ppm, which reduces overlap with the strong NBu_4 signal at $\delta = 1.63$ ppm (* = diethyl ether).

overlapping with intense NBu_4 multiplets, some signals of the $Ge(CH_2)_2CONHCH_2C{\equiv}CH$ function could be detected and quantified only with the help of homodecoupling experiments. The amide and ethynyl protons give rise to triplets at $\delta = 6.69$ and 2.42 ppm, respectively, due to coupling with the propargylic protons (complex multiplet, $\delta = 3.91$ ppm). The signals from the *t*Bu groups (singlet, $\delta = 1.02$ ppm) and the methylene groups adjacent to CO and Ge (complex multiplets centered at $\delta = 2.45$ and 1.55 ppm, respectively) are nearly unaffected by the coupling. As for **1**, relative integration of the different multiplets is consistent with the chemical formula, that is, three NBu_4^+ cations for one hybrid anion. The IR spectra also consistently showed the disappearance of the $\nu(CO_2H)$ band at 1732 cm^{-1} and the appearance of the ν(C(O)NH) band at 1674 cm^{-1}.

*$(NBu_4)_4[PW_{11}O_{39}Ge(CH_2)_2CO_2H]$ (**3**)*: The ^{31}P NMR spectrum of $[PW_{11}O_{39}Ge(CH_2)_2CO_2H]^{4-}$ (**3a**) exhibits a signal at $\delta = -13.48$ ppm, shifted by $\delta = 1.1$ ppm to a lower frequency relative to that of the monovacant precursor $[H_2PW_{11}O_{39}]^{5-}$ ($\delta = -12.39$ ppm) This is consistent with our previous observations of the progressive increase of ^{31}P shielding on going from vacant to saturated P-centered POMs.[46,47]

Apart from the four multiplets from the tetrabutylammonium cations, the ^{1}H NMR spectrum of **3** exhibits one complex multiplet centered at $\delta = 2.62$ ppm that is assigned to the methylene group adjacent to CO_2H (see the Supporting Information, Figure S3). As the in case of **1**, this multiplet may arise from magnetic nonequivalence of the two protons (AA′XX′ system). According to integration, the signal from the methylene group adjacent to Ge is likely hidden under the strong NBu_4 signal at $\delta = 1.40$ ppm; this was indirectly demonstrated by a homodecoupling experiment with irradiation at $\delta = 1.40$ ppm, whereby the multiplet at $\delta = 2.62$ ppm reduced to a singlet.

The $\{^1H\}^{13}C$ spectrum of **3a** displays three low-intensity signals at $\delta = 176.77$ (COOH), 30.16, and 21.66 ppm (methylene groups). It should be noted that the signal assigned to the CH_2 attached to the germanium atom ($\delta = +21.66$ ppm) is shifted to a higher frequency by $\delta = 8$ ppm relative to that of **1a** ($\delta = 13.89$ ppm).

The ^{183}W NMR spectrum exhibits the expected six-line pattern of a monosubstituted Keggin derivative with overall C_s symmetry (see the Supporting Information, Figure S4). Whereas five lines are observed in a narrow δ range between $\delta = -90$ and -114 ppm, the sixth one is shifted to a low frequency at $\delta = -187.9$ ppm and should be assigned to one pair of W nuclei close to Ge. Full assignment of this spectrum will be discussed below, along with that of $[PW_{11}O_{39}Ge(CH_2)_2C(O)NHCH_2C{\equiv}CH]^{4-}$ (**4a**).

*$(NBu_4)_4[PW_{11}O_{39}Ge(CH_2)_2C(O)NHCH_2C{\equiv}CH]$ (**4**)*: The ^{31}P and ^{183}W NMR spectra of **4a** are very similar to those of **3a**. As in the case of the $[PW_9O_{34}(t\text{BuSiO})_3]^{3-}$ platform (vide supra) success of the amide-coupling reaction is demonstrated by ^{1}H NMR spectroscopy with the help of homodecoupling experiments (see the Supporting Information, Figure S5) Among the different signals from the anion, the amide and ethynyl protons give rise to triplets at $\delta = 6.84$ and 2.39 ppm, respectively, due to coupling with the propargyl protons (doublet of doublets, $\delta = 3.92$ ppm). The signals of the methylene groups adjacent to CO and Ge (AA′XX′ multiplets centered at $\delta = 2.48$ and $\delta = 1.35$ ppm,

respectively) are slightly shifted to a lower frequency relative to that of **3a**.

The $\{^1H\}^{13}C$ NMR spectrum of **4a** is characterized by six peaks at 174.39 (***C***O), 81.85 (***C***≡CH), 71.50 (C≡***C***H), 31.60 (***C***H_2CO), 29.29 (N***C***H_2), and 21.74 (Ge***C***H_2).

As already noted, the ^{183}W NMR spectrum of **4a** is quite similar to that of **3a**. It displays six doublets with relative integrated intensity ratio 2:2:2:1:2 in agreement with an overall C_s symmetry of the POM framework. Under ^{31}P decoupling all doublets become narrow singlets (Figure 3). Ob-

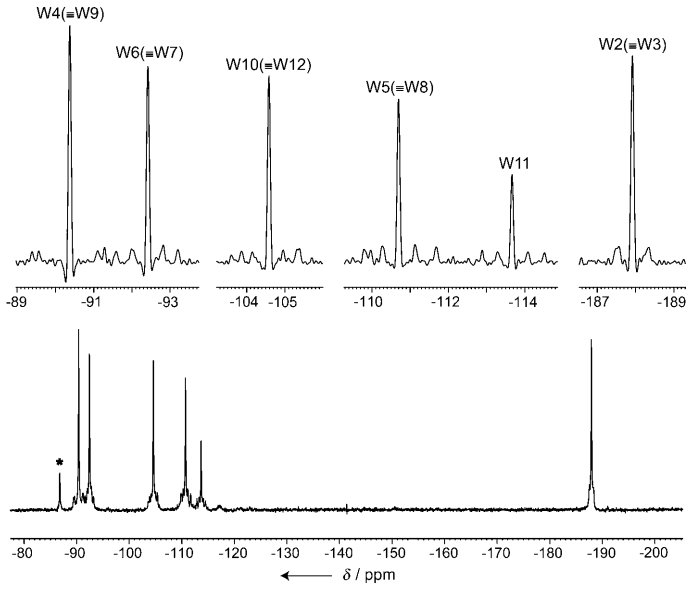

Figure 3. $\{^{31}P\}^{183}W$ NMR spectrum of $[PW_{11}O_{39}Ge(CH_2)_2C(O)NHCH_2C{\equiv}CH]^{4-}$ (**4a**) in DMF/CD_3CN. Bottom: full spectrum after apodization of the FID by exponential function before Fourier transform (the small peak marked by an asterisk at $\delta = -86.8$ ppm corresponds to less than 3% of $PW_{12}O_{40}^{3-}$ impurity). Top: abscissa expansion of the six resonances after resolution enhancement through the Gaussian function to show the tungsten satellites.

servation of well-defined tungsten satellites allows accurate measurement of the homonuclear $^2J_{W-W}$ coupling constants and determination of tungsten–tungsten connectivity. The results of the assignments are given in Table 1 (see the Supporting Information for an explanation of the strategy). The atom numbering is given according to IUPAC convention[48] with Ge at position 1 (Figure 4).

As the linker could influence the electronic interaction between the surface and the POM subunit in surface-grafted POMs, it is worth comparing the ^{183}W NMR spectroscopic

Table 1. Comparison of the ^{183}W chemical shifts [ppm] for $[PW_{11}O_{39}\{O(SiEt)_2\}]^{3-}$, $[PW_{11}O_{39}Ge(CH_2)_2C(O)NHCH_2C{\equiv}CH]^{4-}$ (**4a**), and $[PW_{11}O_{39}\{Sn(CH_2)_2CO_2H\}]^{4-}$.

	$[PW_{11}O_{39}\{O(SiEt)_2\}]^{3-}$[49]	**4a**	$[PW_{11}O_{39}\{Sn(CH_2)_2CO_2H\}]^{4-}$[50]
W2(≡W3)	−251.5	−187.9	−165.1
W4(≡W9)	−198.7	−90.3	−71.4
W5(≡W8)	−121.8	−110.7	−115.5
W6(≡W7)	−99.0	−92.4	−93.0
W10(≡W12)	−104.0	−104.6	−113.2
W11	−108.0	−113.7	−127.6

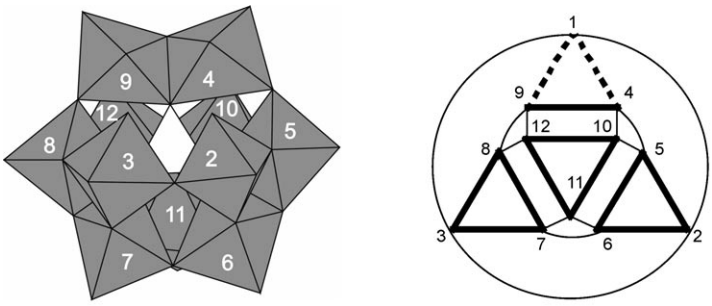

Figure 4. Representation of the POM framework of **3** and **4** with atom numbering according to IUPAC convention.[48] Left: polyhedral representation with Ge omitted for clarity. Right: schematic plane representation, —— and —— hold for intra- and intertrimetallic group W-O-W junctions, respectively (----- represent Ge-O-W junctions).

data for structurally related POMs with different linkers, namely organosilyl, -germyl and -stannyl groups. Derivatives of the monovacant tungstophosphate allow such a comparison (Table 1), even if the structure of the Si species $[PW_{11}O_{39}\{O(SiR)_2\}]^{3-}$ differ from those of Ge and Sn species $[PW_{11}O_{39}(ER)]^{4-}$ (E = Ge, Sn) by the nature of the grafted fragment, that is, a dimeric RSi–O–SiR or a monomeric ER group, respectively.

For the three derivatives, the resonances of the tungsten nuclei remote from the substituent are observed in a very narrow δ range spanning less than $\delta = 30$ ppm. For the remaining nuclei, that is, W2(≡W3) and W4(≡W9), there are large differences between the three species. The most shielded nuclei are always W2(≡W3), which are connected via corners to the substituting element. This agrees with previous observations made by Domaille on various monosubstituted Keggin-type polyoxotungstates.[51] Shielding of the W2(≡W3) nuclei decreases along the series Si ≫ Ge > Sn. A similar sequence is observed for W4(≡W9), which are connected via edges to the substituting element. In the case of the tin and germanium compounds, the W4(≡W9) pair is the least shielded of all the tungsten nuclei. A more detailed comparison of the ^{183}W NMR spectroscopic data of the three derivatives including homonuclear coupling constants is presented in the Supporting Information.

Crystal structure of $(NBu_4)_3[PW_9O_{34}(t\text{BuSiO})_3Ge(CH_2)_2CO_2H]\cdot H_2O$: Colorless crystals of **1**·H_2O were obtained upon slow evaporation of a solution of **1** in DMF in air at room temperature. They belong to the trigonal *R*3c space group. The asymmetric unit contains one tetrabutylammonium cation, one third of the anion, located at a C_3 axis, going through O(11), P(1), Ge(1), and C(5), and a water molecule H-bonded to the carboxylic acid function. A disorder model has been introduced for the $CH_2CH_2CO_2H$ and the *tert*-butyl groups (see the Experimental Section). The overall molecular structure of the anion (Figure 5) is similar to that of other derivatives of the type $[\alpha\text{-A-}PW_9O_{34}(RSiO)_3(RSi)]^{3-}$.[42b,52] The W–O bond lengths fall in the range expected for terminal- (1.711(11) to 1.744(11) Å), doubly- (1.871(11) to 1.965(12) Å), and triply-bridging oxo ligands

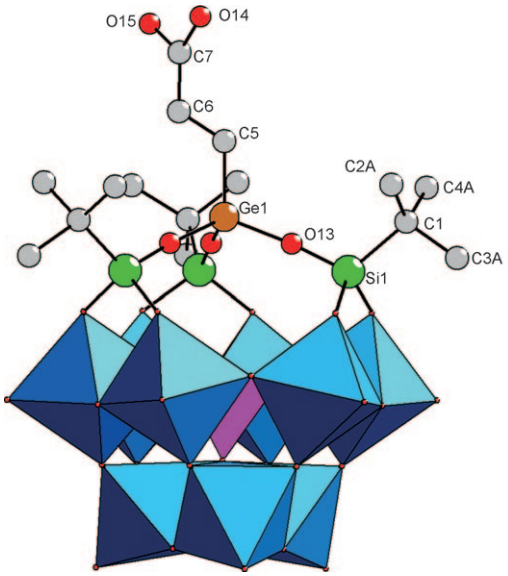

Figure 5. Mixed polyhedral and ball-and-stick representation of $[PW_9O_{34}(t\text{BuSiO})_3Ge(CH_2)_2CO_2H]^{3-}$ (**1a**).

(2.358(10) to 2.402(10) Å). The Ge(1)–O(13) distance of 1.822(14) Å is consistently longer than the Si(1)–O(13) distance of 1.558(15) Å.

Electrochemical studies:

*Electrochemical characterization of $(NBu_4)_3[PW_9O_{34}(tBuSiO)_3Ge(CH_2)_2CO_2H]$ (**1**) and $(NBu_4)_3[PW_9O_{34}(tBuSiO)_3Ge(CH_2)_2CONHCH_2C{\equiv}CH]$ (**2**) in solution*: We have investigated the electrochemical behavior of the organogermyl species **1a** and **2a** by cyclic voltammetry in acetonitrile at a glassy carbon electrode, by using NBu_4BF_4 as the supporting electrolyte. Representative cyclic voltammograms for $(NBu_4)_3$**1a** and $(NBu_4)_3$**2a** are shown in Figure 6 together with that of $(NBu_4)_3[PW_9O_{34}(t\text{BuSiOH})_3]$ for comparison. It must be pointed out that the voltammograms of **1a** and **2a** were obtained after repeated cycles between 0 and −2.5 V, whereas the initial voltammograms displayed an additional feature that progressively disappeared under cycling (see the Supporting Information, Figure S6 and S7; electrochemical data are gathered in Table 2). Each of the three polyoxotungstate hybrids $[PW_9O_{34}(t\text{BuSiOH})_3]^{3-}$, **1a** and **2a**, displays three reversible waves. They correspond to one-electron redox processes as it is known to be the case for Keggin-type POMs in nonaqueous solvents when no protonation accompanies reduction.[53,54] The reduction waves of **1a** and **2a** are only slightly shifted to more negative potentials with respect to $[PW_9O_{34}(t\text{BuSiOH})_3]^{3-}$.

Table 2. Electrochemical data.[a]

Compound	Process	E_{pa}[b]	E_{pc}[b]	$^1/_2(E_{pa}+E_{pc})$[b]	$E_{pa}-E_{pc}$[c]
$[PW_9O_{34}(t\text{BuSiOH})_3]^{3-}$	I	−0.619	−0.671	−0.645	52
	II	−1.103	−1.155	−1.129	52
	III	−1.793	−1.845	−1.819	52
1a	I	−0.756	−0.798	−0.777	42
	II	−1.220	−1.284	−1.252	64
	III	−1.891	−1.976	−1.933	85
2a	I	−0.692	−0.745	−0.718	53
	II	−1.173	−1.237	−1.205	64
	III	−1.841	−1.918	−1.879	77

[a] $c=1\times10^{-3}$ mol L^{-1} in acetonitrile, 0.1 mol L^{-1} NBu_4BF_4, 20 mV s^{-1}. [b] V vs. SCE. [c] mV.

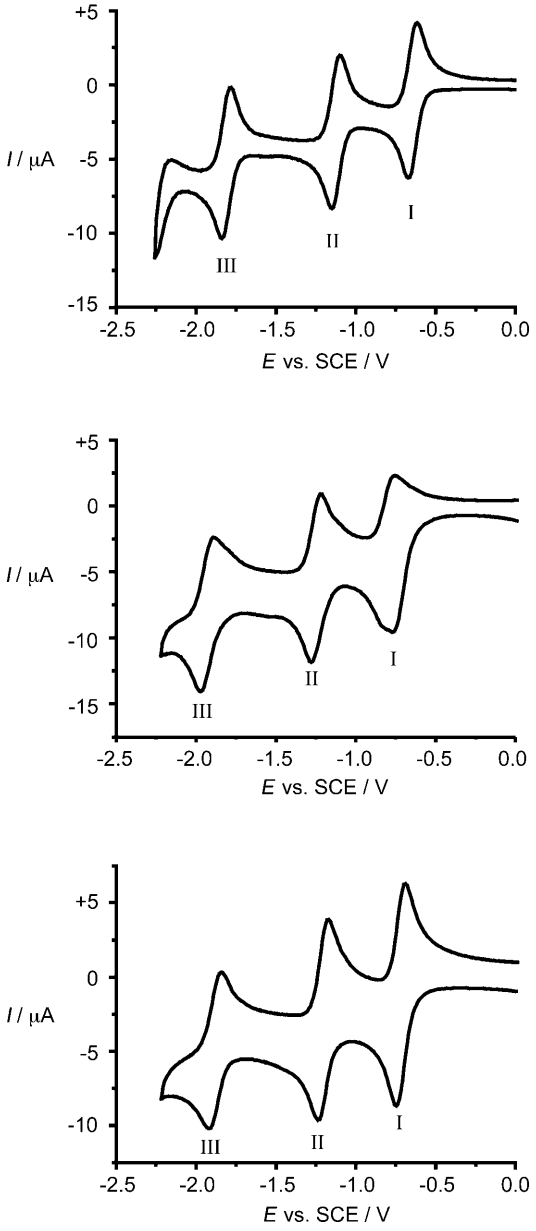

Figure 6. Cyclic voltammograms of $(NBu_4)_3[PW_9O_{34}(t\text{BuSiOH})_3]$ (top), $(NBu_4)_3[PW_9O_{34}(t\text{BuSiO})_3Ge(CH_2)_2CO_2H]$ (**1**) (middle), and $(NBu_4)_3[PW_9O_{34}(t\text{BuSiO})_3Ge(CH_2)_2CONHCH_2{-}C{\equiv}CH]$ (**2**) (bottom) at a glassy carbon electrode. ([POM] $=1\times10^{-3}$ mol L^{-1} in acetonitrile, 0.1 mol L^{-1} NBu_4BF_4, 20 mV s^{-1}).

Electrochemical grafting onto silicon substrates: Electrografting of **2a** onto an n-type highly doped Si surface was achieved by passing an anodic current through a solution of

$(NBu_4)_3$**2a** (1 mmol L^{-1}) and NBu_4BF_4 (0.1 mol L^{-1}) in CH_3CN, by using a protocol adapted from the literature[55] and schematically represented in Scheme 1. The cyclic voltammograms obtained in a three-electrode cell made up of the POM-modified Si electrode as the working electrode

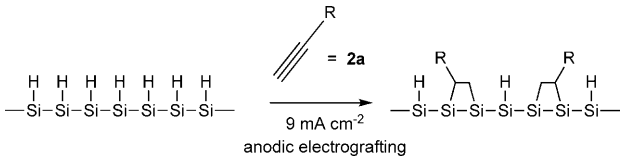

Scheme 1. Schematic representation of the electrografting procedure utilized in this paper.[55a]

and platinum reference and counter electrodes are shown in Figure 7. Three quasi-reversible redox processes are observed with formal potentials of −0.51, −0.93, and −1.38 V versus Pt wire. They are reminiscent of those observed for **2a** in solution, although they are less well-resolved, and thus are assigned to successive reductions of W centers. The working electrode potential was scanned from the lower to higher limit and back at scan rates varying from 20 to 500 mV s^{-1}. The second cathodic peak current (II) shows a linear dependence on the scan rate (see Figure 7 inset), which indicates that the electroactive species are indeed surface-confined. For immobilized species, the theoretical potential difference value between the anodic and cathodic peaks should be zero. The observed value of 80 mV at the scan rate of 500 mV s^{-1} could be interpreted as a slower charge transfer at the Si surface due to the organic spacer. An increase of the potential difference between peaks with the spacing arm length is classically observed in SAMs made of redox species attached at the end of an alkyl chain.[56] These electrochemical results indicate that the POM-modified Si is electrochemically active. There is no evidence for a limited electron transfer between the clusters

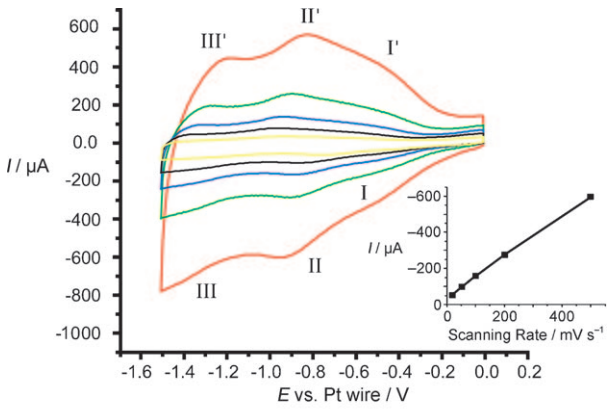

Figure 7. Cyclic voltammograms at the POM-Si modified electrode at different scan rates: 20, 50, 100, 200, 500 mV s^{-1} (acetonitrile, 0.1 mol L^{-1} Bu_4NBF_4). Inset) Linear dependency of peak II current on scan rate.

and the Si substrate contrary to covalently grafted organoimido hexamolybdates on p-type Si wafers.[38]

Conclusion

New organosilyl/-germyl Keggin-type polyoxotungstates have been synthesized for covalent grafting onto Si surfaces. They were characterized by multinuclear NMR spectroscopy and cyclic voltammetry, and, for one of them, by single-crystal X-ray diffraction. Electrografting of $[PW_9O_{34}(t\text{BuSiO})_3Ge(CH_2)_2CONHCH_2{-}C{\equiv}CH]^{3-}$ has been achieved on n-type Si(100) wafers and the resulting films proved to be electrochemically active. Such materials are promising components for the design of multilevel molecular memories.

Experimental Section

General: $(NBu_4)_3[PW_9O_{34}(t\text{BuSiOH})_3]$,[42a] $(NBu_4)_4[H_3PW_{11}O_{39}]$,[57] and $Cl_3Ge(CH_2)_2CO_2H$[43] were prepared as described in the literature and their purity was checked by ^{31}P and ^1H NMR spectroscopy. Unless otherwise noted, all the chemical compounds were purchased from Aldrich. Sulfuric acid (H_2SO_4, 96%), hydrogen peroxide (30%), hydrofluoric acid (1%), acetone, ethanol, and dichloromethane were used as received. Acetonitrile was dried and freshly distilled over CaH_2 before use. NBu_4BF_4 was dried overnight under vacuum at 110 °C. Elemental analyses were performed by the Service de Microanalyses (Université Pierre et Marie Curie) and the Laboratoire Central d'Analyse of the CNRS (Vernaison, France).

Methods

IR spectroscopy: IR spectra were obtained as KBr pellets on a Bio-Rad Win-IR FTS 165 FTIR spectrophotometer.

NMR spectroscopy: The ^1H (300.13 MHz), $\{^1H\}^{13}C$ (75.5 MHz), and $\{^1H\}^{31}P$ (121.5 MHz) NMR spectra were obtained at room temperature in 5 mm o.d. tubes on a Bruker AvanceII 300 spectrometer equipped with a QNP probehead. The $\{^1H\}^{29}Si$ (59.6 MHz) and ^{183}W (12.5 MHz) NMR spectra were recorded in 10 mm o.d. tubes on the Bruker AvanceII 300 spectrometer equipped with a tunable BBO probehead and a special low-frequency VSP probehead, respectively. For ^1H and ^{13}C NMR spectra, chemical shifts are referenced with respect to TMS ($SiMe_4$) by using the solvent signals as secondary standard (CHD_2CN: $\delta(^1H)=1.94$, $\boldsymbol{C}D_3CN$: $\delta(^{13}C)=1.32$, $\boldsymbol{C}D_3CO\boldsymbol{C}D_3$: $\delta(^{13}C)=29.84$ ppm).[58] For other nuclei, chemical shifts were measured by the substitution method and they are given with respect to TMS (^{29}Si), 85% H_3PO_4 (^{31}P), and to external alkaline 2 M Na_2WO_4 aqueous solution (^{183}W), respectively. For ^{183}W, a saturated aqueous solution of $H_4SiW_{12}O_{40}$ was used as secondary standard ($\delta=-103.8$ ppm).[59]

Electrochemistry: All electrochemical measurements were performed at room temperature under argon in a standard three-electrode cell connected to an Autolab PGSTAT100 potentiostat (Eco Chemie BV) equipped with general-purpose electrochemical system software. Freshly cleaned glassy carbon and Pt electrodes (3 mm diameter) were used as the working and auxiliary electrode, respectively. A Pt wire served as the pseudo-reference electrode. Ferrocene (Fc) was added to the solutions as an internal standard. Potentials are given with respect to aqueous SCE ($E_{Fc^+/Fc}=+0.415$ V vs. SCE).

Si surface preparation: The single-crystal phosphorous-doped Si(100) wafers were polished and sliced into rectangular strips of about 0.5 × 1.5 cm^2 in size. A 0.4 × 0.5 cm^2 Cr/Au top contact layer (thickness: 25 nm/500 nm) was deposited on the silicon substrate electrode for cyclic voltammetry measurements. n-Si (phosphorus-doped, two-sides polished, 8×10^{-3}–2.2×10^{-2} Ω cm resistivity) electrodes were used for the experiments.

To remove the organic residues on the surface, the Si(100) wafers were immersed in a 96 wt.% mixture of concentrated 70% H_2SO_4 and 30% H_2O_2 (piranha solution) for about 30 s. After rinsing with copious amounts of water, the Si(100) wafers were blow-dried with purified argon and then immersed in 1% HF for 1 min to remove the oxide film and to leave behind a hydrogen-ended wafer.

Electrografting: Electrografting was performed in a three-electrode cell placed inside a N_2-purged dry-box (Plas Labs). The working electrode was a hydrogenated n-Si wafer with an area of 0.75 cm^2, exposing a 0.45 cm^2 area (for both sides a total area of 0.9 cm^2), in a solution of the reactant ($(NBu_4)_3$**2a**, 0.1 mmol L^{-1}) and the supporting electrolyte (NBu_4BF_4, 0.1 mol L^{-1}) in CH_3CN. Platinum reference and counter electrodes were used. Electrografting was carried out at a constant anodic-current density of 9 mA cm^{-2} for 10^3 s. Following completion of the reaction, the sample was rinsed with CH_3CN, ultrasonicated in CH_3CN for 3 min (×3), to remove any adsorbed species, and dried under a flow of argon. The POM-modified Si surface was characterized by cyclic voltammetry, by using a solution of NBu_4BF_4 in CH_3CN (0.1 mol L^{-1}) and platinum reference and counter electrodes.

Syntheses

*$(NBu_4)_3[PW_9O_{34}(tBuSiO)_3Ge(CH_2)_2CO_2H]$ (**1**)*: An excess of $Cl_3Ge(CH_2)_2CO_2H$ (0.801 g, 3.170 mmol) was added to a solution of $(NBu_4)_3[PW_9O_{34}(tBuSiOH)_3]$ (2.016 g, 0.633 mmol) in dry acetonitrile (80 mL). The reaction mixture was kept overnight at room temperature, then the solvent was removed in vacuo after checking for completion of the reaction by ^{31}P NMR spectroscopy. The residue was dissolved in acetone (10 mL) and compound **1** was precipitated by the addition of a mixture of diethyl ether and ethanol (10:1), filtered off, and dried in air (1.8 g, 83%). Colorless crystals of **1**·H_2O, suitable for single-crystal X-ray crystallography, were grown from a DMF solution by slow evaporation in air at room temperature. IR (KBr): $\tilde{\nu}$ = 2963 (m), 2935 (m), 2876 (w), 2860 (w), 1732 (w), 1677 (w), 1487 (m), 1475 (s), 1384 (w), 1107 (s), 1036 (m), 974 (s), 951 (s), 866 (s), 806 (s), 726 (m), 603 (w), 580 (w), 530 (w), 505 (w), 482 (w), 425 (w), 391 (m), 363 cm^{-1} (m); ^{31}P NMR (CD_3CN): δ = −16.34 ppm; ^1H NMR (CD_3CN): δ = 0.98 (t, 36H; $NCH_2CH_2CH_2C\mathbf{H_3}$), 0.99 (s, 27H; *t*Bu), 1.40 (sextet, 24H; $NCH_2CH_2C\mathbf{H_2}CH_3$), 1.55 (m, 2H; $GeC\mathbf{H_2}CH_2COOH$), 1.63 (m, 24H; $NCH_2C\mathbf{H_2}CH_2CH_3$), 2.57 (m, 2H; $GeCH_2C\mathbf{H_2}COOH$), 3.13 ppm (m, 24H; $NC\mathbf{H_2}CH_2CH_2CH_3$); ^{13}C NMR (DMF, CD_3COCD_3): δ = 13.78 ($NCH_2CH_2CH_2\mathbf{C}H_3$), 13.89 ($GeCH_2CH_2CO_2H$), 19.51 ($\mathbf{C}(CH)_3$), 20.03 ($(NCH_2CH_2\mathbf{C}H_2CH_3$), 24.11 ($NCH_2\mathbf{C}H_2CH_2CH_3$), 27.07 ($C(\mathbf{C}H_3)_3$), 28.05 ($GeCH_2\mathbf{C}H_2COOH$), 58.78 ($N\mathbf{C}H_2CH_2CH_2CH_3$), 174.06 ppm ($GeCH_2CH_2\mathbf{C}OOH$); ^{29}Si NMR (DMF, CD_3COCD_3): δ = −58.34 ppm ($^2J_{W-Si}$ = 8 Hz); ^{183}W NMR (DMF, CD_3COCD_3): δ = −156.0 (d, 6W, $^2J_{W-P}$ = 1.4, $^2J_{W-W}$ = 22.4 Hz), −79.4 ppm (d, 3W, $^2J_{W-P}$ = 0.8, $^2J_{W-W}$ = 22.4 Hz); elemental analysis calcd (%) for $C_{63}H_{140}GeN_3PO_{39}Si_3W_9$ (3406.28): C 22.21, H 4.14, Ge 2.13, N 1.23, P 0.91, Si 2.47, W 48.58; found: C 22.37, H 3.96, Ge 1.66, N 1.30, P 0.95, Si 2.44, W 46.77.

$(NBu_4)_3[PW_9O_{34}(tBuSiO)_3Ge(CH_2)_2C(O)NHCH_2C{\equiv}CH]$ (**2**): Triethylamine (43 μL, 0.307 mmol), isobutylchloroformiate (40 μL, 0.307 mmol), and, after 25 min, propargylamine (36 μL, 0.521 mmol) were added successively to a solution of $(NBu_4)_3[PW_9O_{34}(tBuSiO)_3Ge(CH_2)_2CO_2H]$ (**1**) (0.888 g, 0.261 mmol) in dry acetonitrile (10 mL). The solution was stirred overnight and then evaporated to dryness. The residue was dissolved in acetone (10 mL) and compound **2** was precipitated by the addition of a mixture of diethyl ether and ethanol (10:1), filtered off, and dried in air (0.67 g, 74%). IR (KBr): $\tilde{\nu}$ = 2963 (m), 2935 (m), 2877 (w), 2860 (w), 1674 (w), 1485 (m), 1474 (s), 1384 (w), 1107 (s), 1037 (m), 973 (s), 951 (s), 865 (s), 807 (s), 726 (m), 603 (w), 580 (w), 530 (w), 506 (w), 482 (w), 452 (w), 392 (m), 364 cm^{-1} (m); ^{31}P NMR (CD_3CN): δ = −16.35 ppm; ^1H NMR (CD_3CN): δ = 0.98 (t, 36H; $NCH_2CH_2CH_2C\mathbf{H_3}$), 1.02 (s, 27H; *t*Bu), 1.39 (sextet, 24H; $NCH_2CH_2C\mathbf{H_2}CH_3$), 1.55 (m, 2H; $GeC\mathbf{H_2}CH_2C(O)NHCH_2C{\equiv}CH$), 1.63 (m, 24H; $NCH_2C\mathbf{H_2}CH_2CH_3$), 2.42 (t, 1H, $^4J_{H-H}$ = 2.54 Hz; $GeCH_2CH_2C(O)NHCH_2C{\equiv}C\mathbf{H}$,), 2.45 (m, 2H; $GeCH_2C\mathbf{H_2}C(O)NHCH_2C{\equiv}CH$), 3.13 (m, 24H; $NC\mathbf{H_2}CH_2CH_2CH_3$), 3.91 (dd, 2H, $^3J_{H-H}$ = 5.56, $^4J_{H-H}$ = 2.53 Hz; $GeCH_2CH_2C(O)NHC\mathbf{H_2}C{\equiv}CH$), 6.69 ppm (brt, 1H, $^3J_{H-H}$ ≈ 5.6 Hz); elemental analysis calcd (%) for $C_{66}H_{143}GeN_4PO_{38}Si_3W_9$ (3443.35): C 23.02, H 4.19, Ge 2.11, N 1.63, Si 2.45, W 48.05; found: C 22.60, H 4.27, Ge 1.94, N 1.65, Si 2.93, W 48.25.

*$(NBu_4)_4[PW_{11}O_{39}Ge(CH_2)_2CO_2H]$ (**3**)*: $Cl_3Ge(CH_2)_2COOH$ (0.250 g, 0.992 mmol) and triethylamine (210 μL, 1.505 mmol) were added successively to a solution of $(NBu_4)_4[H_3PW_{11}O_{39}]$ (4 g, 1.096 mmol) in dry acetonitrile (160 mL). The solution was stirred for 5 h and then evaporated to dryness. The residue was dissolved in acetone (10 mL). The white product that precipitated by addition of a mixture of diethyl ether and ethanol (10:1) was filtered off and dried in air (3.9 g). It proved to be a mixed NEt_3H^+/NBu_4^+ salt on the basis of ^1H and ^{13}C NMR spectroscopic analyses. Analytically pure NBu_4^+ salt (**3**) was obtained by recrystallization in DMF. IR (KBr): $\tilde{\nu}$ = 2963 (m), 2935 (m), 2875 (w), 1654 (w), 1485 (m), 1382 (w), 1099 (m), 1072 (s), 963 (s), 886 (s), 808 (s), 738 (sh), 519 (w), 389 cm^{-1} (s); ^{31}P NMR (CD_3CN): δ = −13.48 ppm; ^1H NMR (CD_3CN): δ = 0.99 (t, 48H; $NCH_2CH_2CH_2C\mathbf{H_3}$), 1.40 (m, 34H; $NCH_2CH_2C\mathbf{H_2}CH_3 + GeC\mathbf{H_2}CH_2COOH$), 1.65 (m, 32H; $NCH_2C\mathbf{H_2}CH_2CH_3$), 2.62 (m, 2H; $GeCH_2C\mathbf{H_2}COOH$), 3.15 ppm (m, 32H; $NC\mathbf{H_2}CH_2CH_2CH_3$); ^{13}C NMR (DMF, CD_3CN): δ = 9.66 ($NCH_2\mathbf{C}H_3$), 14.42 ($NCH_2CH_2CH_2\mathbf{C}H_3$), 20.64 ($(NCH_2CH_2\mathbf{C}H_2CH_3$), 21.66 ($GeCH_2CH_2COOH$), 24.72 ($NCH_2\mathbf{C}H_2CH_2CH_3$), 30.16 ($GeCH_2\mathbf{C}H_2COOH$), 47.40 ($N\mathbf{C}H_2CH_3$), 59.26 ($N\mathbf{C}H_2CH_2CH_2CH_3$), 176.77 ppm ($GeCH_2CH_2\mathbf{C}OOH$); ^{183}W NMR (DMF, CD_3CN): δ = −187.9 (2W, $^2J_{W-P}$ ≈ 1.2 Hz), −113.8 (1W, $^2J_{W-P}$ ≈ 1.3 Hz), −110.5 (2W, $^2J_{W-P}$ ≈ 0.9 Hz), −104.5 (2W, $^2J_{W-P}$ ≈ 1.1 Hz), −92.4 (2W, $^2J_{W-P}$ ≈ 1.2 Hz), −90.4 ppm (2W, $^2J_{W-P}$ ≈ 1.5 Hz); elemental analysis calcd (%) for $C_{67}H_{149}GeN_4PO_{41}W_{11}$ (3792.85): C 21.22, H 3.96, Ge 1.91, N 1.48, P 0.82, W 53.32; found: C 21.14, H 3.67, Ge 1.46, N 1.67, P 0.96, W 52.45.

*Synthesis of $(NBu_4)_4[PW_{11}O_{39}Ge(CH_2)_2C(O)NHCH_2C{\equiv}CH]$ (**4**)*: Triethylamine (81 μL, 0.630 mmol), isobutylchloroformiate (87 μL, 0.630 mmol), and, after 25 min, propargylamine (72 μL, 1.050 mmol) were added successively to a solution of $(NBu_4)_4[PW_{11}O_{39}Ge(CH_2)_2COOH]$ (**3**) (2 g, 0.53 mmol) in dry acetonitrile (20 mL). The solution was stirred overnight, filtered, and then evaporated to dryness. The residue was redissolved in acetone (10 mL) and compound **4** was precipitated by the addition of a mixture of diethyl ether and ethanol (10:1), filtered off, and dried in air (1.8 g, 89%). IR (KBr): $\tilde{\nu}$ = 2963 (m), 2937 (m), 2875 (w), 1668 (w), 1485 (m), 1382 (w), 1100 (m), 1072 (s), 963 (s), 886 (s), 807 (s), 518 (w), 506 (sh), 388 cm^{-1} (s); ^{31}P NMR (CD_3CN): δ = −13.50 ppm (−12.81 impurity 15%); ^1H NMR (CD_3CN): δ = 0.99 (t, 48H; $NCH_2CH_2CH_2C\mathbf{H_3}$), 1.41 (sextet, 32H; $NCH_2CH_2C\mathbf{H_2}CH_3$), 1.35 (m, 2H; $GeC\mathbf{H_2}CH_2C(O)NHCH_2C{\equiv}CH$), 1.65 (m, 32H; $NCH_2C\mathbf{H_2}CH_2CH_3$), 2.39 (t, 1H, $^4J_{H-H}$ = 2.55 Hz; $GeCH_2CH_2C(O)NHCH_2C{\equiv}C\mathbf{H}$), 2.48 (m, 2H; $GeCH_2C\mathbf{H_2}C(O)NHCH_2C{\equiv}CH$), 3.17 (m, 32H; $NC\mathbf{H_2}CH_2CH_2CH_3$), 3.92 (dd, 2H, $^3J_{H-H}$ = 5.59, $^4J_{H-H}$ = 2.47 Hz; $GeCH_2CH_2C(O)NHC\mathbf{H_2}C{\equiv}CH$), 6.84 ppm (brt, 1H, $^3J_{H-H}$ ≈ 5.4 Hz); ^{13}C NMR (CD_3CN): δ = 13.98 ($NCH_2CH_2CH_2\mathbf{C}H_3$), 21.74 ($GeC\mathbf{H_2}CH_2C(O)NHCH_2C{\equiv}CH$), 20.49 ($(NCH_2CH_2\mathbf{C}H_2CH_3$), 24.49 ($NCH_2\mathbf{C}H_2CH_2CH_3$), 29.29 ($GeCH_2CH_2C(O)NH\mathbf{C}H_2C{\equiv}CH$), 31.60 ($GeCH_2\mathbf{C}H_2C(O)NHCH_2C{\equiv}CH$), 59.37 ($N\mathbf{C}H_2CH_2CH_2CH_3$), 71.50 ($GeCH_2CH_2C(O)NHCH_2C{\equiv}\mathbf{C}H$), 81.85 ($GeCH_2CH_2C(O)NHCH_2\mathbf{C}{\equiv}CH$), 174.39 ppm ($GeCH_2CH_2\mathbf{C}(O)NHCH_2C{\equiv}CH$); ^{183}W NMR (DMF, CD_3CN): δ = −187.9 (d, 2W, $^2J_{W-P}$ = 1.5, $^2J_{W-W}$ = 10.7, 8.8 Hz), −113.7 (d, 1W, $^2J_{W-P}$ = 1.4, $^2J_{W-W}$ = 20.4, 9.9 Hz), −110.7 (d, 2W, $^2J_{W-P}$ = 1.2, $^2J_{W-W}$ = 23.6, 21.4, 10.6 Hz (2W)), −104.6 (d, 2W, $^2J_{W-P}$ = 1.1, $^2J_{W-W}$ = 21.4, 19.1, ca. 10 Hz), −92.4 (d, 2W, $^2J_{W-P}$ = 1.3, $^2J_{W-W}$ = 20.2, ca. 10 Hz (2W)), −90.3 ppm (d, 2W, $^2J_{W-P}$ = 1.6, $^2J_{W-W}$ = 23.5, 19.2 Hz); elemental analysis calcd (%) for $C_{70}H_{152}GeN_5PO_{40}W_{11}$ (3829.91): C 21.95, H 4.00, Ge 1.90, N 1.83, P 0.81, W 52.80; found: C 21.18, H 3.56, Ge 1.66, N 1.87, P 0.91, W 52.35.

X-ray diffraction study: Crystal data for $(NBu_4)_3[PW_9O_{34}(tBuSiO)_3Ge(CH_2)_2CO_2H]\cdot H_2O$ (**1**·H_2O): $C_{63}H_{140}GeN_3PO_{39}Si_3W_9$; M = 3424.28; colorless crystals; trigonal; space group = $R\bar{3}c$; a = b = 22.284(4), c = 36.880(6) Å; $\alpha = \beta = 90$, $\gamma = 120°$; U = 15860(5) $Å^3$; Z = 6; T = 200(2) K; μ = 10.15 mm^{-1}; 23428 reflections measured, 7333 independent (R_{int} = 0.046), 5525 observed with $I > 2\sigma(I)$, 375 variables refined, final R indices R_1 [$I > 2\sigma(I)$] = 0.0386 and wR_2 (all data) = 0.1161; GOF on F^2 = 1.21; max/min residual electron density = 2.819/−3.025 e $Å^{-3}$. Measurements were performed with a Bruker-Nonius Kappa-CCD diffractometer by using graphite-monochromated $Mo_{K\alpha}$ radiation. Unit-cell parameter de-

termination, data collection strategy, and integration were carried out with the Nonius EVAL-14 suite of programs.[60] The data were corrected from absorption by a multiscan method.[61] The structure was solved by direct methods by using the SHELXS-97 program and refined anisotropically by full-matrix least-squares on F^2 by using the SHELXL-97 software package.[62] Graphics were carried out by using DIAMOND.[63] All non-H atoms, except those of the pending $CH_2CH_2CO_2H$ on the anion, were refined anisotropically. Hydrogen atoms of the cation were introduced at calculated positions and refined isotropically. $CH_2CH_2CO_2H$ is disordered due to the three-fold axis: its geometry was restrained and isotropic displacement parameters of the oxygen atoms were fixed at 0.18, slightly above that of the carbon atom to which they are attached (0.17). The three terminal methyl groups of the *t*Bu group are also disordered over two equally occupied positions. The displacement parameters of related carbon atoms have consequently been fixed to be equal. CCDC-705019 contains the supplementary crystallographic data for this paper. These data can be obtained free of charge from The Cambridge Crystallographic Data Centre via www.ccdc.cam.ac.uk/data_request/cif.

Acknowledgements

This work was supported by a grant from the European Community under the FP6—Marie Curie Host Fellowships for Early Stage Research Training (EST) "CHEMTRONICS" contract number MEST-CT-2005-020513.

[1] a) M. T. Pope, *Heteropoly and Isopoly Oxometalates*, Springer, Berlin, **1983**; b) M. T. Pope, A. Müller, *Angew. Chem.* **1991**, *103*, 56–70; *Angew. Chem. Int. Ed. Engl.* **1991**, *30*, 34–48.
[2] M. T. Pope, *Inorg. Chem.* **1972**, *11*, 1973–1974.
[3] I. A. Weinstock, *Chem. Rev.* **1998**, *98*, 113–170.
[4] M. Sadakane, E. Steckhan, *Chem. Rev.* **1998**, *98*, 219–237.
[5] B. Keita, L. Nadjo, *J. Mol. Catal. A* **2007**, *262*, 190–215.
[6] L. Cheng, J. A. Cox, *Chem. Mater.* **2002**, *14*, 6–8.
[7] a) M. Zynek, M. Serantoni, S. Beloshapkin, E. Dempsey, T. McCormac, *Electroanalysis* **2007**, *19*, 681–689; b) L.-H. Bi, T. McCormac, S. Beloshapkin, E. Dempsey, *Electroanalysis* **2007**, *20*, 38–46.
[8] A. Proust, R. Thouvenot, P. Gouzerh, *Chem. Commun.* **2008**, 1837–1852.
[9] a) D.-L. Long, L. Cronin, *Chem. Eur. J.* **2006**, *12*, 3698–3706; b) D.-L. Long, E. Burkholder, L. Cronin, *Chem. Soc. Rev.* **2007**, *36*, 105–121.
[10] a) S. Liu, D. G. Kurth, D. Volkmer, *Chem. Commun.* **2002**, 976–977; b) S. Liu, D. Volkmer, D. G. Kurth, *Anal. Chem.* **2004**, *76*, 4579–4582.
[11] G. L. Turdean, A. Curulli, I. C. Popescu, C. Rosu, G. Palleschi, *Electroanalysis* **2004**, *16*, 1550–1556.
[12] M. Ammam, B. Keita, L. Nadjo, J. Fransaer, *Sens. Actuators B* **2009**, *142*, 347–354.
[13] T. Yamase, *Chem. Rev.* **1998**, *98*, 307–325.
[14] S. Liu, H. Möhwald, D. Volkmer, D. G. Kurth, *Langmuir* **2006**, *22*, 1949–1951.
[15] a) D. R. Vernon, F. Meng, S. F. Dec, D. L. Williamson, J. A. Turner, A. M. Herring, *J. Power Sources* **2005**, *139*, 141–151; b) R. J. Stanis, M.-C. Kuo, A. J. Rickett, J. A. Turner, A. M. Herring, *Electrochim. Acta* **2008**, *53*, 8277–8286.
[16] a) M. Lu, B. Xie, J. Kang, F.-C. Chen, Y. Yang, Z. Peng, *Chem. Mater.* **2005**, *17*, 402–408; b) B. Xu, M. Lu, J. Kang, D. Wang, J. Brown, Z. Peng, *Chem. Mater.* **2005**, *17*, 2841–2851.
[17] A. K. Cuentas-Gallegos, M. Lirá-Cantu, N. Casañ-Pastor, P. Gómez-Romero, *Adv. Funct. Mater.* **2005**, *15*, 1125–1133.
[18] a) A. M. Douvas, E. Makarona, N. Glezos, P. Argitis, J. A. Mielczarski, E. Mielczarski, *ACS NANO* **2008**, *2*, 733–742; b) E. Kapetanakis, A. M. Douvas, D. Velessiotis, E. Makarona, P. Argitis, N. Glezos, *Org. Electron.* **2009**, *10*, 711–718.
[19] C. Li, W. Fan, B. Lei, D. Zhang, S. Han, T. Tang, X. Liu, Z. Liu, S. Asano, M. Meyyapan, J. Han, C. Zhou, *Appl. Phys. Lett.* **2004**, *84*, 1949–1951.
[20] Q. Li, S. Surthi, G. Mathur, S. Gowda, Q. Zhao, T. A. Sorenson, R. C. Tenent, K. Muthukumaran, J. S. Lindsey, V. Misra, *Appl. Phys. Lett.* **2004**, *85*, 1829–1831.
[21] G. Bidan, E. Jalaguier, PCT Int. Appl., WO 2007015010A1 20070208, **2007**.
[22] a) N. Glezos, D. Velessiotis, G. Chaidogiannos, P. Argitis, D. Tsamakis, X. Zianni, *Synth. Met.* **2003**, *138*, 267–269; b) G. Chaidogiannos, D. Velessiotis, P. Argitis, P. Koutsolelos, C. D. Diakoumakos, D. Tsamakis, N. Glezos, *Microelectron. Eng.* **2004**, *73–74*, 746–751; c) D. Velessiotis, N. Glezos, V. Ioannou-Sougleridis, *J. Appl. Phys.* **2005**, *98*, 084503; d) N. Glezos, A. M. Douvas, P. Argitis, F. Saurenbach, J. Chrost, C. Livitsanos, *Microelectron. Eng.* **2006**, *83*, 1757–1760; e) E. Makarona, E. Kapetanakis, D. M. Velessiotis, A. Douvas, P. Argitis, P. Normand, T. Gotszalk, M. Woszczyna, N. Glezos, *Microelectron. Eng.* **2008**, *85*, 1399–1402.
[23] a) T. He, J. He, M. Lu, B. Chen, H. Pang, W. F. Reus, W. M. Nolte, D. P. Nackashi, P. D. Franzon, J. M. Tour, *J. Am. Chem. Soc.* **2006**, *128*, 14537–14541; b) T. He, S. Ding, N. Peor, M. Lu, D. A. Corley, Y. Gao, S. Itzchaik, J. M. Tour, *J. Am. Chem. Soc.* **2008**, *130*, 1699–1710.
[24] W. G. Klemperer, C. G. Wall, *Chem. Rev.* **1998**, *98*, 297–306.
[25] B. Keita, A. Belhouari, R. Contant, L. Nadjo, *C. R. Acad. Sci. Paris* **1998**, *1*, 333–342.
[26] a) B. Keita, D. Bouaziz, L. Nadjo, *J. Electroanal. Chem.* **1988**, *255*, 307–313; b) B. Keita, D. Bouaziz, L. Nadjo, A. Deronzier, *J. Electroanal. Chem.* **1990**, *279*, 187–203.
[27] a) G. Bidan, E. M. Genies, M. Lapkowski, *J. Chem. Soc. Chem. Commun.* **1988**, 533–535; b) G. Bidan, E. M. Genies, M. Lapkowski, *J. Electroanal. Chem. Interfacial Electrochem.* **1988**, *251*, 297–306.
[28] M. Carraro, M. Gardan, G. Scorrano, E. Fontananova, M. Bonchio, *Chem. Commun.* **2006**, 4533–4535.
[29] a) S. J. Dong, W. Jin, *J. Electroanal. Chem.* **1993**, *354*, 87–97; b) S. J. Dong, M. J. Liu, *J. Electroanal. Chem.* **1994**, *372*, 95–100.
[30] a) P. Judeinstein, *Chem. Mater.* **1992**, *4*, 4–7; b) P. Judeinstein, H. Schmidt, *J. Sol-Gel Sci. Technol.* **1994**, *3*, 189–197.
[31] D. G. Kurth, *Sci. Technol. Adv. Mater.* **2008**, *9*, 014103.
[32] a) C. R. Mayer, V. Cabuil, T. Lalot, R. Thouvenot, *Angew. Chem.* **1999**, *111*, 3878–3881; *Angew. Chem. Int. Ed.* **1999**, *38*, 3672–3675; b) C. R. Mayer, R. Thouvenot, T. Lalot, *Chem. Mater.* **2000**, *12*, 257–260; c) C. R. Mayer, R. Thouvenot, T. Lalot, *Macromolecules* **2000**, *33*, 4433–4437.
[33] R. C. Schroden, C. F. Blanford, B. J. Melde, B. J. S. Johnson, A. Stein, *Chem. Mater.* **2001**, *13*, 1074–1081.
[34] H. Chen, L. Xie, H. Lu, Y. Yang, *J. Mater. Chem.* **2007**, *17*, 1258–1261.
[35] A. R. Moore, H. Kwen, A. M. Beatty, E. A. Maatta, *Chem. Commun.* **2000**, 1793–1794.
[36] a) Y. Wei, B. Xu, C. L. Barnes, Z. Peng, *J. Am. Chem. Soc.* **2001**, *123*, 4083–4084; b) B. Xu, Y. Wei, C. L. Barnes, Z. Peng, *Angew. Chem.* **2001**, *113*, 2353–2356; *Angew. Chem. Int. Ed.* **2001**, *40*, 2290–2292.
[37] Y. Zhu, L. Wang, J. Hao, P. Yin, J. Zhang, Q. Li, L. Zhu, Y. Wei, *Chem. Eur. J.* **2009**, *15*, 3076–3080.
[38] M. Lu, W. M. Nolte, T. He, D. A. Corley, J. M. Tour, *Chem. Mater.* **2009**, *21*, 442–446.
[39] R. J. Errington, S. S. Petkar, B. R. Horrocks, A. Houlton, L. H. Lie, S. N. Patole, *Angew. Chem.* **2005**, *117*, 1280–1283; *Angew. Chem. Int. Ed.* **2005**, *44*, 1254–1257.
[40] Y.-F. Song, N. McMillan, D.-L. Long, S. Kane, J. Malm, M. O. Riehle, C. P. Pradeep, N. Gadegaard, L. Cronin, *J. Am. Chem. Soc.* **2009**, *131*, 1340–1341.
[41] C. Dablemont, A. Proust, R. Thouvenot, C. Afonso, F. Fournier, J.-C. Tabet, *Dalton Trans.* **2005**, 1831–1841.
[42] a) A. Mazeaud, N. Ammari, F. Robert, R. Thouvenot, *Angew. Chem.* **1996**, *108*, 2089–2091; *Angew. Chem. Int. Ed. Engl.* **1996**, *35*,

1961–1964; b) D. Agustin, C. Coelho, A. Mazeaud, P. Herson, A. Proust, R. Thouvenot, *Z. Anorg. Allg. Chem.* **2004**, *630*, 2049–2053.
[43] G. Sazani, M. T. Pope, *Dalton Trans.* **2004**, 1989–1994.
[44] J. Li, R. Tan, R. Li, X. Wang, E. Li, F. Zhai, S. Zhang, *Inorg. Chem. Commun.* **2007**, *10*, 216–219.
[45] H. Günther, *Angew. Chem.* **1972**, *84*, 907–920; *Angew. Chem. Int. Ed. Engl.* **1972**, *11*, 861–874.
[46] R. Massart, R. Contant, J.-M. Fruchart, J.-P. Ciabrini, M. Fournier, *Inorg. Chem.* **1977**, *16*, 2916–2921.
[47] L. Alloul, N. Ammari, C. R. Mayer, A. Mazeaud, R. Thouvenot, *J. Chim. Phys.* **1998**, *95*, 289–294.
[48] Y. Jeannin, M. Fournier, *Pure Appl. Chem.* **1987**, *59*, 1529–1548; Y. Jeannin, *Chem. Rev.* **1998**, *98*, 51–76.
[49] D. Agustin, J. Dallery, C. Coelho, A. Proust, R. Thouvenot, *J. Organomet. Chem.* **2007**, *692*, 746–754.
[50] S. Bareyt, R. Thouvenot, unpublished results.
[51] P. J. Domaille, *J. Am. Chem. Soc.* **1984**, *106*, 7677–7687.
[52] a) J. Niu, M. Li, J. Wang, *J. Organomet. Chem.* **2003**, *675*, 84–90; b) J. Niu, J. Zhao, J. Wang, M. Li, *J. Mol. Struct.* **2003**, *655*, 243–250.
[53] V. Artero, A. Proust, *Eur. J. Inorg. Chem.* **2000**, 2393–2400.
[54] a) S. Himeno, M. Takamoto, *J. Electroanal. Chem.* **2002**, *528*, 170–174; b) S. Himeno, M. Takamoto, A. Higuchi, M. Maekawa, *Inorg. Chim. Acta* **2003**, *348*, 57–62.
[55] a) H. C. Choi, J. M. Buriak, *Chem. Mater.* **2000**, *12*, 2151–2156; b) E. G. Robins, M. P. Stewart, J. M. Buriak, *Chem. Commun.* **1999**, 2479–2480.
[56] K. Huang, F. Duclairoir, T. Pro, J. Buckley, G. Marchand, E. Martinez, J.-C. Marchon, B. De Salvo, G. Delapierre, F. Vinet, *ChemPhysChem* **2009**, *10*, 963–971.
[57] E. Radkov, R. H. Beer, *Polyhedron* **1995**, *14*, 2139–2143.
[58] H. E. Gottlieb, V. Kotlyar, A. Nudelman, *J. Org. Chem.* **1997**, *62*, 7512–7515.
[59] R. Acerete, C. F. Hammer, L. C. W. Baker, *J. Am. Chem. Soc.* **1979**, *101*, 267–269.
[60] A. J. M. Duisenberg, L. M. J. Kroon-Batenburg, A. M. M. Schreurs, *J. Appl. Crystallogr.* **2003**, *36*, 220–229.
[61] R. H. Blessing, *Acta Crystallogr. Sect. A* **1995**, *51*, 33–38.
[62] SHELXL 97: Program for the crystal structure determination, G. M. Sheldrick, University of Göttingen, Göttingen, **1997**.
[63] Diamond, K. Brandenburg, M. Berndt, Crystal Impact GbR, Bonn, **1999**.

Received: December 4, 2009
Published online: March 26, 2010

No.	
1	 $[PW_{11}O_{39}]^{7-}$
2	 $[PW_9O_{34}]^{9-}$
Silyl compounds derived from $[PW_9O_{34}(t\text{BuSiOH}_3)]^{3-}$ anion	
3	 $[PW_9O_{34}(t\text{BuSiOH})_3]^{3-}$
4	 $[PW_9O_{34}(t\text{BuSiO})_3(\text{Si-H})]^{3-}$
5	 $[PW_9O_{34}(t\text{BuSiO})_3(\text{Si-CH=CH}_2)]^{3-}$
6	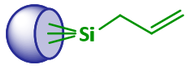 $[PW_9O_{34}(t\text{BuSiO})_3(\text{Si-CH}_2\text{-CH=CH}_2)]^{3-}$
7	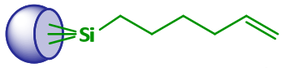 $[PW_9O_{34}(t\text{BuSiO})_3(\text{Si-(CH}_2)_4\text{-CH=CH}_2)]^{3-}$
8	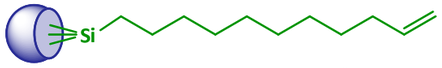 $[PW_9O_{34}(t\text{BuSiO})_3(\text{Si-(CH}_2)_9\text{-CH=CH}_2)]^{3-}$
9	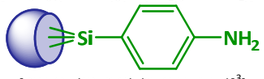 $[PW_9O_{34}(t\text{BuSiO})_3(\text{Si-C}_6\text{H}_4\text{-NH}_2)]^{3-}$
Silyl compounds derived from $[PW_9O_{34}]^{9-}$ anion	
10	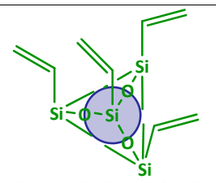 $[PW_9O_{34}(\text{CH}_2\text{=CH-SiO})_3(\text{Si-CH=CH}_2)]^{3-}$
11	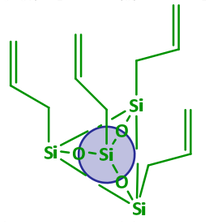 $[PW_9O_{34}(\text{CH}_2\text{=CH-CH}_2\text{-SiO})_3(\text{Si-CH}_2\text{-CH=CH}_2)]^{3-}$
12	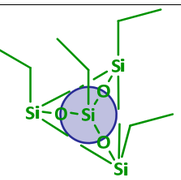 $[PW_9O_{34}(\text{CH}_3\text{-CH}_2\text{-SiO})_3(\text{Si-CH}_2\text{-CH}_3)]^{3-}$
Germyl compounds derived from $[PW_9O_{34}(t\text{BuSiOH}_3)]^{3-}$ anion	
14	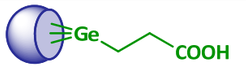 $[PW_9O_{34}(t\text{BuSiOH})_3(\text{GeCH}_2\text{CH}_2\text{COOH})]^{3-}$
15	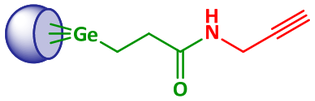 $[PW_9O_{34}(t\text{BuSiOH})_3(\text{GeCH}_2\text{CH}_2\text{C(O)NHCH}_2\text{C}\equiv\text{CH})]^{3-}$
17	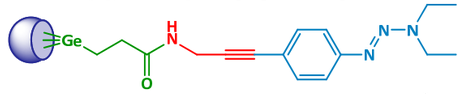 $[PW_9O_{34}(t\text{BuSiOH})_3(\text{GeCH}_2\text{CH}_2\text{C(O)NHCH}_2\text{C}\equiv\text{CC}_6\text{H}_4\text{N}_3\text{Et}_2)]^{3-}$
19	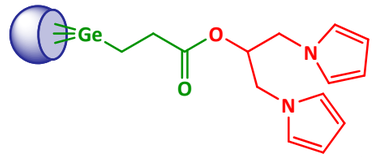 $[PW_9O_{34}(t\text{BuSiOH})_3(\text{GeCH}_2\text{CH}_2\text{COOCH(CH}_2\text{NC}_4\text{H}_4)_2)]^{3-}$
20	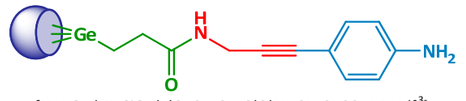 $[PW_9O_{34}(t\text{BuSiOH})_3(\text{GeCH}_2\text{CH}_2\text{C(O)NHCH}_2\text{C}\equiv\text{CC}_6\text{H}_4\text{NH}_2)]^{3-}$
Germyl compounds derived from $[PW_{11}O_{39}]^{7-}$ anion	
21	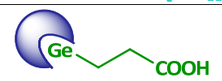 $[PW_{11}O_{39}(\text{GeCH}_2\text{CH}_2\text{COOH})]^{4-}$
22	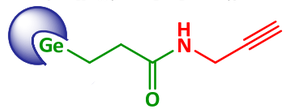 $[PW_{11}O_{39}(\text{GeCH}_2\text{CH}_2\text{C(O)NHCH}_2\text{C}\equiv\text{CH})]^{4-}$
Stannyl compounds derived from $[PW_{11}O_{39}]^{7-}$ anion	
24	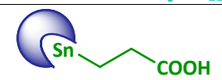 $[PW_{11}O_{39}(\text{SnCH}_2\text{CH}_2\text{COOH})]^{4-}$
25	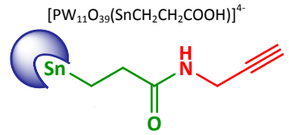 $[PW_{11}O_{39}(\text{SnCH}_2\text{CH}_2\text{C(O)NHCH}_2\text{C}\equiv\text{CH})]^{4-}$

Abstract – The aim of the present thesis is to study the miniaturization of non-volatile memory devices, FLASH type, by replacing the floating gate with monolayers of redox molecules, polyoxometalates. Towards this goal, I was engaged in a program aimed at constructing devices that use the properties of polyoxometalates (POMs) to store information. In a general approach, a redox-active molecule attached to an electroactive surface serves as the active storage medium, and information is stored in the discrete redox states of the molecule (POM).

This work is organized in four parts and begins with a short introduction into the molecular memory and polyoxometalates field. It continues with the experimental results systematized in Part 2, synthesis and characterization of functionalized polyoxometalates; Part 3, polyoxometalates modified electrodes and Part 4, electrical investigation of the polyoxometalates modified capacitors.

Keywords: Molecular memory, Organic-inorganic hybrid composites, Polyoxometalates, Silicon, Surface chemistry

Résumé – L'objectif de cette thèse est d'étudier la miniaturisation des dispositifs à mémoire non-volatile, de type FLASH, en remplaçant la grille flottante avec des monocouches de molécules redox, les polyoxométallates. Dans ce but, j'ai été engagé dans un programme visant à construire des dispositifs qui utilisent les propriétés des polyoxométallates (POMs) pour stocker des informations. Dans une approche générale, une molécule redox-active fixée à une surface d'électrode de silicium sert de support de stockage actif, et l'information est stockée dans les états d'oxydo-réduction discrets de la molécule (POM).

Ce travail est organisé en quatre parties et commence par une brève introduction sur les mémoires moléculaires et les polyoxométallates. Il continue avec les résultats expérimentaux en Partie 2, la synthèse et la caractérisation des polyoxométallates fonctionnalisés; en Partie 3, les électrodes modifiés par des polyoxométallates et en Partie 4, l'étude électrique des condensateurs modifiés par des polyoxométallates.

Mots clés: Mémoire moléculaire, Composites organique-anorganique hybrides, Polyoxométallates, Silicium, Chimie de surface